# POLYIMIDE ULTRAFILTRATION MEMBRANES FOR NON-AQUEOUS SYSTEMS

Monique Beerlage

# POLYIMIDE ULTRAFILTRATION MEMBRANES FOR NON-AQUEOUS SYSTEMS

**Proefschrift**

ter verkrijging van
de graad van doctor aan de Universiteit Twente,
op gezag van de rector magnificus
prof. dr. Th.J.A. Popma,
volgens besluit van het College van Promoties
in het openbaar te verdedigen
op vrijdag 6 mei 1994 te 15.00 uur

door

**Monique Anne Marie Beerlage**

geboren op 26 augustus 1965
te Oldenzaal

Dit proefschrift is goedgekeurd door de promotor prof. dr. ing. H. Strathmann, de co-promotor prof. dr. C.A. Smolders en de assistent-promotor dr. ing. M.H.V. Mulder.

**Acknowledgement**

The work described in this thesis was financially supported by the Dutch Ministry of Economic Affairs, in the framework of the Dutch research program on membranes (IOP-m), X-Flow BV, and Tollens Coatings BV.

CIP-DATA KONINKLIJKE BIBLIOTHEEK, DEN HAAG

Beerlage, Monique Anne Marie

Polyimide ultrafiltration membranes for non-aqueous systems / Monique Anne Marie Beerlage. -[S.l. : s.n.]. - Ill.
Thesis Enschede. -With ref. - With summary in Dutch.
ISBN 90-9007140-7
Subject headings: ultrafiltration membranes

# Voorwoord

Een proefschrift schrijven is iets wat je niet alleen kunt doen, gelukkig niet! Bij de totstandkoming van dit proefschrift zijn dan ook erg veel mensen direct of indirect betrokken geweest, waarvan ik er hier een aantal wil noemen.

Mijn promotoren, Heiner Strathmann en Kees Smolders, ben ik zeer erkentelijk voor hun begeleiding, kritische vragen en nieuwe suggesties. Marcel Mulder, als assistent-promotor was je niet alleen een uitmuntende mentor op membraangebied, maar je wist ook altijd precies de juiste steun te bieden en alles te relativeren.
Robert Meertens en José Nolten, ik wil jullie graag bedanken voor de grote bijdrage die jullie als technisch assistenten geleverd hebben aan het praktische werk, en uiteraard voor de bijzonder plezierige samenwerking. Afstudeerders Marjo Peeters, Martin Heijnen en Sjoerd Visser, bedankt voor jullie enthousiaste inzet en voor de discussies die vaak tot nieuwe ideëen en resultaten leidden.
Erik Rolevink en Piotr Adamczak wil ik graag bedanken voor het uitvoeren van de verffiltraties. Clemens Padberg was onmisbaar voor de GPC-metingen en andere "probeersels", en Richard Bouma voor het opzetten van de wiskundige afleidingen. Marjo Peeters, Antoinette van Bennekom en Remko Boom, bedankt voor het kritisch doorlezen en corrigeren van het concept van dit proefschrift.
De praktische toepasbaarheid van het onderzoek was voor mij een grote stimulans. Daarom wil ik de contactpersonen van de participanten bedanken voor het regelmatige overleg: Ingo Blume en Erik Roesink van X-Flow BV en dhr. van Kooij van Tollens Coatings BV.
Een speciaal woordje van dank nog voor Ingo; in de beginperiode van het onderzoek was je als collega een enorm deskundige steun en toeverlaat, die (bijna) overal een antwoord op had of oplossing voor wist. Bedankt!
Dank ook aan mijn kamergenoten, voor hun geduld èn gezelligheid: Wei Zhang, Arnold Broek, Antoine Kemperman, Christel Wijers en Ljubo Germic.

Een plezieriger werkomgeving dan de onderzoeksgroep Membraantechnologie kan ik me bijna niet voorstellen: iedereen heeft op verschillende manieren wel iets bijgedragen aan dit onderzoek, in de vorm van vragen stellen, discussies, clusteroverleg, literatuur, of letterlijk "een handje helpen". Voor dit laatste ben ik ook veel dank verschuldigd aan John Heeks, en zonder de hulp van Greet van der Voort en Bartie Bruggink waren een heleboel haastklusjes heel wat minder

soepel verlopen.
De gezelligheid in de groep is minstens zo belangrijk geweest door alle koffie-pauzes, barbecues, fietstochten, volleybalwedstrijden, excursies, etc. etc. Iedereen uit de membranengroep: hartstikke bedankt!

De Arriba-dames wil ik ook zeker niet vergeten: jarenlang twee tot drie keer in de week lekker intensief basketballen in een gezellig team doet niet alleen wonderen voor je conditie, maar ook voor je motivatie.

Mijn dank gaat ook uit naar familie en vrienden voor hun interesse en begrip, vooral tijdens mijn schrijfperiode. Dit geldt in het bijzonder voor mijn ouders, en Karin en Arjan: de belangstelling en onvoorwaardelijke steun die ik van jullie heb gekregen, heeft altijd erg veel voor mij betekend.
En Carel, voor mijn dank aan jou voldoet maar één woord: je bent grandioos!

Monique

# Contents

# Chapter 1

# Introduction: ultrafiltration membranes for non-aqueous systems

M.A.M. Beerlage, M.H.V. Mulder, C.A. Smolders, H. Strathmann

## 1.1 Membrane separation technology

### 1.1.1 Introduction

During the last three decades, membrane filtration has emerged as a separation technology which is competitive in many ways with conventional separation techniques, such as distillation, adsorption, absorption, extraction etc.
The key component in all membrane separation processes is the membrane. A membrane can be described as a thin barrier between two bulk phases, that permits transport of some components but retains others. A driving force is necessary to allow mass transport across the membrane. A schematic drawing illustrating a membrane process is given in figure 1.

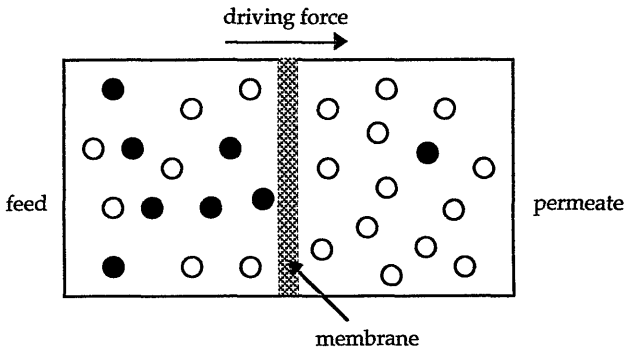


*Figure 1. Schematic drawing illustrating a membrane separation process.*

A review of the historical developments in membrane science and technology in general has been given by Lonsdale [1] and Mason [2]. Reviews on the ultrafiltration process in particular have been presented by Cheryan [3] and

Michaels [4].

### 1.1.2 Membrane processes

Figure 1 provides a general illustration of all types of membrane separation processes, but there are some differences between the various processes.
The actual separation mechanism can be based on differences in the size of the permeating components (sieving effect), or in the membrane affinity towards the feed solution constituents. The solute chemical nature or electrical charges, as well as the vapour pressure of the different components in a mixture often play an important role in membrane separation processes. The two phases separated by the membrane, i.e., the feed and the permeate, can be present in the liquid or in the gaseous state. The driving force that is necessary for the transport is a transmembrane pressure gradient $\Delta P$, a concentration or activity gradient $\Delta c$ or $\Delta a$, respectively, an electrical potential gradient $\Delta E$, or a temperature gradient $\Delta T$. Based on these differences, membrane separation processes can be classified as shown in table 1 [5].

***Table 1.*** *Overview of membrane processes, driving force, separation mechanism, and states of feed and permeate [5].*

| membrane process | driving force | feed state | permeate state | separation mechanism |
|---|---|---|---|---|
| microfiltration (MF) | $\Delta P$ | liq | liq | size |
| ultrafiltration (UF) | $\Delta P$ | liq | liq | size |
| nanofiltration (NF) | $\Delta P$ | liq | liq | size/affinity |
| reverse osmosis (RO) | $\Delta P$ | liq | liq | size/affinity |
| piezodialysis (PD) | $\Delta P$ | liq | liq | affinity |
| gas separation (GS) | $\Delta P$ | gas | gas | affinity/size |
| pervaporation (PV) | $\Delta P$ | liq | gas | affinity |
| dialysis (D) | $\Delta c$ | liq | liq | size |
| osmosis (O) | $\Delta c$ | liq | liq | affinity |
| liquid membranes (LM) | $\Delta c$ | liq | liq | chemical nature |
| electrodialysis (ED) | $\Delta E$ | liq | liq | charge |
| thermo-osmosis (TO) | $\Delta T$, $\Delta p$ | liq | liq | vapour pressure |
| membr. distillation (MD) | $\Delta T$, $\Delta p$ | liq | liq | vapour pressure |

The first four processes mentioned in table 1 utilize a hydrostatic pressure difference as driving force and are closely related to each other. In table 2, the pore sizes are given in relation to their ability to separate solutes. The characteristics of microfiltration, ultrafiltration, nanofiltration, and reverse

osmosis have often been described in literature, and a summary is given in table 2 [1,5-8].

***Table 2.*** *Comparison of pressure-driven liquid (aqueous) phase membrane processes [1,5-8].*

| process | pore size [nm] | materials retained | materials passed | pressure [bar] |
|---|---|---|---|---|
| MF | > 50 | particles (bacteria, yeasts etc) | water, salts macromolecules | < 2 |
| UF | 1 - 100 | macromolecules, colloids, latices solutes $M_w$ > 10,000 | water, salts, sugars | 1 - 10 |
| NF | ≈ 1 | solutes $M_w$ > 500, di- and multivalent ions | water, sugars, monovalent ions | 5 - 20 |
| RO | not relevant | all dissolved and suspended solutes (salts, sugars) | water | 15 - 80 |

In this research project mainly ultrafiltration has been studied. The term "ultrafiltration" has been introduced by Bechhold in 1907 [9], to discriminate this process from separation by filtration, where much larger particles are separated (> 1 μm).

## 1.2 Membrane morphology

Membranes can be classified as symmetric or asymmetric. The difference between these two types is the presence of a pore size gradient in asymmetric membranes: the pores in the toplayer have a different size compared with the pores at the bottom side. It is also possible that the toplayer is non-porous, or even made of a different material as in so-called composite membranes. In porous symmetric membranes, the pores can either form long channels, or the membrane can have a porous sponge-type structure; a symmetric membrane can also be non-porous, i.e., a homogeneous film. Nevertheless, in all three cases a structural gradient is absent in the membrane cross section.
A schematic overview of symmetric and asymmetric membrane cross sections and the processes in which they are used is given in figure 2.

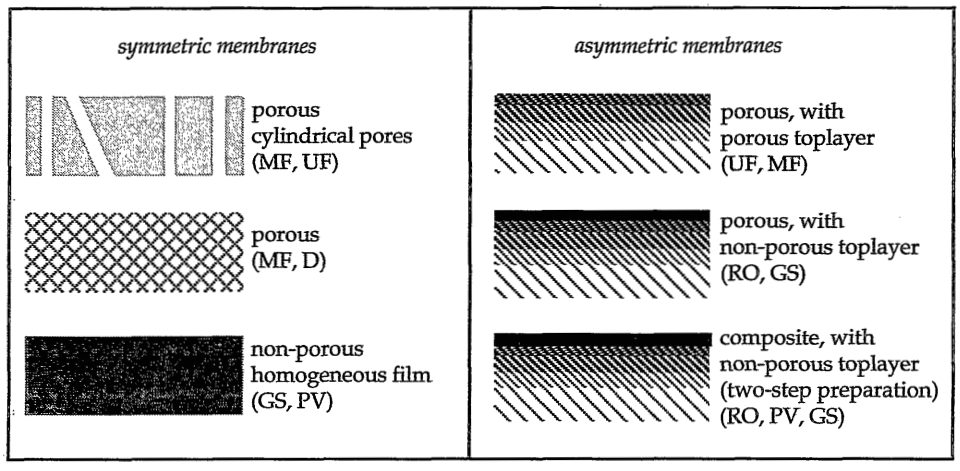


*Figure 2. Schematic drawing illustrating cross sections of symmetric and asymmetric membranes.*

Most ultrafiltration membranes have an asymmetric structure; they are porous with a porous toplayer. Both polymers and inorganic materials are used for the preparation of membranes. Polymeric UF-membranes are very often prepared by the immersion precipitation process. For this purpose, a solution of the polymer is cast as a thin film, and immersed in a coagulation bath that contains a non-solvent for the polymer. Solvent starts to diffuse out of the homogeneous liquid polymer film, whereas non-solvent diffuses into the film. Due to the presence of the non-solvent, phase separation takes place in the polymer film and the polymer precipitates as a solid phase to form a porous asymmetric membrane structure. More detailed information about membrane preparation techniques can be found in literature [5].

## 1.3 Characterization techniques for ultrafiltration membranes

### 1.3.1 General overview

After the preparation of the ultrafiltration membranes they must be characterized. The purpose of this characterization is to obtain information about:

- the membrane morphology: the pore size and pore size distribution, the skin thickness, and the chemical composition of the surface
- the membrane performance: solvent (or gas) permeability, separation properties, retention and fouling behaviour

An elaborate overview of various ultrafiltration membrane characterization techniques has been given by Cuperus and Smolders [10], who classified these methods as morphology or performance related. The most important methods to characterize asymmetric polymeric ultrafiltration membranes are summarized in table 3.

*Table 3. Characterization techniques suitable for asymmetric polymeric UF-membranes [10].*

| morphology related characterization methods | state of membrane during characterization | performance related characterization methods | state of membrane during characterization |
|---|---|---|---|
| microscopy methods | dry/wet | solvent flux meas. | wet |
| liq.-liq. displacement | wet | gas flux measurements | dry |
| permporometry | dry | retention measurements | wet |
| gold sol filtration | wet | fouling measurements | wet |
| surface charact. methods | dry/wet | | |

The state in which the membrane is characterized, i.e., wet or dry state, has been given as well, since a drying procedure may alter the characteristics of the membrane.

### 1.3.2 Aqueous and non-aqueous characterization methods: the effect of water as a test medium

In general, wet-state characterization methods are performed in an aqueous environment, since most membranes are employed in aqueous solutions. For application in non-aqueous mixtures, usually only aqueous characterization techniques are used as well [11-15].
However, the choice of the liquid medium is a very important parameter, especially for performance related characterization methods. Flux measurements for different liquids through the cylindrical pores of the same inert membrane can be compared with each other by normalization to the solvent viscosity and the pressure, according to the Hagen-Poiseuille equation:

$$J_{liq} = \frac{n \pi r_p^4 \Delta P}{8 \eta_{liq} \tau \Delta x} \qquad (1.1)$$

Here, $J_{liq}$ [m/s] is the solvent flux, $\eta_{liq}$ [Ns/m$^2$] is the solvent viscosity, $\Delta P$ [Pa] is the transmembrane pressure, n [/m$^2$] is the number of pores, $r_p$ [m] is the pore

size and $n\pi r_p^2$ [-] is the porosity of the membrane surface, i.e., the total area of the pores per membrane surface, $\tau$ [-] is the tortuosity and $\Delta x$ [m] is the membrane thickness. For a given membrane, n, $r_p$, $\tau$, and $\Delta x$ are constants, which means that at the same pressure the flux is only dependent on the solvent viscosity.
On the other hand, retention and fouling measurements obtained with aqueous polymer solutions may give distinct results when these membranes are employed in non-aqueous applications. Some reasons for this discrepancy are:

- water has an extremely high hydrogen bonding ability
- water can form clusters [16]
- water-soluble polymers cannot be compared to organic-soluble polymers, due to differences in adsorption behaviour

The latter point needs some clarification. Contrary to organic-soluble polymers, water-soluble polymers can have a negative heat of dilution and a lower critical solution temperature (LCST) [17,18]. In addition, water-soluble polymers can have a strong tendency to aggregate and adsorb, either by hydrophobic bonding or by polar interactions. For these reasons, it is likely that in retention and fouling measurements, a water-soluble polymer in aqueous solution behaves very different from a polymer that is soluble in non-aqueous solution, even if their molecular weights are similar.
In conclusion, membranes for non-aqueous ultrafiltration applications require non-aqueous wet-state characterization methods.

## 1.4 Ultrafiltration membrane materials and their chemical stability

### 1.4.1 Membrane materials

Membrane technology became commercially attractive with the development of asymmetric cellulose acetate RO-membranes by Loeb and Sourirajan in 1962 [19]. Cellulose acetate (CA), a derivative of the natural polymer cellulose, has been the main membrane material in the first decade for ultrafiltration. CA-membranes are relatively easy to prepare, with a high flux and a high salt retention (for RO). Nevertheless, the chemical stability of this class of materials is low; it has a relatively narrow range of pH-tolerance, and it is highly biodegradable [3]. Furthermore, CA-membranes cannot be used at temperatures above 30°C, and the membrane performance changes in time due to polymer creep.
Therefore, other polymers were introduced as membrane material. Polymers used very successfully were polysulfone (PSF) and polyethersulfone (PES). Ultrafiltration membranes prepared from these materials show a wide range of pH- and temperature-resistance, and are fairly resistant to chlorine, which means that sterilization and cleaning in dairy and pharmaceutical applications can be carried out by hypochlorite solutions, which is a standard procedure in these

industries. On the other hand, irreversible membrane fouling by adsorption of feed components at the membrane surface, e.g, proteins, may cause a very severe flux decline. In addition, PSF- and PES-membranes are not very resistant to hydrocarbon media.
Therefore, a number of other polymers have been investigated as ultrafiltration membrane material, such as hydrophilic polymers or polymer blends to prevent irreversible protein fouling, and more or less chemically stable polymers (regenerated cellulose, polyacrylonitrile, polyvinylchloride, polyimide, polyvinylidenefluoride, etc.) for other applications [3,5].
Inorganic membranes are gaining importance as ultrafiltration membranes, because of their extremely high chemical and thermal stability. They can be made from glass, metals, or ceramic materials. The excellent stability, combined with the expected longer lifetime, makes these inorganic membranes more favourable for harsh applications than polymeric membranes. On the other hand, inorganic membranes are generally more expensive than polymeric membranes, and are often quite brittle. Ceramic membranes are generally based on aluminum oxide ($\gamma$-$Al_2O_3$) or zirconium oxide ($ZrO_2$); glass membranes are prepared from silicon oxide ($SiO_2$). More information on inorganic membranes can be found in literature [20,21]

### 1.4.2 Chemical stability of polymers

By far most of the industrial applications of pressure-driven membrane processes (i.e., MF, UF, NF, RO) are related to aqueous solutions. Relatively new processes like pervaporation are finding their way to the separation of organic feed mixtures. Examples are solvents with similar boiling points, e.g., isomers, or azeotropic mixtures which are difficult to be separated by conventional separation processes, such as distillation [22-25]. Another example for the application of pervaporation is the dehydration of organic solvents, such as ethanol [26] or acetic acid [27].
In the case of reverse osmosis, the traditional cellulose acetate membranes have been tested for their ability to separate organic liquid mixtures [28,29]. Also other materials like cellulose, polyacrylonitrile, polyolefins, polybenzimidazole, polypiperazinamides and polyvinylalcohol have been investigated for these applications [30-34].
For ultrafiltration, some attempts have been made to prepare membranes that can be used in applications involving organic solvents. A very important problem is the maintenance of the porous structure. In general, a polymer is considered "chemically resistant" to a solvent when it does not dissolve; nevertheless, the solvent can also induce polymer swelling, i.e., sorption of the solvent by the polymer, or even form cracks and crazes, a phenomenon that is related to swelling [35-37].

A high degree of swelling may strongly alter the membrane pore size distribution, so that solvent permeability (corrected for solvent viscosity) and separation characteristics are dependent on the solvent used [38]. Therefore, a membrane material is preferred that does not dissolve, nor swell upon contact with a broad range of solvents. The phenomenon of crack and craze formation is probably more important for non-porous membranes, since for porous membranes propagation of defects caused by this process will hardly be possible due to the discontinuous polymer structure.

The objective of this study is the preparation of chemically resistant polymeric ultrafiltration membranes by the immersion precipitation process. This means that the membrane polymer (or prepolymer) has to be soluble in at least one suitable solvent or class of solvents. On the other hand, the resulting membrane should not dissolve nor swell in a range of organic solvents.
There are two ways to overcome this problem:

- The polymer is soluble in one solvent (or class of solvents) and insoluble in all others.
- After membrane preparation, the membrane is subjected to a special treatment, such as cross linking, that reduces the solubility and increases the chemical stability.

The first approach implies that the membrane morphology will not be altered by the solvent used in the application. Here, the membranes cannot be used for all organic solvents. The second approach includes the possibility of morphology changes by the treatment, while high cross linking densities are necessary to exclude swelling effects.
In the present study the first approach has been emphasized; therefore, a polymer with a high chemical stability is needed.
The chemical stability of polymers is often related to the thermal stability, i.e., factors that favour thermal stability often favour chemical stability as well. The higher the glass transition temperature, the more rigid the polymer is and in general the higher is its stability in solvents. Much research has been directed at the development of thermally stable polymers [39-43]. Unfortunately, many of these polymers are completely insoluble. In general, polymer bulk materials are more rigid when:

- the flexibility of the main chain of the polymer decreases
- the polymer molecular weight is high
- crystallinity is promoted

The flexibility of the main chain can be reduced by avoiding certain groups in the backbone, such as aliphatic chains, carboxyl and ether linkages; furthermore, para substituted aromatic groups contribute much more to rigidity than meta or ortho substituted groups. The presence of bulky side groups causes loss of flexibility by

decreasing the rotational freedom of the backbone. Crystallinity is promoted by structural symmetry, intermolecular interaction such as hydrogen bond formation, and the absence of randomly placed side groups.
In addition, the chemical resistance is promoted by [44]:

- aromatic or heterocyclic backbone structures, i.e., the presence of resonance structures
- absence of "reactive" groups such as unsaturated bonds, -OH groups, free -NH groups, aliphatic groups
- presence of high bond energies that cause strong chemical bonds, e.g., C-F, C-Si, C-P
- polybonding: atoms are linked to the polymer chain with two or more bonds, which implies that chains cannot be broken by the rupture of one single bond, e.g., in ladder polymers

Some examples of classes of highly resistant polymers were discussed by Critchley et al. [43]; a short summary is given in table 4.

***Table 4.*** *Overview of classes of chemically and thermally resistant polymers [43].*

| polymer class | stability promoted by | examples |
|---|---|---|
| thermosetting | high cross linking density | phenol-formaldehyde resin |
| fluorinated | strong chemical bonds | polytetrafluorethylene |
| inorganic | strong chemical bonds | polyphosphazene, polysiloxane |
| aromatic | resonance stability | polyphenylene, aromatic polyamide |
| heterocyclic | resonance stability | polyimide, polybenzimidazole |
| ladder polymers | polybonding, resonance | polypyrrone |

For a long time, polysulfone and polyethersulfone have been regarded as the chemically resistant alternative for cellulose acetate. Several other commercially available polymers have been considered as chemically resistant ultrafiltration membrane material; some examples are polyacrylonitrile [38], polybenzimidazole [45], polyaramide [11,46,47], polyvinylidenefluoride [14,48], polyetheretherketone [49,50], polyimide [12,13,34,51,52]. Furthermore, a large number of "new" polymers have been synthesized that may be very interesting as ultrafiltration membrane material, like polyoxadiazole and polytriazole [44,53], polyamideimide [54], and ladder polymers [55,56].
Nevertheless, the commercial availability of solvent resistant ultrafiltration membranes is limited. Examples are the Nitto 4200 membrane (polyimide) [34,52,57], and Pennwalt's Kynar (polyvinylidenefluoride) [14]; some characteristics of these membranes are summarized in table 5.

*Table 5.* *Characteristics of solvent-resistant ultrafiltration membranes [57,14].*

| | | | |
|---|---|---|---|
| Nitto 4208 | pure toluene flux: 45 l/m$^2$hr bar (25°C) | MWCO: | 8000 |
| Nitto 4220 | pure toluene flux: 100 l/m$^2$hr bar (25°C) | MWCO: | 20000 |
| Kynar | flux for an aqueous solution of 0.4% PVA 125,000 (52°C): | | flux: 12 l/m$^2$hr bar<br>retention: 97% |

## 1.5 Industrial applications of ultrafiltration processes

The number of industrially relevant applications of ultrafiltration is very large. An overview of the most important applications is given by Cheryan [3] and Kulkarni et al. [58]. Some of these applications are summarized in table 6.

*Table 6.* *Summary of important industrial applications of ultrafiltration.*

Environmental applications, such as waste water treatment and recovery of valuable products can be found in:

- electrocoat paint recovery
- oily waste water treatment
- textile industry (synthetic sizing agents and dyes)
- pulp and paper industry (printing ink recovery)
- leather and tanning industry effluents treatment
- abattoir effluents treatment

Applications in the food industry can be found in:

- dairy industry (fabrication of cheese and recovery of proteins from whey)
- sugar refining
- concentration of fruit juices, clarification of beverages
- vegetable protein processing
- egg white concentration

Biotechnological applications are:

- enzymes and micro-organisms separation and harvesting
- bioreactor processes and tissue culture systems

Preparation of ultra-pure water (biotechnology, pharmaceutical and electronics industry)

Hemofiltration (separation of microsolutes from blood)

Polymer industry: concentration of latex emulsions

The most recent economical evaluation of the membrane industry has been given by Strathmann in 1990 [59]. At that moment, the most important ultrafiltration application was hemofiltration: the filtration of blood, to remove toxic metabolisms from the blood stream, such as urea, but retaining proteins

and blood cells. The growth of the total membrane industry was estimated at 12-15% per year. The sales of the membrane industry in total (all types of membranes and modules) and of ultrafiltration membranes and modules in particular, are given in table 7.

*Table 7.* *Sales (in million US $ per year) of the membrane industry [59].*

| branch | total sales million US $ | ultrafiltration sales million US $ |
|---|---|---|
| medical devices | 1050 | 130 |
| water treatment | 490 | 60 |
| chemical industry | 200 | 15 |
| food industry | 169 | 44 |

## 1.6 Applications of ultrafiltration in non-aqueous systems

The industrial, environmental, and medical ultrafiltration applications that were summarized in the previous paragraph, are almost without exception applications for aqueous mixtures. However, there is an enormous potential field for the application of ultrafiltration in non-aqueous systems, provided that there are commercially available membranes and modules that are suitable for applications involving organic solvents. The possible applications are solvent recovery and reuse in the (petro)chemical, painting, and polymer manufacturing industry, as well as upgrading of several product streams.
There are only a few examples for applications of ultrafiltration in non-aqueous solutions described in literature. Most of these descriptions can be found in the patent literature, and it often concerns separations of systems, which are very difficult or even impossible to separate by conventional separation techniques. In this section, some examples will be discussed in more detail.

### 1.6.1. Paint solvent recovery [34,52]

During paint manufacturing and in automated painting baths, it is necessary to frequently change the type and colour of the paint. For this purpose, the just applied paint has to be removed from the mixing vessels and filling lines by means of rinsing with paint solvents. The solvents, contaminated with resins and pigments, are usually disposed of by incineration [60].
When applying an ultrafiltration process, paint solvents can be recovered from the waste stream, and can be reused for rinsing or as fresh paint solvents. The membranes used in this case [34,52] are solvent resistant polyimide membranes

from Nitto; the paint solvents were mixtures of approximately 60% aromatic hydrocarbons (toluene, xylene), 30% methyl ethyl ketone, and 10% of other ingredients (alcohols, esters).

### 1.6.2. Recovery of dewaxing aids during oil dewaxing processes [61,62]

Crude waxy hydrocarbon oils are usually dewaxed by using mixtures of aliphatic ketones (acetone, methyl ethyl ketone), aromatic hydrocarbons (toluene, xylene) and halogenated hydrocarbons (chloroform, dichloroethane). In the patent literature there are a number of examples for the application of reverse osmosis to recover solvent from the dewaxed oil [63-65].
The dewaxing aids, i.e., polyalkylacrylates, polyethyleneoxides, polyvinyl-pyrrolidone, etc., remain in the solvent-free wax; recovery of these components by conventional separation techniques is very difficult and costly. However, the dewaxing aids can be recovered by ultrafiltration of the wax at 70-100°C through a polyethersulfone or a polyimide membrane, while the purified wax can be used for other purposes.

Ultrafiltration can also be employed in the dewaxing process itself. During the Exxon-DILCHILL process, the waxy oil is heated to just above its cloud point. Cold dewaxing solvent is added in small amounts to this mixture, so that small crystallites are formed. These crystallites can be removed by ultrafiltration [66].

### 1.6.3. Heavy oil upgrading or deasphalting [67-69]

A vacuum distillation step is one of the typical processes during crude oil refinery. Products from this step are the so-called middle boiling distillates and heavy vacuum residual oil (HVR). The HVR is unsuitable for conventional cracking methods, since it contains several sulfur and metal containing compounds as well as polar components, that foul and deactivate the cracker catalysts. The general deasphalting step is performed in a flasher-stripper combination [70]; however, upgrading can be done more energy-efficiently by ultrafiltration of a mixture of HVR with toluene, chloroform, hexane or heptane through various ultrafiltration membranes.

### 1.6.4. Treatment of used lubricating oil [71]

Used lubricating oil contains several degraded components such as polymers, dispersion agents, and antioxydants, as well as contaminants like asphaltenes, lead, and combustion by-products. After removal of these degraded components and contaminants, the regenerated oil can be reused as fuel. Ultrafiltration of a mixture of the used oil with solvent (hexane) through polyacrylonitrile

membranes showed very promising results, and most of the contaminants were removed from the oil.

### 1.6.5 Edible oil processing [72-74]

In the edible oil industry, oil is extracted from its raw material (e.g., oilseeds, fruit pulps, animal remains or fish), with solvents such as hexane, ethanol, or isopropanol. After extraction, the mixture of 70-75% solvent with extracted oil (the miscella) is usually separated by distillation; however, an ultrafiltration or reverse osmosis process is also very effective and much more energy efficient [72].
Köseoglu et al. tested various "tight" commercial ultrafiltration and reverse osmosis membranes for this separation [73]. They found that only one of these membranes was resistant enough to the miscella and was able to retain the oil: the Osmonics Sepa polyamide membrane (a reverse osmosis membrane with a MWCO of 300-400). In a Japanese patent this separation has been described using Nitto polyimide ultrafiltration membranes [74].

### 1.6.6 Applications of ultrafiltration in the polymer processing industry (Japanese patents [75-78])

Some applications of non-aqueous ultrafiltration in the polymer industry have been described in Japanese patents.
After manufacturing of diallylphtalate polymers in xylene [75], or polyolefins in hexane [76], or thermosetting resins in a toluene/xylene/DMF-mixture [77], the unreacted monomers and low molecular weight products can be removed by ultrafiltration; for all three processes, Nitto polyimide membrane modules have been used.
Another application of ultrafiltration is the treatment of contaminated rinsing streams after washing of plastic molding or metal parts, using solvents such as trichloroethylene. The contaminated solvent can be cleaned by a hybrid process of settling and ultrafiltration [78]. For this purpose polysulfone membranes have been used.

## 1.7 The structure of this thesis

It is obvious that ultrafiltration of non-aqueous mixtures has hardly been explored, in spite of the enormous field of potential applications. Nowadays, there are only a few commercial applications, and the number of commercially available ultrafiltration membranes that are suitable for use in organic environment is very small, too. Furthermore, it is difficult to correlate the ultrafiltration characteristics of aqueous solutions to non-aqueous systems.

The aim of the research described in this thesis is the development of polymeric ultrafiltration membranes, prepared by immersion precipitation, which can be employed in a range of potential applications in separating non-aqueous mixtures, i.e., which have a good chemical stability in organic solvents. A commercially available polyimide has been chosen as membrane material; the structure of this polyimide is depicted in figure 3. This polymer is readily soluble in aprotic polar solvents, such as dimethylformamide (DMF), dimethylacetamide (DMAc), n-methylpyrrolidone (NMP), and is insoluble and/or poorly swelling in most of the other organic solvents.

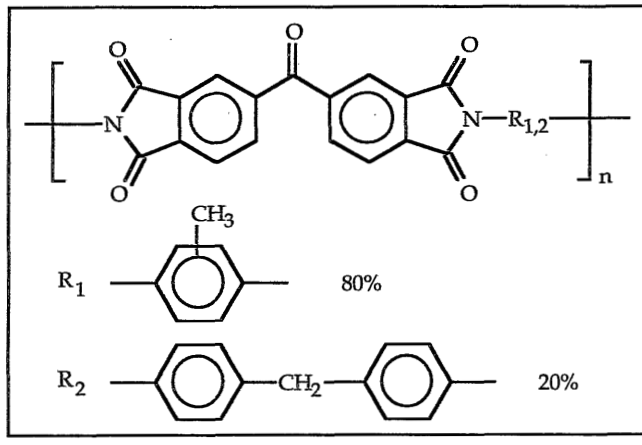


***Figure 3.*** *Structure formula of polyimide used in this thesis.*

In *chapter 2*, the choice of this particular polyimide will be rationalized, and the high chemical stability and properties of polyimides in general will be discussed. The preparation of ultrafiltration membranes by means of immersion precipitation will be described for several ternary systems, consisting of non-solvent/solvent/polyimide; this preparation step will be related to membrane morphology and properties.

The influence of low molecular weight additives in the casting solution on the membrane formation process and the membrane morphology will be discussed in *chapter 3*. A mechanism will be proposed for the membrane formation of quaternary systems, consisting of water or ethanol/dimethylformamide/polyimide/dicarboxylic acids. It will be shown that important parameters in the membrane formation procedure are the steric conformations of the dicarboxylic acid additive and the polyimide repeating unit, as well as the solubility of the additive in the coagulant, which is water or ethanol.

The various membrane characterization techniques that are used in this study

will be described in more detail in *chapter 4*. Particular interest will be directed to the comparison of membrane properties determined by permporometry, and those obtained by pure solvent and gas permeability measurements.
A discussion on the effect of drying procedures on the membrane properties and morphology will be given in the *appendix to chapter 4*.

In *chapter 5*, it will be outlined that it is not possible to perform retention measurements as characterization technique using dilute non-aqueous model systems, because flow-induced deformation plays a determining role during these measurements. The discrepancy of aqueous retention results described in literature will be discussed as well.
It is suggested that flow-induced deformation measurements can be used as a qualitative technique to compare various ultrafiltration membranes. In addition, a mechanism for the flow-induced deformation will be given, which may explain the peculiar flux and retention behaviour during these measurements.

The hindered diffusion of flexible polymers in dilute non-aqueous solutions through polyimide ultrafiltration membranes has been described in *chapter 6*. Mono- and polydisperse feed solutions will be compared, as well as diffusive permeability results for various membranes. The suitability of hindered diffusion experiments as a non-aqueous membrane characterization technique will be discussed. In the *appendix to chapter 6*, a derivation of the diffusive permeability as a function of the membrane pore size distribution will be presented.

In *chapter 7*, the suitability of the developed polyimide ultrafiltration membranes for an actual non-aqueous application will be discussed: the recovery of paint solvent from an organic paint waste stream. The influence of concentration polarization and (in particular) membrane fouling will be investigated.

## 1.8 References

[1] H.K. Lonsdale; The growth of membrane technology; J. Membrane Sci., 10(1982)81
[2] E.A. Mason; From pig bladders and cracked jars to polysulfones: an historical perspective on membrane transport; J. Membrane Sci., 60(1991)125
[3] M. Cheryan; Ultrafiltration handbook; Technomic, Lancaster, 1986
[4] A.S. Michaels; Fifteen years of ultrafiltration: problems and future promises of an adolescent technology; A.R. Cooper (Ed.); Ultrafiltration membranes and applications; Polymer science and technology volume 13; Plenum Press, New York, 1980; p.1
[5] M.H.V. Mulder; Basic principles of membrane technology; Kluwer, Dordrecht, 1991
[6] J.E. Cadotte, F. Forester, M. Kim, R.J. Petersen, T. Stocker; Nanofiltration membranes

broaden the use of membrane separation technology; Desalination, 70(1988)77

[7] P. Eriksson; Nanofiltration extends the range of membrane filtration; Environm. Progr., 7(1988)58

[8] R.J. Petersen; Composite reverse osmosis and nanofiltration membranes; J. Membrane Sci., 83(1993)81

[9] H. Bechold; Koloidstudien mit der Filtrationsmethode; Z. Phys. Chem. Sto. Verw., 60(1907)257

[10] F.P. Cuperus, C.A. Smolders; Characterization of ultrafiltration membranes. Membrane characteristics and characterization techniques; Adv. Colloid Interface Sci., 34(1991)135

[11] P. Zschocke, H. Strathmann; Solvent resistant membranes from poly-(p-phenylene-terephtalamide); Desalination, 34(1980)69

[12] B. Dong, K. Zhu; Preparation and properties of polyimide ultrafiltration membranes; J. Membrane Sci., 60(1991)63

[13] H. Strathmann; Asymmetric polyimide membranes for filtration of non-aqueous solutions; Desalination, 26(1978)85

[14] W.D. Benzinger, B.S. Parekh, J.L. Eichenberger; High temperature ultrafiltration with Kynar PVDF membranes; Sep. Sci. Techn., 15(1980)1193

[15] M.N. Sarbolouki; Properties of asymmetric polyimide ultrafiltration membranes. 1. Pore size and morphology characterization; J. Appl. Polym. Sci., 29(1984)743

[16] S. Vinogradov, R.H. Linnell; Hydrogen bonding; Van Nostrand Reinhold, New York, 1971; p. 207

[17] S.W. Shalaby, C.L. McCormick, G.B. Butler (Eds.); Water-soluble polymers; ACS Symp. Ser. 467, Washington, 1991

[18] C.A. Finch (Ed.); Chemistry and technology of water-soluble polymers; Plenum Press, New York, 1983

[19] S. Loeb, S. Sourirajan; Sea water demineralization by means of an osmotic membrane; Advan. Chem. Ser., 38(1962)117

[20] H.P. Hsieh; Inorganic membranes; AIChE Symp. Ser. 84, 261(1988)1

[21] H.P. Hsieh, R.R. Bahve, H.L. Fleming; Microporous alumina membranes; J. Membrane Sci., 39(1988)221

[22] R.C. Binning, R.J. Lee, J.F. Jennings, E.C. Martin; Separation of liquid mixtures by permeation; Ind. Eng. Chem., 53(1)(1961)45

[23] P.Aptel,N. Challard, J. Cuny, J. Néel; Application of the pervaporation process to separate azeotropic mixtures; J. Membrane Sci., 1(1976)271

[24] I. Cabasso; Organic liquid mixtures separation by permselective polymer membranes. 1. Selection and characteristics of dense isotropic membranes employed in the pervaporation process; Ind. Eng. Chem. Prod. Res. Dev., 22(1983)313

[25] H.-C. Park; Separation of alcohols from organic liquid mixtures by pervaporation; Ph.D. thesis, University of Twente, 1993

[26] J.W.F. Spitzen, E. Elsinghorst, M.H.V. Mulder, C.A. Smolders; Solution-diffusion aspects in the separation of ethanol/water mixtures with PVA; Proc. 2nd Intern. Conf. Pervaporation processes in the chemical industry; San Antonio, U.S.A., march 1987, p. 209

[27] G.-H. Koops, J.A.M. Nolten, M.H.V. Mulder, C.A. Smolders; Poly(vinylchloride) polyacrylonitrile composite membranes for the dehydration of acetic acid; J. Membrane Sci., 81(1993)57

[28] H. Nomura, S. Yoshida, M. Seno, H. Takahashi, T. Yamabe; Permselectivities of some aromatic compounds in organic medium through cellulose acetate membranes by reverse osmosis; J. Appl. Polym. Sci., 22(1978)2609

[29] J. Kopecek, S. Sourirajan; Performance of porous cellulose acetate membranes for the reverse osmosis separation of mixtures of organic liquids; Ind. Eng. Chem. Process Dev., 9-1(1970)5

[30] W.J. Adam, B. Luke, P. Meares; The separation of mixtures of organic liquids by hyperfiltration; J. Membrane Sci., 13(1983)127

[31] H. Nomura, M. Seno, H. Takahashi, T. Yamabe; Permselectivities of various polymeric membranes toward some aromatic compounds in organic media in the reverse osmosis process; J. Membrane Sci., 5(1979)189

[32] B. Farnand; Reverse osmosis fractionation of organic solutes in non-aqueous solutions; National Research Council of Canada; Advances in reverse osmosis and ultrafiltration; NRCC rep. 29895, 1989; p. 177

[33] L.C. Sawyer, R.S. Jones; Observations on the structure of first generation polybenzimidazole reverse osmosis membranes; J. Membrane Sci., 20(1984)147

[34] A. Iwama, Y. Kazuse; New polyimide ultrafiltration membranes for organic use; J. Membrane Sci., 11(1982)297

[35] G.A. Bernier, R.P. Kambour; The role of organic agents in the stress crazing and cracking of poly(2,6-dimethyl-1,4-phenylene oxide); Macromolecules, 1(1968)393

[36] R.P. Kambour, E.E. Romagosa, C.L. Gruner; Swelling, crazing and cracking of an aromatic copolyether-sulfone in organic media; Macromolecules, 5(1972)335

[37] C.C.M. Ma, C.L. Lee, N.H. Tai; Chemical resistance of carbon fiber-reinforced poly(ether-etherketone) and poly(phenylene sulfide) composites; Polym. Comp., 13(1992)435

[38] Q.T. Nguyen, P. Aptel, J. Néel; Characterization of ultrafiltration membranes. Part 1. Water and organic solvent permeabilities; J. Membrane Sci., 5(1979)235

[39] P.E. Cassidy; Thermally stable polymers; Marcel Dekker, New York, 1980

[40] P.E. Cassidy; History of heat-resistant polymers; J. Macromol. Sci., Chem. A, 15(1981)1435

[41] H.F. Mark; Polymers for extreme service conditions; Macromolecules, 10(1977)881

[42] C. Arnold; Stability of high-temperature polymers; J. Polym. Sci., Macromol. Rev., 14(1979)265

[43] J.P. Critchley, G.J. Knight, W.W. Wright; Heat resistant polymers; Plenum Press, New York, 1983

[44] B. Gebben; Thermally stable and chemically resistant polymer membranes. Aromatic polyoxadiazoles and polytriazoles; Ph.D. thesis, University of Twente, 1988

[45] M.J. Sansone; Process for the production of polybenzimidazole ultrafiltration membranes; US 4,693,824; 1987

[46] M. Haubs, F. Herold, C.-P. Krieg, D. Skaletz; Makroporöse, asymmetrische, hydrophile Membran aus Polyaramid; EP 325,962; 1989

[47] H. Strathmann, P. Zschocke; Integralasymmetrische Ultrafiltrationsmembrane; DE 2,940,447; 1981

[48] F. Vigo, C. Uliana, B. Cavazza, F. Salvemini; Mechanical, chemical and bacterial resistance of modified polyvinylidenefluoride membranes suitable for ultrafiltration of oily emulsions; J. Membrane Sci., 21(1984)295

[49] J.Y. Koo, J.R. Racchini, C.-C. Chau, R.A. Wessling, M.T. Bishop; Microporous polyetheretherketone membranes and the preparation thereof; EP 368,003; 1989

[50] H.M. Colquhoun, K. Roberts, A.F. Simpson, T.M.C. Taylor, G.C. East, J.E. McIntyre, V.

Rogers; Polyetherketones - New high-performance polymers for ultrafiltration membranes; Effective Ind. Membrane Proc., Conf. Proceedings (1993)

[51] W. Schumann, H. Strathmann; Polyimide membrane and process for making same; US 3,925,211; 1975

[52] Y. Isooka, Y. Imamura, Y. Sakamoto; Recovery and reuse of organic solvent solutions; Metal Finish., 82(1984)113

[53] B. Gebben, M.H.V. Mulder, C.A. Smolders; Gas separation properties of a thermally stable and chemically resistant polytriazole membrane; J. Membrane Sci., 46(1989)29

[54] M Ghosh; Heat resistant polyamideimides. 3. Synthesis, characterization and evaluation of thermal and other properties; Angew. Makromol. Chem., 172(1989)165

[55] L. Yu, L.R. Dalton; Synthesis and characterization of new polymers exhibiting large optical non linearities. 1. Ladder polymers from 3,6-disubstituted 2,5-dichloroquinone and tetra-aminobenzene; Macromolecules, 23(1990)3439

[56] I. Sideridou-Karayannidou, G. Karayannidis; Synthesis of pyrrones based on the reduction and cyclization of their o-nitrosubstituted polyimides precursors; Angew. Makromol. Chem., 180(1990)121

[57] Nitto Electric Industrial Co.; Commercial brochure 4200-series ultrafiltration membranes

[58] S.S. Kulkarni, E.W. Funk, N.N. Li; Ultrafiltration - Applications and economics; chapter 30; W.S.W. Ho, K.K. Sirkar (Eds.); Membrane handbook; Van Nostrand Reinhold, New York, 1992; p. 446

[59] H. Strathmann; Economic assessment of membrane processes; N.N. Li, J.M. Calo (Eds.); Separation and purification technology; Marcel Dekker, New York, 1992; p. 1

[60] I. Smallwood; Solvent recovery handbook; Edward Arnold, London, 1993; p. 133

[61] J.A. Thompson; Method and apparatus for separating filter aid from separated wax by selective permeation through a membrane; EP 146,298; 1985

[62] B.P. Anderson; Ultrafiltration polyamide membrane and its use for recovery of dewaxing aid; US 4,908,134; 1990

[63] D.L. Wernick, N.J. Elizabeth; Preparation of cellulose acetate membrane and its use for polar solvent-oil separation; US 4,678,555; 1987

[64] M.M. Hafez, H.W. Pauls; Method for preparing thin regenerated cellulose membranes of high flux and selectivity for organic liquids separations; US 4,496,456; 1985

[65] J.G.A. Bitter, J.P. Haan; Process for separating a fluid mixture containing hydrocarbons and an organic solvent; EP 254,359; 1988

[66] L.Y. Lafrenière; Method for reducing the cloud point of materials using an ultrafiltration separation process; US 4,874,523; 1989

[67] E.J. Osterhuber; Upgrading heavy oils by solvent dissolution and ultrafiltration; US 4,797,200; 1989

[68] E.W. Funk, S.S. Kulkarni, Y.A. Chang; Membrane separation of hydrocarbons; US 4,617,126; 1986

[69] S.S. Kulkarni, E.W. Funk, N.N. Li; Hydrocarbon separations with polymeric membranes; AIChE Symp. Ser. no. 250, 82(1986)78

[70] W. Gerhartz (exec. ed.); Ullmann's encyclopedia of industrial chemistry; Volume B3, Unit operations 2; VCH, Weinheim, 1988, 5th edition; p. 6-36

[71] D. Desfives, R. Avrillon, C. Miniscloux, R. Roullet, X. Marze; Regénération des huiles lubrifiantes usagées par ultrafiltration; Inform. Chimie., 175(1978)127

[72] S.S. Köseoglu, D.E. Engelgau; Membrane applications and research in the edible oil industry, an assessment; J. Am. Oil Chem. Soc., 67(1990)239

[73] S.S. Köseoglu, J.T. Lawhon, E.W. Lusas; Membrane processing of crude vegetable oils: pilot plant scale removal of solvent from oil miscellas; J. Am. Oil Chem. Soc., 67(1990)315

[74] Rinoru Oil Mills Co., Nitto Electric Industrial Co.; Purification of crude glyceride compositions; JP 59,20,394; 1982; from Chem. Abstr. 100:212073j

[75] W. Tanaka, M. Osuga, T. Kuri; Purification of diallyl phtalate polymers; JP 60,243,105; 1985; from Chem. Abstr. 105:7344k

[76] Chisso Co.; Separating organic solvents from waste solvents containing low-molecular olefins; JP 58,42,605; 1983; from Chem. Abstr. 99:71603d

[77] Nitto Electric Industrial Co.; Treatment of resin-containing organic solutions; JP 81,161,803; 1981; from Chem. Abstr. 96:164887c

[78] J. Aikawa; Regeneration of spent washing agents by membranes; JP 61,125,407; 1986; from Chem. Abstr. 105:136057t

# Chapter 2

## Preparation of polyimide ultrafiltration membranes Part 1. Ternary systems

M.A.M. Beerlage, R.M. Meertens, M.H.V. Mulder, C.A. Smolders, H. Strathmann

**Summary**

The first part of this chapter describes the chemical resistance of some commercially available polymers. The choice of a soluble polyimide as a basis material for highly chemical resistant ultrafiltration membranes is motivated. It is shown by permeability measurements using different organic media, that the developed membranes can be employed in a wide range of non-aqueous ultrafiltration applications.

The second part describes the membrane formation by the immersion precipitation from a ternary membrane forming system, non-solvent/solvent/polymer.

The influence of some membrane formation parameters on the membrane morphology and permeability has been investigated. DMF was found to be the most suitable solvent for the preparation of polyimide membranes, and combined with ethanol as a non-solvent less brittle membranes were obtained compared to other solvent/non-solvent combinations.

It is shown that the polymer concentration in the casting solution is the main parameter to vary morphology and permeability.

## 2.1 Introduction

Highly chemical resistant polymeric membranes can be employed in several organic media. In this chapter, the chemical stability of some commercially available polymers will be compared, and the most suitable materials for the preparation of ultrafiltration membranes will be selected.
Furthermore, membrane formation by immersion precipitation will be discussed briefly. In this chapter, the ternary systems non-solvent/solvent/polymer will be described, while in chapter 3 of this thesis the addition of low molecular weight casting additives will be discussed.

## 2.2 Material selection

### 2.2.1 Chemical resistance of polymers

The chemical resistance of a polymer is a rather arbitrary property, because it depends strongly on the application. A polymer that is exposed to a chemical environment, can change its physico-chemical properties. McCarthy [1] used a quite general definition: "The chemical resistance of a polymeric material is its ability to withstand chemical attack with minimal change in appearance, dimensions, mechanical properties, and weight over a period of time."
When an ultrafiltration membrane absorbs a certain organic solvent to more than 10% of its original weight, then the membrane matrix is swollen in such a way that the pores become narrower. This implies that the membrane properties will be altered by the swelling and therefore, it is required that the solvent/polymer interaction is as low as possible. In general, rubbery polymers are much more sensitive to swelling than glassy polymers. This makes glassy polymers more favourable for the preparation of ultrafiltration membranes for non-aqueous applications.

However, the phase-inversion process demands that the polymer is well soluble in at least one solvent, and this means that the membrane cannot be used in this solvent or in this class of solvents. The solubility of a polymer is very difficult to predict. Hildebrand developed a solubility parameter theory [2]. Here the solubility parameter of a component i, $\delta_i$, is defined as:

$$\delta_i = \left( \frac{\Delta U_{v,i}}{V_i^o} \right)^{1/2} = (CED)^{1/2} \qquad (2.1)$$

where $\Delta U_{v,i} / V_i^o$ is the energy of vaporization per unit volume of i [J/m$^3$], or the cohesive energy density (CED). This theory only accounts for the contribution of

the mixing enthalpy to the free energy of mixing, and it predicts that when the difference of the δ-values of polymer and solvent is small, the polymer is soluble.
Hansen [3] developed a three-dimensional solubility parameter, $\delta_{t,i}$ (t=total), containing three contributions: dispersion forces (d), polar forces (p) and hydrogen bonding effects (h):

$$\delta_{t,i}^2 = \delta_{d,i}^2 + \delta_{p,i}^2 + \delta_{h,i}^2 \qquad (2.2)$$

Extensive tabulations of solubility parameters of many liquids are available [4]. For polymers it is much more difficult to determine the cohesive force, i.e., to obtain solubility parameters. Usually this is done by determining the dissolution behaviour of a polymer in a series of liquids, after which the "solubility region" is defined [5-7]. For many polymers the estimated solubility parameters can be found in literature [8]; for others these parameters might be estimated by solubility experiments, by a calculation method making use of the group contribution approach [4,9,10], or by correlations with physical quantities [11].

Several attempts were made to standardize chemical stability tests, especially for swelling experiments [12]. The ASTM-D543 method is the most frequently used standard test method, which is suitable for all polymeric materials [13]. For this test, a polymer sample must be disk-shaped or bar-shaped with a thickness of 3.175 mm (i.e., 1/8th inch). These weighed samples are then put in several organic solvents for 7 days at 23°C, after which the swelling value is determined by measurement of the weight gain.
A simple calculation illustrates that this test may give reliable results for rubbery polymers, but for glassy polymers it takes much more time before the equilibrium swelling value is reached. The diffusion coefficients of ethanol and hexane in glassy polyvinylchloride are about $6*10^{-13}$ $cm^2/s$ and $2*10^{-15}$ $cm^2/s$, respectively [14]. According to the penetration theory assuming Fickian diffusion, the diffusion front reaches the center of a 3.175 mm thick sample after 106 and > 30,000 years, respectively: for these thick samples no equilibrium swelling value can be obtained after 7 days. When the interaction between polymer and solvent is very good (e.g. when the polymer is strongly swollen by, or soluble in the solvent), the diffusion may be accelerated by the solvent uptake.

Several tables are available in literature, that compare the chemical stability of polymers exposed to various classes of solvents [15-17]. Tables of solvents and non-solvents can be very useful for material selection as well [10,18,19].
In general, most factors that promote a high $T_g$, also promote a high chemical resistance (see chapter 1). Therefore, the thermal stability of polymers can give additional information about polymers with a high chemical stability [19-21].

One of our objectives was to make membranes from a commercially available polymer, soluble in at least one solvent to allow a phase-inversion process. Some soluble commercially available polymers are polysulfone (PSF), polyethersulfone (PES), polyacrylonitrile (PAN), polyvinylidenefluoride (PVDF), polyetherimide (PEI) and BTDA-based polyimide (PI) (BTDA = benzophenone tetracarboxylic dianhydride). In table 1 the chemical resistances of these polymers are compared, based on information by suppliers, from literature [15-18], and our own experiments. The chemical environments are summarized in several solvent classes, based on their functional groups.

***Table 1.*** *Stability of commercially available polymers in several solvent classes; "+" means: stable, no visible change; "-" means: not stable, highly swelling or soluble; h.c. = hydrocarbons.*

| solvent class | PSF | PES | PAN[a] | PVDF | PEI | PI[b] |
|---|---|---|---|---|---|---|
| alcohols | + | + | +/- | + | + | + |
| aliphatic h.c. | + | + | + | + | + | + |
| aromatic h.c. | - | + | + | + | - | + |
| ethers | - | +/-[c] | + | + | +/-[c] | + |
| esters | - | - | + | - | + | + |
| ketones | - | - | + | - | + | + |
| aliphatic acids | + | + | + | + | - | +/-[d] |
| amides | - | - | - | - | - | - |
| halogenated h.c. | - | - | + | + | - | + |

a: pure polyacrylonitrile
b: soluble BTDA-copolyimide: P84 / PI 2080 (see section "Polyimides")
c: not stable in tetrahydrofuran
d: stable in aqueous dilutions, not stable in concentrated acid

Table 1 only gives a very rough comparison of the chemical resistance of these polymers, since "resistance" is defined in different ways depending on the source. As an example: according to the supplier, PEI is resistant to aromatic hydrocarbons. However, it was observed experimentally that PEI swells visibly upon immersion in aromatic solvents.
From this table it seems that polyacrylonitrile (PAN) is a very resistant polymer; however, commercial PAN is very often a copolymer (e.g., with polyvinyl-chloride) with a much lower chemical resistance. Pure PAN is soluble in a few solvents only, i.e., amides such as DMF and DMAc, but it is also known for its strong plasticization in a number of polar solvents [22-24]. This makes PAN less suitable for use in different organic media.
The soluble (co)polyimide shows a very good chemical resistance as well; for

chemically resistant ultrafiltration membranes it seems the best candidate material. In literature only data are available for swelling in water, which is only a few weight percent [25-27].
The properties of polyimides will be discussed further in the next section.

### 2.2.2 Polyimides

Polyimides are generally known as polymers with excellent thermal stability because of their high glass transition temperature. They are also chemically resistant, which in the past was quite problematic for processing purposes. The first polyimides, which were completely insoluble, were prepared according to a two-step process (see figure 1 [28]).

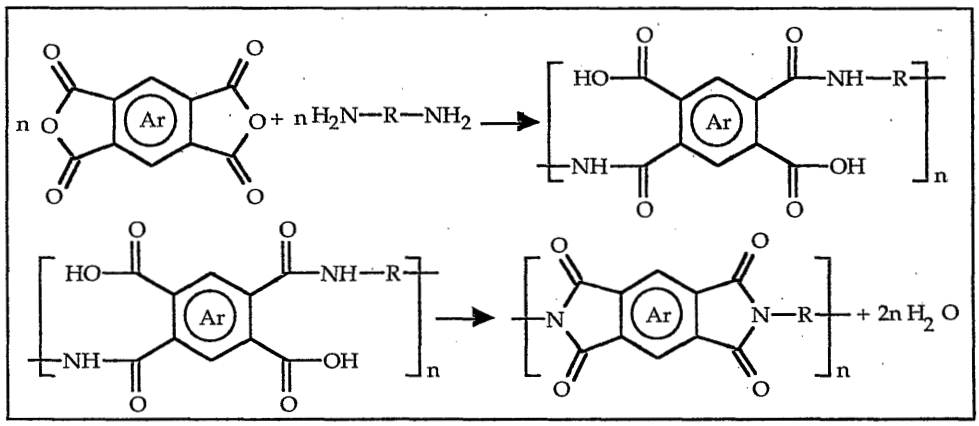


*Figure 1.* *Reaction scheme of the synthesis of polyimides from dianhydrides and diamines by the two-step process.*

Firstly, polycondensation of aromatic dianhydrides with aromatic diamines is necessary to form a soluble prepolymer, a poly(amic acid). The poly(amic acid) is shaped into the desired product, after which the product is imidized through a dehydration step, usually by heating [29,30].
It is also possible to synthesize polyimides by polycondensation of dianhydrides and diisocyanates. In this case the polymer is imidized by removal of carbon dioxide (see figure 2 [28]).

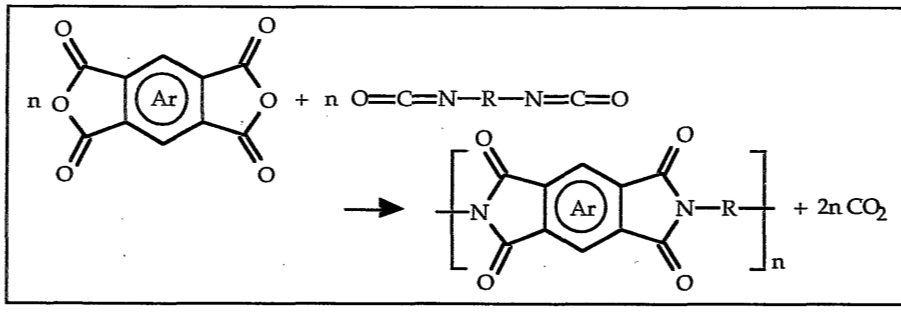


*Figure 2. Reaction scheme of the synthesis of polyimides from dianhydrides and diisocyanates.*

Some commercially available polyimides are summarized in figure 3. In general, polyimides are represented by abbreviations of their monomer units (often acronyms of conventional names for these units), to distinguish between the several types. The overview in figure 3 is restricted to "pure" polyimides. Neither modified polyimides such as polyetherimide or polyamideimide, nor imide oligomers (e.g., for adhesives) have been considered.

The first three polyimides mentioned in figure 3 are soluble resins, which makes them suitable phase-inversion membrane materials.
P84 has the same chemical structure as PI 2080, a polymer originally developed by Upjohn [31], but P84 is produced according to a somewhat different procedure [32,33]. P84 is amorphous, probably due to the random 20:80 copolymerization, which hinders the symmetry. The chemical resistance is excellent: P84 is resistant to almost all organic solvents, whereas it is well soluble in amides. Like many other polyimides, it is not resistant to aqueous alkaline solutions [34]. The $T_g$ of P84 is 315°C, and permanent application at 260°C (in air) does not cause any damage.
The chemical resistance of the two other soluble resins (Matrimid and Sixef) is somewhat worse: next to solubility in amides, these polymers are soluble in THF and some chlorinated hydrocarbons as well [35,36].
Kapton (insoluble [37]) and Upilex are commercially available as films.
The sixth commercial polyimide, BTDA-4pDA (Aldrich), is insoluble, probably due to its high crystallinity [28].

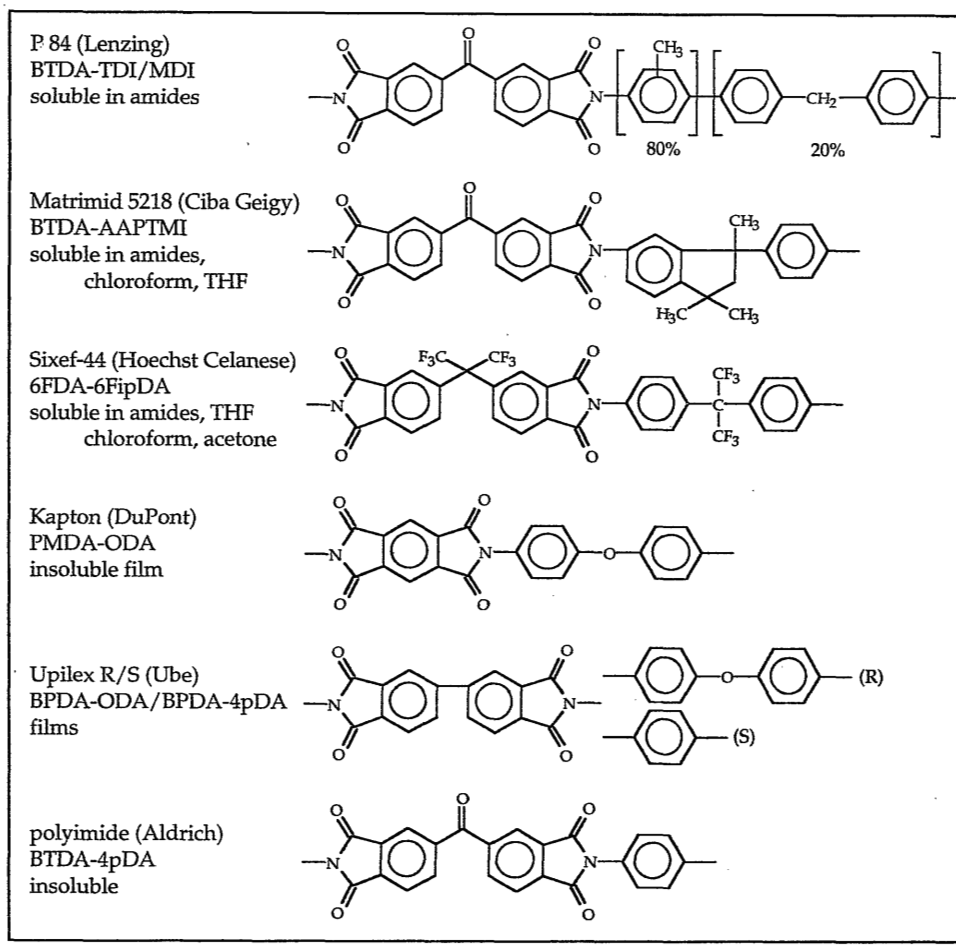


***Figure 3.*** *Commercially available polyimides (information according to suppliers).*

*BTDA:* *benzophenone-3,3',4,4'-tetracarboxylic dianhydride*
*TDI:* *toluene diisocyanate*
*MDI:* *4,4'-methylene bis(phenyl isocyanate)*
*AAPTMI:* *5(6)-amino-1-(4'-aminophenyl)-1,3-trimethylindane*
*6FDA:* *5,5-[2,2,2-trifluoro-1-(trifluoromethyl)-ethylidene]-bis-1,3-isobenzofuranedione*
*6FipDA:* *hexafluoro-2,2-bis(4-aminophenyl)propane*
*PMDA:* *pyromellitic dianhydride*
*ODA:* *4,4'-oxydianiline*
*BPDA:* *biphenyl-3,3',4,4'-tetracarboxylic dianhydride*
*4pDA:* *1,4-diaminobenzene*

Several attempts have been and are still made to synthesize new types of

polyimides, that are soluble in at least a few solvents. These attempts can be classified into four categories:

1. Introduction of flexible groups in the dianhydride or diamine part (e.g., C=O or -$CH_2$-), including the preference for more flexible ortho- and meta-linkages in the diamine [38,39].
2. Substitution of bulky groups in the polymer backbone [40-42] (e.g., Matrimid and Sixef).
3. Hindrance of symmetry by application of random copolymerization [7,43] (e.g., P84).
4. Preparation of modified polymers based on polyimides, like cardo-polyimides, polyamideimides, polyphenyleneimides and quinoxaline-imide polymers [44-46].

The structure - $T_g$ - solubility relationship and other properties of polyimides have often been reviewed in literature [36,37,39,47-54].

Despite their excellent chemical resistance, relatively few examples exist in literature concerning preparation of porous membranes from polyimides. One of the earliest publications on this subject was by Strathmann [55,56], who prepared ultrafiltration and reverse osmosis membranes from a prepolymer, that was imidized afterwards. In patents some actual membrane applications (mostly reverse osmosis) were described, using membranes made from soluble polyimides, as Upjohn's PI 2080 or Ciba Geigy's XU 218 (later Matrimid 5218) [57-60]. Ultrafiltration membrane preparation based on these two polymers has also been described by Sarbolouki [61]. Recently, Dong and Zhu [62] prepared PI-membranes by imidization of membranes prepared from prepolymers.
Nitto Electric Industrial Co. is until now the only company that produces polyimide ultrafiltration membranes. These membranes are prepared using a soluble polyimide from the monomers BPDA and MDA (= methylene dianiline, which results in the same "unit" as MDI). This polymer is also soluble in amides [63-65].

## 2.3 Membrane formation by immersion precipitation for ternary systems

### 2.3.1 The phase inversion process by immersion precipitation

Membrane formation by phase-inversion can be achieved in four ways [66]:

- evaporation of the solvent
- thermal precipitation, i.e., quenching of the solution to a lower temperature

- immersion precipitation, i.e., immersion of the polymer solution into a non-solvent coagulation bath
- vapour precipitation, i.e., contacting the solution with a non-solvent vapour

All membranes described in this thesis have been prepared by immersion precipitation. For this reason the phase separation process by immersion precipitation will be discussed here briefly.

In general, (at least) three components are necessary for the immersion precipitation process: a polymer (P), a solvent (S) and a non-solvent (NS). Certain initial compositions of this ternary system are not homogeneous: they lie within the demixing area of a ternary phase diagram. An example of such a diagram, based on equilibrium thermodynamics, is given in figure 4.

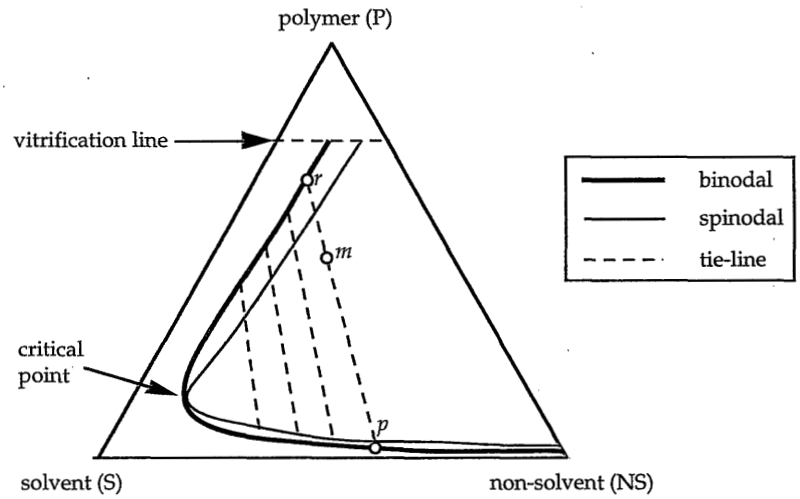


*Figure 4. Ternary phase diagram representing the miscibility behaviour of a polymer (P), a solvent (S) and a non-solvent (NS).*

The tie-lines in this figure connect two equilibrium compositions at the binodal. An unstable mixture *m* inside the spinodal area demixes into the two phases at each end of the tie-line, which are a phase that is poor (lean) in polymer, *p*, and a phase that is rich in polymer, *r*. The area between the binodal and the spinodal curve is a metastable region. For these compositions phase separation takes place by nucleation and growth of the nuclei being formed. Inside the spinodal region, the solutions are unstable. In principle, they demix immediately by spinodal decomposition, during which a bicontinuous network is formed [67-69].

Generally, a polymer solution is cast as a film on a support (glass plate or non-woven) with a casting knife. Then this film is immersed into a coagulation bath containing a non-solvent. At the moment of immersion, solvent diffuses out of the film, while non-solvent diffuses into the film. Due to its immiscibility with the non-solvent, its relatively high molecular weight and low diffusion coefficient, the relative velocity of the polymer molecules is very low, therefore, diffusion takes place in a polymer frame of reference.
The change of compositions inside the film can be represented by a composition path. The concept of the composition path can be used to distinguish between two types of demixing processes: instantaneous demixing and delayed demixing [70]. When phase separation starts at the moment of immersion, visible by the immediate turbidity of the film, the composition path crosses the binodal and instantaneous demixing takes place. In the case of delayed demixing, it takes some time before the composition path crosses the binodal. This difference in composition path between instantaneous and delayed demixing is shown in figure 5 (the composition at the skin side (s) and the bottom side (b) of the membrane are represented). In the case of instantaneous demixing, the toplayer of the membrane has demixed in two phases, a polymer-rich phase s' and a polymer-lean phase s". These two phases together have the composition v, which is a virtual composition.

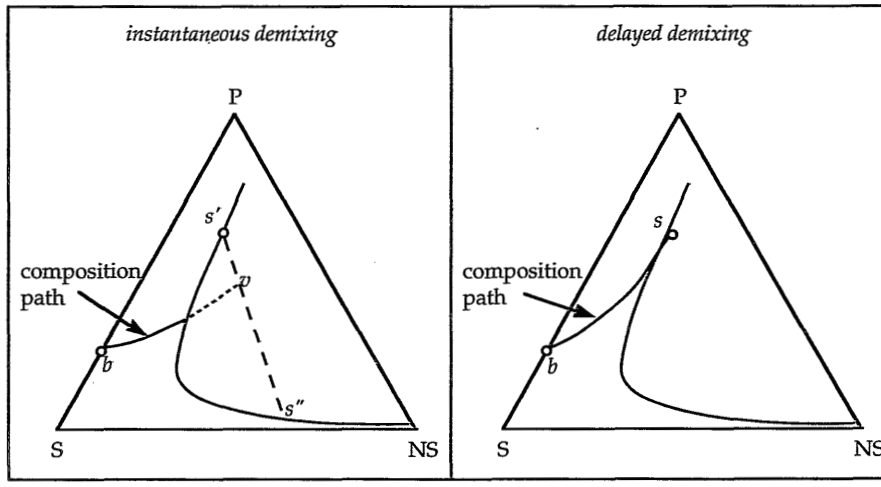


***Figure 5.*** *Composition path of instantaneous demixing (fig. a) and delayed demixing (fig b), after a short period of time (e.g. 1 second).*

This difference in type of demixing ultimately leads to a difference in membrane morphology: instantaneous demixing results in porous membranes (ultrafiltration or microfiltration), while delayed demixing results in membranes with a dense skin layer (reverse osmosis, gas separation or pervaporation).

### 2.3.2 Macrovoid formation [71]

In the sublayers of ultrafiltration membranes very often large voids are present. The formation of these macrovoids can be suppressed by:

- a solvent/non-solvent combination with a lower tendency of mixing
- increasing the polymer concentration in the casting solution (or application of an evaporation step before the immersion in the coagulation bath)
- addition of solvent to the coagulation bath

There are several theories that describe macrovoid formation. The initiation of macrovoids is proposed to be caused by:

- formation of convective cells close to the film/bath interface [72-74]
- rupture of the toplayer by mechanical stresses [75]
- presence of "weak" points in the toplayer (i.e., locally looser packing) [76]
- nucleation of droplets of the polymer-lean phase [71,77]

The latter mechanism is the most likely, because it is the only theory that can account for the presence of macrovoids that do not start at the membrane skin; in addition, nucleation of the polymer-lean phase below the skin is very well possible during membrane formation by liquid-liquid demixing.
Based on this mechanism, Reuvers [78] and Smolders et al. [71] suggested that the growth of a macrovoid is inherent to the growth of the nucleus. In a nucleus of the polymer-lean phase a mixture of solvent and non-solvent will be present. It is possible that the solvent concentration in the nucleus becomes so high, that on a local scale a delayed demixing process is favoured. This means that around the nucleus the polymer solution is relatively stable and no new nuclei are formed, so that the original nucleus can grow, thereby forming a macrovoid.

When the affinity between non-solvent (1) and solvent (2) is high, i.e., when the interaction parameter $g_{12}$ is low, the solvent in the nascent membrane will tend to flow very quickly to the polymer-lean phase nuclei, whereby the solvent concentration in the nucleus increases drastically and macrovoid formation is favoured. At a lower affinity, the solvent flow to the polymer-lean nuclei will be slower, and the propagating diffusion front will be able to form new nuclei deeper in the membrane; these new nuclei will hinder the growth of the older nuclei and macrovoid formation will be hindered.
An increase in polymer concentration will slow down the indiffusion of non-solvent, thereby promoting macrovoid formation, since on a local scale delayed demixing is promoted. On the other hand, with an increase in polymer

concentration, the solvent concentration in the coagulation bath (and the polymer-lean nucleus) necessary to induce delayed demixing is also strongly increasing [71], thus the tendency to form macrovoids will be decreased. Smolders et al. suggested that above a certain concentration the second phenomenon is dominant.
The addition of solvent to the coagulation bath suppresses macrovoid formation, since delayed demixing is promoted. The addition of a second polymer to the casting solution can also suppress the formation of macrovoids, as explained by Boom et al. [79,80].

### 2.3.3 Formation of nodular structures in the toplayer

The toplayer of most ultrafiltration membranes consists of nodules, that are smallest at the surface (diameter < 50 nm) and are larger deeper inside the toplayer. The formation of nodular structures cannot be explained by liquid-liquid demixing by means of the nucleation and nucleus growth mechanism, since at these polymer concentrations (i.e., above the critical point) nucleation of the polymer-lean phase is expected. Boom et al. [79] described the formation of these nodules by spinodal decomposition, based on the original theory developed by Cahn [67]. The basis of this theory is the presence of concentration fluctuations in unstable solutions, which grow in amplitude until phase separation takes place and a bicontinuous network is formed.
However, the toplayer of ultrafiltration membranes is not bicontinuous, but consists of nodules. Wienk et al. [81] explained this phenomenon by a collapse of the highly entangled polymers into clusters, due to the very rapid change in environment, i.e., from "solvent" to "non-solvent". This collapse is accompanied by a disentanglement process, which is stopped abruptly at the moment of vitrification. Therefore, in the resulting membrane many nodules will still be interconnected, which explains the low porosity of ultrafiltration membranes prepared by immersion precipitation.
Li [82] explained nodule formation as follows. In the metastable region there are concentration fluctuations present in the solution, due to the clustering tendency of the entangled polymers (see above). However, before stable nuclei of the polymer-lean phase are formed (i.e., "low concentration areas"), the polymer-rich phase domains may reach the vitrification concentration. Due to this preliminary vitrification of the polymer-rich phase, nodules are formed, while the not yet nucleated polymer-lean phase forms the small pores in between these nodules.
Pinnau and Koros [83] suggested that the (partial) breaking up of the bicontinuous structure into spherical nodules may be caused by the interfacial surface tensions between the two phases. In a later stage, the nodules can coalesce because of these tensions. By instantaneous vitrification of the nodular structure, this coalescence is at least partially prevented, resulting in a porous toplayer.

During delayed demixing, the coalescence of the nodules can proceed, resulting in membranes with a non-porous toplayer (gas separation membranes).

### 2.3.4 Membrane formation parameters

Several membrane formation parameters can affect the final membrane morphology:

- type of solvent
- polymer concentration in the casting solution
- type of non-solvent
- temperature of the coagulation bath
- addition of extra components (i.e., additives) to the casting solution

The choice of solvent is determined by the choice of the polymer: for the chemically resistant polyimide P84, the class of amides are used as solvents. The non-solvent must be completely miscible with the solvent. Furthermore, to promote instantaneous demixing, the non-solvent/solvent pair should have a high mutual affinity, i.e., a low interaction parameter $g_{12}$ [84]. Aprotic amide solvents generally have a very high mutual affinity with water. They show a negative excess free enthalpy of mixing ($G_M^E$) [85]. Values for $G_M^E$ of amides in combination with other non-solvents are rarely found in literature, but it is expected that at least for ethanol the mutual affinity is still rather high.
In this chapter the polyimide membrane formation for different non-solvent/solvent pairs will be compared using light transmission measurements [70]. The solvent used for these measurements was DMF and as non-solvent water and a range of low-molecular weight alcohols were employed.

The polymer concentration is a very important parameter during immersion precipitation. If the concentration is above the critical point, nucleation of the polymer-lean phase takes place, so that a membrane will be formed finally, because the polymer-rich phase is the continuous phase. If the concentration is below the critical point, the polymer-rich phase will form nuclei inside a continuous polymer-lean phase matrix, so that a latex will be formed instead of a membrane.
When the composition of the polymer-rich phase crosses the vitrification line (see figure 4), the polymeric matrix will be vitrified. Because the polymers used in this study are amorphous, a discussion of crystallization phenomena is beyond the scope of this thesis. A high initial polymer concentration leads to a high polymer concentration in the toplayer of the membrane. This implies that the membrane is less permeable for water or ethanol.
The effect of an additive to the casting solution will be discussed further in chapter 3 of this thesis.

## 2.4 Experimental

### 2.4.1 Materials

The polyimide P84 (Lenzing AG, Austria; 325 mesh (<45 μm), chargenr. 8170914) was kindly supplied by X-Flow BV. Dimethylformamide (DMF), methanol, ethanol, n-propanol and n-butanol were purchased from Merck, analytical grade, and used as received. Demineralized water and technical ethanol were used as non-solvent coagulation media. Technical grade ethanol was also used as storage medium.

### 2.4.2 Membrane preparation

Casting solutions were prepared from dried PI-powder (drying time 24 hours in a vacuum oven at 150°C); the PI was dissolved immediately in the solvent after removal from the oven. The air inside the erlenmeyer was replaced by nitrogen. The erlenmeyer was closed tightly. The polymer was dissolved by magnetic stirring for 24 hours, without heating. The polymer solution was then filtered under nitrogen through a Bekipor® 25 μm stainless steel filter from Bekaert Filter Technologies to remove (gel) particles. The solutions were degassed overnight.
The filtrated polymer solution was spread as a thin film on a dry and clean glass plate by a stainless steel casting knife, with a casting gap of 0.20 mm. The glass plate with the film was immersed immediately in the non-solvent coagulation bath at the desired coagulation temperature, without evaporation. The residence time in the coagulation bath was at least ten minutes. All membranes precipitated instantaneously.
The membranes were rinsed with tap water for 24 hours to remove traces of the solvent. To confirm that this procedure is sufficient, the DMF-content after rinsing was determined using TGA and found to be negligible. After the rinsing procedure, the water was replaced by ethanol in at least three washing steps, and the membranes were stored in closed containers with ethanol.
During the whole preparation, storage and testing procedure special care was taken that the membranes were not dried. A discussion about drying of ultrafiltration membranes can be found in the appendix to chapter 4.

### 2.4.3 Scanning Electron Microscopy

SEM (Scanning Electron Microscopy) has been used for the investigation of the sublayer morphology of the prepared membranes. The membrane samples were coated with a thin gold layer to enable the transport of electrons from the electron beam that are not reflected or transformed to secondary electrons.
This layer, which is about 5 nm in thickness, can have an important effect on the

quality and reliability of the final image. The preparation of membrane samples is very crucial. Cross sections are obtained by cryogenic breaking of the membrane in liquid nitrogen. The sample was placed in a sample holder and evacuated for at least 16 hours in a Balzers Union SCD 040 sputter coater; during this step, the ethanol evaporates. After this, the pressure in the coating chamber was set at 0.05 mbar using argon. The samples were sputtered for 300 seconds at a current of 15 mA.
SEM is only used here as a technique to compare the morphology of the sublayer or membrane matrix of different membranes. No information can be obtained about the toplayer by this technique. It is assumed here that the drying step does not drastically change the morphology of the matrix, whereas it will probably change the toplayer. The influence of drying on the toplayer, overall membrane surface and membrane performance will be discussed in the appendix to chapter 4.

### 2.4.4 Other characterization techniques

Three different techniques were used for membrane characterization. For all membranes the permeability for ethanol was determined. For some dried membranes the dry-state pore size distribution has been obtained by permporometry, or the nitrogen flux has been determined. More information about these characterization techniques can be found in chapter 4.

### 2.4.5 Light transmission measurements

Reuvers performed light transmission experiments to investigate the demixing behaviour of the system cellulose acetate-acetone-water [70]. This method distinguishes between instantaneous demixing and delayed demixing.
A large petri dish was filled with a mixture of solvent and non-solvent at the desired temperature. Below this coagulation bath a light sensor was placed, coupled to a recorder. A light source was used above the coagulation bath.
The polymer solution was cast on a small glass plate using a knife with a casting thickness of 0.20 mm. A second glass plate was placed above the first one on top of four stubs to reduce the convective movement induced by the immersion in the coagulation bath. The experimental set-up is illustrated in figure 6.
As soon as the glass plates are immersed in the bath, diffusion of non-solvent into and of solvent out of the film starts; the light transmission through the system is measured as a function of time. When demixing starts, i.e., when the film becomes turbid, the light transmittance decreases: $I_t < I_o$, with $I_o$ the initial intensity. Delayed demixing occurs when the decrease in light transmission starts only after a certain period of time. If this process starts at the moment of immersion, instantaneous demixing occurs.

The completely demixed membrane will still allow some light to pass, i.e., the transmittance of light through the final membrane, $I_\infty$, is not zero. However, the value of $I_\infty$ has no physical meaning. It is assumed that the slope of the transmittance curve is in some way dependent on the demixing velocity. When systems with the same solvent but different non-solvents are compared, this slope gives a qualitative impression of the non-solvent/solvent affinity. The results of these measurements are represented by values for $t_{25/75}$, i.e., the time necessary for the polymer film to proceed from 25% transmittance decrease (i.e., $0.75(I_0-I_\infty)$) to 75% transmittance decrease (i.e., $0.25(I_0-I_\infty)$) (see figure 6).

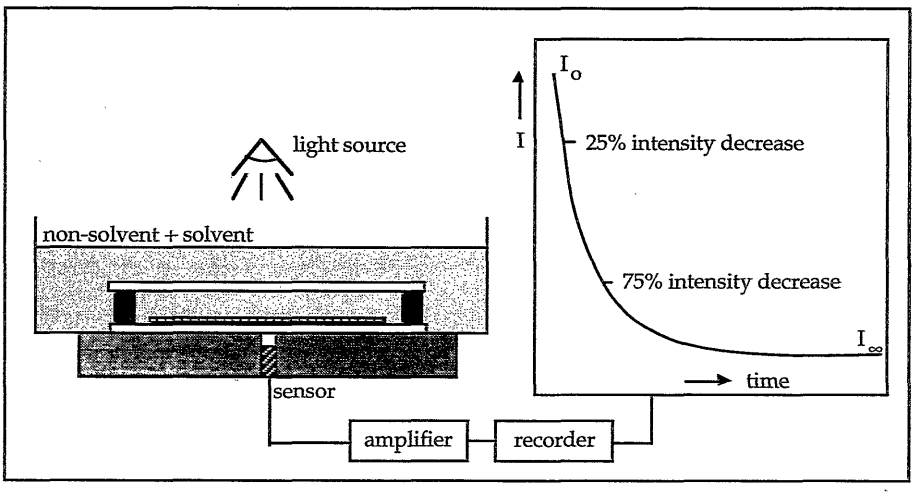


*Figure 6. Experimental set-up for light transmission measurements.*

### 2.4.6 Swelling experiments

Homogeneous polymer films with a thickness of 100-120 μm have been obtained by evaporation of the solvent from a thin polymer solution film in a dry nitrogen atmosphere for two weeks. The films were cut to strips of about 5 cm * 3 cm, which were dried for several weeks at 150°C vacuum. The dry weight of each film has been determined, directly before immersion in closed jars containing an organic solvent. After removal from the solvent, the films were carefully wiped with tissues, after which a swelling value was determined by measuring the weight increase relative to the dry weight (i.e., percentage weight gain). The determined swelling values are *not* equilibrium swelling values, but only give a very rough comparison of the chemical resistance of the polymeric material (see section 2.2.1).

## 2.5 Results of chemical resistance tests of polyimide P84

To achieve some information about the swelling behaviour of polyimide in several solvents, swelling experiments were used. The results are summarized in table 2. The homogeneous films were very brittle, so special care had to be taken during storage and handling to avoid breaking. One has to keep in mind that the values presented in table 2 are not equilibrium swelling values (see paragraph 2.2.1).

*Table 2. Swelling of polyimide P84 in several organic solvents.*

| solvent | swelling [wt%] | time [days] | solvent | swelling [wt%] | time [days] |
|---|---|---|---|---|---|
| methanol | 12.2 | 120 | n-hexane | 1.4 | 600 |
| ethanol | 8.0 | 316 | cyclohexane | 2.4 | 40 |
| 1-propanol | 1.8 | 316 | ethyl acetate | 2.8 | 185 |
| isopropanol | <1 | 316 | toluene | 2.7 | 288 |
| demin. water | 5.8 | 316 | trichloroethylene | 4.7 | 96 |

It is obvious from table 2 that the swelling of polyimide in almost all cases is lower than 10%, which means that no significant differences in porous structures are to be expected upon immersion of a polyimide ultrafiltration membrane in any of these solvents. An exception is methanol. It is possible that the relatively high swelling of polyimide in methanol is caused by specific polymer-solute interactions.
Homogeneous polyimide films became extremely brittle or were stress-cracked upon immersion in dioxane, methylene chloride, or cyclohexanone.

Asymmetric dry polyimide membranes were kept for 24 hours in several boiling solvents. For none of these membranes any visual changes could be observed after this treatment, and the dry weight of the membrane was not altered by this procedure. These test results are shown in table 3.

*Table 3. Solvents used for boiling tests of polyimide membranes.*

| | | |
|---|---|---|
| chloroform | ethyl acetate | methyl ethyl ketone |
| toluene | p-xylene | trichloroethylene |
| tetrahydrofuran | n-hexane | ethanol |
| acetone | acetonitrile | white spirit |

A batch of PI-membranes, prepared from a 23 wt% PI/DMF-solution and coagulated in ethanol, was used to determine the permeability for four different solvents: ethanol, n-hexane, toluene, and acetone. For this purpose, fresh membranes were pre-conditioned in these solvents for at least two days. In table 4 the permeability results are presented. In this table also normalized permeabilities are given, i.e., permeabilities of different solvents multiplied by the solvent viscosity, $\eta_{medium}$: $P_{norm} = P * \eta_{medium}$.

***Table 4.*** *Permeability (P) and normalized permeability ($P_{norm}$) of PI-membranes (23 wt% PI in solvent DMF; coagulated in ethanol) for different organic media.*

| medium | P [kg/m$^2$ hr bar] | $\eta_{medium}$ [Pa s] | $P_{norm} = P * \eta_{medium}$ [kg Pa s/m$^2$ hr bar] |
|---|---|---|---|
| ethanol | 120 | $1.13*10^{-3}$ | $135*10^{-3}$ |
| n-hexane | 681 | $0.30*10^{-3}$ | $206*10^{-3}$ |
| toluene | 248 | $0.58*10^{-3}$ | $144*10^{-3}$ |
| acetone | 513 | $0.32*10^{-3}$ | $162*10^{-3}$ |

From this table it is clear that the normalized permeabilities are comparable with each other. This implies that the differences in swelling are small enough to exclude the occurrence of significant differences in pore size when comparing the morphology of the membrane in various organic media. Experiments have been done to compare the permeability of different membranes for ethanol and ethyl acetate as well. These results will be described in chapter 4.

In conclusion, P84 has a very high chemical resistance, i.e., it has a low degree of swelling in a range of organic solvents. Especially the high resistance to esters and ketones is significant, since many potential non-aqueous applications may be found based on these solvents (see also chapter 1). Nevertheless, one has to be careful when using this material in methanol, dioxane, methylene chloride, or cyclohexanone.

## 2.6 Results for polyimide membrane preparation

### 2.6.1 Influence of solvent

Polyimide solutions with 20 wt% polymer were prepared in different solvents: DMF (dimethylformamide), DMAc (dimethylacetamide), and NMP (n-methyl-2-pyrrolidone). The membranes were cast on glass plates with a thickness of 0.20

mm, and coagulated in ethanol or water.
The scanning electron microscopy photographs of the various membranes are given in figure 7 (next page).

As can be seen from these photographs the shape of the macrovoids present in the various membranes coagulated in ethanol differs clearly. Membranes from NMP show long cigar-shaped macrovoids, while membranes from DMF- and DMAc-solutions have smaller and triangular-shaped macrovoids. This difference in morphology also has an influence on the integrity of the membranes: membranes from NMP show much more defects and pinholes than membranes from DMF and DMAc, probably because some of the long macrovoids in NMP-cast membranes are extended over the whole membrane thickness, including the toplayer.

The membranes also differ in brittleness and fragility. PI itself is already a brittle material, typically caused by the rigid structure. Ethanol-coagulated membranes from NMP and DMAc solutions are much more fragile than membranes from DMF. SEM-magnifications of the sublayers of these membranes also show subtle differences: the sublayers of the former membranes consist mainly of loosely packed nodular aggregates, while the matrix of DMF-cast membranes resembles more a spongy, bicontinuous structure (see figure 8). It is expected that a spongy substructure is mechanically more resistant to external forces, whereas the structure with nodular aggregates easily breaks.
The membranes coagulated in water are very brittle. These membranes all have sublayers that consist of large nodular aggregates. The differences in morphology for different solvents are less obvious than in the case of ethanol as non-solvent. From this point of view, DMF is the most suitable polyimide solvent for membrane formation by immersion precipitation.

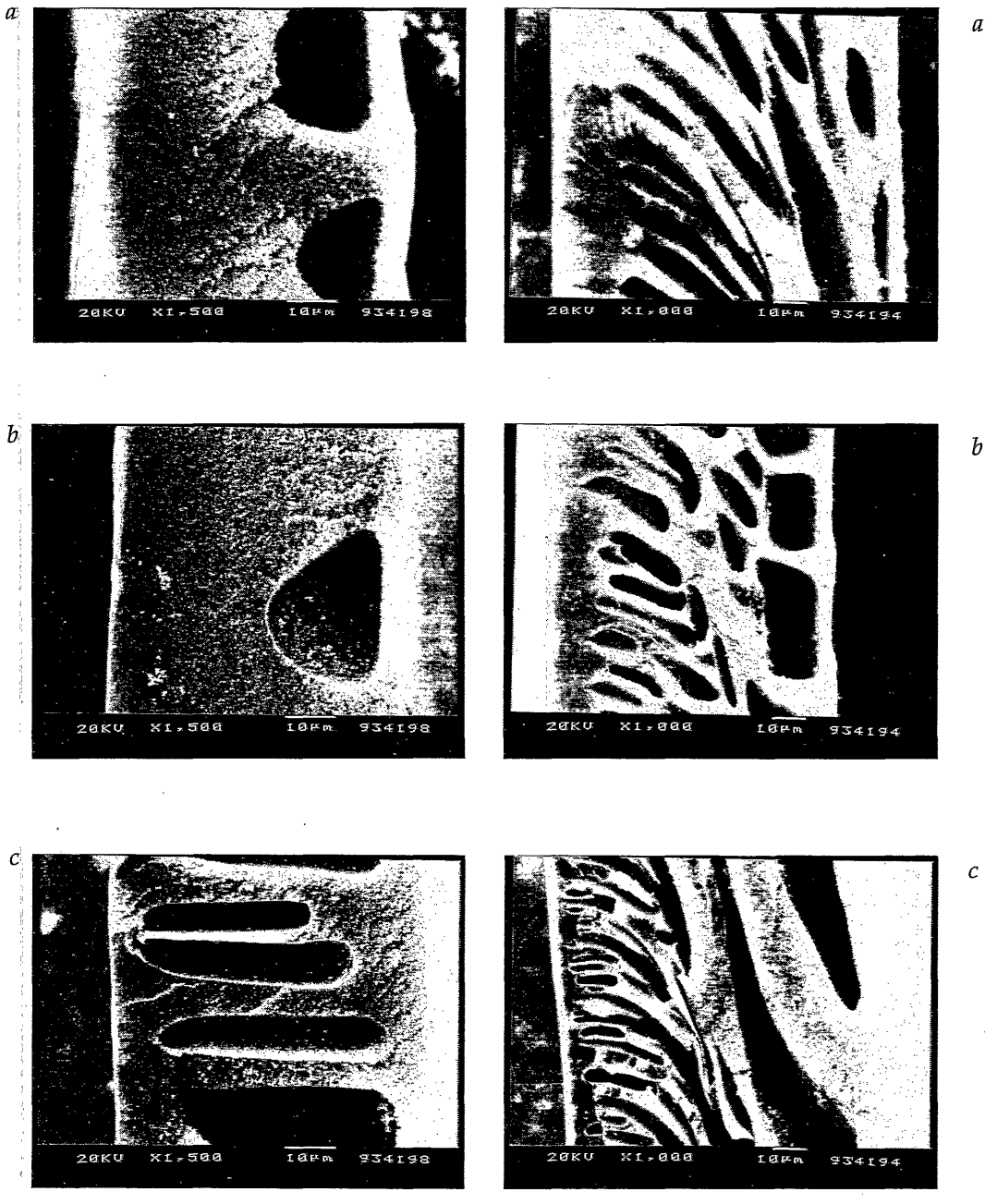


*Figure 7. SEM-photographs of membranes prepared from 20 wt% PI-solutions in DMF (a), DMAc (b), and NMP (c); membranes on the left hand side are coagulated in ethanol, membranes on the right hand side are coagulated in water.*

a

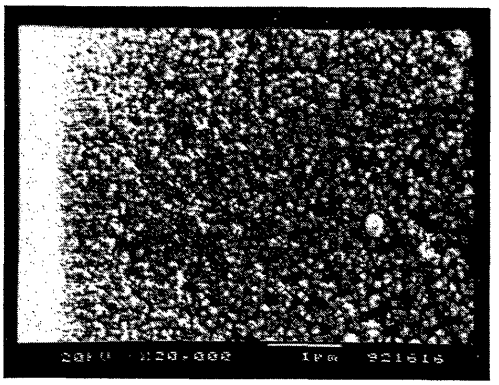

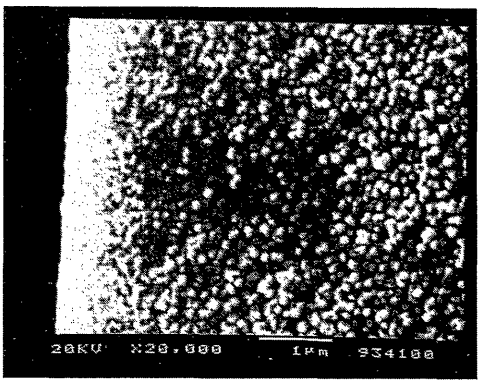


b

*Figure 8.* *Magnifications of the region directly beneath the toplayer of PI-membranes (prepared from 20 wt% casting solutions, coagulated in ethanol); fig. a: membrane from a DMF-solution (flexible membrane), fig. b: membrane from a DMAc-solution (brittle membrane).*

*Solubility parameter* $\delta$

The casting solution solvent affects the membrane formation process. An important property related to the solvent is the solubility of the membrane polymer in the solvent. The solubility parameter approach roughly can predict the solubility of polymers in solvents. Bottino et al. [86], Ventoza and Lloyd [87], Kinzer et al. [88], and Tam et al. [89] used this theory to compare solvents for several membrane forming systems.
For polyimides there is only one set of data available [7], but this PI has a different chemical structure than the one used by us, P84. Therefore, two calculation methods using group contributions were applied to estimate the solubility parameters of P84: the method of Van Krevelen and Hoftijzer (method A), and the method of Hoy (method B), see ref. [9]. For the first method molar volumes were calculated according to a group contribution table by Fedors [9], while the second method already includes a molar volume calculation. The results of these calculations are presented in table 5. For comparison, also the literature data for a different PI are shown, as well as the solubility parameters for the three solvents [4].

***Table 5.*** *Solubility parameters for polyimides and solvents. The values for P84 were calculated according to van Krevelen and Hoftijzer (A) or Hoy (B).*

| component | $\delta_d$ $[J/m^3]^{1/2}$ | $\delta_p$ $[J/m^3]^{1/2}$ | $\delta_h$ $[J/m^3]^{1/2}$ | $\delta_t$ $[J/m^3]^{1/2}$ | $\Delta\delta_{PS}$ $[J/m^3]^{1/2}$ |
|---|---|---|---|---|---|
| P84 (method A) | 27.7 | 9.8 | 9.7 | 31.0 | |
| P84 (method B) | 13.1 | 14.8 | 10.8 | 22.6 | |
| P84 (mean) | 20.4 | 12.3 | 10.3 | 26.8 | |
| BTDA-TMPDA [7] | 21.7 | 10.8 | 10.8 | 26.5 | |
| DMF | 17.4 | 13.7 | 11.3 | 24.8 | 3.5 |
| DMAc | 16.8 | 11.5 | 10.2 | 22.7 | 3.7 |
| NMP | 18.0 | 12.3 | 7.2 | 22.9 | 3.9 |

Method A and method B give quite different results. This is also pointed out by Van Krevelen, who suggested to take the mean values of the two methods. These mean values are rather close to the solubility parameters of the BTDA-TMPDA-polyimide, that were determined by solubility experiments.
Van Krevelen states that a liquid is a good solvent for a polymer when $\Delta\delta_{PS} \leq 5$, where:

$$\Delta\delta_{PS} = \left[\left(\delta_{d,P}-\delta_{d,S}\right)^2 + \left(\delta_{p,P}-\delta_{p,S}\right)^2 + \left(\delta_{h,P}-\delta_{h,S}\right)^2\right]^{1/2} \qquad (2.3)$$

The calculated values for $\Delta\delta_{PS}$, based on the mean calculated values for P84 and the values from literature for the solvents, are also given in table 5. It is obvious that according to the criteria mentioned above, DMF, DMAc and NMP are good solvents for this polyimide. DMF has the lowest value for $\Delta\delta_{PS}$, but the differences are so small that hardly any relevant conclusion can be drawn from the solubility parameter approach. Therefore, the solubility parameter theory cannot be used to explain the differences in membrane morphology in relation to these solvents.

*Interaction parameter* $g_{12}$

The non-solvent/solvent interaction parameter, $g_{12}$, is another solvent-related thermodynamic property important for membrane formation. This concentration-dependent parameter can be determined from excess free enthalpy of mixing data ($G_M^E$) [84], or from vapour-liquid phase equilibrium data of mixtures, via the calculation of activity coefficients, according to [84]:

$$\Delta G_M^E = nRT(x_1 \ln\gamma_1 + x_2 \ln\gamma_2) \qquad (2.4)$$

$$g_{12} = \frac{1}{x_1\varphi_2}\left(x_1 \ln\frac{x_1}{\varphi_1} + x_2 \ln\frac{x_2}{\varphi_2} + \frac{\Delta G_M^E}{nRT}\right) \qquad (2.5)$$

Here, $x_i$ is the mol fraction of component i [-], $\varphi_i$ is the volume fraction of component i [-] and $\gamma_i$ is the activity coefficient of component i [-], with i=1,2.
For water/DMF [84], and water/NMP [90], some values of $g_{12}$ are given in literature, obtained by calculation of activity coefficients at high temperature (T>100°C) that were extrapolated to room temperature. Li et al. presented $g_{12}$-data for water/DMAc [91], calculated via the excess heat of mixing, $H_M^E$. In figure 9 these literature data are summarized by dashed lines.

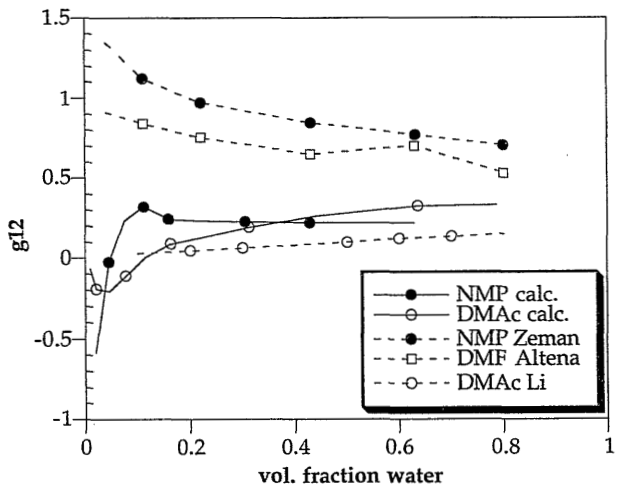


*Figure 9. Concentration-dependent water/solvent interaction parameters $g_{12}$; dashed lines: data directly from literature; full lines: data calculated from vapour-liquid equilibrium data at 20°C.*

For water/DMAc [92] and water/NMP [93] also experimental equilibrium data are available for pressure variation at room temperature, and the $g_{12}$-parameters for these two systems were calculated at 20°C and atmospheric pressure. These curves are represented in figure 9 by full lines. These calculated values are much lower over the whole range than the literature values for water/DMF and water/NMP.
The $G_M^E$-value of water/NMP, presented by Zeman and Tkacik [90], was found to be positive over the whole concentration range. The $g_{12}$-data that were used by Altena [84], are also based on positive values for $G_M^E$ [94]. On the other hand, $G_M^E$

is negative over the whole concentration range in the case of water/DMAc [95]. The data presented by Li et al. [91] are obtained by an approximation procedure via Redlich-Kister equations, but the values calculated from vapour-liquid equilibrium data are much more accurate.
Unfortunately, no vapour-liquid equilibrium data are available for water/DMF at 20°C, but it is expected that the $g_{12}$-curve is located at lower values than the curves for water/NMP and water/DMAc, based on the literature data mentioned above. Consequently, water/DMF will have a higher mutual affinity than water/DMAc or water/NMP.

*Ethanol permeability*

The average pore size and the pore size distribution in the toplayer determine the ethanol permeability of ultrafiltration membranes. The ethanol permeability of PI-membranes, prepared from 20 wt% solutions in DMF, DMAc, or NMP, and coagulated in water or ethanol, are given in table 6.

***Table 6.*** *Ethanol permeability of PI-membranes (20 wt%), from various solvents and non-solvents.*

| solvent | non-solvent | ethanol permeability [kg/m$^2$hr bar] |
|---|---|---|
| DMF | water | 258 |
| DMF | ethanol | 291 |
| DMAc | water | 166 |
| DMAc | ethanol | 192 |
| NMP | water | 119 |
| NMP | ethanol | 129 |

It is obvious from table 6 that there are differences in pore size and pore size distributions between these membranes. DMF as solvent results in the highest permeability, and NMP gives the lowest ethanol permeability.
The membrane formation process is not only influenced by thermodynamic parameters, like polymer solubility and non-solvent/solvent interaction, but is also strongly dependent on kinetic parameters, like diffusion coefficients and driving forces. Especially during the formation of the nodular toplayer the kinetic parameters will be crucial, since the concentration gradients at the film-bath interface will be very large.
Tkacik and Zeman [96] measured "slow mode" and "fast mode" diffusion coefficients for the systems water/NMP/PES, water/DMF/PES, and water/NMP/PES, and "fast mode" diffusion coefficients for ethanol/NMP/PES,

using the quasi elastic light scattering technique. The fast mode diffusion coefficient corresponds to diffusive movement of polymer segments, i.e., center-of-mass movement of the total network, whereas the slow mode diffusion coefficient represents center-of-mass movement of single polymer chains, or reptation [97]. The comparison of DMF and NMP as solvents showed that both the fast and the slow mode diffusion coefficients are larger for DMF than for NMP. Diffusion coefficients for PI membrane forming systems are not known, but we expect the trend to be similar.
It is suggested that in the case of DMF as a solvent, the nodules in the final membrane are less interconnected due to a rapid disentanglement of the contracting polymer chains (i.e., higher diffusion coefficients). This results in larger pore sizes when compared with membranes prepared from NMP- or DMAc-solutions, where the disentanglement process will be slower due to the lower diffusion coefficients. The more interconnected nodular structure in the toplayer of membranes from NMP and DMAc causes a lower solvent permeability. This explanation supports the nodule formation hypothesis by Wienk et al. [81].

### 2.6.2 Influence of polymer concentration

Polyimide solutions in DMF were prepared with different polymer concentrations (18, 20, and 25 wt%, respectively), and coagulated in ethanol or water (see figure 10).

An increase in polymer concentration causes a decrease in the number of macrovoids. In the case of ethanol as non-solvent, the 25 wt%-membrane contains no macrovoids at all, whereas the 20 wt%- and 18 wt%-membranes contain some macrovoids (18 wt%-membranes contain even more macrovoids than 20 wt%-membranes. This is not very clear from figure 10, but it has been concluded from several other SEM-investigations). For water-coagulated membranes also a decrease in number of macrovoids can be correlated with an increase in polyimide concentration.
The polymer concentration also has a strong influence on the toplayer structure of the membrane. This has been investigated by ethanol permeability measurements for wet membranes, and nitrogen flux measurements for dry membranes. The membranes were dried according to an ethanol-hexane-air displacement procedure to minimize capillary forces during the drying process. Both the gas flux and the solvent permeability decrease drastically with an increase of the PI concentration. These results are given in figures 11 and 12, respectively.

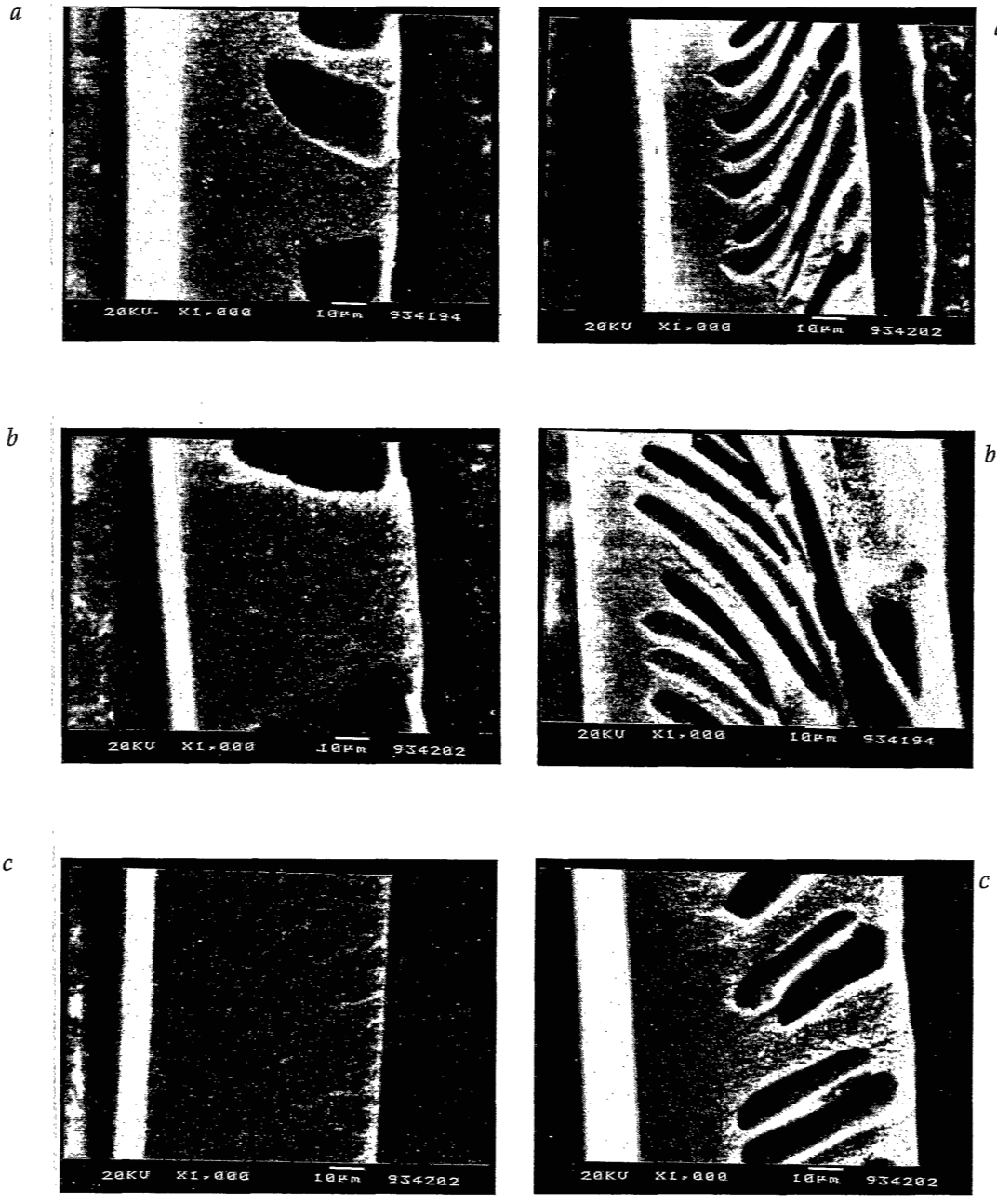


***Figure 10.*** *Variation of polyimide concentration in the casting solutions. Fig.a: 18 wt% PI, fig. b: 20 wt% PI, fig. c: 25 wt% PI. Membranes on the left hand side are coagulated in ethanol; membranes on the right hand side are coagulated in water.*

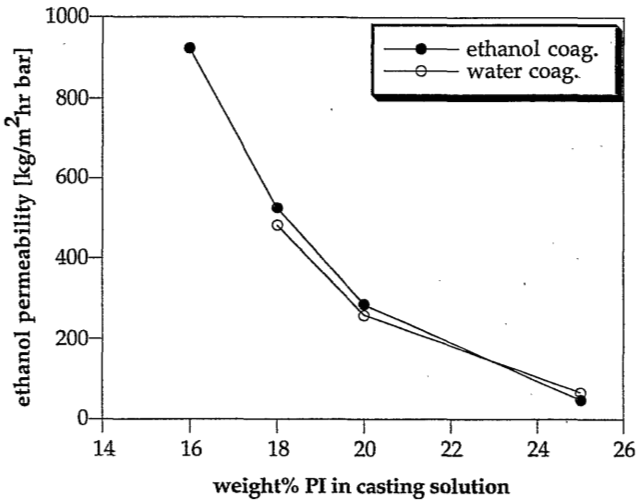


*Figure 11.* *Ethanol permeability as a function of the polyimide concentration in the casting solution for membranes coagulated in water or ethanol (solvent: DMF).*

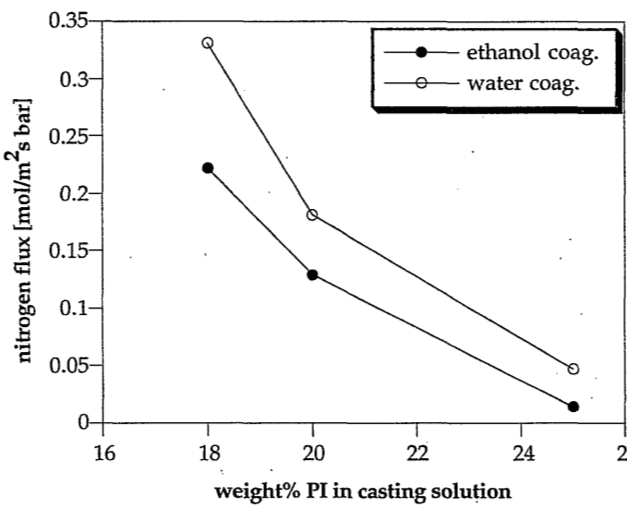


*Figure 12.* *Nitrogen flux as a function of the polyimide concentration in the casting solution for membranes coagulated in water or ethanol (solvent: DMF).*

The dried membranes were characterized using permporometry with cyclohexane as condensable vapour [98]. A more detailed discussion of this method is given in chapter 4 of this thesis.

The pore size distributions of membranes prepared from 18, 20, and 25 wt% polyimide casting solutions, coagulated in water and ethanol, are given in chapter 4. From these graphs it can be seen that with an increase in polymer concentration, the number of large pores decreases, and the maximum of the pore peak shifts to lower pore radii. In table 7, these maxima are summarized for the different membranes.

*Table 7. Position of maximum in pore size distributions for different membranes, obtained by permporometry (see chapter 4).*

| PI-concentration in casting solution [wt%] | NS: ethanol position of maximum [nm] | NS: water position of maximum [nm] |
|---|---|---|
| 18 | 7.0 | 5.0 |
| 20 | 5.4 | 3.8 |
| 25 | 4.0 | 3.8 |

It must be noticed that the pore size distributions have been determined for dry membranes.

The experimental results described in this section can be explained as follows. A higher initial polymer concentration in the casting solution corresponds with a composition path that is situated closer to the polymer corner in the phase diagram, thereby inducing a larger concentration of polymer-rich phase in the toplayer of the membranes; this explains the strong dependence of ethanol permeability (and nitrogen flux) on the casting polymer concentration.
Furthermore, a higher polymer concentration suppresses the formation of macrovoids [71,99].

### 2.6.3 Influence of non-solvent

In figures 7 and 10 SEM-photographs can be compared of membranes coagulated in ethanol or water. An obvious difference between these membranes is the morphology of the sublayer. Water results in a substructure with more macrovoids compared to ethanol. The presence of macrovoids is especially of interest because of the fragility of macrovoid-containing membranes.
This difference might be explained by the difference in non-solvent/solvent interaction parameter for these systems. The affinity between water and amide solvents is extremely high, which favours macrovoid formation. The affinity between ethanol and amides is expected to be lower, because of the lower polarity of ethanol compared to water, thus the tendency towards macrovoid formation

will be less pronounced in the case of ethanol [71].
The demixing experiments may give qualitative information about the phase-inversion process for these two systems. It was found experimentally that for membranes from 20 wt% PI casting solutions in DMF the type of demixing changes from instantaneous to delayed in coagulation baths consisting of DMF/water with between 5 and 10 vol% water; for ethanol this transition lies between 10 and 15 vol% ethanol. This means that the demixing area for the system water/DMF/PI is larger than for the system ethanol/DMF/PI. The same conclusion was drawn by Tkacik and Zeman [96] for the systems water/NMP/PES and ethanol/NMP/PES, and by Mulder et al. [100] and Wijmans et al. [101] for the systems water/DMAc/PSF and ethanol/DMAc/PSF.
Mulder et al. and Wijmans et al. concluded that for these systems the position of the binodal is mainly determined by the interaction between non-solvent and polymer. When the affinity increases (i.e., $\chi_{13}$ decreases), more non-solvent is required to induce phase separation. The swelling experiments for polyimide have shown that the affinity (i.e., swelling) between PI and ethanol is higher than the affinity between PI and water, which is in agreement with the results presented above.

The ethanol permeability of several membranes, coagulated in ethanol and water, did not show significant differences (see figure 11 and table 6). On the other hand, the pore size distributions of these membranes in the dry state are different (see table 7 and chapter 4): ethanol as non-solvent results in broader dry-state pore size distributions than water, and the maxima of the peaks are located at lower pore radii in the case of water. Comparison of the nitrogen fluxes also shows some differences (see figure 12). These dry-state properties are very difficult to explain, because the drying procedure will change the pore size distribution irreversibly. Therefore, differences between membranes in the wet-state are more significant. Additional research is necessary, using wet-state characterization techniques to achieve information on the pore size distributions of these membranes in relation to the non-solvent used.

A 20 wt% solution of PI in DMF (containing 5 wt% glycerol) was used to cast membranes, that were coagulated in different alcohols at 25°C, i.e., methanol, ethanol, n-propanol, and n-butanol. All these membranes were formed by instantaneous demixing. The permeability results are given in table 8, and it can be seen that the membranes became less permeable by coagulation in higher alcohols.
In table 8 also results are presented that were obtained by light transmission experiments of 20 wt% PI in DMF, coagulated in 75 vol% DMF + 25 vol% alcohol at 25°C. The values for $t_{25/75}$ represent the times necessary for the respective membranes to go from 25% relative intensity decrease to 75% relative intensity decrease. The value of $t_{25/75}$ increases with increasing alcohol length, which

means that the higher the alcohol, the slower the diffusion front proceeds across the membrane.

*Table 8.* *Influence of non-solvents from a series of alcohols on the ethanol permeability of the final membranes, compared with the demixing velocity (represented by the time necessary for a casting solution immersed in 75/25 DMF/NS to go from 25% intensity decrease to 75% intensity decrease).*

| non-solvent | ethanol permeability [kg/m$^2$ hr bar] | $t_{25/75}$ [s] |
|---|---|---|
| methanol | 312 | 156 |
| ethanol | 256 | 180 |
| n-propanol | 172 | 246 |
| n-butanol | 35 | 300 |

There may be two effects responsible for this slower demixing process (that is still instantaneous). Firstly, the decreasing polarity of higher alcohols might cause the non-solvent/solvent affinity to decrease, thus the interaction parameter $g_{12}$ to increase. Unfortunately, in literature there are no experimental data available in order to calculate $g_{12}$ for DMF combined with $C_1$-$C_4$-alcohols. Secondly, higher alcohols will have a lower diffusion coefficient, so that the indiffusion of non-solvent into the nascent membrane will be lower for higher alcohols. Both effects will cause the membranes to become less permeable for ethanol, purely by differences in morphology.

In addition, in this homologue series of non-solvents differences in swelling may even enlarge the differences in ethanol permeability. An example: the ethanol permeability of a membrane coagulated in methanol is higher than that for a similar membrane coagulated in ethanol. The swelling value of polyimide in methanol (>12%) is higher than the swelling in ethanol (8%). The polymeric matrix of a membrane coagulated in methanol will shrink upon storage in ethanol, thus the pores may become larger. On the other hand, membranes coagulated in higher alcohols such as propanol and butanol (which have a low swelling value for PI) will swell upon storage in ethanol, and therefore have a lower ethanol permeability.
However, two remarks have to be made. Firstly, the swelling values summarized in table 2 are not equilibrium swelling values. Secondly, this comparison is only valid for non-solvents that do not differ much in non-solvent/solvent interactions, which means that water as a non-solvent can not be compared in this way to the homologue series of alcohols.

Anyway, the choice of the non-solvent is shown to be an important formation parameter to vary the ethanol permeability of the membranes.

### 2.6.4 Influence of the coagulation bath temperature

It is expected that a higher temperature of the coagulation bath increases the diffusion coefficients during the membrane formation process (especially the non-solvent indiffusion), so that more permeable membranes are obtained. An increase in coagulation bath temperature resulted in a small increase in ethanol permeability, while the morphology of the sublayer did not change as deduced from SEM-photographs.
The temperature of the nascent film during precipitation is difficult to determine, since all non-solvent/solvent combinations used here show exothermic mixing behaviour, the temperature at the interface bath/film will increase. Consequently, this may affect the rate of diffusion of solvent and non-solvent. Nevertheless, the influence of the temperature on the membrane performance is much smaller than, e.g., the influence of the polymer concentration or the type of non-solvent.

## 2.7 Conclusions

The soluble polyimide P84 was found to have a high chemical resistance. It is well soluble in amides, and insoluble and poorly swelling in almost all other organic media. The low-swelling behaviour implies that this polyimide is very suitable for the preparation of porous membranes for non-aqueous applications.
Membranes cast from DMF-solutions were less brittle and fragile than membranes from NMP- or DMAc-solutions. A difference in the structure of the layer beneath the toplayer probably is responsible for this difference in integrity. An explanation for this difference on the basis of preparation parameters has not yet been found, in part due to the fact that quantitative $g_{12}$-data appeared rather unreliable. The effect of the choice of solvent on the toplayer morphology could be explained reasonably well by qualitative differences in ternary diffusion coefficients.
With water and ethanol as non-solvents only minor differences in ethanol permeability were observed. However, permporometry and gas flux measurements indicate that the pore size distributions of the toplayers in the dry state are rather different. This phenomenon may also be caused by differences in non-solvent/solvent interaction, combined with differences in driving forces and binary diffusion coefficients. Membranes from DMF-solutions that are coagulated in ethanol are less brittle than similar membranes coagulated in water. A difference in structure beneath the toplayer is responsible for this

difference in brittleness.
The effect of a series of alcohols on the demixing behaviour and the ethanol permeability of the final membranes also has been investigated. The higher the alcohol, the slower is the demixing process (probably by a higher $g_{12}$ and lower diffusion coefficients) and the less permeable the toplayer.
The influence of the polymer concentration in the casting solution was found to be consistent with theory. The effect of temperature was only of minor importance compared to the effect of polymer concentration. The polymer concentration was found to be the most important parameter to obtain membranes in a wide range of ethanol permeabilities.

## 2.8 References


[1] R.A. McCarthy; Chemically resistant polymers; H.F. Mark, N.M. Bikales, C.G. Overberger, G. Menges (Eds.); Encyclopedia of polymer science and engineering; J. Wiley, New York, 1985; Vol. 3, p. 412

[2] J. Hildebrand, R. Scott; The solubility of non-electrolytes; Reinhold Publ. Corp., New York, 1949 (3rd edition)

[3] C.M. Hansen; The three-dimensional solubility parameter - key to paint-component affinities: 1. solvents, plasticizers, polymers, and resins; J. Paint Technol., 39(1967)104

[4] A.F.M. Barton; Handbook of solubility parameters and other cohesion parameters; 2nd edition, CRC press, Boca Raton, 1991

[5] K.E. Kinzer, D.R. Lloyd, M.S. Gay, J.P. Wightman, B.C. Johnson, J.E. McGrath; Phase inversion sulfonated polysulfone membranes; J. Membrane Sci., 22(1985)1

[6] E. Klein, J.K. Smith; The use of solubility parameters for solvent selection in asymmetric membrane formation; H.K. Lonsdale, H.E. Podall (Eds.); Reverse osmosis membrane research; Plenum Press, New York, 1972

[7] H.-R. Lee, Y.-D. Lee; Solubility of an organic soluble polyimide; J. Appl. Polym. Sci., 40(1990)2087

[8] A.F.M. Barton; Handbook of polymer-liquid interaction parameters and solubility parameters; CRC Press, Boca Raton, 1990

[9] D.W. van Krevelen; Properties of polymers. Their correlation with chemical structure, their numerical estimation and prediction from additive group contributions; 3rd edition, Elsevier, Amsterdam, 1990

[10] J. Brandrup, E.H. Immergut; Polymer Handbook; 3rd edition, Wiley, New York, 1989

[11] D.M. Koenhen, C.A. Smolders; The determination of solubility parameters of solvents and polymers by means of correlations with other physical quantities; J. Appl. Polym. Sci., 19(1975)1163

[12] R.P. Brown; Handbook of plastics test methods; Longman, London, 1988, p. 345

[13] American Society for Testing and Materials; Standard test method for resistance of plastics to chemical reagents; test D543-84, Annual book of ASTM standards, 1987, Vol. 08.01

[14] W.J. Koros, M.W. Hellums; Transport properties; H.F. Mark, N.M. Bikales, C.G. Overberger, G. Menges (Eds.); Encyclopedia of polymer science and engineering; J. Wiley, New York, 1985; Supplement, p. 771

[15] International Plastics Selector; D.A.T.A. Digest, edition 12 (1991); Vol. 1, P. A-101

[16] H.W. Hill, D.G. Brady; Polyarylenesulfides; H.F. Mark, N.M. Bikales, C.G. Overberger, G. Menges (Eds.); Encyclopedia of polymer science and engineering; J. Wiley, New York, 1985; Vol. 11, p 531

[17] R.E. Kesting; Synthetic polymeric membranes; McGraw Hill, New York, 1971; p 20

[18] R.A. Orwoll; Solubility of polymers; H.F. Mark, N.M. Bikales, C.G. Overberger, G. Menges (Eds.); Encyclopedia of polymer science and engineering; J. Wiley, New York; Vol. 15, p 380

[19] J.A. Brydson; Plastics materials, 5th edition; Butterworths, London, 1989

[20] P.E. Cassidy; Thermally stable polymers; Dekker, New York, 1980

[21] J.P. Critchley, G.J. Knight, W.W. Wright; Heat resistant polymers; Plenum, New York, 1983

[22] S. Rosenbaum; Polyacrylonitrile fiber behaviour. 2. Dependence on structure and environment; J. Appl. Polym. Sci., 9(1965)2085

[23] Z. Gur-Arieh, W. Ingamells, R.H. Peters; The effect of plasticizing compounds on acrylic fibers; J. Appl. Polym. Sci., 20(1976)41

[24] G. Henrici-Olivé, S. Olivé; Molecular interactions and macroscopic properties of polyacrylonitrile and model substances; Adv. Polym. Sci., 32(1979)123

[25] C.R. Moylan, M. Evans Best, M.Ree; Solubility of water in polyimides: quartz crystal microbalance measurements; J. Polym. Sci., B, Polym. Phys., 29(1991)87

[26] H. Pranjoto, D.D. Denton; Gravimetric measurements of steady-state moisture uptake in spin-coated polyimide films; J. Appl. Polym. Sci., 42(1991)75

[27] B.S. Lim, A.S. Nowick, K.-W. Lee, A. Viehbeck; Sorption of water and organic solutes in polyimide films and its effect on dielectric properties; J. Polym. Sci., B, Polym. Phys., 31(1993)545

[28] D. Wilson, H.D. Stenzenberger, P.M. Hergenrother; Polyimides; Blackie, Glasgow, 1990

[29] W.M. Edwards, I.M. Robinson; Polyimides of pyromellitic acid; US 2,710,853; 1955

[30] W.F. Gresham, M.A. Naylor; Polyimide intermediates; US 2,712,543; 1955

[31] L.M. Alberino; Mischpolyimide; Ger. DE 2143080; 1971

[32] E. Wanek, J. Baumgartinger; Verfahren zur herstellung von hochtemperaturbeständigen polymerisaten in pulverform sowie anlage zur durchführung des verfahrens; AT-OS 387.227; 1988

[33] K. Weinrotter, S. Seidl; Produkte aus aromatischen Polyimiden; Ö. Chem. Z. , 7-8(1990)228

[34] K. Weinrotter; Properties and applications of the new polyimide fiber P84; Polyimides, synthesis, characterization and application; Proc. 2nd Intern. Conf. on polyimides, New York, 1985; p. 253

[35] J. Bateman, D.A. Gordon; Soluble polyimides derived from phenylindane diamines and dianhydrides; US 3.856.752; 1974

[36] F.W. Harris, L.H. Lanier; Structure-solubility relationships in polyimides; F.W. Harris, R.B. Seymour (Eds.); Structure-solubility relationships in polymers; Academic Press, New York, 1977; p. 183

[37] T.L. StClair, A.K. StClair, E.N. Smith; Solubility-structure study of polyimides; F.W. Harris, R.B. Seymour (Eds.); Structure-solubility relationships in polymers; Academic Press, New York, 1977; p. 199

[38] T.L. StClair, A.K. StClair, E.N. Smith; Solubility properties of novel polyimides; Polym. Prepr., 17(2)(1976)359

[39] C.E. Sroog; Polyimides; J. Polym. Sci., Macromol. Rev., 11(1976)161

[40] J.-K. Lin, Y. Yuki, H. Kunisada, C. Miyagawa, S. Kondo; Synthesis and characterization of new comb-like aromatic polyamides, polyimides, and polyureas containing 1,3,5-triazine rings in their side chains; Polym. J., 21(1989)709

[41] J.-K. Lin, Y. Yuki, H. Kunisada, S. Kondo; Synthesis and characterization of new aromatic polyamides, polyimides, and polyureas containing 1,3,5-triazine rings; J. Appl. Polym. Sci., 40(1990)2113

[42] H.-J. Jeong, Y. Oishi, M.-A. Kakimoto, Y. Imai; Synthesis and characterization of new soluble aromatic polyimides from 3,4-bis(4-aminophenyl)-2,5-diphenylfuran and aromatic tetracarboxylic dianhydrides; J. Polym. Sci., Polym. Chem., 29(1991)39

[43] H. Sheffer; Cresylic soluble polyimides; J. Appl. Polym. Sci., 26(1981)3837

[44] F.W. Harris, W.A. Feld, L.H. Lanier; Structure-solubility relationships in aromatic polyimides; Polym. Prepr., 17(2)(1976)353

[45] F. Akutsu, S. Kuze, K. Matsuo, K. Naruchi, M. Miura; Preparation of polyimides from 2,3-bis(4-aminophenyl)quinoxalines and aromatic tetracarboxylic dianhydrides; Makromol. Chem., Rapid Commun., 11(1990)673

[46] M. Ghosh; Heat resistant polyamideimides. 3. Synthesis, characterization and evaluation of thermal and other properties; Angew. Makromol. Chem., 172(1989)165

[47] M.I. Bessonov, M.M. Koton, V.V. Kudryavtsev, L.A. Laius; Polyimides: thermally stable polymers; Consultants bureau, New York, 1987

[48] C.J. Lee; Polyimides, polyquinolines, and polyquinoxalines: Tg-structure relationships; J. Macromol. Sci.-Rev. Macromol. Chem. Phys., 29(4)(1989)431

[49] E. Smit, H.A. Teunis, R.M. Meertens, K.M.P. Kamps, B.A.M. Venhoven, M.H.V. Mulder, C.A. Smolders; Diffusion of carbon dioxide through membranes of novel polyimides: relation between diffusivity D and heat capacity jump, $\Delta C_p$, at $T_g$; Proc. Int. Conf. on membranes and membrane processes, ICOM '90, Chicago, U.S.A., august 1990; p. 786

[50] E. Smit, M.H.V. Mulder, C.A. Smolders, H. Karrenbeld, J. van Eerden, D. Feil; Modelling of the diffusion of carbon dioxide in polyimide matrices by computer simulation; J. Membrane Sci., 73(1992)247

[51] W.J. Koros, G.K. Fleming; Membrane-based gas separation; J. Membrane Sci., 83(1993)1-80

[52] S.A. Stern, Y. Mi, H. Yamamoto, A.K. St. Clair; Structure/permeability relationships of polyimide membranes. Applications to the separation of gas mixtures; J. Polym. Sci., B, Polym. Phys., 27(1989)1887

[53] H. Yamamoto, Y. Mi, S.A. Stern, A.K. St. Clair; Structure/permeability relationships of polyimide membranes. 2; J. Polym. Sci., B, Polym. Phys., 28(1990)2291

[54] M.I. Bessonov, V.A. Zubkov; Polyamic acids and polyimides. Synthesis, transformations, and structure; CRC Press, Boca Raton, 1993

[55] H. Strathmann; Asymmetric polyimide membranes for filtration of non-aqueous solutions; Desalination, 26(1978)85

[56] W. Schumann, H. Strathmann; Polyimide membrane and process for making same; US 3.925.211; 1975

[57] L.E. Black, H.A. Boucher; Process for separating alkylaromatics from aromatic solvents and the separation of the alkylaromatic isomers using membranes; US 4.571.444; 1986

[58] M.M. Hafez, L.E. Black; Membrane separation of unconverted carbon fiber precursors from flux solvent and/or antisolvent; US 4.606.903; 1986

[59] L.E. Black, P.G. Miasek, G. Adriaens; Aromatic solvent upgrading using membranes; US

4.532.029; 1985

[60] H.F. Shuey, W.Wan; Asymmetric polyimide reverse osmosis membrane, method for preparation of same and use thereof for organic liquid separations; EP 125.908; 1984

[61] M.N. Sarbolouki; Properties of asymmetric polyimide ultrafiltration membranes. 1. Pore size and morphology characterization; J. Appl. Polym. Sci., 29(1984)743

[62] B. Dong, K. Zhu; Preparation and properties of polyimide ultrafiltration membranes; J. Membrane Sci., 60(1991)63

[63] A. Iwama, Y. Kazuse; New polyimide ultrafiltration membranes for organic use; J. Membrane Sci., 11(1982)297

[64] Y. Isooka, Y. Imamura, Y. Sakamoto; Recovery and reuse of organic solvent solutions; Metal Finishing, 82(1984)113

[65] Nitto non-aqueous tubular UF module for treating organic solutions; commercial brochure

[66] M.H.V. Mulder; Basic priciples of membrane technology; Kluwer, Dordrecht, 1992

[67] J.W. Cahn; Phase separation by spinodal decomposition in isotropic systems; J. Chem. Phys., 42(1965)93

[68] J.J. van Aartsen; Theoretical observations on spinodal decomposition of polymer solutions; Eur. Polym. J., 6(1970)919

[69] C.A. Smolders, J.J. van Aartsen, A. Steenbergen; Liquid-liquid phase separation in concentrated solutions of non-crystallizable polymers by spinodal decomposition; Koll. Z. u. Z. Pol., 243(1971)14

[70] A.J. Reuvers, C.A. Smolders; Formation of membranes by means of immersion precipitation. 2. The mechanism of formation of membranes prepared from the system cellulose acetate-acetone-water; J. Membrane Sci., 34(1987)67

[71] C.A. Smolders, A.J. Reuvers, R.M. Boom, I.M. Wienk; Microstructures in phase-inversion membranes. Part 1. Formation of macrovoids; J. Membrane Sci., 73(1992)259

[72] M.A. Frommer, R.M. Messalem; Mechanism of membrane formation. 4. Convective flows and large void formation during membrane precipitation; Ind. Eng. Chem. Prod. Res. Dev., 12(1973)328

[73] R. Matz; The structure of cellulose acetate membranes. 1. The development of porous structures in anisotropic membranes; Desalination, 10(1972)1

[74] R.J. Ray, W.B. Krantz, R.L. Sani; Linear stability theory model for finger formation in asymmetric membranes; J. Membrane Sci., 23(1985)155

[75] H. Strathmann, K. Kock, P. Amar, R.W. Baker; The formation mechanism of asymmetric membranes; Desalination, 16(1975)179

[76] L. Broens, F.W. Altena, C.A. Smolders; Asymmetric membrane structures as a result of phase separation phenomena; Desalination, 32(1980)33

[77] V. Gröbe, G. Mann, G. Duwe; Ausbildung von strukturen bei der koagulation von polyacrylnitrillösungen; Fasenforsch. Textiltechn., 17(1966)142

[78] A.J. Reuvers; Membrane formation. Diffusion induced demixing processes in ternary polymeric systems; Ph.D. thesis, University of Twente, 1987

[79] R.M. Boom, I.M. Wienk, Th. van den Boomgaard, C.A. Smolders; Microstructures in phase inversion membranes. Part 2. The role of a polymeric additive; J. Membrane Sci., 74(1992)277

[80] R.M. Boom, H.H.M. Rolevink, Th. van den Boomgaard, C.A. Smolders; Microscopic structures in phase inversion membranes: the use of polymer blends for membrane formation by immersion precipitation; Makromol. Chem., Macromol. Symp., 69(1993)133

[81] I.M. Wienk, Th. van den Boomgaard, C.A. Smolders; The formation of nodular structures in

the toplayer of ultrafiltration membranes; accepted for publication in J. Appl. Polym. Sci.

[82] S. Li; Preparation of hollow fiber membranes for gas separation; Ph.D. thesis, University of Twente, 1993

[83] I. Pinnau, W.J. Koros; A qualitative skin layer formation mechanism for membranes made by dry/wet phase inversion; J. Polym. Sci., B, Polym. Phys., 31(1993)419

[84] F.W. Altena, C.A. Smolders; Calculation of liquid-liquid phase separation in a ternary system of a polymer in a mixture of a solvent and a nonsolvent; Macromolecules, 15(1982)1491

[85] J. Wisniak, A. Tamir; Mixing and excess thermodynamic properties; Elsevier, Amsterdam, 1978

[86] A. Bottino, G. Capanelli, S. Munari, A. Turturro; Thermodynamic approach to prepare asymmetric membranes of poly(vinylidene fluoride); B. Sedlacek, J. Kahovec (Eds.); Synthetic polymeric membranes; Walter de Gruyter, Berlin, 1987; p. 141

[87] T.P. Ventoza, D.R. Lloyd; Poly(ether sulfone) membranes for desalination: membrane preparation and characterization; Desalination, 56(1985)381

[88] K.E. Kinzer, D.R. Lloyd, J.P. Wightman, J.E. McGrath; Asymmetric membrane preparation from nonsolvent casting systems; Desalination, 46(1983)327

[89] C.M. Tam, M. Dal-Cin, M.D. Guiver; Polysulfone membranes. 4. Performance evaluation of Radel A/PVP membranes; J. Membrane Sci., 78(1993)123

[90] L. Zeman, G. Tkacik; Thermodynamic analysis of a membrane-forming system water/n-methyl-2-pyrrolidone/polyethersulfone; J. Membrane Sci., 36(1988)119

[91] S. Li, C. Jiang, Y. Zhang; The investigation of solution thermodynamics for the polysulfone-DMAc-water system; Desalination, 62(1987)79

[92] T.M. Lesteva, G.I. Logunova; Zh. Prikl. Khim. (Leningrad), 52(1979)1986; summarized in: Vapour-liquid equilibria; Dechema Data series

[93] L.A. Rogozilnikova; Fazov. Ravnovesiya I Prakt. Aspekty Protsessov Razdelneya Produktov; (1980)117; summarized in: Vapour-liquid equilibria; Dechema Data series

[94] S. Saphon, H.-J. Bittrich; Physikalisch-chemische untersuchungen in binären systemen von dimethylformamid mit äthylenglykol, diäthylenglykol und wasser; Z. Phys. Chemie Leipzig, 252(1973)113

[95] A. Carli, S. Di Cave, E. Sebastiani; Thermodynamic characterization of vapour-liquid equilibria of mixtures acetic acid-dimetylacetamide and water-dimethylacetamide; Chem. Eng. Sci., 27(1972)993

[96] G. Tkacik, L. Zeman; Component mobility analysis in the membrane-forming system water/n-methyl-2-pyrrolidone/polyethersulfone; J. Membrane Sci., 31(1987)273

[97] P.G. de Gennes; Scaling concepts in polymer physics; Cornell University Press, New York, 1979

[98] F.P. Cuperus, D. Bargeman, C.A. Smolders; Permporometry. The determination of the size distribution of active pores in UF membranes; J. Membrane Sci., 71(1992)57

[99] L. Zeman, T. Fraser; Formation of air-cast cellulose acetate membranes. Part 1. Study of macrovoid formation; J. Membrane Sci., 84(1993)93

[100] M.H.V. Mulder, J. Oude Hendrikman, J.G. Wijmans, C.A, Smolders; A rationale for the preparation of asymmetric pervaporation membranes; J. Appl. Polym. Sci., 30(1985)2805

[101] J.G. Wijmans, J. Kant, M.H.V. Mulder, C.A. Smolders; Phase separation phenomena in solutions of polysulfone in mixtures of a solvent and a non-solvent: relationship with membrane formation; Polymer, 26(1985)1539

# Chapter 3

## Preparation of polyimide ultrafiltration membranes Part 2. Quaternary systems: the effect of low molecular weight additives

M.A.M. Beerlage, J.A.M. Nolten, R.M. Meertens, M.H.V. Mulder, C.A. Smolders, H. Strathmann

**Summary**

Low molecular weight aliphatic dicarboxylic acids have been used as additives for the membrane-forming system with polyimide as polymer, dimethylformamide as solvent, and water or ethanol as non-solvents. It is shown that some of these additives are effective in suppressing the formation of macrovoids. Furthermore, they affect the pore size distribution of the membrane.
Turbidity measurements have been carried out to determine cloud point curves for these quaternary systems. Membranes prepared from quaternary systems have been characterized by scanning electron microscopy, ethanol permeability measurements and permporometry.
A mechanism is proposed to explain the role of these additives on the macrovoid formation and on the membrane toplayer formation.

## 3.1 Introduction

In chapter 2, it has been shown that polyimide (PI) membranes prepared from solutions in dimethylformamide (DMF) and coagulated in ethanol gave less macrovoids, compared with coagulation in water. A known method to suppress the formation of macrovoids is the addition of polyvinylpyrrolidone to polymeric casting solutions [1]. However, this second polymer will be partly trapped in the membrane matrix. Polyvinylpyrrolidone has a much lower chemical resistance than polyimide. Since our objective is to develop membranes for non-aqueous applications, addition of polyvinylpyrrolidone is not an option. However, other additives may be employed.

In this chapter, the influence of the addition of low molecular weight aliphatic dicarboxylic acids to the casting solutions of PI in DMF will be discussed. Especially macrovoid formation and the membrane pore size distribution as a function of the type of additive will be investigated.

## 3.2 Theoretical background

### 3.2.1 Metal salts and formamide as additives to the casting solution

Already in 1950, Biget described the preparation of cellulose acetate (CA) desalination membranes, from aqueous solutions containing metal perchlorate salts [2]. Based on this work, Loeb and Sourirajan [3] prepared CA-membranes from a casting solution of acetone as solvent with magnesium perchlorate and water as additives. Since then, several researchers added small amounts of various salts to cellulose acetate casting solutions to improve the water flux of the resulting membranes.
Keilin [4,5] postulated that salts "swell" cellulose acetate by complexation between the strongly hydrated cations and the nucleophilic hydroxyl and acetate groups of cellulose acetate. He also showed that after rinsing the membranes, the salts were removed completely. The presence of salts during membrane preparation induces the formation of a more open porous membrane network. This mechanism has also been described by Kesting [6].
Manjikian used formamide as additive instead of water and magnesium perchlorate [7]. The membrane performance was similar, formamide is also a swelling agent for CA.

Kesting and Menefee [8] and later Kunst et al. [9] proposed a membrane formation mechanism based on the assumption that supermolecular aggregates are already present in the casting solution, before the immersion step. These

aggregates are larger when the solution composition is located closer to the binodal, which could be induced by the presence of a casting additive. The nature of these aggregates was not defined. It was also suggested, that inside the aggregates the polymer molecules "dissociate" and exist as individual molecules. However, polymer chains in concentrated polymer solutions are highly entangled but do not form aggregates, because this latter phenomenon only occurs by the nucleation and growth mechanism if the composition is brought inside the binodal. Therefore, the mechanism of changing the aggregate size by the additive is without meaning for solutions of polymers. In addition, characteristics obtained for cellulose acetate systems can be very different when compared with systems of other polymers.

A general mechanism to describe the effect of low molecular weight additives on the membrane formation process does not exist, because these effects are very system specific. Additives may have an effect on the following factors: they may

- change the viscosity of the casting solution
- shift the position of the binodal
- cause specific interactions between polymer and additive, solvent and additive, coagulant and additive
- change the diffusion rate of the non-solvent into the casting solution
- change the diffusion rate of the solvent into the coagulation bath
- influence the solidification process of the membrane (influence on $T_g$, crystallization, toplayer formation, etc.)

Upon addition of low molecular weight components to the casting solution, the membrane formation process will be altered by a combination of the effects mentioned above.

A broad range of chemicals has been used as additives in CA-solutions. Most of these studies are based on the swelling mechanism suggested by Keilin and Kesting, where additives have been considered as swelling agents for the aggregates in solution. With the use of other membrane polymers, the search for "flux-increasing" additives still continued. Some researchers adapted the casting solution aggregate formation mechanism, e.g., Fan et al. for polysulfonamide [10], Hou et al. for polysulfone [11], Kraus et al. for polyamide [12]. Nevertheless, most studies on low molecular weight additives are based on trial-and-error procedures.

Kesting et al. [13,14] used additives from a group of Lewis acids (monofunctional acids) for the preparation of so-called "second generation" gas separation membranes from polysulfone. These are non-solvents for the polymer, but they can form transient Lewis acid:base complexes with the solvent NMP. It was shown that the high molar volume of these complexes decreases the polymer

packing density inside coalesced nodules, which results in a higher free volume and a higher gas permeability of the membrane. The complexes are hydrolytically unstable, they disintegrate upon contact with water. In this way, the diffusion processes during immersion precipitation will not be hindered, which would be the case when a solvent is used that has a high molar volume itself.

### 3.2.2 Dicarboxylic acids as additives

The use of dicarboxylic acids as additives, especially maleic acid, has been mentioned for cellulose acetate in several reports of the Office of Saline Water [15-17]. The addition of dicarboxylic acids increases the permeability of the final membrane, but an explanation was not given in any of these reports. However, King et al. [18,19] suggested that the dicarboxylic acids form hydrogen bonds with the ketone and hydroxyl groups of CA, thereby acting as "swelling agents".
Bokhorst et al. [20] performed phase separation experiments using cellulose acetate with dioxane, methanol, water and maleic acid (< 6 wt%). They found that with an increase in maleic acid concentration, the solution requires more non-solvent to demix, i.e., the binodal has been shifted to the polymer/non-solvent axis.
Vásárhelyi et al. [21] compared the membrane formation process of cellulose acetate/cellulose triacetate/acetone/dioxane/water with and without the addition of maleic acid, based on a patent by Wafilin [22]. Light transmission experiments with the additive-containing system showed a two-step curve, which has been ascribed to the formation of polymer aggregates. SEM-photographs of these membranes showed in the case of the additive-containing system a very porous intermediate layer between the membrane toplayer and the sublayer. It has been suggested that this aggregate formation is similar to polymer crystallization effects. Titration experiments showed that maleic acid preferentially remained in the polymer-rich phase during phase separation by immersion precipitation, probably through hydrogen bonding between CA and maleic acid.
Ronner et al. [23] examined the same system by Pulse Induced Critical Scattering (PICS). They also concluded that the aggregates are induced by crystallization. The addition of maleic acid causes a decrease in the size of the demixing gap; perhaps this offers a greater chance for crystal nucleation to take place. That crystallization may play an important role is also indicated by time-dependent effects [21,23]. The casting solutions must be used immediately, and the "cloud points" are very much dependent on time and temperature. This means that the function of maleic acid as additive is not simply that of a swelling agent, as suggested by Vásárhelyi et al.
Friedrich et al. [24] added several acids to casting solutions of sulfonated polysulfone, like acetic, glycolic, lactic, malonic, maleic, succinic, and tartaric acid.

They found that these additives cause an increase in water permeability of reverse osmosis membranes, and small enhancements or decreases in salt retention, which was caused by an increase in casting solution viscosity. However, it is very likely that the charged sulfonate groups are strongly swollen by the acids, so that the acids may be partial solvents for the sulfonated polysulfone.

### 3.3.3 Scope of this chapter

All the literature data mentioned above concern the preparation of dense reverse osmosis or gas separation membranes. In this chapter, the influence of a series of low molecular weight aliphatic dicarboxylic acids as additives on the preparation of polyimide ultrafiltration membranes will be discussed; especially the macrovoid-suppressing effect of certain dicarboxylic acids on the membrane sublayer can be very strong, as will be shown. Furthermore, the effect of these additives on the pore size distributions of the membranes will be investigated.

## 3.4 Experimental

### 3.4.1 Materials

Polyimide P84 (Lenzing AG, Austria; 325 mesh, chargenr. 8170914) was kindly supplied by X-Flow BV. Dimethylformamide (DMF) was purchased from Merck (analytical grade) and used as received. Technical grade ethanol and demineralized water have been used as coagulation bath media. The casting additives were purchased from Merck or Aldrich; they were of the highest purity grade available and used as received.

### 3.4.2 Membrane preparation

The preparation of membranes from ternary systems has already been described in detail in chapter 2. For membranes from quaternary systems (i.e., with an additive), the casting solution additive was dissolved completely in DMF, after which the dried polyimide was added to prepare a homogeneous solution.

### 3.4.3 Membrane characterization techniques

The presence of macrovoids in the sublayers of the membranes was investigated by Scanning Electron Microscopy (SEM).
Ethanol flux measurements were performed for all prepared membranes.
Dry-state pore size distributions were determined by permporometry. For this purpose the membranes were dried according to an ethanol-hexane-air

displacement sequence. Permporometry as a characterization technique will be discussed in more detail in chapter 4.

### 3.4.4 Cloud point measurements

Cloud point data have been determined for ternary and quaternary systems with ethanol as non-solvent with a simple titration method. A mixture of DMF and ethanol was added dropwise and very slowly to a stirred polymer solution in a closed vessel at 25°C. Because the solutions had a dark brown colour, it was not possible to observe inhomogeneities visually. Therefore, the vessels were covered with black tape, a small light source was placed on one side of the vessel and a light sensor on the other side. Inhomogeneities could be detected very easily by means of this method by a sharp decline in light transmittance; when this decline was observed, the solution was allowed to homogenize before a new addition of solvent/non-solvent mixture was carried out.
It is assumed that the cloud point is reached when the solution was still turbid after two days following the last addition step. These cloud point compositions were plotted in a pseudo-ternary phase diagram (PI/DMF/ethanol), by "excluding" this additive fraction. The concentration at the cloud point was between 2.5-3.5 wt% for all additives.

## 3.5 Results

### 3.5.1 Presence of macrovoids in the membrane sublayer

Membranes with many macrovoids are more brittle and showed more defects than membranes without macrovoids. Experimental results presented in chapter 2 also showed, that the formation of macrovoids can be suppressed during the immersion precipitation process by an increase of the polymer concentration in the casting solution, and by coagulation in ethanol instead of water.
It has been found experimentally, that the addition of a few weight% of some additives to the casting solution is also very effective in suppressing macrovoid formation, even for membranes coagulated in water. Therefore, SEM-investigation has been used to compare various membranes, prepared from a 20 weight% PI solution in DMF without additive or with 3 weight% additive, and coagulated in ethanol or water.
A series of dicarboxylic acids has been used as additives. Furthermore, ethanol, glycerol, and acetic acid were used as reference additives. The chemical structures of these additives are given in figure 1.

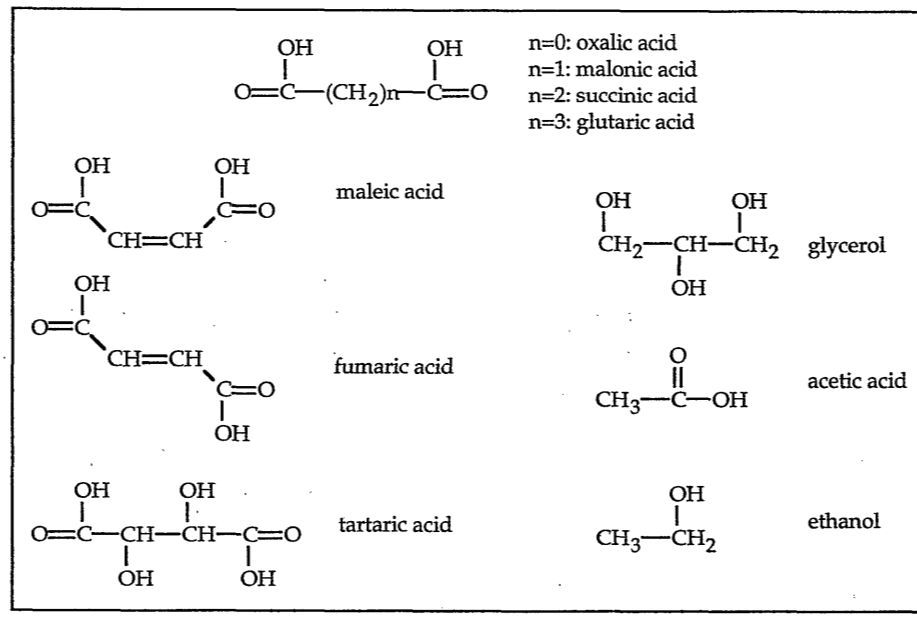


*Figure 1. Chemical structures of additives used in the casting solutions of polyimide in DMF.*

A qualitative comparison of the presence of macrovoids for different membranes is given in figure 2. The membranes that were prepared from casting solutions containing oxalic acid showed the lowest number of macrovoids, for coagulation in water and ethanol.

*membranes coagulated in ethanol:* ⟶ decreasing macrovoid formation

ethanol > no additive / fumaric acid / glutaric acid > malonic acid / succinic acid / acetic acid > glycerol > maleic acid / tartaric acid > oxalic acid

*membranes coagulated in water:* ⟶ decreasing macrovoid formation

no additive / malonic acid / glycerol > maleic acid / fumaric acid / succinic acid / acetic acid > tartaric acid / ethanol > glutaric acid > oxalic acid

*Figure 2. Qualitative comparison of presence of macrovoids for membranes coagulated in ethanol or water, respectively.*

As an illustrative example four different membranes are given in figure 3, which

shows scanning electron micrographs of various membranes cross sections. These membranes were prepared from a 20 wt% PI-solution in DMF without additives (figures 3.a and 3.b), and from a 20 wt% PI-solution in DMF with 3 wt% oxalic acid (figures 3.c and 3.d). The upper photographs represent membranes coagulated in ethanol, the lower photographs represent membranes coagulated in water. It is obvious from these figures that the number of macrovoids has been decreased drastically by the presence of oxalic acid in the casting solution.

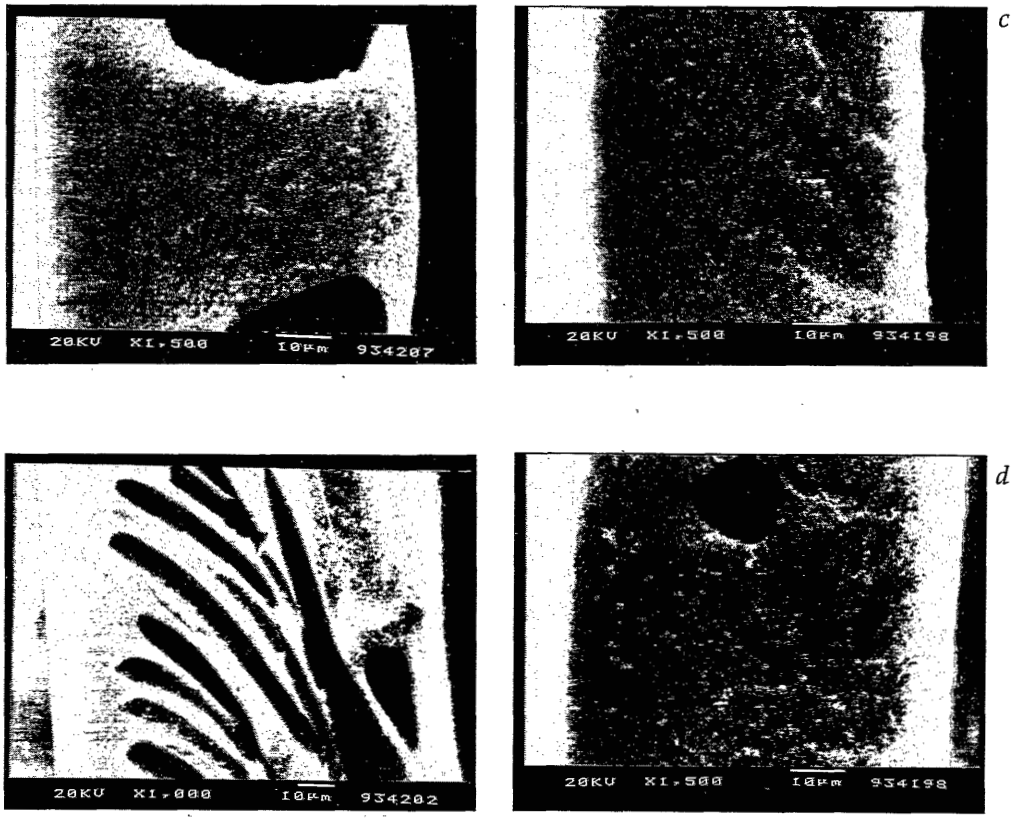


***Figure 3.*** *Scanning Electron Micrographs of membranes prepared from a 20 wt% casting solution of PI in DMF. Fig. a: no additive, coagulation in ethanol, fig. b: no additive, coagulation in water, fig. c: 3% oxalic acid, coagulation in ethanol, fig. d: 3% oxalic acid, coagulation in water.*

### 3.5.2 Influence of additives on ethanol permeability

The ethanol permeabilities of the different membranes have been determined and the results are given in table 1. For two additives, oxalic acid and fumaric acid, the ethanol permeability was determined as a function of the additive concentration in the casting solution. These results are presented in table 2.

*Table 1.* *Ethanol permeability of membranes prepared from a 20 wt% PI solution in DMF.*

| *non-solvent ethanol* | | *non-solvent water* | |
|---|---|---|---|
| additive | $P_{ethanol}$ [kg/m$^2$hr bar] | additive | $P_{ethanol}$ [kg/m$^2$hr bar] |
| no additive | 291 | 3% ethanol | 307 |
| 3% succinic acid | 282 | no additive | 258 |
| 3% glutaric acid | 278 | 3% glycerol | 255 |
| 3% malonic acid | 275 | 3% glutaric acid | 254 |
| 3% ethanol | 274 | 3% tartaric acid | 246 |
| 3% glycerol | 274 | 3% malonic acid | 229 |
| 3% tartaric acid | 247 | 3% succinic acid | 225 |
| 3% acetic acid | 231 | 3% maleic acid | 214 |
| 3% maleic acid | 185 | 3% acetic acid | 197 |
| 3% fumaric acid | 156 | 3% oxalic acid | 173 |
| 3% oxalic acid | 64 | 3% fumaric acid | 169 |

*Table 2.* *Influence of additive concentration on ethanol permeability for membranes coagulated in ethanol and water.*

| casting solution | mol. ratio PI/additive [mol/mol] | *non-solvent ethanol* $P_{ethanol}$ [kg/m$^2$hr bar] | *non-solvent water* $P_{ethanol}$ [kg/m$^2$hr bar] |
|---|---|---|---|
| no additive | | 291 | 258 |
| 1% oxalic acid | 4.3 | 92 | 152 |
| 3% oxalic acid | 1.4 | 64 | 173 |
| 5% oxalic acid | 0.9 | 75 | 151 |
| 7% oxalic acid | 0.6 | 34 | 49 |
| 1% fumaric acid | 5.5 | 223 | 186 |
| 3% fumaric acid | 1.8 | 156 | 169 |
| 5% fumaric acid | 1.1 | 195 | 188 |
| 7% fumaric acid | 0.8 | 216 | 184 |

### 3.5.3 Influence of additives on the membrane pore size distribution

Some of the membranes have been characterized by permporometry. These membranes were dried according to an ethanol-hexane-air displacement sequence. This implies that the obtained pore size distributions refer to membranes in the dry state. A detailed discussion on permporometry is given in chapter 4.

The pore size distributions of four different types of membranes are given in figure 4. The casting solutions used for the preparation of the membranes contained 20 wt% PI in DMF, with 3 wt% maleic acid, 1 wt% oxalic acid, and 3 wt% glycerol, respectively, and they were coagulated in ethanol. No macrovoids were present in any of these membranes. As a reference, the pore size distribution for a membrane made from a 20 wt% PI solution in DMF without additives and coagulated in ethanol is given in the same figure (see chapter 4).

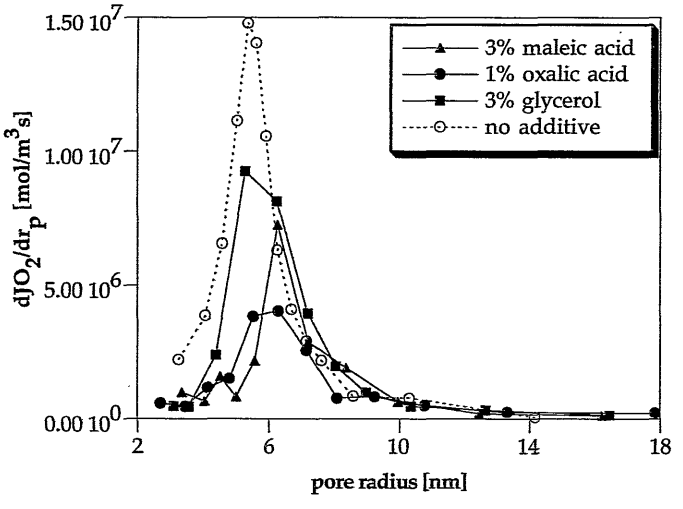


*Figure 4. Pore size distributions for different membranes prepared from 20 wt% PI casting solutions in DMF and coagulated in ethanol, determined by permporometry. Influence of maleic acid, oxalic acid, and glycerol as additive.*

It can be seen from this figure, that the position of the maximum does not vary much, but the number of pores decreases when additives to the solutions are applied. The most drastic effect is observed for oxalic acid, and even more so when considering that for this additive a concentration of only 1% has been used here.

In figure 5, the pore size distributions of membranes prepared from 20 wt% PI in DMF with 3 wt% fumaric acid and coagulated in water and ethanol are compared with the pore size distributions of membranes prepared from solutions without additives. Also in these cases the location of the maxima are hardly influenced by the presence of fumaric acid.

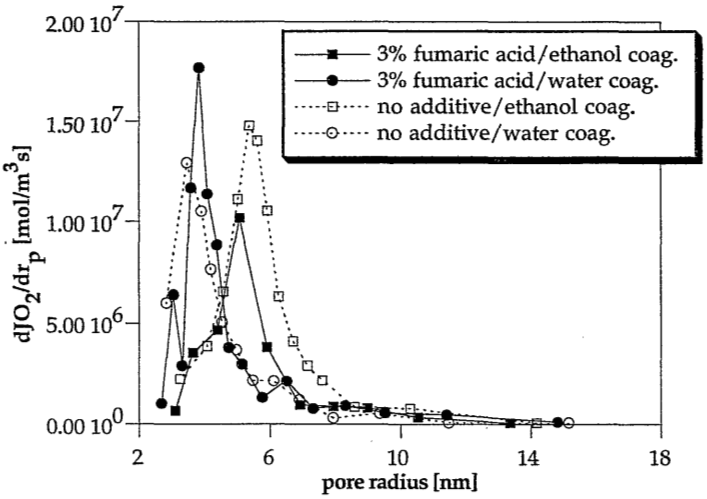


*Figure 5.* *Pore size distributions for different membranes prepared from 20 wt% PI in DMF casting solutions, obtained by permporometry. Influence of fumaric acid as an additive and type of coagulation bath.*

### 3.5.4 Influence of additives on the cloud point curve

For some of the additives, cloud points were determined by turbidity measurements with ethanol as non-solvent. The results for the quasi-ternary system ethanol/DMF/PI with five different additives is presented in figure 6. The additive concentration was 3% in all cases.

It can be seen that by the presence of the additives the binodal curves are shifted to the solvent/polymer axis. Especially in the case of oxalic acid, maleic acid, and tartaric acid as additives, this effect is strong. For the system with fumaric acid or glycerol only small changes in the binodal were observed compared to the ternary system.

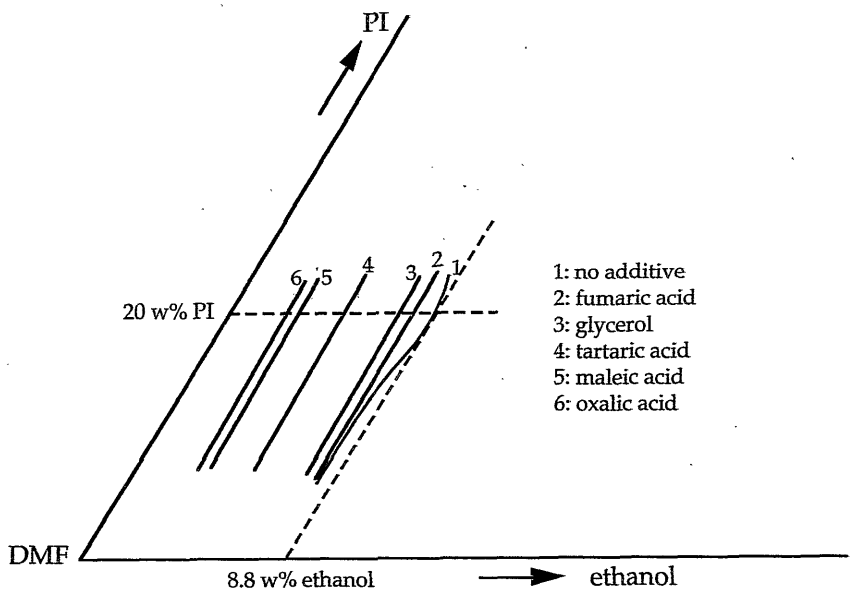


*Figure 6. Schematic representation of cloud point curves for the system PI/DMF/ethanol and various additives.*

## 3.6 Discussion

The results show that the addition of some of the additives to the polyimide solution can have a large effect on membrane morphology. This can be shown by the disappearance of macrovoids and by the change in pore size distribution in the membrane toplayer, indicated by permporometry and ethanol permeability measurements.

To understand why the additives have different effects, some of the physical properties must be compared. The acidity (only in water), solubility in ethanol, and solubility in water of the additives are given in table 3. Chemical structures have already been given in figure 1.

*Table 3. Comparison of acidity and solubility of additives.*

| additive | $pKa_1$ [-] | additive | solubility in ethanol[a] [g/100ml] | additive | solubility in water[b] [g/100ml] |
|---|---|---|---|---|---|
| oxalic acid | 1.27 | ethanol | ∞ | ethanol | ∞ |
| maleic acid | 1.97 | acetic acid | ∞ | acetic acid | ∞ |
| malonic acid | 2.85 | glycerol | ∞ | glycerol | ∞ |
| tartaric acid | 2.89 | glutaric acid | ∞ | tartaric acid[a] | 139.5 |
| fumaric acid | 3.02 | maleic acid | 69.9 | maleic acid | 78.9 |
| succinic acid | 4.21 | malonic acid | 57 | malonic acid | 73.5 |
| glutaric acid | 4.34 | oxalic acid | 23.7 | glutaric acid | 63.9 |
| acetic acid | 4.75 | tartaric acid | 20.4 | oxalic acid | 8.0 |
| glycerol | 14.15 | succinic acid | 7.5 | succinic acid | 5.8 |
| ethanol | -- | fumaric acid | 5.75 | fumaric acid | 0.4 |

a: from ref. [25]
b: from ref. [26]

Based on a comparison of table 3 and figure 1 in relation to the presence of macrovoids in the membrane (figures 2 and 3), the following conditions can be given for the suppression of macrovoid formation:

- presence of at least two approachable -OH groups (also from -COOH)
- low solubility in the coagulation bath
- no intramolecular hydrogen bonding possible

Firstly, ethanol and acetic acid have hardly any influence on the presence of macrovoids. They both have only one -OH group. The most surprising difference can be found between the isomers maleic acid and fumaric acid in the case of ethanol-coagulated membranes: maleic acid (the cis-isomer) is a very effective macrovoid suppresser, whereas fumaric acid (the trans-isomer) has no effect on the presence of macrovoids at all. The other very effective additives also have at least two approachable -OH groups: oxalic acid (ethanol and water as non-solvent), maleic acid and tartaric acid (ethanol as non-solvent), and glutaric acid (water as non-solvent).
Secondly, the differences of membranes from solutions containing glutaric acid and tartaric acid, coagulated in ethanol or water, can be explained by their solubility behaviour. In general, when the solubility in the coagulation bath is low, the additives suppress macrovoid formation (i.e., tartaric acid/ethanol, glutaric acid/water); when the solubility is higher, the additives have almost no effect (i.e., tartaric acid/water, glutaric acid/ethanol). Oxalic acid, with a low

solubility, is very effective. The acidity of the additive probably is not of importance, especially not in ethanol.
The third condition applies to maleic acid, which is able to form intramolecular hydrogen bonds (see figure 7) [27]. In this case there are not two free -OH groups available anymore. The formation of this intramolecular hydrogen bonding can occur more easily in water than in ethanol [28]. Therefore, maleic acid can suppress macrovoid formation far more effectively for ethanol-coagulated membranes than for water-coagulated membranes, despite the similar solubilities of maleic acid in ethanol and water.

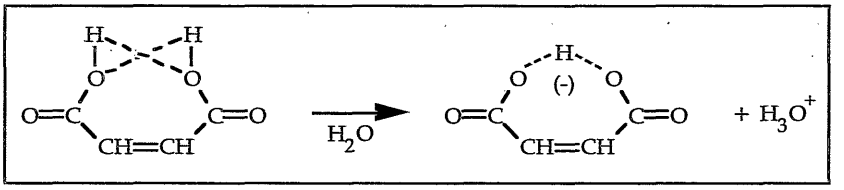


*Figure 7. Intramolecular hydrogen bonding of maleic acid.*

The fact that some -OH groups have to be present in the additives indicates the possibility of hydrogen bonding with the polymer. This has already been suggested for dicarboxylic acids and cellulose acetate by King et al. [18,19]. From our results it is obvious that at least two -OH groups have to be present that are able to approach each other. This means that double hydrogen bonds are formed as a kind of bridge, at a fixed distance.
Since the unsaturated dicarboxylic acid isomers maleic acid and fumaric acid have a rather rigid structure (because of the double bond), they were used here as model solutes to calculate these specific distances. The most probable distances between the protons of the two acid groups of maleic and fumaric acid were estimated at:

maleic acid: 2.5 Å
fumaric acid: 4.8 Å

It is expected that the hydrogen bond bridge "fits" on two proton accepting groups of the polyimide. Because the BTDA-unit of the polyimide is very rigid, it is possible to calculate distances between several proton accepting groups. A schematic overview of these distances is given in figure 8.

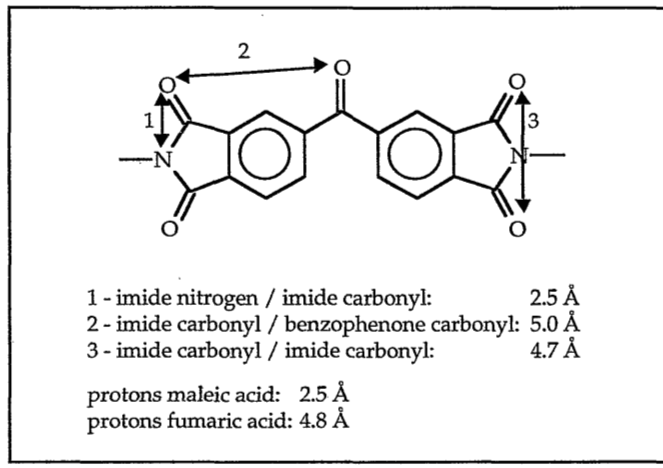


*Figure 8. Calculated distances between proton accepting groups in the rigid BTDA-unit of polyimide.*

From figure 8 it can be concluded that the distance between the protons of the OH groups of maleic acid is about the same as the distance between the nitrogen and the carbonyl oxygen of the imide group, whereas the distance between the protons of the two OH groups of fumaric acid is about the same as the distance between the oxygens of the imide carbonyl and the benzophenone carbonyl or the distance between the oxygens of two carbonyls of the same imide group. This means that the two bridges are formed at different places for these two additives. All the other additives are much more flexible, so it is assumed that the distances between the protons of their OH groups varies to a large extent.

It is very likely that the polymer properties are changed by the bridge-complex formation. In addition, the position of the bridge is important, since it can influence the flexibility of the polymer chain during the vitrification of the membrane. Smit [29] has shown that for several glassy polyimides the imide nitrogen atom serves as a"pivot point", i.e., a flexible link.
For the polymer-additive combinations this means that a "fit" on the imide carbonyl and nitrogen, position 1 in figure 8 (i.e., maleic acid, oxalic acid), can cause a decrease in polymer chain flexibility due to the steric hindrance at the pivot point, whereas the other additives (i.e., fumaric acid) will have only a minor influence on the chain flexibility when they form a bridge at the oxygen groups (positions 2 or 3 in figure 8).
The decrease in flexibility will be an important factor during the vitrification of the membrane toplayer. According to Wienk et al. [30], the nodules in the toplayer are formed by collapse of the entangled polymer structure, due to the rapid change in environment from solvent to non-solvent conditions. During

the collapse, the polymer chains will (partly) disentangle, thereby forming nodules with pores between the nodules where the chains are disentangled. The presence of an additive in the polymer solution will hinder the disentanglement process. When the solubility of the additive in the non-solvent is low, the effect will be larger. However, when the additive has some interaction with the polymer chains combined with a low solubility, the disentanglement process will be disturbed very severely. In that case, the nodules will still be highly interconnected at the moment of vitrification, which results in smaller or fewer pores and a low liquid permeability.
Oxalic acid causes the strongest decrease in ethanol permeability, and this can be explained by this mechanism: oxalic acid has a low solubility in ethanol and water, and it is able to form an hydrogen bond bridge that affects the chain flexibility.
Within one repeating unit of PI, there are two of these sites available at the same time (position 1 in figure 8, at the left N and at the right N). This means that all sites are occupied when the molar ratio of PI/oxalic acid approaches 0.5, so then the flexibility loss will be the largest. From table 2 it can be seen that at 7 wt% oxalic acid, this ratio is 0.6. At this concentration the lowest ethanol permeability is obtained, for ethanol-coagulated membranes as well as water-coagulated membranes. For fumaric acid, an increasing additive concentration affects the ethanol permeability much less strongly.

From permporometry (figures 4 and 5), it was observed that the presence of the additive did not change the position of the pore peak maximum. On the other hand, the number of pores is in some cases significantly lower than for the membrane prepared without additives. Especially oxalic acid causes a large decrease in the number of pores.
The ethanol permeability measurements (table 1) showed that almost all additives decrease the ethanol permeability of the membrane. Once again, oxalic acid shows the strongest effect.

The fact that the solubility of the additives in the non-solvent influences the membrane formation, indicates that diffusional aspects must be considered. During the immersion precipitation process of a ternary system, non-solvent (1) diffuses into the polymer film, and solvent (2) diffuses out of the polymer film. Assuming that the polymer phase (3) is fixed as a frame of reference, the diffusive fluxes can be represented by [31]:

$$J_i = \sum_{j=1}^{2} \underline{v}_i L_{ij} \{\varphi_1, \varphi_2\} \frac{\partial \mu_j}{\partial x} \qquad (3.1)$$

Here, $J_i$ is the volume flux of component i relative to component 3 [$m^3/m^2s$], $\underline{v}_i$

is the specific volume of component i [$m^3/kg$], $\varphi_i$ is the volume fraction of component i [-], $\partial\mu_j/\partial x$ is the chemical potential gradient in the polymer film [J/mol m], and $L_{ij}$ are phenomenological coefficients [mol s/$m^3$]. For a quaternary system consisting of non-solvent (1)/solvent (2)/ polymer (3)/additive (4), this results in [31]:

$$-\frac{\partial J_i}{\partial x} = \frac{\partial\left(\frac{\varphi_i}{\varphi_3}\right)}{\partial t} = \underline{v}_i \frac{\partial}{\partial x}\left(\sum_{j=1,2,4} \varphi_3 L_{ij} \frac{\partial \mu_j}{\partial x}\right) \qquad (3.2)$$

The chemical potential of mixing of component 4, $\Delta\mu_4$, can be related to the free enthalpy of mixing:

$$\Delta\mu_4 = \left(\frac{\partial \Delta G_M}{\partial n_4}\right)_{P,T,n1,n2,n3} \qquad (3.3)$$

Here, $n_4$ is the number of moles of component 4 [mol], and $\Delta G_M$ is the free enthalpy of mixing [J]. The free enthalpy of mixing can be written as [1,31-33]:

$$\frac{\Delta G_M}{RT} = n_1 \ln\varphi_1 + n_2 \ln\varphi_2 + n_3 \ln\varphi_3 + n_4 \ln\varphi_4 + n_1\varphi_2 g_{12}\{u_2\} + n_1\varphi_3\chi_{13} + n_1\varphi_4 g_{14}\{u_4\} + n_2\varphi_3 g_{23}\{v_2\} + n_2\varphi_4 g_{24}\{w_2\} + n_3\varphi_4 g_{34}\{v_3\} \qquad (3.4)$$

Here, $u_i$, $v_i$, $w_i$ are semi-binary volume fractions (e.g., $u_2 = \varphi_2/(\varphi_2 + \varphi_1)$), $g_{ij}$ are binary interaction parameters depending on components i and j and on concentration, and $\chi_{ij}$ is a concentration independent interaction parameter.

Comparing different additives, it is assumed that the variations in $J_1$ and $J_2$ are much smaller than those in $J_4$. The variation in $J_4$ will be mainly caused by differences in $g_{14}$ and $g_{34}$ between the various additives and the other components. The solubility in the coagulation bath affects $g_{14}$, and the interaction between the additive and the polymer will determine $g_{34}$.
Therefore, when the additive is well soluble and has no interaction with the polymer, it can easily diffuse from the polymer-rich phase to the polymer-lean phase, so that the macrovoid formation process will be comparable to the ternary systems (without additives), since $J_4$ is very large. However, if the solubility of the additive in the non-solvent is low and the additive interacts with the polymer, the additive will remain preferably in the polymer-rich phase.

Boom [34] has developed a mass transfer model for the first moments of immersion for a quaternary membrane forming system, where the additive is a second polymer. He explained that during this very short time the movement of

the two polymers is negligible, when compared with the movement of solvent and non-solvent. A certain minimum molecular weight of the second polymer is necessary to achieve a drastic decrease in polymer-(polymeric) additive diffusion, and the only further demand is that the polymers are miscible. Based on the assumption that the two polymers act as one single network (kinetic restriction), Boom was able to calculate phase diagrams for quaternary systems that are only valid for this short time scale, which indicated that the polymer solution becomes more compatible with the non-solvent upon addition of the polymeric additive, i.e., the size of the *virtual* demixing gap is decreased. In reality, the solution is very incompatible, which is indicated by the fact that the *real* cloud point curve (for longer time, thus including kinetic effects) is situated very close to the polymer/solvent axis.
Because the polymer network is very immobile, the polymer solution is allowed to enter deeply into the real demixing gap, since during very short times the smaller virtual demixing gap is valid. Boom showed that for these systems delayed demixing is promoted because the polymers do not demix, while at the same time the solvent concentration in the coagulation bath increases drastically. Therefore, as soon as the polymers start to phase separate, the solution is very unstable and demixes without giving macrovoid formation a chance.

When comparing the quaternary systems investigated by Boom with the systems described in the present study, two important differences can be pointed out:

- the present additives have low molecular weights, whereas the additive used by Boom is polymeric
- in the system of Boom, interaction of the additive with the polymer is not important, whereas in the present systems the interaction of the additive with the polymer is a crucial parameter

It is suggested here that the decrease of the chain flexibility due to interaction of certain dicarboxylic acids with polyimide has a similar effect as the high molecular weight of the polymeric additive. These systems have in common that the mobility of the polymeric network is decreased and the demixing process is hindered. Since the demixing on a local scale is delayed, macrovoid formation will not be possible. Therefore, the flexibility decreasing interaction combined with the low solubility of the additive in the non-solvent bath is essential, since during non-solvent/solvent exchange these additives will not simply be removed directly from the polymer chain, but proceed in diminishing the polymeric movement.
However, further research is necessary to test this hypothesis, and to compare the quaternary systems used here with the system used by Boom.

The cloud point data presented in figure 6 indicate that the presence of each one of these casting additives reduces the stability of the casting solutions, since the

demixing gaps for the quaternary system are larger than for the ternary system. These are binodals for the real demixing gap, so including kinetic effects. The parameters necessary to calculate the hypothetical virtual binodals are not available for our systems.

The SEM-photographs of membranes prepared from a 20 wt% PI-solution in DMF containing 7 wt% oxalic acid showed a different morphology than those with a lower concentration of oxalic acid: a kind of closed-cell structure is obtained, with an irregular structure in between the pores (see figure 9).

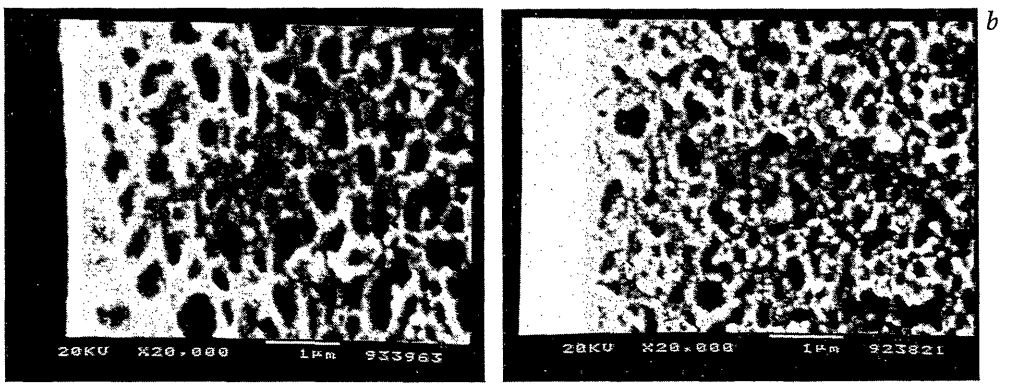


*Figure 9. SEM-photographs of membranes from 20 wt% PI-solution in DMF, containing 7 wt% oxalic acid; coagulated in ethanol (a) or in water (b).*

A similar structure has been found by Boom [35] for a membrane from a 15 wt% polyethersulfone/10 wt% polystyrene solution in NMP (coagulated in water). Boom explained the formation of this co-continuous structure by assuming that inside the polymer-rich phase the two polymers have phase separated on a smaller scale. It is not clear why these structures are comparable. The basic materials are different, i.e., either two polymers or a polymer combined with a low molecular weight component.

If interaction should preferably take place between the DMF and the acids, then fewer solvent molecules will be available for polymer-solvent interaction. This means that solvent is squeezed out of the polymer coil, so that the coil contracts and the viscosity will decline. However, the viscosity of polyimide solutions increases upon addition of effective additives (visual observation), thus interaction between DMF and the additives is not very probable.

## 3.7 Conclusions

A hypothetical mechanism has been proposed for the influence of aliphatic dicarboxylic acid additives on the polyimide membrane formation process, i.e., the presence of macrovoids and the pore size distribution of the toplayer. An additive is able to suppress macrovoid formation in polyimide membranes, when:

- it has two approachable OH groups
- it does form intramolecular hydrogen bonds
- it has a low solubility in the coagulation bath

It has been suggested that the first two conditions imply that a hydrogen bond bridge has to be formed at a specific site of the polyimide chain, while this interaction will remain during the immersion precipitation process by the low solubility of the additive in the coagulation bath. In addition, the hydrogen bond bridge and the low solubility have been shown to affect the toplayer pore size distribution.
Experimental cloud point curves showed that all the investigated additives reduce the stability of polyimide/DMF casting solutions.

## 3.8 References


[1] R.M. Boom, I.M. Wienk, Th. van den Boomgaard, C.A. Smolders; Microstructures in phase-inversion membranes. Part 2. The role of a polymeric additive; J. Membrane Sci., 74(1992)277

[2] A.M. Biget; A chemically inert gel; Ann. Chim. (Paris), 5(1950)66

[3] S. Loeb, S. Sourirajan; Sea water demineralization by means of an osmotic membrane; Advan Chem. Ser., 38(1962)117

[4] B. Keilin; Office of Saline Water report no. 84; United States, Department of the Interior; 1964

[5] B. Keilin; The mechanism of desalination by reverse osmosis; Office of Saline Water report no. 117; United States, Department of the Interior; 1964

[6] R.E. Kesting; Semipermeable membranes of cellulose acetate for desalination in the process of reverse osmosis. 1. Lyotropic swelling of secondary cellulose acetate; J. Appl. Polym. Sci., 9(1965)663

[7] S. Manjikian; Desalination membranes from organic casting solutions; I. E. C. Prod. Res. Dev., 6(1967)23

[8] R.E. Kesting, A. Menefee; The role of formamide in the preparation of cellulose acetate membranes by the phase inversion process; Kolloid-Z. u. Z. fur Polymere, 230(1969)341

[9] B. Kunst, D. Skevin, G. Dezelic, J.J. Petres; A light-scattering and membrane formation study on concentrated cellulose acetate solutions; J. Appl. Polym. Sci., 20(1976)1339

[10] G. Fan, C. Zhang, L. Zheng; The study of action of organic additives in polysulfonamide UF membranes; Desalination, 56(1985)325

[11] T.-P. Hou, S.-H. Dong, L.-Y. Zheng; The study of mechanism of organic additives action in the polysulfone membrane casting solution; Desalination, 83(1991)343

[12] M.A. Kraus, M. Nemas, M.A. Frommer; The effect of low molecular weight additives on the properties of aromatic polyamide membranes; J. Appl. Polym. Sci., 23(1979)445

[13] R.E. Kesting, A.K. Fritzsche, M.K. Murphy, C.A. Cruse, A.C. Handermann, R.F. Malon, M.D. Moore; The second generation polysulfone gas-separation membrane. 1. The use of Lewis acid:base complexes as transient templates to increase free volume; J. Appl. Polym. Sci., 40(1990)1557

[14] R.E. Kesting, A.K. Fritzsche, C.A. Cruse, M.D. Moore; The second-generation polysulfone gas-separation membrane. 2. The relationship between sol properties, gel macrovoids, and fiber selectivity; J. Appl. Polym. Sci., 40(1990)1575

[15] C.W. Saltonstall; Development of new and improved cellulose ester reverse osmosis membranes; Office of Saline Water report no. 434; United States, Department of the Interior; 1969

[16] D.L. Hoernschemeyer, C.W. Saltonstall, O.S. Schaeffler, L.W. Schoellenbach, A.J. Secchi, A.L. Vincent; Research and development of new and improved cellulose ester membranes (for desalination of water); Office of Saline Water report no. 556; United States, Department of the Interior; 1970

[17] D.L. Hoernschemeyer, R.W. Lawrence, C.W. Saltonstall, O.S. Schaeffer, A.J. Secchi; New and improved cellulose ester membranes; Office of Saline Water report no. 700; United States, Department of the Interior; 1971

[18] W.M. King, P.A. Cantor; Reverse osmosis and process and composition for manufacturing cellulose acetate membranes wherein the swelling agent is a di- or tri- basic aliphatic acid; US 3,673,084; 1972

[19] W.M. King, D.L. Hoernschemeyer, C.W. Saltonstall; Cellulose acetate blend membranes; H.K. Lonsdale, H.E. Podall (Eds.); Reverse osmosis membrane research; Plenum, New York, 1972; p. 131

[20] H. Bokhorst, F.W Altena, C.A. Smolders; Formation of cellulose acetate membranes; Desalination, 38(1981)349

[21] K. Vásárhelyi, J.A. Ronner, M.H.V. Mulder, C.A. Smolders; Development of wet-dry reversible reverse osmosis membranes with high performance from cellulose acetate and cellulose triacetate blends; Desalination, 61(1987)211

[22] Wafilin BV; Membrane for filtration made using two aqueous baths; Neth. Appl. 78,12664; 1979

[23] J.A. Ronner, S. Groot Wassink, C.A. Smolders; Investigation of liquid-liquid demixing and aggregate formation in a membrane-forming system by means of pulse-induced critical scattering (PICS); J. Membrane Sci., 42(1989)27

[24] C. Friedrich, A. Driancourt, C Noel, L. Monnerie; Asymmetric reverse osmosis and ultrafiltration membranes prepared from sulfonated polysulfone; Desalination, 36(1981)39

[25] BDH Biochemical Reagents catalogue; BDH Limited

[26] Ullmann's Encyclopedia of industrial chemistry; fifth edition; W. Gerhartz (exec. ed.); VCH, Weinheim, 1987; Vol. A.8, p. 525

[27] S. Vinogradov, R.H. Linnell; Hydrogen Bonding; Van Nostrand Reinhold, New York, 1971; p. 43

[28] M. Usman, B. Bhan Singh; Ionization constants of maleic, fumaric, citraconic and mesaconic

acids in methanol-water mixtures; Trans. SAEST, 18(1983)309

[29] E. Smit; Modelling of the diffusion of gases through membranes of novel polyimides; Ph.D. thesis, University of Twente, 1991

[30] I.M. Wienk, Th. van den Boomgaard, C.A. Smolders; The formation of nodular structures in the toplayer of ultrafiltration membranes; accepted for publication in J. Appl. Polym. Sci.

[31] A.J. Reuvers, J.W.A. van den Berg, C.A. Smolders; Formation of membranes by means of immersion precipitation. Part 1. A model to describe mass transfer during immersion precipitation; J. Membrane Sci., 34(1987)45

[32] J. Flory; Principles of polymer chemistry; Cornell University Press, New York, 1953

[33] H. Tompa; Polymer solutions; Butterworths, London, 1956

[34] R.M. Boom; Membrane formation by immersion precipitation: the role of a polymeric additive; Ph. D. thesis, University of Twente, 1992

[35] Ref. 34; chapter 5, p134, figure 3.a

# Chapter 4

## Characterization of polyimide ultrafiltration membranes

M.A.M. Beerlage, M.L. Heijnen, M.H.V. Mulder, C.A. Smolders, H. Strathmann

### Summary

The characterization methods that were described in previous chapters are discussed in this chapter in more detail, i.e., liquid flux measurements, gas flux measurements and permporometry. Six different types of polyimide ultrafiltration membranes were used as standard membranes. For gas flux measurements and permporometry the membranes were dried following an ethanol-hexane displacement sequence.
From permporometry measurements pore size distributions for the dried membranes were calculated. With the pore size distributions obtained a theoretical oxygen flux and a theoretical (liquid) ethanol permeability was calculated for all membranes, with the dry state parameters. The theoretical oxygen fluxes derived from permporometry were of the same order as the experimental gas flux measurements. The theoretical ethanol permeabilities were two orders of magnitude lower than the experimental measurements. This is probably caused by the drying procedure: upon drying of an ultrafiltration membrane the pore size distribution has changed.
Permporometry is a very suitable method to characterize ultrafiltration membranes that are to be used in the dry state. Membrane characteristics that are obtained by dry characterization techniques are only applicable for membranes in dry states.

## 4.1 Introduction

In the past much research has been directed to the characterization of ultrafiltration membranes. The primary goal of most characterization efforts was to predict the actual performance of the membrane during ultrafiltration; for that reason the pore size and pore size distribution in the toplayer of the membrane is one of the most important parameters for characterizing ultrafiltration membranes.

In chapters 2 and 3 of this thesis, the membrane formation parameters were related to membrane properties using scanning electron microscopy, organic liquid and gas flux measurements and permporometry.
In this chapter the latter characterization techniques will be discussed in more detail, for six different types of polyimide ultrafiltration membranes.

## 4.2 Background and applicability of characterization techniques

### 4.2.1 Overview of ultrafiltration characterization techniques

There is an enormous amount of literature and research concerning the characterization of ultrafiltration membranes. Each technique has both advantages and disadvantages, and the suitability of a certain technique depends strongly on the membrane material, morphology and specific properties.
An extensive overview and discussion on characterization methods is given by Cuperus and Smolders [1], who classified methods as morphology related and performance related. Characterization techniques can also be classified as "dry" or "wet", depending on the state in which the membrane samples are characterized; this distinction is meaningful, because drying an ultrafiltration membrane generally alters the characteristics of the membranes, i.e., the morphology in the wet state and dry state is not the same.

Microscopy methods are very widely used, especially Scanning Electron Microscopy (*SEM*). SEM can only give qualitative information about the membrane morphology and an estimation of the membrane skin thickness, because the resolution is not high enough to visualize the pores in the skin of an ultrafiltration membrane [2]. In principle it is also possible to combine a cryo-preparation technique with SEM; in that case cryogenically broken wet membrane samples are kept some time at about 190 K to sublimate the water, after which a thin gold layer is sputtered on the surface. The resolution is comparable to resolutions obtained by the normal SEM procedure. Wienk [3] showed that this sublimation step is often not sufficient, because some bound

water is still present in the membrane. After application of a second sublimation step inside the microscope, membranes show the same morphology as the membranes that are not prepared according to the cryo-technique, but simply dried.

*FESEM* (Field Emission Scanning Electron Microscopy) has a much better resolution, of about 1 nm [3,4]. For FESEM, as well as for SEM, membranes have to be dried and then coated with a charge conducting layer, with a thickness of the order of some nm, which is also the size of the smaller pores in the membranes; this might cause problems in interpreting the obtained electron micrographs.

For *TEM* (Transmission Electron Microscopy) dry membranes have to be embedded in a resin, after which a thin slice has to be cut from the membrane. TEM has a very high resolution (< 1 nm), but often small cracks can be seen in the samples, caused by the cutting procedure. Also the influence of the embedding resin on the membrane structure is not clear [3,4]. An alternative preparation technique is the freeze-etching replica method; this way of preparation, however, may also induce crack formation.

*AFM* (Atomic Force Microscopy) is a wet technique developed only very recently [5]. Wienk [3] showed that membranes from a blend of polyethersulfone and polyvinylpyrrolidone can easily be damaged using this technique, when too high operating forces are applied. She also mentioned that the nodules present in the skin are roughly of the same size as the tip of the scanning needle (10-20 nm), which may cause unreliable results.

*Liquid-liquid displacement* is a wet characterization technique, making use of the immiscibility of two liquids, usually water and water-saturated isobutanol [3,6] or water and water-saturated isobutanol/methanol [7,8,9]. The method combines the principles of bubble pressure measurements with liquid permeability measurements. The pressure required to replace the liquid within a pore by a second immiscible liquid, so that the pore is open to liquid permeation, is related to the size of the pore and the interfacial tension between the two liquids. Unfortunately, polyimide membranes appeared not to be chemically resistant enough to the liquids used in this technique, so reliable results could not be obtained and other liquid mixtures are required.

*Mercury porosimetry*, a technique where mercury is forced under relatively high pressure into the pores of a dry membrane, is not suitable for characterization of pores in polymeric ultrafiltration membranes. Liabastre and Orr [10] showed that the structure of Nuclepore microfiltration membranes was severely damaged by the high pressures needed.

*Gas adsorption/desorption* does not only measure the small pores in the toplayer of the membrane, but also the small pores present in the sublayer of asymmetric phase inversion membranes. This was shown by Cuperus [1], who used this technique to characterize polysulfone membranes. Gas adsorption/

desorption is more suitable to characterize dry symmetric polymeric or ceramic membranes [11,12].
*Thermoporometry* measures the freezing or melting point depression of a liquid or frozen liquid inside pores; this depression is related to the size of the pores [13]. Zeman et al. [14] showed that the application of this method also is disturbed by the presence of pores in the membrane sublayer.
*Permporometry* is a dry characterization technique, based on a combination of controlled pore blocking by capillary condensation and counter diffusion of inert gases through the opened pores. This characterization method will be discussed further in section 4.2.4.
*NMR spin-lattice relaxation* is a wet technique to determine pore size distributions. This method is developed only recently and was tested for symmetric membranes [11,15]; it seems to be rather sensitive to the choice of the liquid, the field strength and calibration techniques.
*Gold sol filtration* was developed by Cuperus et al. [16] to determine the toplayer thickness of ultrafiltration membranes.
The hydrophobicity of a membrane is an important parameter related to the fouling behaviour; it can be determined quantitatively by *contact angle measurements* [9,17] or qualitatively by *fouling experiments* [18].
Surface analysis techniques can be used to characterize the chemical nature of the membrane surface, which may be necessary for the investigation of solute adsorption or other solute-membrane interactions, e.g., for affinity membranes. There are several techniques described in literature to analyse the surface of the membrane chemically; *ESCA/XPS* (X-ray Photoelectron Spectroscopy), *FTIR-ATR* (Fourier Transform Infrared spectroscopy - Attenuated Total Reflectance) and *SIMS* (Secondary Ion Mass Spectrometry) are the best known examples [17,19-21].

*Liquid* and *gas flux measurements* can be used to compare the permeability of membranes. These methods are often used as a first characterization method to relate permeation properties to morphology or to membrane formation parameters, as was done in chapters 2 and 3. These methods will be discussed further in sections 4.2.2 and 4.2.3, respectively.
Probably, the most widely used characterization method for ultrafiltration membranes are *retention measurements*. The amount of literature on this subject is enormous. Non-aqueous retention measurements using polyimide ultrafiltration membranes will be discussed in chapter 5.

A schematic overview of characterization techniques for ultrafiltration membranes is given in tables 1 and 2. Liquid-liquid displacement, permporometry, and gold sol filtration could also be seen as performance related methods, because in all cases permeation is involved; since the characteristics obtained by

these techniques are morphology related (e.g. pore size distribution and toplayer thickness), they are classified here as morphology related techniques.

*Table 1. Morphology related characterization methods for ultrafiltration membranes.*

| characterization method | determined membrane property | membrane state during characterization |
|---|---|---|
| microscopy methods | | |
| SEM | toplayer thickness, morphology | dry |
| cryo-SEM | toplayer thickness, morphology | wet/dry |
| FESEM | pore size distribution, porosity | dry |
| TEM | pore size distribution, porosity | dry |
| AFM | pore size distribution, porosity | wet |
| liquid-liquid displacement | pore size distribution | wet |
| mercury porosimetry | pore size distribution | dry |
| gas adsorption/desorption | pore size distribution | dry |
| thermoporometry | pore size distribution, pore shape | wet |
| permporometry | pore size distribution | dry |
| NMR spin relaxation | pore size distribution | wet |
| gold sol filtration | toplayer thickness | wet |
| contact angle | hydrophobicity/fouling | wet |
| ESCA/XPS | surface chemical analysis | dry |
| FTIR-ATR | surface chemical analysis | dry |
| SIMS | surface chemical analysis | dry |

*Table 2. Performance related characterization methods for ultrafiltration membranes.*

| characterization method | determined membrane property | membrane state during characterization |
|---|---|---|
| liquid permeation | permeability, hydraulic pore size | wet |
| gas permeation | permeability, "mean" pore size | dry |
| retention measurements | solute retention | wet |
| fouling experiments | hydrophobicity/fouling | wet |

### 4.2.2 Liquid flux measurements

Liquid flux measurements are a very simple way to compare ultrafiltration membranes. In literature, water is very often used as flux medium for this purpose. Assuming a capillary (cylindrical) pore shape in the skin, the Hagen-Poiseuille equation can be used to determine the liquid flux [22]:

$$J_{liq} = \frac{n \pi r_p^4 \Delta P}{8 \eta_{liq} \tau \Delta x} \qquad (4.1)$$

where $J_{liq}$ is the liquid flux [$m^3/m^2s$ = m/s], n is the number of pores at the membrane surface [$1/m^2$], $r_p$ the pore radius [m], $\eta_{liq}$ the liquid viscosity [$Ns/m^2$], $\tau$ the membrane tortuosity [-], $\Delta P$ the transmembrane pressure [Pa] and $\Delta x$ the toplayer thickness [m].
For membranes with a nodular toplayer, i.e., a layer of close packed spheres, the liquid flux can be described by the Kozeny-Carman equation [23]:

$$J_{liq} = \frac{\varepsilon^3 \Delta P}{K \eta_{liq} S^2 (1-\varepsilon)^2 \Delta x} \qquad (4.2)$$

where $\varepsilon$ is the volume fraction of the pores [-], K is the Kozeny-Carman constant [-] (which depends on the tortuosity, the packing density and the pore shape) and S is the specific surface area of the spherical particles [$m^2/m^3$].
Liquid flux measurements can give a qualitative measure of the permeability of a membrane in the wet state.
When several liquids are used the fluxes should be normalized by a viscosity correction; however, care should be taken since the swelling of the membrane in these liquids may differ. An example of the suitability of polyimide ultrafiltration membranes in different flux media has been given in chapter 2 (table 4).
Liquid fluxes can also be normalized by correcting the values for the transmembrane pressure; if this is done, the term "liquid permeability" will be employed, $P_{liq}$, with the units [$kg/m^2hr$ bar].

### 4.2.3 Gas flux measurements

The principle of gas flux measurements is comparable to liquid flux measurements, with the exception that in the case of gases membranes are characterized in the dry state. Upon drying the morphology may have changed. The transport regime is dependent on the pore size: when relatively large pores are present (> 10 nm), the gas flux is mainly determined by viscous flow [24,25]. At smaller pores (1 < $r_p$ < 10 nm), the gas flux is mainly determined by Knudsen

diffusion, described by equation (4.3)[26]:

$$J_{k,g} = \frac{P_{k,g}\,\Delta P_{m,g}}{\Delta x} = \frac{n\,\pi\,r_p^2\,D_{k,g}\,\Delta P_{m,g}}{R\,T\,\tau\,\Delta x} \qquad (4.3)$$

where $J_{k,g}$ is the gas flux [mol/m$^2$ s], $P_{k,g}$ is the permeability coefficient [mol/m s bar], n the number of pores [1/m$^2$], $r_p$ the pore radius [m], $\Delta P_{m,g}$ the pressure difference between the membrane up and down stream side [Pa], R the gas constant [J/mol K], T the temperature [K], $\tau$ the membrane tortuosity [-], $\Delta x$ the toplayer thickness [m] and $D_{k,g}$ the Knudsen diffusion coefficient [m$^2$/s], which can be calculated from equation (4.4):

$$D_{k,g} = 0.66\,r_p\sqrt{\frac{8\,R\,T}{\pi\,M_g}} \qquad (4.4)$$

where $M_g$ is the molar mass of the gas [kg/mol].
The proper gas transport regime can be obtained by measuring the fluxes for two gases at low transmembrane pressures. When the ratio of the fluxes is about equal to the reciprocal ratio of the square root of the molecular masses of the two gases, the main transport mechanism is Knudsen diffusion:

$$\frac{J_{g,1}}{J_{g,2}} = \sqrt{\frac{M_{g,2}}{M_{g,1}}} \qquad (4.5)$$

Comparison of these values for several membranes can give an estimation of the permeability of the membranes in the dry state. The permeability coefficient is the gas flux normalized to the transmembrane pressure, time, and membrane area, with units [mol/m s bar].

### 4.2.4 Permporometry

Permporometry is a characterization technique to determine pore size distributions of active pores in ultrafiltration membranes; the method was first described by Eyraud [27] as gas-liquid permporometry and later modified by Mey-Marom and Katz [28] and Katz and Baruch [29]. In our laboratory, Cuperus et al. [30] designed an improved setup to perform permporometry measurements and a similar setup was used by Cao et al. [12].

Permporometry is based on capillary condensation of a vapour inside the pores of an ultrafiltration membrane, combined with simultaneous counterdiffusion of inert gases through the pores that are not blocked by condensed vapour.
An important parameter is the relative vapour pressure, $P_R$, which is defined as the ratio of the vapour pressure during the measurement to the saturated

vapour pressure. At $P_R$ =0, all the pores are open: the membrane is in a dry state. When $P_R$ increases, first adsorption of a thin condensed layer on the pore walls takes place; this is the so-called t-layer [12,31,32], and it has a thickness of about 0.5 nm, dependent on the type of vapour [30]. When $P_R$ increases further, capillary condensation occurs first in the smallest pores; the relation between $P_R$ and the Kelvin radius of a pore, $r_k$, is given by the Kelvin relation [23]:

$$\ln P_R = \ln \frac{P}{P_S} = \left(-\frac{\gamma V_m}{R T}\right) \cos\theta \left(\frac{1}{r_{k1}} + \frac{1}{r_{k2}}\right) \qquad (4.6)$$

where $P_S$ is the saturated vapour pressure at the measuring temperature [Pa], P is the measurement vapour pressure [Pa], $P_R$ is the relative vapour pressure [-], $\gamma$ is the interfacial tension of the condensed vapour [$N/m^2$], $V_m$ is the molar volume of the condensate [$m^3/mol$], $\theta$ is the contact angle [-], and $r_{k1}$ and $r_{k2}$ are the Kelvin radii of the curvature of the gas-liquid interface inside the pore [m].

With a progressive increase in relative vapour pressure, larger pores are filled by condensed vapour until at $P_R$ =1 all the pores are filled. Desorption of the condensed vapour can be realized by lowering $P_R$, first opening the largest pores. During desorption, the gas-liquid interface in a cylindrical pore is hemispherical, which means that $r_{k1} = r_{k2} = r_k$ [23,30].
Assuming complete wettability, implying that $\theta$ = 0, equation (4.6) for the desorption process becomes:

$$\ln P_R = -\frac{2\gamma V_m}{R T r_k} \qquad (4.7)$$

Figure 1 schematically shows the steps during the desorption process, as well as the relation between the Kelvin radius $r_k$, the pore radius $r_p$ and the t-layer.

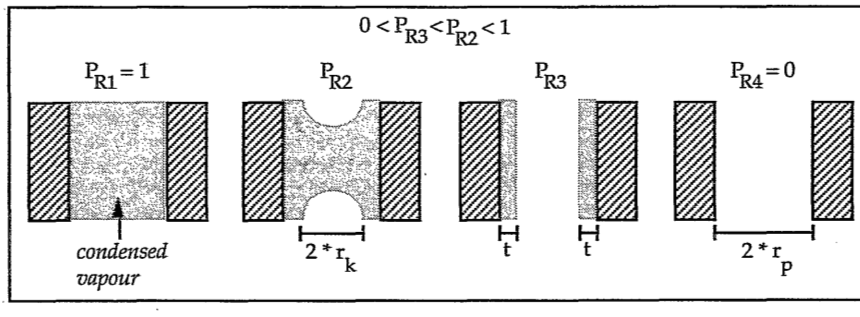


*Figure 1. Permporometry desorption process: stepwise lowering of the relative vapour pressure.*

To determine the number of pores that are opened at a certain relative vapour pressure, counterdiffusion of nitrogen and air is applied. On one side of the membrane a nitrogen stream with a gasflow $\Phi_{N2}$ and $P_R$ has been established and on the other side an air stream with a flow $\Phi_{air}$ and a pressure $P_R$. Very crucial during the measurement is that $\Phi_{N2}$ is exactly equal to $\Phi_{air}$, and that both relative vapour pressures, temperatures and overall pressures are also exactly identical. If this condition is met, then Knudsen diffusional transport of oxygen through the opened pores can occur due to an oxygen concentration gradient. The flux is given by equation (4.8):

$$J_{k,O_2} = n\, r_k^3\, \Delta P_{p,O_2} \frac{0.66}{\tau\, \Delta x} \sqrt{\frac{8\,\pi}{R\,T\,M_{O_2}}} \qquad (4.8)$$

Here, $\Delta P_{p,O2}$ is the partial pressure difference of a gas between the two sides of the membrane [Pa].
With equation (4.7) the oxygen permeation through the membrane $J_{O2}$ at a certain relative vapour pressure $P_R$, which is related to a Kelvin radius $r_k$, allows the calculation of the number of pores of a radius $(r_k+dr_k)$. The real pore radius, $r_p$ [m], can be calculated from equation (4.9):

$$r_p = r_k + t \qquad (4.9)$$

In figure 2 four stages of the permporometry process are represented.

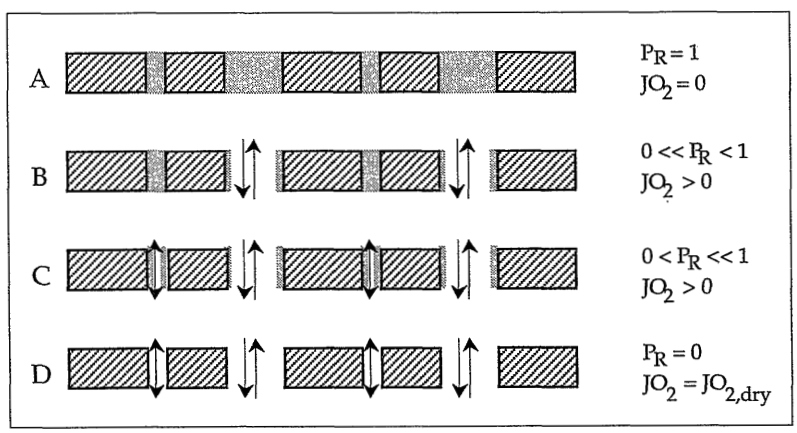


*Figure 2. Principle of permporometry: combination of capillary condensation and counterdiffusion of gases.*

Situation A shows a membrane where all the pores are filled and no oxygen diffusion occurs (in fact, some oxygen will dissolve in the condensed vapour and

will diffuse through this layer, but this diffusion is almost negligible; this will be shown in section 4.4.3). In situation B, desorption just started for the large pores and there is oxygen diffusing through these pores. In situation C, $P_R$ has decreased further so that smaller pores are also opening up, thereby increasing the oxygen diffusion somewhat further. Only the t-layer is still present. In situation D, desorption is complete because also the t-layers are desorbed, since there is no vapour present anymore. In this situation the oxygen diffusion should be of the same order as comparable gas flux measurements for Knudsen flow (described in section 4.2.3).

A disadvantage of permporometry is that membranes have to be dried before the measurements, which might alter the pore size distribution. From permporometry results a theoretical ethanol permeability can be calculated (with dry state parameters!), to be compared with the experimentally determined ethanol permeability.

## 4.3 Experimental

### 4.3.1 Membranes

Six different types of flat sheet polyimide ultrafiltration membranes were used for comparison of the characterization methods. The membrane casting solutions consisted of 18, 20 or 25 weight% P84 polyimide (PI) in dimethylformamide (DMF). P84 powder (Lenzing AG, Austria) was kindly supplied by X-Flow BV, The Netherlands; DMF was purchased from Merck (analytical grade) and used as received.
The preparation conditions of the polymer solutions and the membranes were discussed in more detail in chapter 2.
Six different batches of membranes were obtained by using technical grade ethanol or demineralized water as coagulation bath; after preparation and rinsing with water and ethanol, the membranes were stored in ethanol. Prior to ethyl acetate measurements, the membranes were pre-conditioned in ethyl acetate for at least two days.

### 4.3.2 Drying procedure

It is necessary that the membranes are in a dry state for application of gas flux measurements and permporometry. The membranes were dried following an ethanol-hexane displacement sequence [33-35]: the storage ethanol was replaced by n-hexane, and subsequently the hexane was refreshed at least three times to remove the ethanol completely. The membranes were kept in hexane for three days; then they were put between tissues and glass plates to prevent curling

during drying. After two days at room temperature, the membranes were dry and could be stored.
The subject of membrane drying will be discussed further in the appendix to this chapter.

### 4.3.3 Liquid flux measurements

Fluxes of ethanol and ethyl acetate were determined for wet membranes only. The membranes were cut carefully in an ethanol or ethyl acetate bath to circular pieces of 7.6 cm diameter and placed in a dead-end stainless steel filtration cell of 450 ml. The cell was immediately filled with ethanol or ethyl acetate. The support plate was a very porous stainless steel support and all O-rings were made of highly chemically stable Kalrez® (purchased from Eriks).

The feed tank was pressurized using $N_2$-gas; flux measurements were performed at transmembrane pressures between 0.5 and 1 bar and the permeate flow was determined gravimetrically.
For all membranes the flux reached a constant value after 1 to 2 hours of filtration, after which the liquid flux was determined. The resulting fluxes were normalized to 1 bar transmembrane pressure to obtain the liquid permeability.

### 4.3.4 Gas flux measurements

Dried membranes were cut to circular pieces of 3.9 cm diameter and placed between O-rings in a stainless steel cell. The cell was pressurized to 0.2 - 1 bar with $N_2$-gas. After about 20 minutes the gas flux was determined with a soap bubble meter; measurements were done at two different feed pressures.
The $N_2$ was replaced by $O_2$-gas and the procedure was repeated.

### 4.3.5 Permporometry

Dried membranes were placed in a permporometry cell with an effective surface of 0.91 or 1.54 $cm^2$, depending on the gas permeability. The cells were oval shaped, with a height of 2 mm at each side of the membrane (see figure 3), providing an estimated mean surface diameter of 9 mm. The cell was closed tightly using O-rings to prevent leakage and placed inside the thermostated water bath of the permporometry setup (see figure 3).
As inert gases technical air (21.0% $O_2$ + 79.0% $N_2$) and very pure $N_2$-gas were used. The gas flows were adjusted with mass flow controllers (Brooks 5850TR) to about 1.5 ml/s, and calibrated to obtain exactly equal values. Both gas flows were fed through vapour saturators, containing cyclohexane at about 75 °C, i.e., close to its boiling point of 81°C.

Cyclohexane (Merck, analytical grade) was chosen as condensable vapour for several reasons: PI is chemically almost inert to cyclohexane; cyclohexane is considered as a Van der Waals-gas containing non-interacting, hard, spherical molecules [30]; cyclohexane as a liquid completely wets PI; the use of cyclohexane permits determination of Kelvin radii of 1.5 - 50 nm, which covers almost the whole ultrafiltration range.

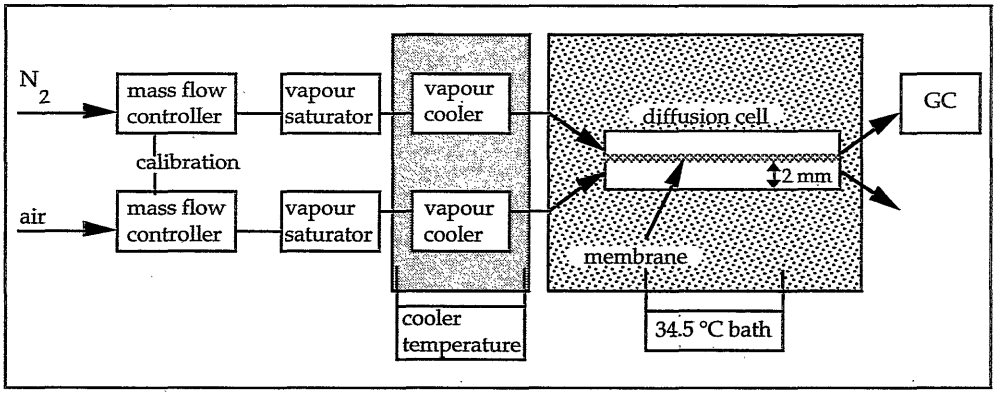


***Figure 3.*** *Schematic representation of the permporometry setup.*

The gas flows, containing cyclohexane vapour, were led through long reversed spiral coolers (at exactly the same temperatures, controlled by a Colora WK 16 thermostat bath filled with ethylene glycol) to adjust the vapour pressure to desired values ($P_R<1$), after which the gas flows entered the two feed sides of the membrane cell. The membrane cell was situated in a thermostath bath at 34.5°C, which is the actual measuring temperature. This temperature is the standard for the saturated vapour pressure, $P_S$.

The cross section of one compartment of the membrane cell resembles a rectangular pipe. The hydraulic diameter ($d_h$ [m]) of a rectangular pipe is given by (2*width*height)/(width+height) = 3.3 mm, and the mean cross sectional area $A = 18*10^{-6}$ m$^2$. The gas flow velocity is $\Phi/A = 0.083$ m/s.
The Reynolds number, Re, is:

$$Re = \frac{\rho_{air}\, v\, d_h}{\eta_{air}} = \frac{1.13 * 0.083 * 3.3*10^{-3}}{18.84*10^{-6}} = 16.4$$

where $\rho_{air}$ [kg/m$^3$] and $\eta_{air}$ [Pa s] are the density and viscosity of air at 34.5°C and 1 bar [36].
In this case Re « 2000, so the flow regime is laminar; this means that the driving force, the partial pressure gradient of oxygen, can be represented by the logarithmical mean value [37]:

$$\overline{\Delta P_{O2}} = \frac{(\Delta P_{O2,in} - \Delta P_{O2,out})}{\ln\left(\frac{\Delta P_{O2,in}}{\Delta P_{O2,out}}\right)}$$

where $\Delta P_{O2,in}$ is the difference in oxygen partial pressure between the two feed streams (= 21 kPa) and $\Delta P_{O2,out}$ is the difference in oxygen partial pressure between the two outlet streams (≤ 21 kPa).
The oxygen concentration in the outlet stream of the nitrogen side was determined using a Varian 3400 gas chromatograph, equipped with a zeolite 13X column. The oxygen content should not exceed 6 kPa (arbitrary value), because in that case the driving force ($\Delta P_{O2,out}$) becomes too low, and not the whole membrane surface is considered. After installation of the membrane, the oxygen diffusion through the membrane was determined in the dry state, to verify this requirement.

The membrane was saturated for at least 16 hours by the gas flows containing vapour at $P_R$ = 1, to ascertain the filling of all the pores with condensed cyclohexane. The measurement itself consisted of a stepwise lowering of the spiral cooler temperatures; after stabilization times of 20 - 30 minutes the oxygen content in the nitrogen stream was determined. In all cases the oxygen diffusion at $P_R$ = 0 (after desorption) was equal to the value before the measurement, so no membrane morphology changes occured during the permporometry cycle.

## 4.4 Results of characterization techniques

### 4.4.1 Liquid flux measurements with ethanol and ethyl acetate as flux media

In chapter 2 it was shown already that the pure liquid permeability of polyimide ultrafiltration membranes for several organic media can be related to each other if corrected for viscosity; this means that the swelling of the polyimide membrane material is comparable for these liquids and that each liquid might be used to determine a pure liquid permeability.
Pure liquid permeabilities of membranes prepared from casting solutions containing 18, 20 or 25wt% PI in DMF and coagulated in ethanol or water were determined for ethanol and ethyl acetate as flux media. The results are given in table 2.

*Table 2.* *Permeability for ethanol and ethyl actetate of several polyimide ultrafiltration membranes.*

| PI-concentr. in casting solution [wt%] | coag. bath | $P_{ethanol}$ [kg/m$^2$hrbar] | $P_{eth.acetate}$ [kg/m$^2$hrbar] | $P_{ethanol}/P_{eth.acet.}$ [-] |
|---|---|---|---|---|
| 18 | ethanol | 526 | 1035 | 0.51 |
| 18 | water | 482 | 950 | 0.51 |
| 20 | ethanol | 291 | 743 | 0.39 |
| 20 | water | 258 | 620 | 0.42 |
| 25 | ethanol | 49 | 143 | 0.34 |
| 25 | water | 67 | 131 | 0.51 |

The last column of table 2 shows that the ratio of the pure liquid permeabilities is within a range of 0.34-0.51. The Hagen-Poiseuille equation (4.1) predicts that the liquid permeability ratio should be equal to the inverse ratio of the liquid viscosities. For ethanol and ethyl acetate this ratio is:

$$\frac{P_{ethanol}}{P_{ethyl\ acetate}} = \frac{\eta_{ethyl\ acetate\ 298\ K}}{\eta_{ethanol\ 298\ K}} = \frac{0.44*10^{-3}}{1.08*10^{-3}} = 0.41$$

This value corresponds reasonably well with the values of the last column of table 2, and this is once again an evidence for the high chemical stability of polyimide ultrafiltration membranes. The experimental irreproducibility in the permeability for different membrane samples of the same type is quite normal for ultrafiltration membranes.

### 4.4.2 Gas flux measurements with oxygen and nitrogen

Membranes that were used for liquid flux measurements, were dried using an ethanol-hexane liquid sequence series. The gas flux of these membranes was determined for oxygen and nitrogen and normalized to 1 bar pressure difference, to obtain the gas permeability. Results of these measurements are summarized in table 3.

*Table 3.* *Fluxes for oxygen and nitrogen of several dried polyimide ultrafiltration membranes [mol/m²s bar].*

| PI-concentr. in casting solution [wt%] | coag. bath | $J_{oxygen}$ [mol/m²s bar] | $J_{nitrogen}$ [mol/m²s bar] | $J_{O2}/J_{N2}$ [-] |
|---|---|---|---|---|
| 18 | ethanol | 0.204 | 0.222 | 0.93 |
| 18 | water | 0.304 | 0.331 | 0.92 |
| 20 | ethanol | 0.115 | 0.129 | 0.90 |
| 20 | water | 0.166 | 0.181 | 0.90 |
| 25 | ethanol | 0.013 | 0.014 | 0.90 |
| 25 | water | 0.043 | 0.047 | 0.92 |

When the transport mechanism is determined by Knudsen diffusion, the ratio of the gas permeabilities of oxygen and nitrogen should be equal to the inverse ratio of the square roots of the gas molecular weights (see eq. (4.5)):

$$\frac{J_{O2}}{J_{N2}} = \frac{\sqrt{M_{N2}}}{\sqrt{M_{O2}}} = \frac{\sqrt{28*10^{-3}}}{\sqrt{32*10^{-3}}} = 0.93$$

This value agrees very well with the experimental permeability ratio, so the main gas transport mechanism is indeed Knudsen diffusion.

### 4.4.3 Permporometry

With the Kelvin relation (equation (4.6)) and equation (4.9) the oxygen content in the outlet stream on the nitrogen side as a function of the relative vapour pressure of cyclohexane can be transferred to a curve representing the oxygen flux versus the pore radius. An example is given in figure 4. The oxygen permeation curve is cumulative: starting from high pore radii, the oxygen flux increases because with every step more pores are available for oxygen diffusion; at very low pore radii, the oxygen flux is the sum of all separate contributions to the permeation.

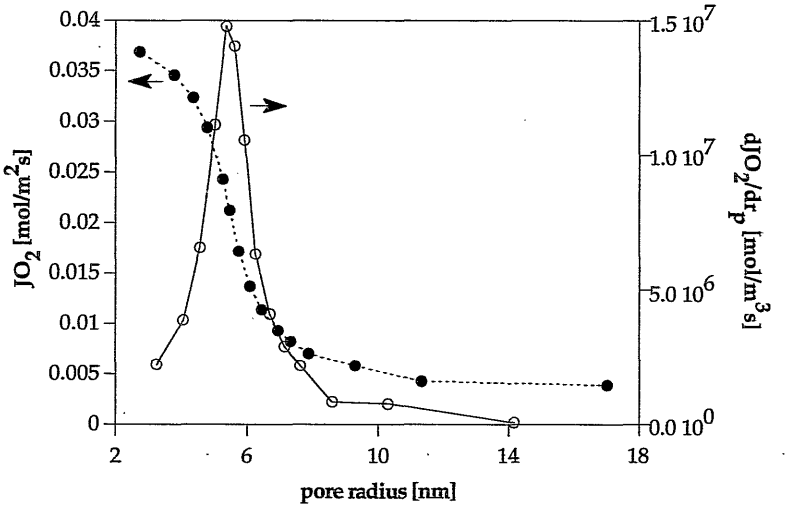


*Figure 4. Example of a cumulative oxygen permeation curve (dashed line) and the resulting differential oxygen permeation curve (solid line), both as a function of the pore radius; for a membrane prepared from a casting solution of 20 wt% PI in DMF and coagulated in ethanol.*

For all membranes the oxygen permeation has a constant value at vapour pressures corresponding to pore radii larger than 20 nm, and it is not zero. This is also indicated by the dashed line in figure 4. It is very unlikely that the membranes contain pores larger than 20 nm, because several other techniques, like Coulter Porometry, retention measurements and bubble pressure measurements excluded the presence of such large pores.
When all the pores are filled with condensed cyclohexane, some oxygen diffusion will take place by solution and diffusion through this layer. The solubility in liquid cyclohexane at 0.21 bar partial oxygen pressure was calculated at $2.35*10^{-3}$ mol/m$^3$ (at 36°C [38]). The diffusion coefficient of oxygen in cyclohexane was estimated at $1.5*10^{-9}$ m$^2$/s, using the Stokes-Einstein equation [39]. Assuming Fickian diffusion, the oxygen diffusive flux through a liquid cyclohexane layer of an estimated thickness of $0.2*10^{-6}$ m, is then:

$$J_{O2} = D_{O2/CH}\frac{\Delta c}{\Delta x} = 1.5*10^{-9} * \frac{2.35*10^{-3}}{0.2*10^{-6}} = 1.76*10^{-5} \text{ mol/m}^2\text{ s}$$

This value is about two orders of magnitude lower than the constant oxygen permeation at vapour pressures corresponding to pore radii larger than 20 nm.
The oxygen diffusion through the pores filled with cyclohexane of an actual ultrafiltration membrane will be even lower, because the porosity is much lower

than 100%. This indicates that oxygen diffusion through liquid cyclohexane cannot explain the permeability of oxygen at high vapour pressures.
It may be possible that there are very small pores present in the membrane, that are too small to be filled by condensed cyclohexane, whereas the smaller oxygen molecules are able to diffuse through them. For further calculation this contribution was neglected.

The cumulative oxygen permeation curves can be differentiated stepwise, resulting in a pore size distribution; on the y-axis values of $dJO_2/dr_k$ are given. The Kelvin radius can be related to a pore radius, by assuming a value for the t-layer; in accordance with Cuperus et al. [30] and Cao et al. [12] a t-layer thickness for cyclohexane condensate of 0.5 nm is assumed here.
In figures 5 and 6 these pore size distributions are compared for ethanol coagulated dry membranes and for water coagulated dry membranes, respectively.

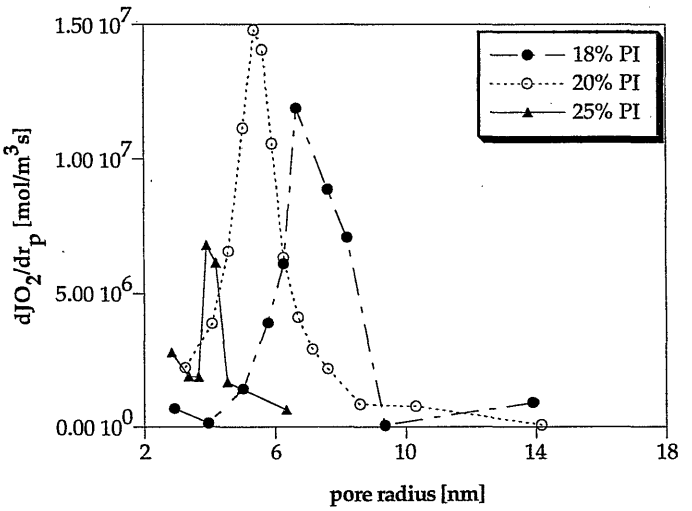


*Figure 5.* *Oxygen diffusion - pore size distributions of membranes prepared from casting solutions containing 18, 20, or 25 wt% PI in DMF, and coagulated in ethanol, calculated from permporometry results.*

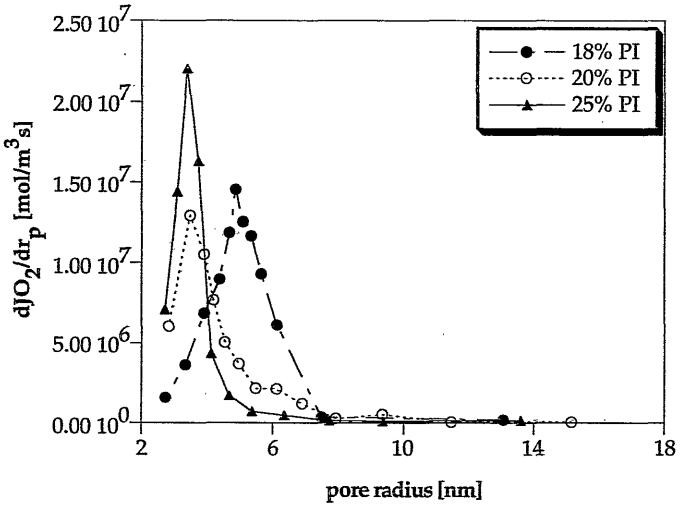


*Figure 6. Oxygen diffusion - pore size distributions of membranes prepared from casting solutions containing 18, 20, or 25 wt% PI in DMF, and coagulated in water, calculated from permporometry results.*

From figure 5 it can be concluded that the pore size distribution of membranes coagulated in ethanol changes with a change in polyimide concentration in the casting solution: 18 wt% PI-membranes have a quite broad distribution with relatively many large pores and a maximum at 7 nm. At 20 wt% PI, the distribution becomes narrower with a maximum at 5.4 nm; for membranes made of 25 wt% PI the distribution is very narrow, with a maximum at 4.0 nm.
For similar membranes coagulated in water the differences are less obvious: the maxima of the curves are much closer to each other, at 5 nm, 3.8 nm and 3.8 nm for 18, 20, and 25 wt% polyimide concentrations in the casting solutions, respectively.
In figures 7, 8 and 9 the pore size distributions are compared for membranes prepared from several PI-concentrations in the casting solutions, but coagulated in different baths; these are the same curves as shown in figures 5 and 6, but represented in different sets.

At lower PI-concentrations in the casting solution (18 and 20 wt% PI, see figures 7 and 8) membranes coagulated in ethanol seem to have many more large pores than membranes coagulated in water, while at 25 wt% PI the water coagulated membranes seem to be more "open" than the ethanol coagulated membranes (see figure 9).

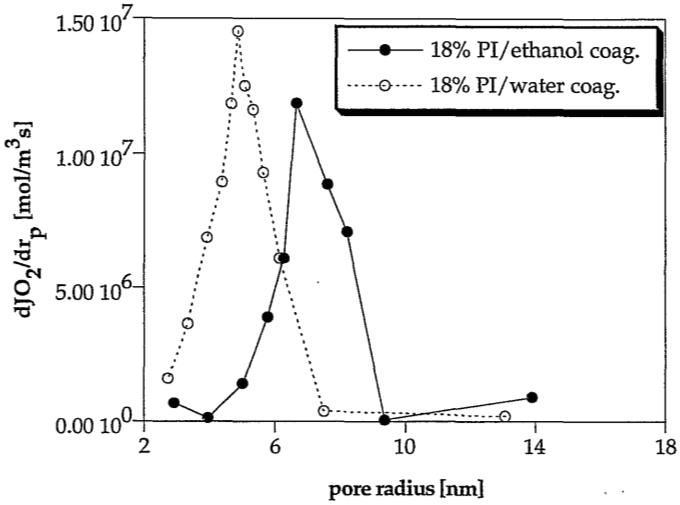


*Figure 7.* *Oxygen diffusion - pore size distributions of membranes prepared from casting solutions containing 18 wt% PI in DMF, calculated from permporometry.*

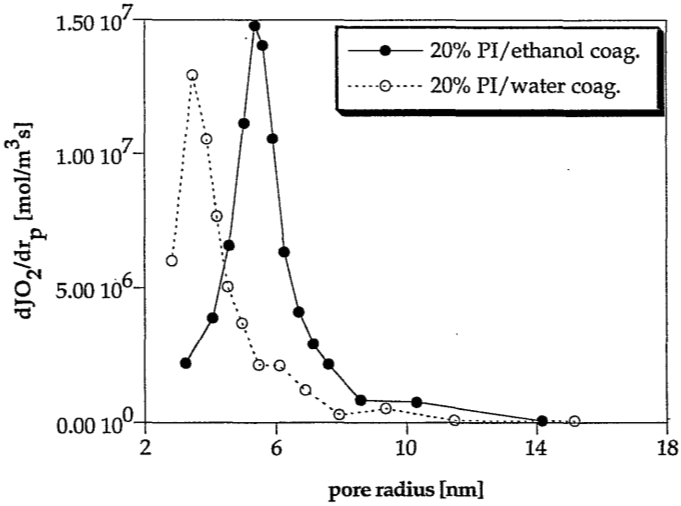


*Figure 8.* *Oxygen diffusion - pore size distributions of membranes prepared from casting solutions containing 20 wt% PI in DMF, calculated from permporometry.*

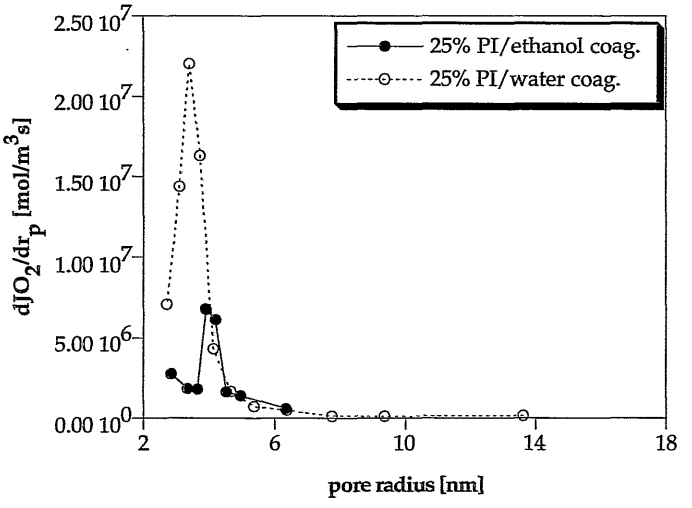


*Figure 9. Oxygen diffusion - pore size distributions of membranes prepared from casting solutions containing 25 wt% PI in DMF, calculated from permporometry.*

The curves of $dJO_2/dr_k$ versus $r_p$ can be translated into a $n(r_p)$ pore size distribution by calculation of the number of pores for each step according to the Knudsen relation (equation (4.7)), which requires the assumption of definite values for the tortuosity, $\tau$, and the toplayer thickness, $\Delta x$. These $n(r_p)$ pore size distributions can be used to calculate a theoretical ethanol permeability (for a *dried* membrane!) as well as a theoretical oxygen permeability. The theoretical permeabilities obtained in this way may be compared with the experimental values from ethanol flux measurements and oxygen permeability determinations. This will be discussed further in the next section.

## 4.5 Discussion: comparison of characterization methods

The $dJO_2/dr_k$-steps from each oxygen diffusion pore size distribution curve, obtained by permporometry, are converted into a differential number of pores - pore size distribution curve, using the Knudsen relation (equation (4.7)); for this purpose $\tau = 1$ and $\Delta x = 0.2$ μm are assumed [30].
An illustrative example for one membrane, prepared from a 20 wt% PI casting solution in DMF and coagulated in ethanol, is given in figures 10-12.

Figure 10 shows the differential pore size distribution for the number of pores vs. the pore radius, as well as the cumulative curve that is obtained by summation of the differential values, starting at high pore radii.

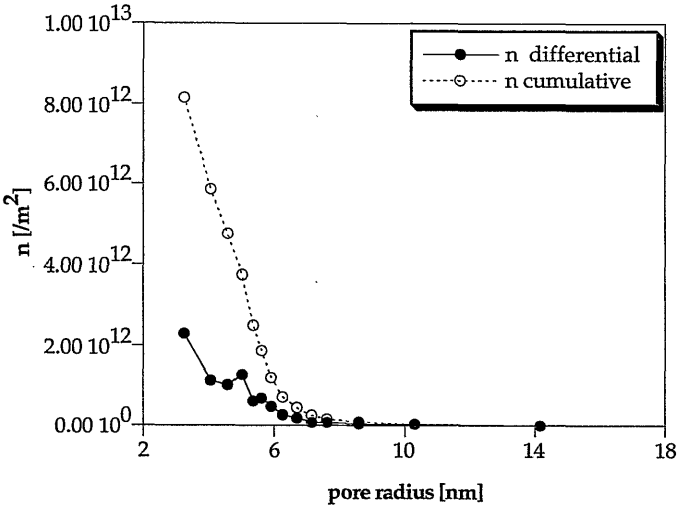


*Figure 10.* *Number of pores - pore size distribution for membranes prepared from a casting solution of 20 wt% PI in DMF, coagulated in ethanol.*

The differental curve is used to calculate a theoretical oxygen flux curve (0.21 bar and 307.7 K) and a theoretical ethanol permeability curve, which are represented in figures 11 and 12, respectively. In these two figures also the cumulative permeability curves are shown.

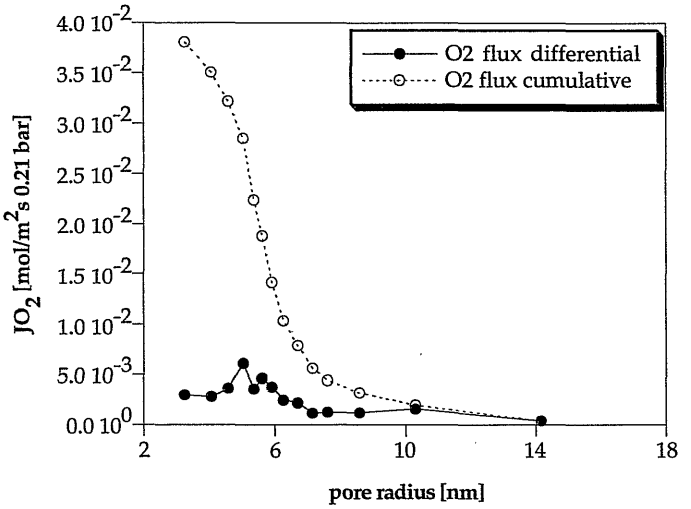


*Figure 11.* *Theoretical oxygen flux curve for membranes prepared from a casting solution of 20 wt% PI in DMF and coagulated in ethanol, at 0.21 bar and 307.7 K.*

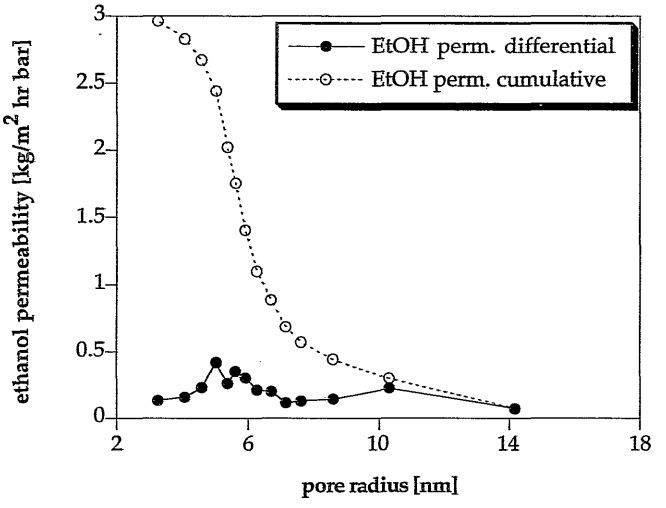


*Figure 12. Theoretical liquid ethanol permeability curve for membranes prepared from a casting solution of 20 wt% PI in DMF and coagulated in ethanol, at 298 K.*

The cumulative theoretical oxygen fluxes at 0.21 bar and 307.7 K (at permporometry conditions) are given in table 4 for the different types of membranes. The values for the experimental oxygen permeability, from table 3, are converted as well to permporometry conditions. In the last column theoretical ethanol permeabilities are calculated from the permporometry pore size distributions.

*Table 4. Theoretical oxygen flux [mol/m²s] at 0.21 bar and 307.7 K from permporometry pore size distributions and experimental gas fluxes at the same conditions. In the last column a theoretical ethanol permeability is given [kg/m²hr bar] for the different membranes.*

| PI-concentr. in casting solution [wt%] | coag. bath | $J_{O2,theor.}$ [mol/m²s] | $J_{O2,experim.}$ [mol/m²s] | $P_{ethanol,theor.}$ [kg/m²hr bar] |
|---|---|---|---|---|
| 18 | ethanol | 0.036 | 0.043 | 3 |
| 18 | water | 0.037 | 0.063 | 4 |
| 20 | ethanol | 0.038 | 0.024 | 2 |
| 20 | water | 0.032 | 0.035 | 3 |
| 25 | ethanol | 0.010 | 0.003 | 2 |
| 25 | water | 0.030 | 0.009 | 1 |

The theoretical oxygen fluxes are clearly of the same order as the experimental values. Deviations might likely be caused by the calculation procedure of the permporometry $n(r_p)$ pore size distribution, because for this purpose a stepwise differentiation procedure was used, which ascribes a certain increase in the number of pores for one interval to one mean pore radius in that interval; this may cause small errors in the final pore size distribution. To approach a more continuous distribution curve, the method would become very laborious.
As a conclusion, permporometry gives a quite reliable pore size distribution for dry ultrafiltration membranes, when applied for gas separation purposes.

The permporometry pore size distributions cannot be used to calculate the (liquid) ethanol permeability. The calculated values are very low and far from the experimental ethanol permeabilities for membranes in the wet state; this difference roughly varies with a factor of 40 to 190. The large discrepancy between the theoretical and the experimental ethanol permeability is a clear indication that drying changes the membrane morphology.

When the membranes used in this study are dried according to an ethanol-hexane displacement sequence and rewetted again, the experimental ethanol permeability is 10-90% lower than the permeability before the drying step. The theoretical ethanol permeability calculated from permporometry parameters is still one order of magnitude lower than this value; this means that rewetting a membrane also changes the membrane morphology, but to a different final wet situation than the original wet state before the drying step.
Consequently, pore size distributions obtained by dry characterization methods are not very reliable for any wet state application.

## 4.6 Conclusions

Liquid flux measurements and gas flux measurements are useful methods to compare polyimide ultrafiltration membranes in a wet and dry state, respectively. Fluxes for ethanol and ethyl acetate are comparable after a correction for the viscosity difference. The transport regime during all gas flux measurements was shown to be Knudsen diffusion; this means that there are hardly any large pores present in the membranes tested.

Using a stepwise differentiation, permporometry results for dry membranes can be used for calculations of pore size distribution curves. Calculation of number of pores - pore size distribution curves from these results requires assumptions for the toplayer thickness and the tortuosity; the number of pores - pore size distribution curves were used to calculate theoretical oxygen fluxes and theoretical ethanol permeabilities.

The results presented in this chapter show that the theoretical oxygen fluxes approach the experimental values for gas separation, while the theoretical (liquid) ethanol permeability (for dry membrane parameters) is in all cases about two orders of magnitude lower than the experimental ethanol permeability (wet membrane, never dried). This means that permporometry is a very good method to determine the pore size distributions of dry membranes, but these distributions should be handled with care when assigned to membranes in a wet state.

## 4.7 References


[1] F.P. Cuperus, C.A. Smolders; Characterization of UF membranes, membrane characteristics and characterization techniques; Adv. Colloid Interface Sci., 34(1991)135

[2] I.M. Watt; The principles and practice of electron microscopy; Cambridge University Press, Cambridge, 1985

[3] I.M. Wienk; Ultrafiltration membranes from a polymer blend; Ph.D. thesis, University of Twente, the Netherlands, 1993

[4] K.J. Kim, A.G. Fane, C.J.D. Fell, T. Suzuki, M.R. Dickson; Quantitative microscopic study of surface characteristics of ultrafiltration membranes; J. Membrane Sci., 54(1990)89

[5] G. Binnig, C.F. Quate, Ch. Gerber; Atomic force Microscope; Phys. Rev. Lett., 12(1986)930

[6] R.M. McDonogh, H. Strathmann. R. Buck, R. Deppich, H. Göhl; Estimation of membrane sieving and rejection from pore size distributions measured by the liquid displacement method; P. Aimar, P. Aptel (Eds.); Récent progrès en génie des procédés; Vol. 6(22)(1992), p.65; Euromembrane 92, Paris

[7] G. Capanelli, F. Vigo, S. Munari; Ultrafiltration membranes - characterization methods; J. Membrane Sci., 15(1983)289

[8] S. Munari, A. Bottino, P. Moretti, G. Capanelli, I. Becchi; Permporometric study on ultrafiltration membranes; J. Membrane Sci., 41(1989)69

[9] V. Gekas, W. Zhang; Membrane characterization using porosimetry and contact angle measurements: a comparison with experimental ultrafiltration results; Process Biochem., oct.(1989)159

[10] A.A. Liabastre, C.J. Orr; An evaluation of pore structure by mercury penetration; J. Colloid Interface Sci., 64(1978)1

[11] C.L. Glaves, D.M. Smith; Membrane pore structure analysis via NMR spin-lattice relaxation experiments; J. Membrane Sci., 46(1989)167

[12] G.Z. Cao, J. Meijerink, H.W. Brinkman, A.J. Burggraaf; Permporometry study on the size distribution of active pores in porous ceramic membranes; J. Membrane Sci., 83(1993)221

[13] C. Eyraud, J.F. Quinson, M.Brun; Characterization of porous solids; K.K. Unger, J. Rouquerol, K.S.W. Sing, H. Kral (Eds.), Elsevier, Amsterdam, 1988

[14] L. Zeman, G. Tkacik, P. Le Parlouer; Characterization of porous sublayers in UF membranes by thermoporometry; J. Membrane Sci., 32(1987)329

[15] C.L. Glaves, P.J. Davis, K.A. Moore, D.M. Smith, H.P.Hsieh; Pore structure characterization of composite membranes; J. Colloid Interface Sci., 133(1989)377

[16] F.P. Cuperus, D. Bargeman, C.A. Smolders; A new method to determine the skin thickness of asymmetric UF-membranes using colloidal gold particles; J. Colloid Interface Sci., 135(1990)486

[17] J.T.F. Keurentjes, J.G. Harbrecht, D. Brinkman, J.H. Hanemaaijer, M.A. Cohen Stuart, K. van't Riet; Hydrophobicity measurements of microfiltration and ultrafiltration membranes; J. Membrane Sci., 47(1989)333

[18] H.D.W Roesink, M.A.M. Beerlage, W. Potman, Th. van den Boomgaard, M.H.V. Mulder, C.A. Smolders; Characterization of new membrane materials by means of fouling experiments. Adsorption of BSA on polyetherimide-polyvinylpyrrolidone membranes; Colloids Surfaces, 55(1991)231

[19] F.F. Stengaard; Characteristics and performance of new types of ultrafiltration membranes with chemically modified surfaces; Desalination, 70(1988)207

[20] M. Oldani, G. Schock; Characterization of ultrafiltration membranes by infrared spectroscopy, ESCA, and contact angle measurements; J. Membrane Sci., 43 (1989)243

[21] M. Fontyn, B.H. Bijsterbosch, K. van 't Riet; Chemical characterization of ultrafiltration membranes by spectroscopic methods; J. Membrane Sci., 36(1987)141

[22] M.H.V. Mulder; Basic principles of membrane technology; Kluwer Academic Publishers, Dordrecht, 1991

[23] A.W. Adamson; Physical chemistry of surfaces; Wiley, New York, 5th ed., 1990; p 58 (Kelvin relation), p. 570 (Kozeny-Carman relation)

[24] H. Yasuda, J.T. Tsai; Pore size of microporous polymer membranes; J. Appl. Polym. Sci., 18(1974)805

[25] F.W. Altena, H.A.M. Knoef, H. Heskamp, D. Bargeman, C.A. Smolders; Some comments on the applicability of gas permeation methods to characterize porous membranes based on improved data handling; J. Membrane Sci., 12(1983)313

[26] E.A. Mason, A.P. Malinauskas; Gas transport in porous media: the dusty gas model; Elsevier, Amsterdam, 1983

[27] C. Eyraud, M. Betemps, J.F. Quinson, F. Chatelut, M. Brun, B. Rasneur; Détermination de la répartition des rayons de pores d'un ultrafiltre par: "permporométrie gaz-liquide", comparaison entre porométrie d'écoulement et porométrie d'équilibre de condensat; Bull. Soc. Chim. France, 9-10(1984)I-237

[28] A. Mey-Marom, M.G. Katz; Measurement of active pore size distribution of microporous membranes - a new approach; J. Membrane Sci., 27(1986)119

[29] M.G. Katz, G. Baruch; New insights into the structure of microporous membranes obtained using a new pore size evaluation method; Desalination, 58(1986)199

[30] F.P. Cuperus, D. Bargeman, C.A. Smolders; Permporometry. The determination of the size distribution of active pores in UF membranes; J. Membrane Sci., 71(1992)57

[31] S.J. Gregg, K.S.W. Sing; Adsorption, surface area and porosity, 2nd ed.; Academic Press, New York, 1982

[32] D.M. Ruthven; Principles of adsorption and desorption processes; J. Wiley & sons, New York, 1984

[33] W. MacDonald, C.-Y. Pan; Method for drying water-wet membranes; US 3.842.515; 1974

[34] P. Manos; Membrane drying process; US 4.080.743; 1978

[35] A. Lui, F.D.F. Talbot, A. Fouda, T. Matsuura, S. Sourirajan; Studies on the solvent exchange technique for making dry cellulose acetate membranes for the separation of gaseous mixtures; J. Appl. Polym. Sci., 36(1988)1809

[36] L'Air Liquide; Encyclopedie des Gaz; Elsevier, Amsterdam, 1976

[37] R.B. Bird, W.E. Stewart, E.N. Lightfoot; Transport phenomena; Wiley, New York, 1960; pp. 467,697

[38] IUPAC solubility data series; Vol. 7, Oxygen and ozone; Pergamon Press, Oxford, 1981; p. 243

[39] E.L. Cussler; Diffusion: mass transfer in fluid systems; Cambridge University Press, Cambridge, 1984; p. 123

# Appendix to chapter 4

## Drying of polyimide ultrafiltration membranes

M.A.M. Beerlage, R.M. Meertens, M.H.V. Mulder, C.A. Smolders, H. Strathmann

### 4.A.1 Introduction

An important problem in characterizing ultrafiltration membranes is the drying process. In chapter 4 it was shown that ultrafiltration membranes show irreversible morphology changes during drying. Moreover, drying of membranes has many advantages over wet membranes with respect to transport, handling and installation.
The effect of various drying procedures on performance and overall surface area of polyimide membranes will be discussed in this appendix.

### 4.A.2 Theory

The toplayer or skin of most asymmetric phase inversion ultrafiltration membranes consists of a tightly packed layer of small nodules. Pores are thought to be formed by the interstitial spaces between the nodules [1-4]. The formation of these nodular structures is still not clear (see chapter 2). Wienk et al. [2] suggested that the highly entangled polymer structure collapses, when brought in contact with the non-solvent during the immersion precipitation process. This collapse results in polymer-rich phase domains (the nodules), with an interconnected structure which contains pores at places where the disentanglement of polymer chains has fully taken place. The disentanglement process is relatively easy as long as much solvent is still present in the nascent membrane which plasticizes the polymer. When most of the solvent has diffused into the non-solvent bath, the system will reach the glassy state, when its glass transition temperature, $T_g$, is well above the temperature of the coagulation bath. In the glassy state, the morphology is effectively frozen, since the relaxation times for polymer movement in the glassy state are extremely large when compared to the rubbery or highly plasticized state.

Most ultrafiltration membranes are stored under wet conditions, because the structure of a membrane changes ("collapses") when the membrane is subjected to a drying procedure. A very simple way to prevent a change of the porous structure is to fill the pores with a non-volatile liquid (glycerol is often used for this purpose [5]). In literature the method is often referred to as a "drying procedure", but strictly speaking it is not a drying process.
In the past several attempts were made to prepare wet-dry reversible membranes, but this was only successful for reverse osmosis or gas separation membranes [6-8]. In the case of ultrafiltration membranes, drying almost without exception induces irreversible loss of solvent permeability, which is thought to be caused by collapse of the porous structure. During the drying procedure, strong capillary forces are present inside the liquid filled pores that are represented by:

$$F_C = \Delta P * A \qquad (4.A.1)$$

where $\Delta P$ is the capillary pressure difference between the gas phase and the liquid phase [Pa] and A is the pore cross sectional area [$m^2$]. The capillary pressure difference is given by the Laplace equation:

$$\Delta P = \frac{2\gamma}{r_p} \cos\theta \qquad (4.A.2)$$

where $\gamma$ is the surface tension of the gas/liquid interface inside the pores [N/m], $r_p$ is the pore radius [m] and $\theta$ is the contact angle between the liquid and the membrane material [°] (see also figure 1).

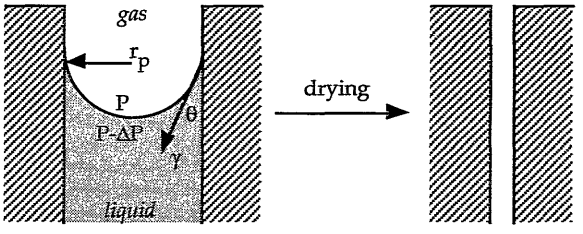


***Figure 1.*** *Schematic drawing illustrating the capillary pressure difference in a pore during the drying process, which may cause a decrease in pore radius or a complete disappearance of the pore.*

The capillary forces can reach large values for the very small pores of ultrafiltration membranes, which might cause the collapse of these pores.
Brown [9] described the coalescence of polymer latex particles by drying during film formation; this process is well comparable with the collapse of pores during

drying of nodular toplayers of ultrafiltration membranes. He stated the resistance of the matrix to deformation opposes the capillary pressure. This resistance of the matrix to deformation, is defined as [9]:

$$F_R = 0.37\ E * A \qquad (4.A.3)$$

E is the tensile modulus of the polymer material [$N/m^2$], and is a measure for the pore wall elasticity. As long as $F_R > F_C$, collapse of the porous structure will not occur, while $F_R < F_C$ is the condition for film formation of the latex particles.
Assuming a tensile modulus of polyimide of $10^9$ $N/m^2$ and $\cos \theta = 1$, then with the surface tension of hexane (i.e., 18 mN/m) and a combination of equations (4.A.1)-(4.A.3), a critical pore radius of 0.1 nm can be calculated. Pores that are larger than this critical radius should not collapse.
However, in equation (4.A.3), E is defined as the tensile modulus of the pure polymeric material. In the case of nodules, the pore wall elasticity is probably lower than the E-modulus of the pure polymer. It is very likely that inside a nodule there is some remaining tension, as well as small voids formed by this tension that are filled with non-solvent, because during the immersion precipitation process the morphology is frozen in a non-equilibrium state. All these factors influence the real wall elasticity of the pores, which complicates the quantitative application of Brown's model to membrane toplayers.

The Laplace equation (4.A.2) indicates that the capillary force is proportional to the surface tension of the liquid that is present during drying. Based on the decrease of surface tension, several patents are aimed to solvent exchange prior to drying of the membranes [10-13], eventually combined with removal of traces of water by addition of molecular sieves to the last solvent bath. The last solvent used is often an aliphatic hydrocarbon like hexane or halogenated hydrocarbons like trichloroethane, since the surface tension of these liquids is relatively low. In this way, $F_C$ is minimized and the porous structure may be maintained if the strength of the matrix is high enough.
Most of these drying procedures are used for asymmetric gas separation membranes, to prevent collapse of the porous structure directly beneath the non-porous skin. For ultrafiltration membranes this is only partly realized, because there is often an irreversible change in performance caused by the drying and rewetting procedure.

For the polyimide ultrafiltration membranes that were used in this study, the characterization results already indicated that there is some discrepancy in morphology between wet and dry membranes, despite the solvent exchange sequence procedure before drying. This discrepancy also made clear that the drying step itself and not the rewetting step is responsible for the morphology

changes. McDonogh [14] measured for polyethersulfone membranes a drying induced reduction in permeability of 10 - 90 %; there was no clear dependence of this reduction on the initial permeability. He also measured the pore size distribution of wet membranes and rewetted membranes using a liquid displacement method; the results showed that pore collapse is dependent on the initial pore size before the drying step: especially in the 2 - 9 nm pore radius range the number of pores is decreased dramatically.

Irreversible changes induced by drying are also present on a somewhat larger scale: the overall geometrical surface of a membrane shrinks during the drying procedure. This might be prevented by casting the membrane on a non-woven that does not shrink. The risk of this procedure is that the shrinking membrane on top of the support may form crazes, which can be more disadvantageous for application than the partial pore collapse of a freely shrinking membrane.

In this appendix the drying of polyimide ultrafiltration membranes will be described. Firstly, the liquid permeabilities of wet and rewetted membranes using an ethanol-hexane solvent exchange sequence as a drying procedure will be compared. The overall surface shrinkage of the membranes will then be compared using different drying procedures.

## 4.A.3 Experimental

### 4.A.3.1 Materials and membranes

Polyimide P84, from Lenzing AG, Austria, was kindly supplied by X-Flow BV, the Netherlands. The preparation of the membranes has already been described in chapters 2 and 3. All solvents were purchased from Merck (analytical grade) and used as received.
Molecular sieves with pore diameters of 5Å were dried at 150 °C under vacuum before use.

### 4.A.3.2 Drying procedures

Ethanol-wet membranes were cut in circular pieces with a diameter of 7.6 cm. The membrane samples were dried by different procedures. Conditioning in liquid exchange baths took place in well-closed beakers to prevent preliminary drying of membranes. A change in type of bath was always accompanied by at least three washing steps with the new bath medium. During the real drying step, from the last bath to air, membranes were kept between tissues and glass plates to prevent curling.
All methods are summarized in table 1.

***Table 1.*** *Overview of drying procedures. E = ethanol, H = hexane, A = air; liquid combinations are given in volume ratios.*

| nr. | procedure: liquid-liquid exchange sequence prior to drying |
|---|---|
| 1 | E - A |
| 2 | E - water (3 days) - A |
| 3 | E - water (3 days) - oven 80 °C (1 day) - A |
| 4 | E - H (3 days) - A |
| 5 | E - H (35 days) - A |
| 6 | E - 1:1 E:H (3 days) - H (3 days) - A |
| 7 | E - 3:1 E:H (3 days) - 2:1 E:H (3 days) - 1:1 E:H (3 days) - 1:2 E:H (3 days) - 1:3 E:H (3 days) - H (3 days) - A |
| 8 | E - H with mol. sieves (3 days) - A |
| 9 | "water-free prepared" membrane - E - H (3 days) - A |
| 10 | E - H (3 days) - supercritical drying from hexane - A |

Method 2 was used to investigate the influence of a liquid with a high surface tension, method 3 also included a faster evaporation speed.
Methods 4 - 7 were normal solvent exchange sequences, using different residence times in the hexane bath or different exchange rates.
Method 8 was employed to remove traces of water from the system, analogous to one of the cases described in literature [11].
For method 9, some membranes were prepared in coagulation baths of ethanol of analytical grade and flushed with fresh analytical grade ethanol instead of water. In this way water-free prepared membranes could be obtained, which were dried according to procedure 4. This water-free method has been used to exclude the presence of water inside the pores that might influence pore collapsing.
Method 10, supercritical drying from hexane, was used to avoid the presence of phase menisci in the membrane pores during the drying step. By evaporation of hexane above the critical point, no liquid-vapour transition occurs, so the surface tension can have no influence during supercritical drying. Hexane was chosen as medium, because the critical point of n-hexane is at a pressure of $P_c = 30.2*10^5$ Pa and a temperature $T_c = 234.8$°C [15], which is well below the $T_g$ of PI (310°C [16]).
For the supercritical drying experiments, an open glass cylinder was filled with n-hexane containing membrane samples and placed in a thermostated autoclave. The pressure was increased to about $35*10^5$ Pa, after which the temperature was raised slowly to 245°C. During the heating process, the pressure inside the autoclave increased due to expansion of the hexane; therefore the pressure build-up was released a few times. After reaching a pressure of $56*10^5$ Pa and a temperature of 245°C, the autoclave was kept under these conditions for 1.5 hours. The pressure was released quickly to about $1*10^5$ Pa; the autoclave was

flushed a few times with dry nitrogen gas at $10*10^5$ Pa to remove traces of hexane vapour. The membranes were then cooled inside the autoclave to room temperature. A schematic representation of the pressure vs. temperature diagram during the supercritical drying is given in figure 2.

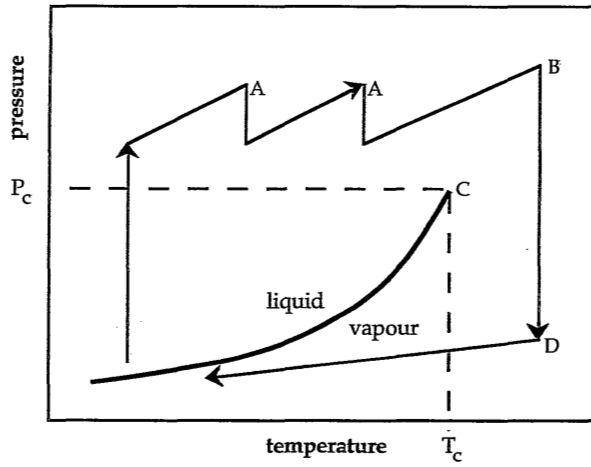


*Figure 2. Schematic representation of supercritical drying. The fat line represents the liquid-vapour phase transition, ending at the critical point of hexane (point C). Points A are releases in pressure, B is the supercritical stabilization stage and at point D all hexane vapour is removed by flushing with nitrogen.*

## 4.A.4 Results

### 4.A.4.1 Ethanol permeability change by drying and rewetting

Several membranes were dried by an ethanol-hexane-air exchange sequence (drying procedure 4 in table 1), during which the membranes were kept for three days in hexane. The geometrical membrane surface shrunk in all cases. After rewetting, the ethanol permeability was determined again.
The results were very irreproducible, but all membranes showed a decline in permeability relative to the initial wet state ranging from 10 - 90 % of the original value. From these results no information on permeability decrease could be obtained.

### 4.A.4.2 Geometrical surface shrinkage

Membrane samples with a fixed diameter of 7.6 cm were dried according to the procedures described in table 1 in the experimental section.

All membranes that were prepared from PI-solutions in DMF or DMAc (with different PI-concentrations and water or ethanol as coagulation bath) showed a similar surface shrinkage of 18%, despite their large differences in initial ethanol permeability. (This is surprising, because it means that a membrane with only 10% permeability decline shows an equal surface shrinkage as a membrane with 90% permeability decline.)
Furthermore, the difference in surface tension had no influence on the overall surface shrinkage, because drying procedures 2 (high $\gamma$), 4 (low $\gamma$) and 10 (no $\gamma$!) all shrunk to the same degree. In addition, a longer residence time in the hexane bath (methods 4 vs. 5), a more gradual solvent exchange (methods 4, 6 and 7) and even waterfree membrane preparation (methods 4 vs. 9) had no influence at all on the final membrane surface dimensions.
On the other hand, membranes that were prepared from PI-solutions in NMP all showed an overall surface shrinkage of 22%.

## 4.A.5 Discussion

The permeability decline by drying (and rewetting) of the membranes used in this study varied to a large extent. The results of McDonogh for polyethersulfone ultrafiltration membranes also showed this kind of behaviour, with about the same variation in permeability decline [14]. This is probably caused by the fact that the pore size distributions of these membranes are situated around the most critical pore range: from 2 - 9 nm pore radius there is a drastic decrease in the number of pores caused by drying, while at about 10 nm there is even an increase [14]. Pores with sizes larger than 20 nm are hardly influenced by the drying step, which explains the almost complete absence of drying shrinkage for microfiltration membranes.
Even for one type of membrane the drying results are also very irreproducible. This might be caused by the relative distribution of pores over the membrane surface: a large pore, which is emptied earlier than a small pore, might be widened when a small pore is situated close to it.
A very strange phenomenon in this respect is that the gas permeability and permporometry results are very reproducible for each separate type of membrane. This means that probably the drying step causes a more or less reproducible change in pore size distribution, whereas the rewetting step causes an irreproducible change. It might be possible that the net effect of the drying procedure on the pure ethanol permeability (theoretically) consists of a very severe decline, while the rewetting procedure is responsible for a partial, but irreproducible, recovery of the ethanol permeability.
This hypothesis is in accordance with the permporometry and ethanol permeability results: the theoretical ethanol permeability (obtained from permporometry parameters) for a dry membrane is 40-190 times lower than the

original ethanol permeability and reproducible for membranes from the same batch, while the experimental permeability for a rewetted membrane is only a factor 1.1-10 lower than the original pure ethanol permeability but irreproducible for membranes from the same batch.
This irreproducibility may be caused by incomplete wetting of the membrane material during the rewetting procedure, i.e., the advancing contact angle is not zero. However, these contact angles are not known for polyimide.

The surface tension of the liquid inside the pores surely has an influence on the collapse of the pores, but the results presented here indicate that the surface tension has little influence on the overall membrane surface shrinkage. Collapse of the pores might cause a decrease in membrane surface; if this is supposed to be the main mechanism to explain the surface shrinkage, then different pore size distributions would result in differences in surface shrinkage. However, the results show that the surface shrinkage is equal in most cases. Furthermore, the surface porosity ($\approx$ 1%) of ultrafiltration membranes is much lower than the surface shrinkage by drying (18-22%). Therefore, the collapse of the pores probably is of minor importance when considering the overall surface shrinkage during drying. The fact that the use of NMP as membrane casting solvent results in an increase in surface shrinkage (when compared to DMF or DMAc) may point at some influence of the membrane preparation conditions on the final membrane surface shrinkage.

During the immersion precipitation process, the formation of nodules is accompanied by disentanglement of the polymer chains between the nodules. At the moment of immersion into the coagulation bath, the toplayer configuration is rapidly frozen in a non-equilibrium state, due to the fast exchange rates of solvent and non-solvent. It is likely that in the skin and the region directly beneath the toplayer, still large tensions are present.
It is not clear why NMP as membrane casting solvent induces higher overall surface shrinkage. During membrane formation DMF, DMAc and NMP all cause instantaneous demixing. It might be possible that due to the relatively lower diffusion coefficient of NMP, at the moment of vitrification there is more NMP left in small voids *inside* the nodules than would be the case for DMF or DMAc. These voids are smaller than the pores of the membranes and probably of the order of the free volume elements of the polymer material. Since the porosity based on capillary pores of ultrafiltration membranes in general is very low, it is likely that the relative "area" of these voids is much larger than the area of the pores between the nodules. After removal of the solvent by rinsing, this would result in a higher void percentage inside the nodules of membranes prepared from NMP-solutions. These voids are now filled with non-solvent. Ree et al. [17] studied the effect of precursor history on residual stress and relaxation of several

polyimides using a wafer bending technique. One of their most important results is that for polyimides with high glass transition temperatures stress relaxation is mainly the result of moisture uptake at ambient conditions. This can explain the presence of small voids filled with non-solvent inside the nodules. As long as non-solvent is filling the voids, the structure of the membrane is supported and stabilized by the incompressible non-solvent. When the membrane is subjected to drying, the voids collapse, so that membranes from NMP-solutions show a higher overall surface shrinkage.
This hypothesis is very difficult to prove experimentally, because microscopic techniques have to be carried out for membranes in the wet and the dry state to compare the differences in size of the nodules before and after drying.

## 4.A.6 Conclusions

Like most ultrafiltration membranes, polyimide membranes show irreversible morphology changes when they are subjected to a drying procedure. These changes manifest themselves in at least two phenomena: a solvent permeability decrease by a change in pore size distribution and an overall membrane surface shrinkage. The solvent permeability decrease was shown to be very irreproducible; it is suggested that the drying procedure causes a reproducible change in pore size distribution, while the rewetting procedure causes an irreproducible change.
Until now, it was generally assumed that surface shrinkage was directly caused by pore collapse, but the results presented in this study made clear that there must be an even more important mechanism next to pore collapsing that determines the shrinkage.
It is suggested that during membrane preparation strong tensions tend to be frozen in, while liquid exchange results in residual small voids *inside* the nodules in the toplayer; these voids also collapse during drying, and are probably the main cause for the surface shrinkage. Experimental (shrinkage) results for membranes prepared from PI-solutions in a different solvent, support this hypothesis.

## 4.A.7 Acknowledgement

The authors would like to thank mr. A.H. Pleiter of the High Pressure Lab of the University of Twente for performing the supercritical drying experiments.

## 4.A.8 References


[1] R.M. Boom, I.M. Wienk, Th. van den Boomgaard, C.A. Smolders; Microstructures in phase inversion membranes. The role of a polymeric additive; J. Membrane Sci., 73(1992)277

[2] I.M. Wienk, Th. van den Boomgaard, C.A. Smolders; The formation of nodular structures in the toplayer of ultrafiltration membranes; accepted for publication in J. Appl. Polym. Sci.

[3] I. Pinnau, W.J. Koros; A qualitative skin layer formation mechanism for membranes made by dry/wet phase inversion; J. Polym. Sci., B, Polym. Phys., 31(1993)419

[4] W.J. Koros, G.K. Fleming; Membrane-based gas separation; J. Membrane Sci., 83(1993)1

[5] W. Stone, P.A. Cantor, B.S. Fischer, W.S. Highley; Dry polycarbonate membranes; Eur. Pat. Appl. EP 46,817; 1982

[6] K. Vásárhelyi, J.A. Ronner, M.H.V. Mulder, C.A. Smolders; Development of wet-dry reversible reverse osmosis membranes with high performance from cellulose acetate and cellulose triacetate blends; Desalination, 6(1987)211

[7] R.E. Kesting; Reverse osmosis membranes by complete evaporation of the solvent system; US 3,884,801; 1975

[8] B.S. Minhas, T. Matsuura, S. Sourirajan; Formation of asymmetric cellulose acetate membranes for the separation of carbon dioxide - methane gas mixtures; Ind. Eng. Chem. Res., 26(1987)2344

[9] G.L. Brown; Formation of films from polymer dispersions; J. Polym. Sci., 22(1956)423

[10] W. MacDonald, C.-Y. Pan; Method for drying water-wet membranes; US 3,842,515; 1974

[11] P. Manos; Membrane drying process; US 4,080,743; 1978

[12] M.-W. Tang, W.M. King, C.G. Wensley; Air dried cellulose actetate membranes; US 4,855,048; 1989

[13] P. Manos; Gas separation membrane drying with water replacement liquid; US 4,080,744; 1978

[14] R.M. McDonogh; unpublished results

[15] K.H. Simmrock, R. Janowsky, A. Ohnsorge; Critical data of pure substances: Ag - C7; p. 468; Chemistry Data Series, Vol 2, part 1; Dechema, 1986

[16] According to supplier: Lenzing AG

[17] M. Ree, S. Swanson, W. Volksen; Effect of precursor history on residual stress and relaxation behaviour of high temperature polyimides; Polymer, 34(1993)1423

# Chapter 5

## Non-aqueous retention measurements: ultrafiltration behaviour of polystyrene solutions and colloidal silver particles

M.A.M. Beerlage, M.L. Heijnen, M.H.V. Mulder, C.A. Smolders, H. Strathmann

**Summary**

The retention behaviour of polyimide ultrafiltration membranes was investigated using dilute solutions of polystyrene in ethyl acetate as test solutions.
It is shown that flow-induced deformation of the polystyrene chains highly affects the membrane retention. This coil-stretch transition is not instantaneous, but gradual. The concept of a deformation resistance has been introduced to explain this behaviour. This concept can be applied to describe the flux behaviour of the membranes during the tests as well. Solute deformation allows to compare the pore size distributions of the membranes qualitatively.
Retention measurements were also performed with silver sol particles that were prepared in mixtures of ethanol and water; these sols remain stable as long as the ethanol concentration does not exceed 57 volume percent. The sols were completely retained by the membranes, which is probably caused by the fact that the effective diameter of the particles is much larger than that observed by transmission electron microscopy.

## 5.1 Introduction

Solute retention measurements are generally regarded as one of the most important techniques to characterize the pore size distributions of ultrafiltration membranes. The major advantage of such measurements is the fact that the characterization conditions can be very well compared to the actual ultrafiltration applications for which the membranes will be used. Complications which interfere with drying of the membranes, as discussed in chapter 4, do not occur. For polyimide membranes which are employed for non-aqueous applications, retention measurements with non-aqueous mixtures can be used as a characterization method as well.
There are still a lot of problems involved with retention measurements, such as concentration polarization, molecular weight distribution or adsorption. Another point is the possible occurrence of flow-induced deformation of flexible polymers that are used as retention model solutes.

In this chapter, the retention and flux behaviour will be described of dilute solutions of polystyrene in ethyl acetate using polyimide membranes. Special attention will be focused on the flow-induced deformation of the flexible polymer chains during these retention measurements.
In addition, the retention behaviour of non-deformable silver sols will be discussed.

## 5.2 Theoretical background and literature

### 5.2.1 Retention measurements

An important industrial application for ultrafiltration membranes is found in the dairy industry, where ultrafiltration is used to concentrate whey proteins [1]. The major problem in the ultrafiltration process is the occurrence of fouling of the membranes by the proteins. The fouling process starts with adsorption at the membrane surface and pore narrowing or blocking by adsorption or plugging of the solutes inside the pores. With some solutes it is possible that a gel layer is formed at the membrane surface. This effect is enhanced by concentration polarization, which results in an increase in solute concentration at the membrane surface due to total or partial retention of the solute by the membrane. Fouling and concentration polarization generally result in an increase in retention, but also cause a drastic decline in flux through the membrane. An overview of membrane fouling and concentration polarization is given in several publications [2-4]. A schematic drawing illustrating the hydrodynamic resistances to transport is given in figure 1. The resistance of the

membrane toplayer is always present during ultrafiltration, whereas the other resistances occur during ultrafiltration of solutions.

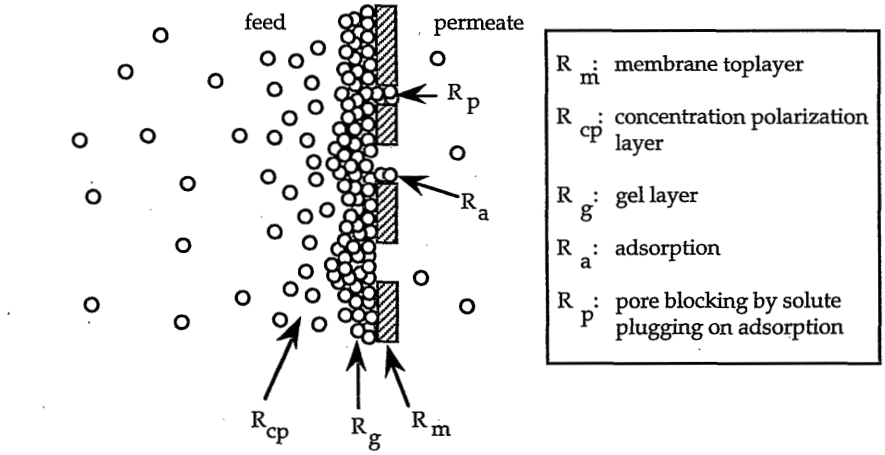


***Figure 1.*** *Schematic drawing illustrating the hydrodynamic resistances that can cause flux decline during ultrafiltration [4]; the resistance of the toplayer is always present.*

For industrial applications of ultrafiltration, a large amount of research has been aimed to prevent or reduce adsorption and fouling, by developing membrane materials which are less sensitive to fouling [5] or by chemical modification of the membrane surfaces [6,7]. Also hydrodynamic conditions of the feed flow can be varied to reduce membrane fouling and concentration polarization. Hydrophobic materials are generally much more sensitive to protein adsorption than hydrophilic materials. A protein molecule consists of hydrophobic and hydrophilic groups. In aqueous environments, a protein molecule is stabilized by intramolecular hydrophobic interactions, i.e., most of the hydrophobic groups will direct themselves to the interior of the globular molecule, whereas most of the hydrophilic groups will be situated on the outside of the protein, in contact with the surrounding water. The adsorption on hydrophilic surfaces will be rather loose and reversible, because the molecule retains its shape. On hydrophobic surfaces, the hydrophobic groups will be brought in contact with the surface, so that the protein will be deformed and adsorption will be irreversible [8].

Bottino et al. [9] described the influence of the hydrodynamic conditions on membrane characterization by retention measurements. They concluded that it is necessary to measure at low transmembrane pressures, high feed flow velocity parallel to the membrane surface and with very low solute concentrations.
For characterization purposes, another way to avoid the specific fouling

problems caused by the use of proteins, is to use synthetic polymers as model solutes in dilute solutions. Almost all characterization retention studies were performed using aqueous sytems. It is very likely that the retention and adsorption behaviour of polymers in organic solution differs from the behaviour in aqueous solutions. This will be discussed in more detail later.
A second important reason to take polymers as model solutes for retention measurements is that in this way a range of molecular weights can be tested without the problem of solute specific properties. For proteins, these specific properties will most likely be different when using a variety of different sizes. In this way, for a range of similar solutes a retention curve can be obtained, which gives the retention coefficient as a function of the solute polymer molecular weight.
The use of gel permeation chromatography to determine the change in molecular weight distribution of polymers in feed and permeate, as described by Cooper and Vanderveer [10], gave an extra impulse to membrane characterization by polymer retention measurements. With this method, the retention coefficient can be determined as a function of the polymer molecular weight by only one retention experiment.
The most frequently used polymers for membrane characterization are water-soluble dextrans and polyethyleneglycols (PEG), because they are commercially availabe in several molecular weight lengths and distributions. However, Baker and Strathmann [11] pointed out already in 1970, that often a discrepancy exists between the retention measurements of proteins and other polymers: the retention of a protein is always higher than the retention of a polymer (dextran or PEG) of the same molecular weight. They also found a retention decline for the polymer with increasing transmembrane pressure, and they ascribed this unexpected behaviour to shear-induced deformation of the flexible polymers in dilute solutions.

The literature concerning retention measurements of solutions of flexible polymers can be divided in two classes: the first group describes the retention behaviour by assuming polymer deformation, the other group shows that the behaviour of polymers can be described by assuming that the solutes are non-permeable or non-draining rigid spheres, like proteins.
In the latter case the sieving mechanism can be used. This mechanism is described mathematically by relations derived by Ferry (equation (5.1)) [12], Mason et al. (5.2.a) [13] or Munch et al. (5.2.b) [14]. These relations describe rejection of non-adsorbing rigid spheres by capillary pores larger than the spheres (i.e., $\lambda<1$; when $\lambda\geq1$: R=1), according to:

$$R = \frac{c_o - c_p}{c_o} = (\lambda(2-\lambda))^2 \qquad (5.1)$$

$$R = 1-(1-\lambda)^2(2-(1-\lambda)^2)\frac{(1-\lambda/3)}{(1-\lambda/3+2\lambda^2/3)} \qquad (5.2.a)$$

$$R = (1-(1-\lambda)^2)^{3/2} \qquad (5.2.b)$$

Here, $c_o$ and $c_p$ are the solute concentrations in the feed and the permeate, respectively, and $\lambda$ is the ratio of solute radius to pore radius: $\lambda = r_s/r_p$, where $r_s$ is defined as the Stokes-Einstein radius or the hydrodynamic radius of the solute. Relation (5.1) was derived for filtration cases where diffusion is dominant, while relations (5.2.a,b) were derived for cases where convection is dominant, thus including hydrodynamic effects. All three equations are valid for $\lambda < 1$; if $\lambda \geq 1$, then $R = 1$. In practice, these equations give about the same retention curves.
In literature several modifications of these equations were given to describe the sieving mechanism in the absence of fouling; the values for the retention resulting from these models also show little variation.

Today researchers still disagree whether the retention of flexible polymers in very dilute solutions is influenced by flow-induced deformation, during which the polymer is able to alter its conformation and pass even very small pores (see also section 5.2.2).
A very important reason for this disagreement was the lack of understanding of the deformation of polymers. A breakthrough came in 1976, when De Gennes formulated his scaling laws for flexible polymers [15]. Daoudi and Brochard [16] used these scaling laws for a physical description of the transport of flexible polymers through cylindrical and conical pores.
Nguyen and Néel [17,18] showed that the flow-induced deformation as described by scaling laws applies qualitatively to their experimental results on filtration of dilute solutions of fractionated PEG and dextran through various ultrafiltration membranes.
Long and Anderson [19], who measured flow-dependent retention of monodisperse polystyrene (PS) in carbon tetrachloride/methanol, showed that flow-induced deformation is not only restricted to water-soluble polymers. By comparing experimentally the molecular weight distribution of PS in permeate and feed they also excluded polymer chain degradation by deformation as possible source for errors in the determination of the concentration difference in permeate and feed. In a later article, Long and Anderson [20] also proved that the deformation is not dependent on the solvent quality (which influences the molecular radius), by using different ratios of carbon tetrachloride to methanol in the mixed solvent.
On the other hand, Mitchell and Deen [21] published results of retention measurements of solutions of BSA (a protein), ficoll (a crosslinked poly-

saccharide) and dextran, from which they concluded that even the dextrans behave like rigid hard spheres and are not susceptible to deformation. However, the interpretation of their results is somewhat problematic since BSA adsorbs on the membrane surface (Nuclepore membranes), while dextran hardly adsorbs, which makes a comparison of the retention of these two solutes troublesome.

Poyen et al. [22] measured the retention of monodisperse PS in cyclohexane for ceramic membranes, and they concluded that the non-draining rigid sphere model is only valid as long as the pore radius is larger than the solute radius, i.e., $\lambda = r_s/r_p < 1$.
Comparison of the results of several retention studies confirms this conclusion: the measurements performed by Mitchell and Deen [21], Liu et al. [23] and Long et al. [24] were done at a $\lambda < 0.5$ (and hence no flow-induced deformation took place), while the measurements of Long and Anderson [21] , Nguyen et al. [17] and Nguyen and Néel [18] used a value of $\lambda \geq 1$ (flow-induced deformation). In another article, Long and Anderson [19] were even more precise. They postulated that when $\lambda \geq 1$, apparently flow-induced deformation takes place, but when $0.5 < \lambda < 1$, then the behaviour of the polymer molecules is some sort of combination of deformation and rigid sphere sieving; the latter situation is very difficult to describe.
Zeman and Wales [25] measured filtration of dextran molecules through Nuclepore membranes. They showed that the experimental retentions agree well with the hard sphere sieving model at low values of $\lambda$, but when $\lambda \geq 0.6$, the experimental retentions deviate from the theoretical values predicted by this model.
Measurements that do not seem to be in agreement with this conclusion are described by Mochizuki and Zydney [26], who measured dextran ultrafiltration at rather high feed concentrations through asymmetric polyethersulfone membranes, over a large range of $\lambda$-values. They concluded that during all these measurements dextran deformation never occurred. The reason for this disagreement seems to be the very high surface porosity of the membranes they used; this will be discussed further in section 5.2.2.
In conclusion: if $\lambda > 0.6$, flow-induced deformation plays an important role during the ultrafiltration of very dilute solutions of flexible polymers.

Davidson and Deen [27] developed a detailed hydrodynamic model on diffusive and convective transport of flexible macromolecules through pores, with $\lambda \leq 1$. Their theory accounted for statistical deformation of the polymer chain, resulting in a chain conformation distribution. Their model is able to describe the lower retention of flexible polymers compared to rigid spheres in the vicinity of $\lambda = 1$, but it can not explain the passage of very large polymers (high molecular weight) through the pores in the case of $\lambda \gg 1$. Davidson and Deen neglected flow-induced deformation, since they assumed that the relaxation time for a polymer

chain is much smaller than the characteristic time for the converging flow near the pore entrance. This is not very realistic for ultrafiltration membranes where the flow velocity near the pore entrance can be extremely high, because of the *low membrane porosity*. Consequently, the influence of a polymer chain conformation distribution might be important when diffusion plays a dominating role.
The dependence of hindered diffusion of flexible polymers through porous membranes on $\lambda$ is now generally accepted. Guillot et al. [28] showed that the effective diffusion coefficient of PS in ethyl acetate through Nuclepore membranes is dependent on $\lambda$; at lower values of $\lambda$, the hindered diffusion of PS-chains can be regarded as diffusion of rigid spheres, while at $\lambda \approx 1$ scaling laws describe chain flexibility much better. However, the pores in Nuclepore membranes are not straight capillaries, but have a sort of "balloon shape" [29]. It is not clear which pore radius is used for the determination of $\lambda$ in this case.
Diffusion of flexible polymers through ultrafiltration membranes is more elaborately discussed in chapter 6.

Most retention studies used a rather broad solute molecular weight distribution, and this polydispersity can have a large effect on the mutual partial retention coefficients, as was shown by Bottino et al. [9]. For this reason the mentioned studies cannot simply be included in a comparison of the influence of $\lambda$ on the polymer behaviour during filtration.
Also the effect of adsorption (solute-membrane interactions) on the retention, hydrodynamic flow through the pores and flow-induced deformation is still far from clear.

Another very important parameter, which is often not recognized, is the choice of the solvent. Until now, most studies were done with water as solvent. Since water has very specific characteristics, the use of organic solvents will give completely different results. Water has an extreme hydrogen bonding ability and may easily form clusters. Polymers that are water-soluble also have very specific properties (e.g., negative heat of dilution, sometimes occurrence of a lower critical solution temperature (LCST), strong tendency to aggregate and adsorb). As a consequence, the normal Flory-Huggins theory is often not valid for these aqueous polymer solutions. Extended reviews on water-soluble polymers are found in literature [30,31].
The major part of water-soluble polymers contain both hydrophobic and hydrophilic moieties. A solution in water may result in a structure similar to globular proteins: intramolecular hydrophobic interaction and stabilization of this structure by strong interactions between the shell of hydrophilic groups and a surrounding layer of bound water [8]. These water-specific interactions may have a very pronounced influence on the magnitude of the elastic restoring

force, and diminish the possibility to deform; the solute molecules might be regarded as rigid spheres, even at very high shear rate. For this reason a comparison of aqueous and non-aqueous retention studies will be very difficult.

Summarizing: there are several demands that need to be fulfilled for reliable retention measurements with flexible macromolecules:

- adsorption must be excluded
- concentration polarization must be minimized
- use of monodisperse solutes excludes mutual effects
- solute-solvent interactions should be understood; solvent-specific interactions have to be minimized

In this chapter, polystyrene (PS) in ethylacetate was chosen as model system. The expected solute to pore radius, $\lambda$, was $\geq 1$ for the majority of pores, as estimated from permporometry measurements for the tested membranes (see chapter 4); anyway, the value of $\lambda$ was always larger than 0.5. The $\lambda$ used here is based on the ratio of the hydrodynamic solute size to the pore size. The results can also be compared to other non-aqueous retention measurements, with PS as solute.
In addition, the adsorption ability of PS on the polyimide membranes has to be examined.

As soon as the phenomenon of flow-induced deformation was recognized, researchers started to look for other solutes to characterize membranes by retention measurements. Some attempts were directed at branching of several macromolecules. Adamski and Anderson [32] compared the retention behaviour of linear comb-branched, and star-branched polystyrenes; their results indicated that branching reduces the flexibility only slightly.
Intramolecular crosslinking of polymers could also be a possibility, but this seems to be far more succesful in aqueous systems (e.g. ficoll: a crosslinked polysaccharide [18]) than in non-aqueous sytems: Antonietti and Sillescu and Antonietti et al. [33,34] showed that intramolecular crosslinking of PS in dichloroethane resulted in only a small reduction in flexibility. Adamski and Anderson [35] filtered dilute solutions of a rigid rod polymer, poly(1,4-phenylene-2,6-benzobisthiazole) in methanesulfonic acid, but the retention in this case is also flow-rate dependent. This can be explained by the long cylindrical shape of a rigid rod: in a flow field towards the pore entrance, the rod is directed perpendicular to the membrane surface and can easily enter the pore.
For aqueous systems it is also possible to use Aerosils®, small silica particles [36]. Unfortunately, these particles are not stable in organic solvents. They can be coated with long polymer chains [37,38], but then the resulting particle will consist of a hard core with a shell of flexible macromolecules, so that also in this case the actual size during retention measurements is an unknown parameter.
The use of micelles [39] is not suitable to characterize PI membranes, because the

surfactant molecules necessary to form the micelles strongly adsorb on the membrane, and in most cases they even chemically attack the polyimide membrane material.
Microemulsions also can be candidates as "nanoparticles"; however, there is hardly any literature on the behaviour of these systems under flow. The structure of microemulsions is very much dependent on interaction forces between the components, and these forces may easily be disturbed by the flow during ultrafiltration. A microemulsion system is an equilibrium system; even if the microemulsions themselves are retained by the membrane, the components in solution will pass the membrane, thereby disturbing the equilibrium. There are a few examples of non-aqueous microemulsions, but there are still a lot of practical problems related to these systems [40]. Friberg and Liang [41] concluded that in the case of non-aqueous systems the concept of "microemulsion structure" is still too premature. One of the major constituent parts in microemulsions are surface-active agents, which are not suitable to characterize a polyimide membrane.

Colloidal systems seem more suitable. In the past metal sols in water have been used for membrane characterization. Cuperus et al. [42] used gold sols in water to determine the skin thickness of ultrafiltration membranes; very recently, Kim et al. [43] used colloidal silver particles in water to characterize commercial membranes.
In literature there are only a few examples of non-aqueous sols [44,45], and an attempt was made here to use the silver sol system of Kim et al., and replace some of the water by ethanol. In this way, the flux of the silver sol system can be related to the pure ethanol permeability; also the contact time of the membrane with the sol solution is restricted to the retention measurement itself (it is not necessary to precondition the membranes), so that degradation of the polyimide is not very likely to occur.

### 5.2.2 Flow-induced deformation

A polymer chain in dilute solution can be regarded as a random coil, with a certain radius of gyration $r_g$, i.e., the weight average value of the root mean square distance between a coil element and the centre of gravity of the coil. The hydrodynamic radius ($r_h$) of a polymer is frequently approximated by the Stokes-Einstein radius of the polymer. This means that the particular polymer coil has the same bulk diffusion coefficient as a rigid spherical particle with a size $r_s$.
When a large mechanical force is exerted on the polymer chain, this coil model is not valid anymore: the chain can be described better by a string of "blobs" [15], all with the characteristic blob size $\xi_p$ (see figure 2). The part of the chain inside one blob is still considered as a random coil, while on a larger scale the polymer

is partly unrolled forming a string of statically and dynamically independent blobs, with a blob size $\xi_p << r_g$.

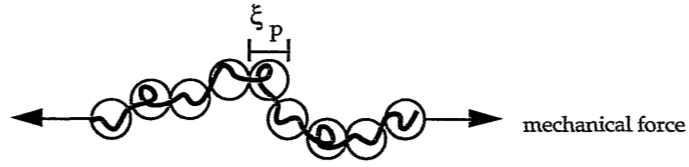


*Figure 2. The string of blobs model for a polymer chain under (externally) applied mechanical force [52].*

Consider an isolated polymer random coil (size $r_g$) in a very dilute solution at the entrance of a pore with size $r_p$, with $r_g > r_p$. When pressure is applied, solvent will flow through the pore. At low pressures the flow through the pore is small, and consequently the shear exerted by the frictional force on the polymer chain is low. The chain tends to return to its original, entropically favourable coil configuration by Brownian movement, due to an elastic force counteracting to the frictional force.
When the transmembrane pressure increases, the flow through the pore increases and so does the frictional force. At a certain flow rate, the two forces are in equilibrium. When this critical shear ($S_c$) is exceeded, the polymer chain unrolls into a chain of blobs that are dynamically independent; this process is called flow-induced deformation. The characteristic size of the polymer is now the blob size, and because this value is smaller than the pore size, the deformed polymer can enter the pore easily. A schematic representation of flow-induced deformation is given in figure 3.
Sometimes also the term "affine deformation" is used for this phenomenon. Affine deformation implies that each volume element within an imaginary box containing the polymer chain deforms in exact proportion to the box itself [47]; since it is not known if this is actually the case for the systems studied in this work, we decided to use the more general term "flow-induced deformation".

The following derivation is mainly based on scaling laws, which implies that numerical coefficients are not included. The scaling relations are indicated by a "≅"-sign.

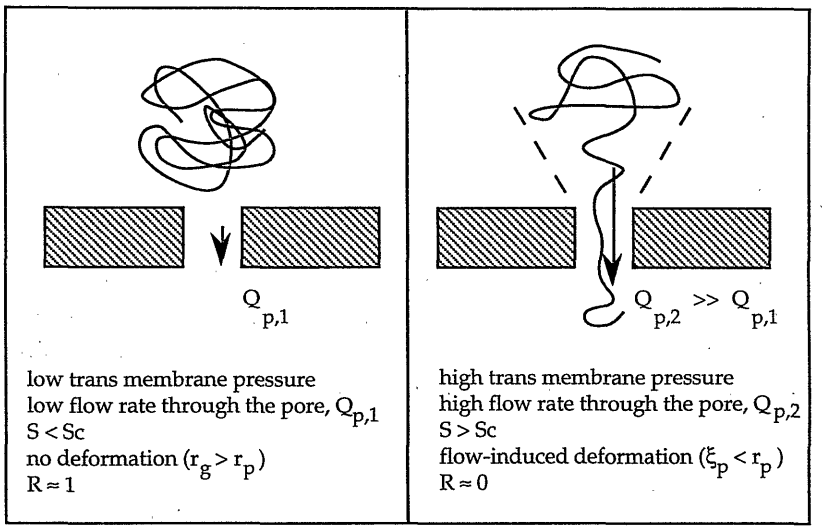


***Figure 3.*** *Schematic drawing illustrating the flow-induced deformation.*

The coil-stretch transition is related to the critical shear $S_c$; $S_c$ is determined by the elastic restoring force. According to Bird et al. [48], $S_c$ is proportional to the Zimm relaxation time:

$$S_c \cong \tau_z^{-1} \cong \frac{k_B T}{\eta_o r_g^3} \qquad (5.3)$$

Here, $k_B$ is the Boltzmann constant [J/K], T is the temperature [K], $\eta_o$ is the solvent viscosity [Pa s], and $\tau_Z$ is the Zimm relaxation time [s]. To correlate this critical shear to a certain critical flow rate through the pore, assumptions about the flow field in the vicinity of the pore are necessary. Daoudi and Brochard [16] assumed the flow entering the pore to be convergent, for which the velocity $v_s$ [m/s] in the "funnel" depends on the distance x to the central line of the funnel [m] (with $x>r_p$) as:

$$v_s \cong Q_p / x^2 \qquad (5.4)$$

Here, $Q_p$ is the volumetric flow rate through the pore [$m^3/s$].
According to Nguyen and Néel [18], the flow rate per pore can be related to the flux per membrane area, J [m/s], by :

$$Q_p \cong \frac{J r_p^2}{\varepsilon} \qquad (5.5)$$

with $\varepsilon$ being the surface porosity $n \pi r_p^2$ [-] and $r_p$ the pore radius [m]. It is assumed that all the pores have the same size $r_p$.
The elongational shear is the derivative of the solution velocity to x, and by combining equations (5.4) and (5.5):

$$S = -\frac{dv_s}{dx} \cong \frac{Q_p}{x^3} \cong \frac{J r_p^2}{\varepsilon x^3} \qquad (5.6)$$

Daoudi and Brochard assumed that the condition for the polymer to enter the pore is that $x_c \approx r_g$, which means that the critical shear has to be reached at a distance from the pore opening that is at least of the order of the size of the dissolved polymer, $r_g$. A combination of equations (5.3), (5.6) and this condition gives:

$$\frac{k_B T}{\eta_o r_g^3} \cong \frac{J_c r_p^2}{\varepsilon (x_c \approx r_g)^3} \qquad (5.7)$$

Here, $J_c$ is the critical flow rate *through the membrane* [m/s], which is then:

$$J_c \cong \frac{k_B T \varepsilon}{\eta_o r_p^2} \qquad (5.8)$$

Because the surface porosity $\varepsilon$ equals $n \pi r_p^2$ (where n is the number of pores per membrane surface area [$/m^2$]), the critical flow rate through the membrane becomes:

$$J_c \cong \frac{k_B T n}{\eta_o} \qquad (5.9)$$

This means that the critical flow rate or the critical flux through the membrane is *not* dependent on the size of the pore, which is of course very surprising. It is also independent of the size of the original polymer coil, and of the polymer concentration (as long as the polymer solution is very dilute). One remark has to be made here: the independence of $J_c$ on the pore radius is mainly a consequence of the demand $x_c \approx r_g$, whereas this demand is only an assumption that is strongly dependent on the flow field. A small deviation in $x_c$ then causes at least some dependence of $J_c$ on the radius of gyration.
On the other hand, $J_c$ is dependent on the *number* of pores, n. The pore geometry is also of importance; according to Daoudi and Brochard a conical (converging) pore has a lower critical flow rate than a cylindrical pore with the same (smallest) size.
The independence of $J_c$ on the pore size has been confirmed by several experimental studies [20,21,49]; also the independency of $J_c$ on the molecular

weight, the radius of gyration or the hydrodynamic Stokes-Einstein radius of the solute has been proven experimentally [18-20,32,49,50]. Almost all these results were obtained for track-etched membranes, with the exceptions of Nobrega et al. [49] and De Balmann and Nobrega [50], who used polysulfone hollow fiber membranes that were prepared by immersion precipitation. The choice of solvent quality is not important as well, as may be deduced from the fact that the radius of gyration, which is solvent-dependent, has no effect on $J_c$.

In this chapter, more attention will be directed to the dependence of the critical flow rate through the membrane on the number of pores, because it is suggested that the comparison of the retention curves for different membranes can give more qualitative information about the number of pores. In this way, deformation studies may form an additional membrane characterization technique. Also a correlation must be found between the retention curves and the permporometry results.

The absence of flow-induced deformation during the experiments of Mochizuki and Zydney [26] has to be elucidated. They claimed that their PES-membranes had an extremely high surface porosity of 0.8, and determined the permeate flow rate per pore for this porosity to be $< 1.1*10^{-4}$ m/s. For polymeric ultrafiltration membranes, prepared by immersion precipitation, a surface porosity of 0.8 is a very unrealistic value; in general, the *overall* porosity is about 0.8 [51], but the surface porosity in a densified skin can be limited to a fraction of a percent.
Consider a membrane with a pure ethanol permeability of 300 $kg/m^2hr$ bar (like some of the membranes used in this study) and a surface porosity of 0.01 or 0.001, which are normal values for asymmetric polymeric ultrafiltration membranes [51], then the values of the permeate flow rates at 1 bar are 0.1 m/s and 0.01 m/s respectively. Therefore, it is suggested that the permeate flow rate per pore for the PES-membranes is severely underestimated by Mochizuki and Zydney, but the flow rate probably is still lower than the critical flow rate.

The flow-induced deformation theory, as described above, is only valid for dilute solutions; this means that the polymer concentration c has to be far below the overlap concentration, c* [52]. Below c*, the polymer coils have no interaction with each other. In the vicinity of c* they start to "overlap", and far above c* polymer chains form an entangled network (see figure 4).

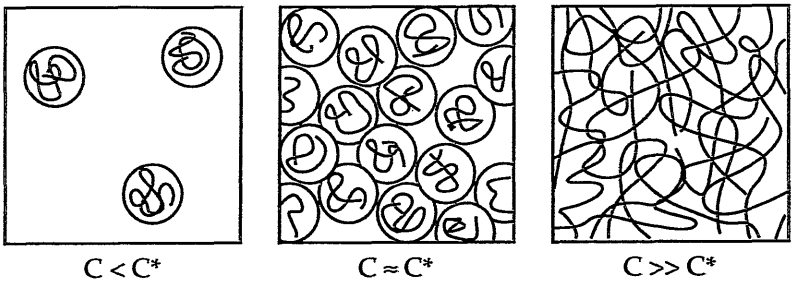


*Figure 4.* *Concentration regimes for polymer solutions; definition of the overlap concentration c* [52].*

The value of the overlap concentration is dependent on the molecular weight of the polymer. A schematic example for polystyrene in good solvents, after Graessley [53], is given in figure 5.

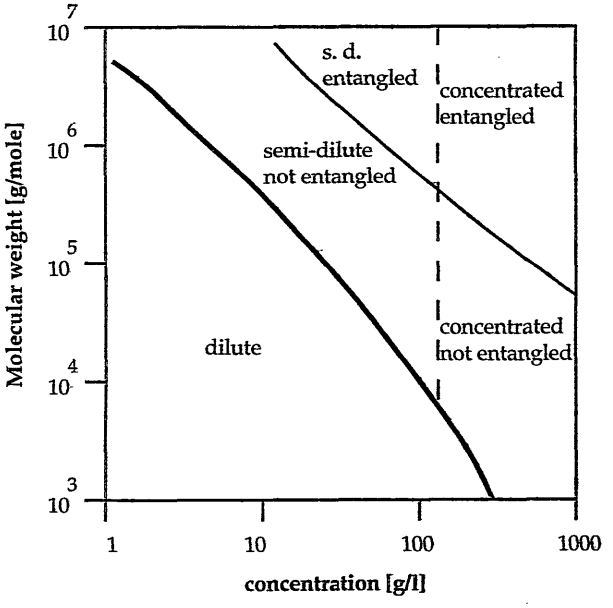


*Figure 5.* *Overlap concentration (fat line) as a function of the molecular weight of polystyrene in good solvents, after Graessley [53]. The other line represents the entanglement concentration.*

According to Nguyen and Néel [18] the critical flow rate decreases sharply with increasing concentration above c*; this is however very difficult to prove experimentally, because concentration polarization plays an important role in

these cases. Furthermore, it is suggested here that their theory for $c>c^*$ probably is restricted to semi-dilute not entangled polymer solutions (i.e., the middle situation in figure 4), because above the entanglement concentration not only the blob size is important, but also the entanglement distance. A detailed discussion on retention behaviour at higher concentrations is beyond the scope of this chapter; the measurements will be restricted to dilute solutions.

Many characteristic phenomena that occur during retention measurements can be understood from scaling concepts combined with the coil-stretch transition (flow-induced deformation). However, there are a number of drawbacks. The first and most important one is the qualitative character of the scaling theory; because scaling laws do not include numerical coefficients, exact values for the critical flow rate can not be predicted.
Also the difference in rigidity of polymers is not included. Adamski and Anderson [32] showed, that an increase in the degree of branching of macromolecules results in a small decrease in deformation. They also correctly mentioned that the convergent flow field, used by Daoudi and Brochard to calculate a critical flow rate, probably is not right; some influence of vortices in the regions near the funnel should be included, especially at high permeate flow rates. This may also introduce at least some dependence of $J_c$ on $r_g$ (see remark on eq. (5.9)).
A very difficult point is the coil-stretch transition itself. De Gennes [54] reasoned that this transition should be very sharp; the expectation was that the retention of a porous membrane for flexible polymers would drop immediately to zero at the critical flow rate. However, Nguyen and Néel [18] experimentally found a more gradual decrease for membranes with toplayers that consist of a distribution of pore sizes. Experiments performed by Long and Anderson [19] and Adamski and Anderson [32] with track-etched mica membranes containing uniform pore sizes, showed a gradual decrease in retention as well.
Larson and Magda [55] used a different model for the polymer chain than De Gennes did, to calculate theoretically a coil-stretch transition. With this model, they reasoned that this transition is at least somewhat more gradual than predicted by De Gennes.

In spite of these disadvantages, the deformation theory may be very helpful to explain qualitatively the typical ultrafiltration behaviour of dilute solutions of flexible polymers, in the absence of concentration polarization.
Despite the criticism about this flow-induced deformation, the coil-stretch transition by flow shear stress has recently been proven experimentally by various research groups. Menasveta and Hoagland [56], Nguyen and Kausch [57] and Narh et al. [58] measured flow birefringence in elongational flows of dilute polystyrene solutions, which is clearly an indication of orientation by stretching.

Menasveta and Hoagland also confirmed equation (5.3) experimentally, which gives the relation between the critical shear and the Zimm relaxation time. Recently, Link and Springer [59] used light scattering techniques to prove the deformation of PS chains under shear flow. Menasveta and Hoagland and Link and Springer also emphasized the need for a more quantitative theory to describe the deformation phenomena.

## 5.3 Experimental

### 5.3.1 Materials

Polyimide P84 (Lenzing AG, Austria) was kindly supplied by X-Flow BV. DMF, ethyl acetate and ethanol were purchased from Merck (analytical grade) and were used as received. Monodisperse polystyrene fractions were purchased via Waters from Tosoh Corp., with $M_w$ = 96,400 g/mol and $M_w/M_n$ = 1.01 (TS-144), and $M_w$ = 355,000 g/mol and $M_w/M_n$ = 1.02 (TS-85).

### 5.3.2 Membrane preparation

PI-powder was dried at least 24 hours at 150°C in vacuum before preparation of the casting solutions. Solutions in DMF were prepared immediately after the drying procedure, and the air inside the erlenmeyer was replaced by nitrogen. After 24 hours of stirring (without heating) the solutions were filtered with a Bekipor® 25 μm stainless steel filter from Bekaert Corp. The solutions were degassed overnight.
A film of 0.20 mm thickness was cast on a dry and clean glass plate and immediately immersed in the coagulation bath, containing ethanol or demineralized water. The residence time in the bath was at least 10 minutes, but the membranes precipitated immediately. The prepared membranes were flushed for 24 hours with water to remove DMF; the water was replaced by ethanol, in which the membranes were stored.
Before the membranes were applied for filtration of ethyl acetate or polymer solutions in ethyl acetate, they were pre-conditioned in this liquid for at least two days.

### 5.3.3 Polymer feed solutions

Polystyrene samples were dissolved in ethyl acetate at various feed solution concentrations, $c_o$, to a maximum of 1 g/l (for the high $M_w$ a feed concentration of 0.7 g/l was used).
To determine hydrodynamic radii for PS 96,400 and PS 355,000, the bulk diffusion coefficients in dilute solution have to be known. Some results, obtained by quasi

elastic light scattering, are presented in literature for PS in dilute solutions in ethyl acetate at 20°C [28,60]. Analogously to Kathawalla and Anderson [61], these data were fitted by a power law dependent on the molecular weight, with an additional temperature and viscosity correction: $D_o \sim 3.296*10^{-8}*M_w^{-0.533}$. Hydrodynamic radii, $r_h$, can then be calculated using the Stokes-Einstein relation (see also chapter 6). The radius of gyration, $r_g$, can be estimated using a relation between $r_g$ and $r_h$ for PS in good solvents [62-64]:

$$\frac{r_g}{r_h} = 1.48 \pm 0.03 \qquad (5.10)$$

Guillot et al. [28] showed that ethyl acetate is a good solvent for PS.
The literature concerning the value of the overlap concentration is quite indistinct, several relations were applied to calculate c*. Because the purpose of the present work is to investigate ultrafiltration behaviour at concentrations far below c*, two examples of calculations are given here. Equation (5.11) shows the overlap concentration according to Doi and Edwards [65], while equation (5.12) gives the overlap concentration according to Des Cloizeaux and Jannink [66]:

$$c^* = \frac{M_w}{\frac{4}{3}\pi r_g^3 N_A} \qquad (5.11)$$

$$c^* = \frac{M_w}{(\sqrt{2}\, r_g)^3 N_A} \qquad (5.12)$$

where $N_A$ is Avogadro's number.
The characteristics of the polystyrenes used in this study are summarized in table 1. The radius of gyration has been estimated from equation (5.10).

***Table 1.*** *Characteristics of the monodisperse polystyrene samples used.*

| PS Mol.w. [g/mol] | $r_h$ [nm] | $r_g$ [nm] | $c^{*a}$ [g/l] | $c^{*b}$ [g/l] |
|---|---|---|---|---|
| 96,400 | 7.07 | 10.5 | 33 | 49 |
| 355,000 | 14.1 | 20.9 | 15 | 23 |

a: from equation (5.11)
b: from equation (5.12)

From table 1 it can be concluded that the feed concentrations used were far below any value of c*, even far below the value of 1/8 c*, which was advised by Bishop et al. [67]. Figure 5, which showed the c* vs. molecular weight relationship, also

indicated high c* values. Teraoka et al. [68] recently showed by measurements of diffusion of PS in porous glasses, that the concentration regime *inside* the pore is definitely dilute, if the ratio of $c_o/c^* \leq 0.2$ and c* has been defined according to equation (5.12). The feed concentrations are also far below this latter value.

Permporometry measurements, as described in chapter 4, showed that for the membranes used the major part of the pore radii is smaller than 7 nm, so here $\lambda = r_s/r_p \geq 1$. In addition, for all pores $\lambda > 0.5$. It should be realized that these pore size distributions were determined for membranes in a dry state, which may result in a change in morphology.
Concentrations of PS-solutions were determined with a Philips PU 8720 UV/Vis scanning spectrophotometer at a wavelength of 260 nm.

### 5.3.4 Silver sols

Silver sols were prepared according to the method described by Creighton et al. [69]: 100 ml of $10^{-3}$ M aqueous $AgNO_3$-solution was added to 300 ml of a $2*10^{-3}$ M aqueous $NaBH_4$ solution at 0°C under vigorous stirring. This mixture was slowly diluted with water to a concentration of $0.1*10^{-3}$ M or $0.11*10^{-3}$ g Ag/l, according to Kim et al. [43]. The resulting sol was light yellow and stable for several months, without any precipitate. The stock solution was then very slowly diluted with the desired ratio of ethanol to water. Three different final concentrations were used: 0/100 v/v, 30/70 v/v, and 57/43 v/v ethanol/water, respectively; these sols remained stable for at least three weeks without any visual changes. An increase of the ethanol concentration above 57% resulted in an immediate colour change to darkbrown or grey, with finally a grey precipitate. The prepared sols were used for retention measurements immediately after preparation. Concentrations of the sols were determined using a Philips PU 8720 UV/Vis scanning spectrophotometer at $\lambda = 393$ nm.
Size distributions of the sols were determined using a Jeol 200 CX High Resolution Transmission Electron Microscope. For this purpose, drops of the sols were placed on a sample holder, after which the solvent was evaporated.

### 5.3.5 Retention measurements

The pure solvent permeability of the membrane for ethyl acetate or ethanol was determined in a dead-end filtration set-up, as described in chapter 4 (3 hours filtration at 1 bar), prior to the actual retention measurement. Directly after this procedure, the supply tank was emptied and the pure solvent in the 400 ml cell was replaced by the solution and stirred immediately at 1200 rpm. After adjusting the pressure the permeate samples were collected and analysed.
The retention was calculated as $R = ((c_o - c_p)/c_o)$; the increase in the feed

concentration, $c_o$, caused by retention, was always much lower than 10%.
For new retention measurements, clean and fresh membranes were used.

## 5.4 Results and discussion of retention measurements obtained with polystyrene solutions

### 5.4.1 Influence of polystyrene molecular weight

For the measurements only one type of membrane was used. The membranes were prepared from a 20 wt% casting solution of polyimide in DMF and coagulated in ethanol. Retention values of these membranes for a solution of PS with a $M_w$ of 96,400 g/mol and a solution of PS with a $M_w$ of 355,000 g/mol were determined. The concentrations of the PS-solutions were 1 g/l for PS 96,400 and 0.7 g/l for PS 355,000.
The retentions were measured at two different transmembrane pressures. The retentions were stable for at least 30 minutes. The results are listed in table 2.

*Table 2.* *Retentions of a membrane prepared from a casting solution of 20 wt% PI in DMF and coagulated in ethanol, for PS-solutions of two different monodisperse PS molecular weights.*

| pressure [bar] | PS 96,400 [g/mol] R [%] | PS 355,000 [g/mol] R [%] |
|---|---|---|
| 0.1 | 90 | 92 |
| 1.0 | 0 | 0 |

The results from table 2 can be explained by the flow-induced deformation theory. An increase in permeate flow causes a decrease in retention, which implies that the polystyrene chains can change their conformation to pass through small pores at higher permeate flow velocities.
It is obvious that the retention behaviour of these membranes is similar for the two PS molecular weights. This means that the critical flow rate through the membrane is independent of the size of the polymer coil ($M_w$), which is conform to equation (5.9). This result agrees also very well with the retention results that were described in literature (see theory).
The solvent flux [g/min] for the 96,400-solution was almost equal to the pure ethyl acetate flux, which means that concentration polarization is negligible. Therefore, pore plugging can not be the cause of such a drastic decrease in retention. On the other hand, the flux for the 355,000-solution was lower than

the pure solvent flux. This will be discussed further in paragraph 5.4.2.

In chapter 4 results have been presented for the pore size distribution of this membrane, obtained by permporometry. This distribution shows that there are some pores present in the membrane that have a radius of 14 nm, which explains that the retention is not complete for neither of these two PS solutes. It seems that the drying procedure (necessary for the permporometry characterization) does not have a large influence on these relatively large pores. Hindered diffusion experiments with dilute polystyrene solutions in ethyl acetate will be described in chapter 6 for the same membrane. For both PS 96,400 and PS 355,000 the diffusive permeability was larger than zero, which means that also according to this characterization technique there are some pores present with a radius of about 14 nm.

In conclusion, permporometry pore size distributions, retention measurements, and hindered diffusion measurements are well in agreement for these relatively large pores.

### 5.4.2 Comparison of retention curves for different membranes

Standard retention curves were measured for six different types of membranes. Three different casting solution polyimide concentrations (18, 20 and 25 wt% PI in DMF) and two different coagulation baths, ethanol or water, were used. The permeabilities of these membranes for pure ethyl acetate vary roughly from 130 kg/m$^2$hr bar for the "tight" membranes (25 wt%PI), to about 1000 kg/m$^2$hr bar for the more "open" membranes (18 wt% PI); these results were described in chapter 4, as well as the pore size distributions obtained for these membranes by permporometry.

Retention curves for these membranes were determined using feed solutions of 1 g/l PS 96,400 in ethyl acetate; the results for the different membranes are given in figures 6 (25 wt% PI), 7 (20 wt% PI) and 8 (18 wt% PI).

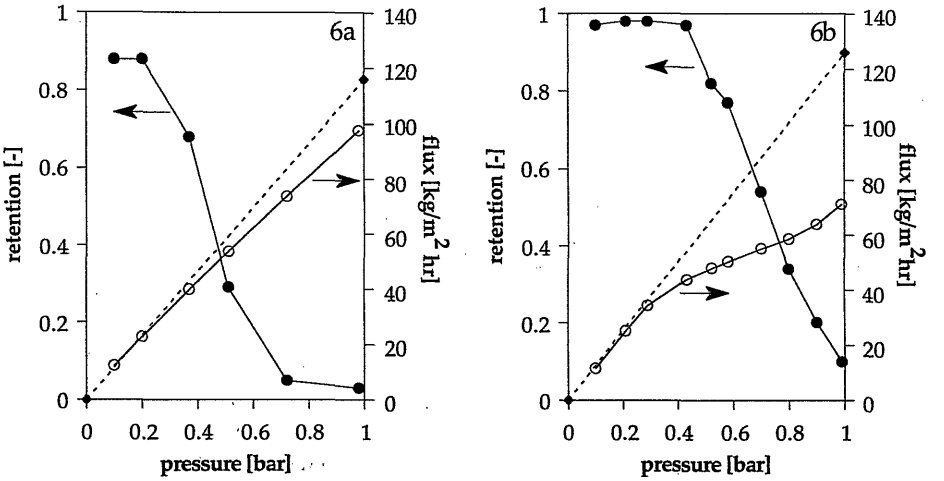


*Figure 6.* *Flux and retention behaviour of membranes prepared from 25 wt% PI in DMF and coagulated in ethanol (6a) or water (6b), for 1 g/l PS (96,400) solution in ethyl acetate. Pure ethyl acetate fluxes are represented by dashed lines.*

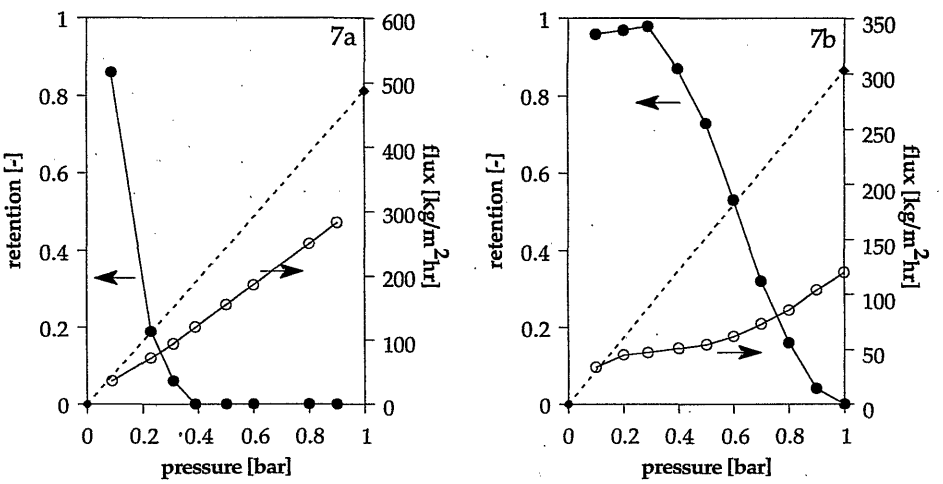


*Figure 7.* *Flux and retention behaviour of membranes prepared from 20 wt% PI in DMF and coagulated in ethanol (7a) or water (7b), for 1 g/l PS (96,400) solution in ethyl acetate. Pure ethyl acetate fluxes are represented by dashed lines.*

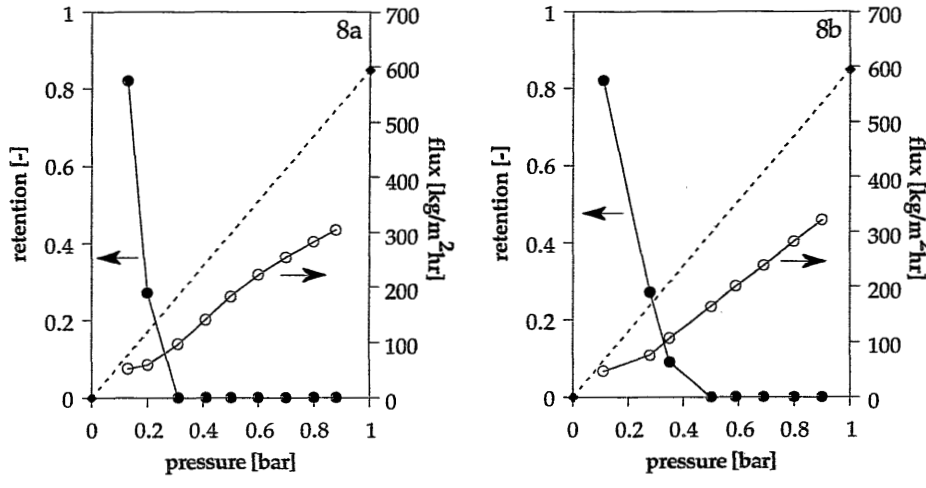


*Figure 8. Flux and retention behaviour of membranes prepared from 18 wt% PI in DMF and coagulated in ethanol (8a) or water (8b), for 1 g/l PS (96,400) solution in ethyl acetate. Pure ethyl acetate fluxes are represented by dashed lines.*

The measurements were very reproducible and different membranes from the same batch resulted in only minor differences in retention behaviour. A stepwise decrease in pressure gave the same results as a stepwise increase. When the same membrane was used twice for similar measurements, changes in the retention curves were negligible.
The form of the retention curves agrees well with literature data and can be explained by flow-induced deformation. For the situations that are given in figures 6a, 6b, and 7b, at very low pressures ( $P \approx 0.1$ bar) almost no deformation takes place and the retention is high and almost constant. When the pressure increases, the critical permeate flow is reached, flow-induced deformation takes place and the retention drops to zero; this happens at different pressures for the different types of membranes. For the situations presented in figures 7a, 8a, and 8b, deformation already occurs at 0.1 bar pressure. It is obvious for all the measurements that the retention decreases with increasing pressure, which is typical for flow-induced deformation.
Furthermore, the retention decrease is indeed gradual, which supports the theoretical model for the coil-stretch transition by Larson and Magda [55].

The flux of the solution is also given in the figures. Note that the flux is given in $kg/m^2hr$ units, and is *not* normalized to the pressure. When the retention is high, so before deformation starts, the flux is equal to the pure ethyl acetate permeability as shown in the figures by a dashed straight line. Despite the high

retention, concentration polarization is negligible. As soon as deformation starts the flux deviates from linear behaviour, but still increases with pressure. When zero retention is reached the flux increases linearly with the pressure again, at a somewhat lower level than the pure solvent flux. This can be made more clear in figure 9, where the results of figure 7 are replotted, using a pressure normalized flux (i.e., the solution permeability).

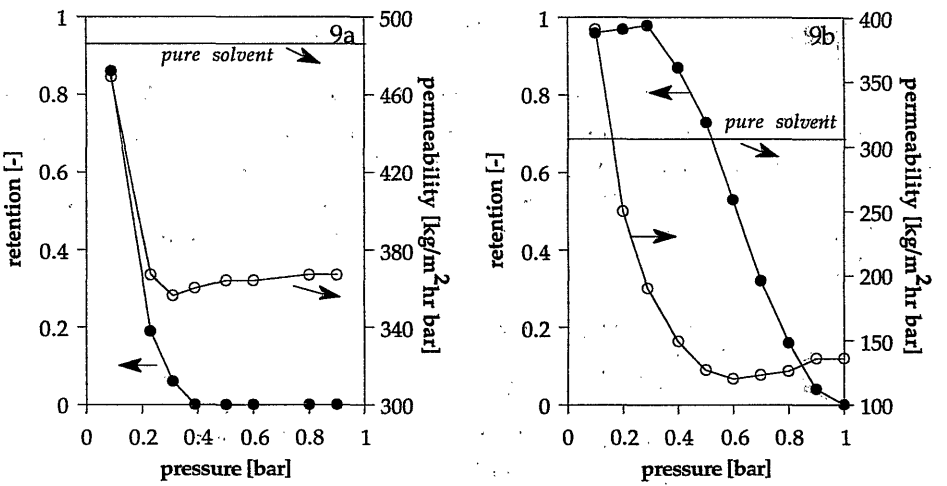


*Figure 9. Retention and solution permeability of membranes prepared from 20 wt% PI in DMF and coagulated in ethanol (9a) or water (9b), for 1 g/l PS/ethyl acetate. The flux results of figure 7 are normalized to the transmembrane pressure difference, units: kg/m² hr bar.*

It is clear that the strong decline in retention by no means can be explained by concentration polarization, because in all cases described in literature where concentration polarization occurs, the permeability finally is decreasing with pressure.

On the gradual change in retention over a broader range of pressure values the following remarks can be made. It is quite plausible that the coil-stretch transition occurring during flow-induced deformation, is not as sharp as De Gennes predicted [54] but is more gradual, as stated theoretically by Larson and Magda [55], and experimentally by Nguyen and Néel [18], Long and Anderson [19], and Adamski and Anderson [32].

The frictional energy, necessary to deform a polymer molecule, is supplied by the kinetic energy of the convective permeate flow. A gradual coil-stretch transition in this respect corresponds with a gradual decrease in kinetic energy of the permeate flow. This decrease results in an additional resistance to permeate flow, a sort of "deformational resistance", that becomes constant when all the polymer molecules are deformed at a retention of zero (see figure 9).

At this point, the flux is again linearly dependent on the pressure, at a somewhat lower level than the pure ethyl acetate permeability line (as in figure 9).
However, part of the loss in kinetic energy of the permeate flow can also be ascribed to the friction of the deformed chain with the pore wall (especially for very small pores, with a pore size that is of the order of the blob size). Nevertheless, it is suggested here that this wall drag resistance that is mainly present in very small pores is only a fraction of the decrease in kinetic energy, that is indicated by the decrease in permeability.

In figure 1, a schematic overview was given for the hydrodynamic resistances during ultrafiltration of a solution with such a concentration, that concentration polarization and fouling do take place (practical application). For the situation of ultrafiltration of a very dilute solution of flexible polymers (retention measurements for membrane characterization), a new resistance model is suggested (see figure 10).

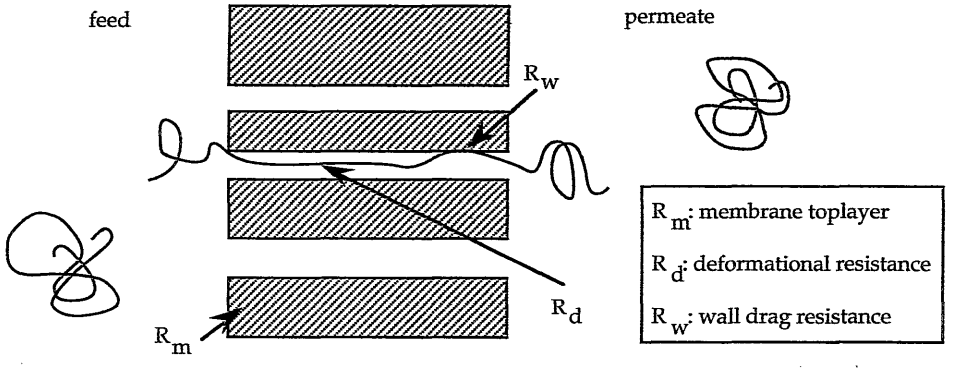


*Figure 10. Schematic drawing depicting the hydrodynamic resistances occurring during ultrafiltration of very dilute solutions of flexible polymers.*

With respect to the deformational resistance, one may conclude from figures 6-8 that in most cases the resistance is higher for membranes coagulated in water, than for membranes coagulated in ethanol. A possible explanation could be that the pores in water-coagulated membranes are longer (thicker toplayer) or more tortuous, so that the deformation that has to be maintained for a longer time requires more energy than in the case of ethanol-coagulated membranes. This hypothesis is very difficult to prove experimentally. There is no other characterization method available to determine the tortuosity of the pores in the toplayer, while for the determination of the skin thickness until now only an aqueous gold-sol filtration method was used [42].
It is also possible that the flow-induced deformation of a polymer with a higher

molecular weight causes a higher deformational resistance than a polymer with a lower molecular weight (see results in paragraph 5.4.1). If this is true, then there is no influence on the form of the retention curve, but the flux at zero retention will be lower for the higher molecular weight polymer. This could be an explanation for the results described in paragraph 5.4.1.

The critical permeate flow for the six membranes is reached at very different pressures, but of course, the pure ethyl acetate permeability of the membranes also shows a large variation. The retention curves of the six types of membranes from figures 6-8 are plotted in figure 11 versus the flux through the membrane.

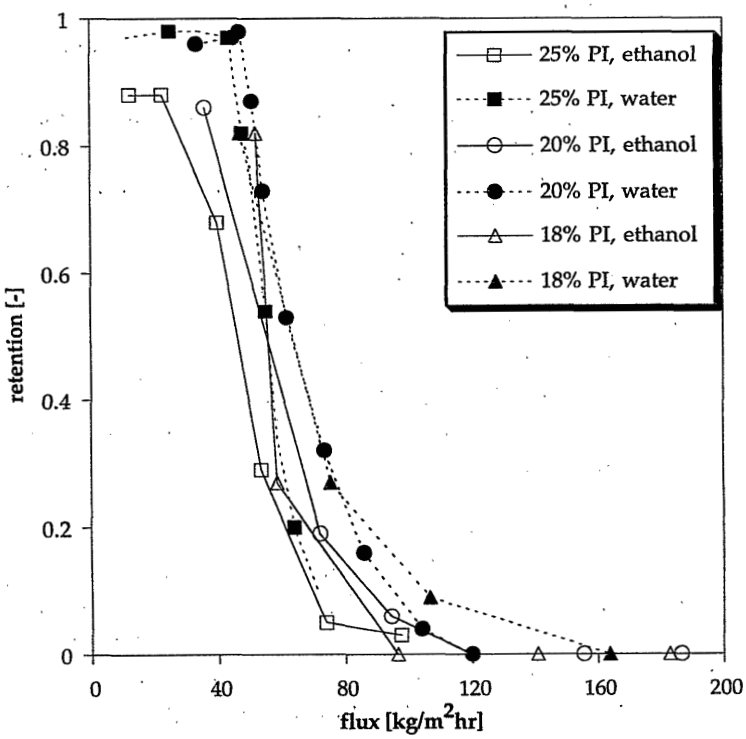


*Figure 11. Retention for 1 g/l solutions of PS (96,400) in ethyl acetate as a function of the flux through the membrane; comparison of six different types of membranes.*

The retention curves of the membranes coagulated in ethanol are situated more to the left hand side compared to the membranes coagulated in water. Because the critical flow rate through one pore, $Q_{p,c}$, is equal for both cases (independent of pore size), this difference in critical flow rate through the membrane, $J_c$, can only result from a difference in the *number* of pores, n, as predicted by equation

(5.9).
This means that a membrane coagulated in water has more pores than a similar membrane coagulated in ethanol ($n_{water} > n_{ethanol}$). Also a trend for the polymer concentration can be observed: membranes from 18 wt%-solutions have more pores than membranes from 20 or 25 wt%-solutions: for these higher concentrations parts of the curves overlap, so $n_{20} \approx n_{25}$. Combining this latter result with the fact that the pure solvent permeability for 20 wt% PI-membranes is about a factor five higher than for 25 wt% PI-membranes, one may conclude that 20 wt% PI-membranes contain larger pores than 25 wt% PI-membranes. This result for wet membranes agrees with the results of permporometry for comparable membranes in the dry state, that were described in chapter 4. (It is also possible that the length of the pores for 25 wt% PI-membranes is larger than for the 20 wt% PI-membranes, but there are no experimental data available for the toplayer thickness.)
However, the retentions for undeformed PS chains are not in agreement with these results. It is assumed here, that as long as the retention is constant at very low pressures deformation hardly occurs, which means that the initial retentions in figures 6a, 6b, and 7b can be compared with each other. It is obvious from these figures that the retention is about equal for a 25 wt%-membrane and a 20 wt%-membrane both coagulated in water, whereas the retention of a 25 wt%-membrane coagulated in ethanol is somewhat lower. Based on the permporometry pore size distributions (see chapter 4), one might expect the retentions of 25 wt%/ethanol and 25 wt%/water to be of the same order, while the retention of 20 wt%/water should be lower. This discrepancy cannot be explained at this stage of our work.

To our knowledge, this is the first time that flow-induced polymer deformation studies are used for membrane characterization purposes. Of course, this type of characterization is only qualitative, but it may be possible to compare pore size distributions of different membranes made of the same material; this last demand is necessary to completely exclude the influence of interactions between solute polymer and membrane material as a complicating factor.
This method may be useful in relation to membrane formation.

### 5.4.3 Influence of feed concentration

Retention curves were determined at a lower feed concentration for two types of membranes. For 25 wt% PI-membranes coagulated in ethanol a feed concentration of 0.34 g/l was used, while for 25 wt% PI-membranes coagulated in water a feed concentration of 0.58 g/l was tested. The results are given in figure 12.

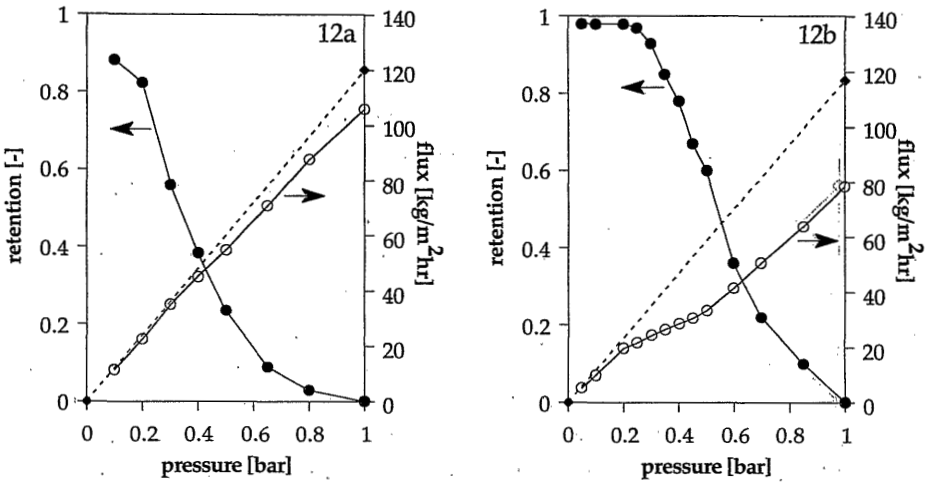


*Figure 12. Influence of feed concentration on flux and retention behaviour of a membrane prepared from 25 wt% PI in DMF and coagulated in ethanol for 0.34 g/l PS solution (12a), and of a membrane prepared from 25 wt% PI in DMF and coagulated in water for 0.58 g/l PS solution (12b).*

The results in figure 6.a and figure 12.a look very similar, even if one takes into account that two different membranes (from the same batch) have been measured. For figure 6.b and figure 12.b, the retention curves are almost similar, but the flux curves seem to deviate a little from each other.
This means that the feed concentration has no influence on the retention curve, which agrees well with the flow-induced deformation theory; the independence of concentration is only valid for feed solutions far below the overlap concentration. This is an experimental proof for equation (5.9), from which it has already been concluded theoretically that the critical flow rate is independent of the (dilute) polymer concentration.
On the other hand, the feed concentration seems to have an influence on the flux behaviour for some of the membranes. As already mentioned in section 5.2, the deformation theory and almost all published experimental results involve the retention behaviour; however, the dependence of the flux was never described satisfactorily. The flux behaviour described here can also be explained by the higher resistance to deformation in the case of water-coagulated membranes. An increase in feed concentration simply means that there are more polymer molecules that have to be deformed and that the friction with the pore wall increases, thus the energy loss is larger. The increased energy loss causes an increase in resistance to permeate flow, so a larger deviation from the pure ethyl acetate flux has been observed, while the same retention curve was maintained.

### 5.4.4 Adsorption tests

The pure ethyl acetate permeability of the membrane after the retention measurement was a little lower than before, about 5%.
To investigate whether this decrease is caused by fouling, membranes were put in a PS 96,400 solution in ethyl acetate for 24 hrs, while similar membranes were put in pure ethyl acetate. The ethyl acetate permeability after this treatment showed about 5% decrease for both tests. This means that the small decrease in permeability after retention measurements is not caused by pore plugging nor by adsorption at the membrane and pore surface, but just by immersion in ethyl acetate. Only after seven days in ethyl acetate, a constant ethyl acetate permeability was observed. Probably the pre-conditioning time in ethyl acetate of two days, as is used for all measurements, is not long enough. Ethyl acetate is the only solvent that showed this behaviour; pre-conditioning times of two days in hexane, toluene or acetone always gave constant permeabilities.
For the ethyl acetate measurements always the same pre-conditioning times were used, i.e., it may be assumed that small differences are negligible or, at least, comparable for all membranes.
Another important conclusion is that polystyrene does not adsorb on polyimide membranes, as was expected.

## 5.5 Retention measurements obtained with silver sols

### 5.5.1 Stability and particle diameters of silver sols

Several attempts were made to obtain silver sols in mixtures of ethanol and water. Experimentally, it has been found necessary to make a standard stock solution based on water only. The presence of only a few percent of ethanol resulted already immediately in a grey mixture with visible particles. Dilution mixtures containing ethanol have to be added very slowly and dropwise, during vigorously stirring. All stable light-yellow solutions showed an absorption peak at $\lambda$ = 393 nm, which agrees with the results by Kim et al. [43]. As soon as the colour of the solution changed, this peak disappeared. This seems to be a very good indication of the stability of the sol.

The maximum ethanol content of the final mixture was found to be 57%; this mixture still had a yellow colour, which was a little bit darker than with 30% ethanol or 100% water, and the sol was stable for at least two weeks. The mixture with 30% ethanol had exactly the same appearance as the 100% water sol. TEM-photographs of three different sols are shown in figure 13.

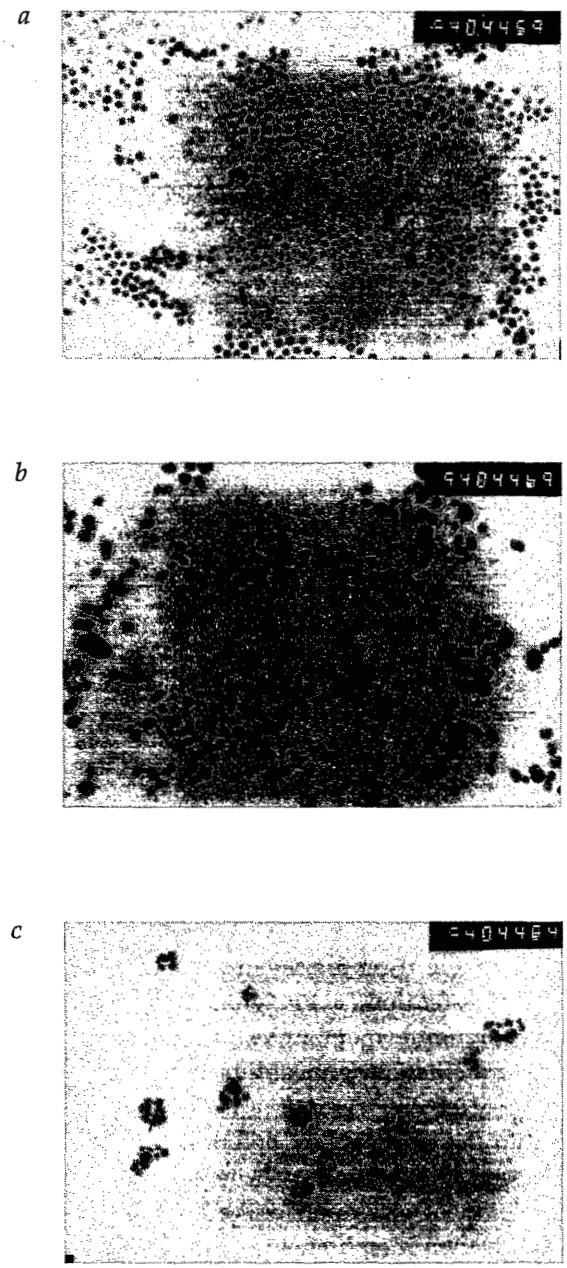

*Figure 13. TEM photographs of silver sols, from three different solvent mixtures: 0/100 ethanol/water (12a), 30/70 ethanol/water (12b) and 57/43 ethanol/water (12c). Magnification: 104,000 times.*

The particles in figures 13.a and 13.b look very much the same. They are well separated. For the sol containing the largest amount of ethanol, the particles start to form aggregates, as is shown in figure 13.c; this sol obviously is close to the stability treshold.
Particle diameter distributions for the first two sols are shown in figure 14. The curves for both sols show a maximum at a particle diameter of 12 nm; both distributions are slightly broader than the distribution determined by Kim et al.

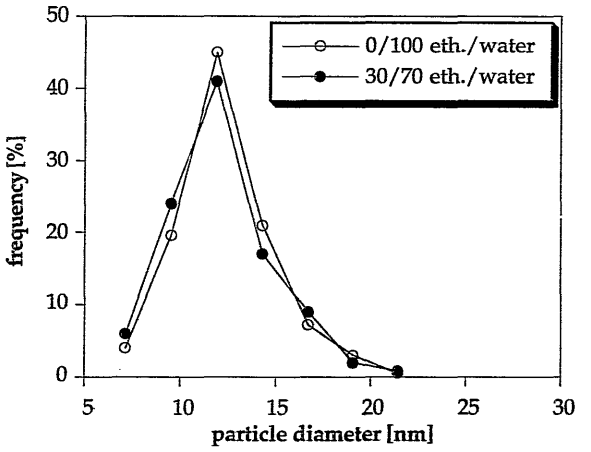


*Figure 14. Particle diameter distributions for silver sols diluted with water or water/ethanol.*

### 5.5.2 Retention measurements with silver sols

The freshly prepared sols were used for retention measurements. All the results showed almost complete retention, even when more open membranes were used, like the 18 wt%-polyimide membranes. The flux of the diluted sol was about the same as the pure ethanol permeability for the sols of 30/70 and 0/100 ethanol to water ratio; after the retention measurements the pure ethanol permeability was equal to the permeability before the retention measurements.
This corresponds quite well to the results of Kim et al. [43], who found complete retention and the formation of an "open" cake layer on top of the membrane surface for PM 30 ultrafiltration membranes.
When the 57/43 ethanol to water ratio sol was used, the flux of the sol and the ethanol permeability after the retention measurement were lower than the pure ethanol permeability before the retention measurement. It is very likely that these sol particles become unstable during the retention measurement, so that they fall apart into smaller components. The smaller molecules may enter the pores and thereby cause pore plugging and an irreversible flux decline.

## 5.6 Comparison of retention measurements of polystyrene and silver sol solutions

Silver sols are undeformable particles. In addition, polystyrene chains remain randomly coiled at very low permeate flows, e.g., at transmembrane pressures slightly larger than zero. The radius of gyration for PS 96,400 in ethyl acetate is about 7.1 nm, while the particle radius for the silver sols (determined by TEM) varies from 4 to 10 nm with a maximium at 6 nm. Despite the smaller size of the majority of the silver sols, the retention of all membranes tested was almost 1.
It may be possible that the PS-chains are already (partly) deformed at a pressure of 0.1 bar (Meireles et al. [70] published results that showed deformation of dextran already at 0.005 bar). However, this does not agree with the theoretical concept of a critical shear (see figure 3).
It is more likely that the specific properties of silver sols are the cause of the complete rejection. The stability of these sols is assured by the presence of a large quantity of water, which is already an indication of the importance of charges. It is possible that the double layer thickness, as given by the Debye length $\kappa^{-1}$, around the sol particles increases the effective size of the silver sols. Kim et al. [43] determined for these silver sols a Debye length of 5-8 nm, which means that the effective particle radius during retention measurements can be twice as large as predicted by TEM.
In chapter 4, pore size distributions were given for these membranes in the dry state. Especially the more open membranes (i.e., 18 wt% PI) showed a reasonable number of pores with radii between 6 and 10 nm and even some larger pores were present. The fact that also for 18 wt% PI-membranes the retention is almost 1, means that the effective sol particle radius should be larger than these dry state pore radii. It might be possible that in a wet state the pore size distribution is shifted to higher pore radii. Then the silver sols are even larger than these wet state pore radii. Unfortunately, no information could be obtained about this wet state pore size distribution.
Anyway, the conclusion can be drawn that the major part of the pores, for all the tested polyimide ultrafiltration membranes, will have radii smaller than 7 nm; based on the high retentions for PS 96,400 at very low pressures; this conclusion agrees well with the dry-state pore size distributions obtained by permporometry.

## 5.7 Conclusions

The retention behaviour of very dilute solutions of polystyrene in ethyl acetate through phase-inversion polyimide membranes could be described by the occurrence of flow-induced deformation. The concept of a deformation resistance was introduced to explain the step-like flux decline, in the absence of concentration polarization.

Flow-induced deformation studies for non-aqueous systems were carried out to compare qualitatively the pore size distributions of six types of PI-membranes. It was found that the number of pores per unit area, n, for membranes coagulated in water is larger than that for similar membranes coagulated in ethanol. In addition, the deformation resistance is larger in the case of membranes coagulated in water, compared to membranes coagulated in ethanol. A possible reason is that the effective pore length in water-coagulated membranes is larger, because of a larger membrane toplayer thickness or a higher tortuosity.
The number of pores in 20 wt% PI-membranes was about equal to the number of pores in 25 wt% PI-membranes, so the large pure solvent permeability difference between these types has to be explained by the presence of relatively larger pores in the 20 wt% PI-membrane. This agrees well with the permporometry results, although these latter results were obtained for dried membranes. Membranes from 18 wt% PI-solutions show more pores than the 20 wt% or 25 wt% PI-membranes.
Flexible polymer deformation studies were shown to be useful to relate qualitatively membrane formation parameters to pore size distributions of the final membranes. Especially the information about the number of pores is crucial, since the results of permporometry should be critically considered as membrane characterization method, since the necessity of the drying procedure. Deformation characterization is a wet-state technique, which is an advantage over the dry-state permporometry.
It is obvious from the results that it is not possible to use this kind of retention measurements, i.e., dilute non-aqueous solutions of flexible polymers, as quantitative characterization technique to calculate membrane pore size distributions. Furthermore, it has been suggested here to be very careful in interpreting aqueous retention measurements, since water as a solvent may have a large influence on the results, which is often not recognized.

Silver sols were prepared in different mixtures of ethanol and water, to obtain small non-deformable solutes. It was found that when the final ethanol concentration exceeds 57%, the sol particles start to form aggregates. A large quantity of water is necessary to ensure the stabilization of the sol particles. The presence of a double layer around the sol particles does increase the effective hydrodynamic diameter, i.e., the effective diameter is larger than the mean particle diameter of 12 nm, as determined by Transmission Electron Microscopy.
The retention for stable silver sols in ethanol/water mixtures or water was almost complete for all membranes. Comparison of this result with the retentions for PS at very low pressures, i.e., molecule deformation may be neglected and the radius of gyration is 7 nm, also supports the presence of a much larger effective diameter of the silver sols.

## 5.8 Acknowledgement

The authors would like to thank mr. S. Visser for performing part of the experiments.

## 5.9 References

[1] S.S. Kulkarni, E.W. Funk, N.N. Li; Ultrafiltration (part 7) in: W.S.W. Ho, K.K. Sirkar (Eds), Membrane Handbook; van Nostrand Reinhold, New York, 1992

[2] A.G. Fane; Ultrafiltration: factors influencing flux and rejection (ch. 4); Progress in filtration and separation; R.J. Wakeman (Ed.); Elsevier, Amsterdam, 1986; p. 101

[3] M. Cheryan; Modelling of ultrafiltration processes (ch. 4). Fouling of ultrafiltration membranes (ch. 6); Ultrafiltration handbook; Technomic Publ. Comp., Lancaster, 1986; p. 73, 171

[4] G.B. van den Berg and C.A. Smolders; Flux decline in ultrafiltration processes; Desalination, 77(1990)101

[5] L.Y. Lafreniere, F.D.F. Talbot, T. Matsuura, S. Sourirajan; Effect of polyvinylpyrrolidone additive on the performance of polyethersulfone ultrafiltration membranes; Ind. Eng. Chem. Res., 26(1987)2385

[6] F.F. Stengaard; Characterization and performance of new types of ultrafiltration membranes with chemically modified surfaces; Desalination, 70(1988)207

[7] L.E.S. Brink, D.J. Romijn; Reducing the protein fouling of polysulfone surfaces and polysulfone ultrafiltration membranes; optimization of the type of presorbed layer; Desalination, 78(1990)209

[8] W. Norde; Adsorption of proteins from solution at the solid-liquid interface; Adv. Colloid Interface Sci., 25(1986)267

[9] A. Bottino, G. Capanelli, A. Imperato, S. Munari; Ultrafiltration of hydrosoluble polymers. Effect of operating conditions on the performance of the membrane; J. Membrane Sci., 21(1984)247

[10] A.R. Cooper, D.S. van der Veer; Characterization of ultrafiltration membranes by polymer transport measurements; Sep. Sci. & Techn. 14(1979)551

[11] R.W. Baker, H. Strathmann; Ultrafiltration of macromolecular solutions with high-flux membranes; J. Appl. Pol. Sci., 14(1970)1197

[12] J.D. Ferry; Ultrafilter membranes and ultrafiltration; Chem Rev., 18(3)(1936)373

[13] E.A. Mason, R.P. Wendt, E.H. Bresler; Similarity relations (dimensional analysis) for membrane transport; J. Membrane Sci., 6(1980)283

[14] W.D. Munch, L.P. Zestar, J.L. Anderson; Rejection of polyelectrolytes from microporous membranes; J. Membrane Sci., 5(1979)77

[15] P.G. de Gennes; Dynamics of entangled polymer solutions. 1. The Rouse model/ 2. Inclusion of hydrodynamic interactions; Macromolecules 9(1976)587/594

[16] S. Daoudi, F. Brochard; Flows of flexible polymer solutions in pores; Macromolecules 11(1978)751

[17] Q.T. Nguyen, P. Aptel, J. Néel; Characterization of ultrafiltration membranes. 2. Mass transport measurements for low and high molecular weight synthetic polymers in water

solutions; J. Membrane Sci., 7(1980)141

[18] Q.T. Nguyen, J. Néel; Characterization of ultrafiltration membranes. 4. Influence of the deformation of macromolecular solutes on the transport through ultrafiltration membranes; J. Membrane Sci., 14(1983)111

[19] T.D. Long, J.L. Anderson; Flow-dependent rejection of polystyrene from microporous membranes; J. Polym. Sci., Polym. Phys. Ed., 22(1984)1261

[20] T.D. Long, J.L. Anderson; Effects of solvent goodness and polymer concentration on rejection of polystyrene from small pores; J. Polym. Sci., Polym. Phys. Ed., 23(1985)191

[21] B.D. Mitchell, W.M. Deen; Effect of concentration on the rejection coefficients of rigid macromolecules in track-etch membranes; J. Colloid Interface Sci., 113(1986)132

[22] S. Poyen, B. Bariou, N. Mameri, M. Portier, M. Bergez; Prediction of rejection coefficients in ultrafiltration; J. Membrane Sci., 43(1989)47

[23] T. Liu, S. Xu, D. Zhang, S. Sourirajan, T. Matsuura; Pore size and pore size distribution on the surface of polyethersulfone hollow fiber membranes; Desalination, 85(1991)1

[24] T.D. Long, D.L. Jacobs, J.L. Anderson; Configurational effects on membrane rejection; J. Membrane Sci., 9(1981)13

[25] L. Zeman, M. Wales; Steric rejection of polymeric solutes by membranes with uniform pore size distributions; Sep. Sci. & Techn., 16(1981)275

[26] S. Mochizuki, A.L. Zydney; Dextran transport through asymmetric ultrafiltration membranes: comparison with hydrodynamic models; J. Membrane Sci., 68(1992)21

[27] M.G. Davidson, W.M. Deen; Hydrodynamic theory for the hindered transport of flexible macromolecules in porous membranes; J. Membrane Sci., 35(1988)167

[28] G. Guillot, L. Léger, F. Rondelez; Diffusion of large flexible polymer chains through model porous membranes; Macromolecules, 18(1985)2531

[29] F.P. Cuperus, D. Bargeman, C.A. Smolders; Permporometry. The determination of the size distribution of active pores in UF membranes; J. Membrane Sci., 71(1992)57

[30] C.A. Finch (Ed.); Chemistry and technology of water-soluble polymers; Plenum Press, New York, 1983

[31] S.W. Shalaby, C.L. McCormick, G.B. Butler (Eds.); Water-soluble polymers; ACS Symp. Ser. 467, Washington, 1991

[32] R.P. Adamski, J.L. Anderson; Configurational effects on polystyrene rejection from microporous membranes; J. Polym. Sci., Polym. Phys. Ed., 25(1987)765

[33] M. Antonietti, H. Sillescu; Diffusion of intramolecular crosslinked and three-arm-star branched polystyrene molecules in different matrices; Macromolecules, 19(1986)798

[34] M. Antonietti, H. Sillescu, M. Schmidt, H. Schuch; Solution properties and dynamic bulk behaviour of intramolecular crosslinked polystyrene; Macromolecules, 21(19880736

[35] R.P. Adamski, J.L. Anderson; Flow-dependent filtration of a rigid-rod polymer; Macromolecules, 24(1991)3562

[36] R.M. McDonogh, K. Welsch, A.G. Fane, C.J.D. Fell; Flux and rejection in the ultrafiltration of colloids; Desalination, 70(1988)251

[37] G. Boven, M.L.C.M. Oosterling, G. Challa, A.J. Schouten; Grafting kinetics of poly(methylmetacrylate) on microparticulate silica; Polymer, 31(1990)2377

[38] M.M. Kops-Werkhoven, H.M. Fijnaut; Dynamic light scattering and sedimentation experiments on silica dispersions at finite concentrations; J. Chem. Phys., 74(1981)1618

[39] I. Issid, M. Lavergne, D. Lemordant; Using micelles to determine the pore size of ultrafiltration membranes; J. Membrane Sci., 74(1992)279

[40] H.-D. Dörfler, C. Swaboda; Some selected problems on non-aqueous microemulsions - phase diagrams and variation of the composition in the quaternary and ternary systems; Colloid Polym. Sci., 271(1993)586

[41] S.E. Friberg, Y.-C. Liang; Microemulsions: structure and dynamics. Ch 3: non-aqueous microemulsions; S.E. Friberg, P. Bothorel (Eds.), CRC Press, Boca Raton, USA, 1987

[42] F.P. Cuperus, D. Bargeman, C.A. Smolders; A new method to determine the skin thickness of asymmetric UF-membranes using colloidal gold particles; J. Colloid Interface Sci., 135(1990)486

[43] K.-J. Kim, V. Chen, A.G. Fane; Ultrafiltration of colloidal silver particles: flux, retention and fouling; J. Colloid Interface Sci., 155(1993)347

[44] C.H. Fischer, A. Henglein; Photochemistry of colloidal semi-conductors.31. Preparation and photolysis of CdS sols in organic solvents; J. Phys. Chem., 93(1989)5578

[45] M. Beaman, S.P. Armes; Preparation and characterization of polypyrrole colloids in non-aqueous media; Colloid Polym. Sci., 271(1993)70

[46] M. Daoud, J.P. Cotton, B. Farnoux, G. Jannink, G. Sarma, H. Benoit, R. Duplessix, C. Picot, P.G. de Gennes; Solutions of flexible polymers. Experiments and interpretation; Macromolecules, 8(1975)804

[47] P.C. Hiemenz; Polymer chemistry. The basic concepts; Marcel Dekker, New York, 1984; p. 145

[48] R.B. Bird, R.C. Armstrong, O. Massager; Dynamics of polymeric liquids, vol.1; Wiley, New York, 1977

[49] R. Nobrega, H. de Balmann, P. Aimar, V. Sanchez; Transfer of dextran through ultrafiltration membranes: a study of rejection data analysed by GPC; J. Membrane Sci. 45(1989)17-36

[50] H. de Balmann, R. Nobrega; The deformation of dextran molecules. Causes and consequences in ultrafiltration; J. Membrane Sci., 40(1989)311

[51] F.P. Cuperus, C.A. Smolders; Characterization of ultrafiltration membranes. Membrane characteristics and characterization techniques; Adv. Colloid Interf. Sci., 34(1991)135

[52] P.G. de Gennes; Scaling concepts in polymer physics; Cornell University Press, Ithaca, New York, 1979

[53] W.W. Graessley; Polymer chain dimensions and the dependence of viscoelastic properties on concentration, molecular weight and solvent power; Polymer, 21(1980)258

[54] P.G. de Gennes; Coil-stretch transition of dilute flexible polymers under ultrahigh velocity gradients; J. Chem. Phys., 60(1974)5030

[55] R.G. Larson, J.J. Magda; Coil-stretch transitions in mixed shear and extensional flows of dilute polymer solutions; Polym. Prepr., 30(1989)93

[56] M.J. Menasveta, D.A. Hoagland; Molecular weight dependence of the critical strain rate for flexible polymer solutions in elongational flow; Macromolecules, 25(1992)7060

[57] T.Q. Nguyen, H.H. Kausch; Chain extension and degradation in convergent flow; Polymer, 33(1992)2611

[58] K.A. Narh, J.A. Odell, A. Keller; Temperature dependence of the conformational relaxation time of polymer molecules in elongational flow: invariance of the molecular weight exponent; J. Polym. Sci., Polym. Phys. Ed., 30(1992)335

[59] A. Link, J. Springer; Light scattering from dilute polymer solutions in shear flow; Macromolecules, 26(1993)464

[60] J. Brandrup, E.H. Immergut; Polymer Handbook; 3d edition, Wiley, New York, 1989

[61] I.A. Kathawalla, J.L. Anderson; Pore size effects on diffusion of polystyrene in dilute solution; Ind. Eng. Chem. Res., 27(1988)866

[62] M. Fukuda, M. Fukutomi, Y. Kato, T. Hashimoto; Solution properties of high molecular weight polystyrene; J. Polym. Sci., Polym. Phys. Ed., 12(1974)871

[63] N. Nemoto, V. Makita, Y. Tsunashima, M. Kurata; Dynamic light scattering studies of polymer solutions. 3. Translational diffusion and internal motion of high molecular weight polystyrenes in benzene at infinite dilution; Macromolecules, 17(1984)425

[64] B.K. Varma, Y. Fujita, M. Takahashi, T, Nose; Hydrodynamic radius and intrinsic viscosity of polystyrene in the crossover region from θ to good-solvent conditions; J. Polym. Sci., Polym. Phys Ed., 22(1984)1781

[65] M. Doi, S.F. Edwards; The theory of polymer dynamics; Clarendon Press, Oxford, UK, 1986

[66] J. des Cloizeaux, G. Jannink; Polymers in solution: their modeling and structure; Clarendon Press, Oxford, UK, 1990

[67] M.T. Bishop, K.H. Langley, F.E. Karasz; Dynamic light-scattering studies of polymer diffusion in porous materials: linear polystyrene in porous glass; Macromolecules, 22(1989)1220

[68] I. Teraoka, K.H. Langley, F.E. Karasz; Diffusion of polystyrene in controlled pore glasses: transition from the dilute to the semi-dilute regime; Macromolecules, 26(1993)287

[69] J.A. Creighton, C.G. Blatchford, M.G. Albrecht; Plasma resonance enhancement of Raman scattering by pyridine adsorbed on silver or gold sol particles of size comparable to the excitation wavelength; J. Chem. Soc. Faraday Trans. 2, 75(1979)790

[70] M. Meireles, P. Aimar, V. Sanchez; Effects of protein fouling on the apparent pore size distribution of sieving membranes; J. Membrane Sci., 56(1991)13

# Chapter 6

## Hindered diffusion of flexible polymers through polyimide ultrafiltration membranes

M.A.M. Beerlage, J.M.M. Peeters, J.A.M. Nolten, M.H.V. Mulder, C.A. Smolders, H. Strathmann

**Summary**

The hindered diffusion of polystyrene in dilute solutions of ethyl acetate through polyimide ultrafiltration membranes has been investigated. The present system did not show specific membrane-solute interactions; furthermore, polystyrene can be considered as a flexible polymer coil.
It is shown that the hindered diffusive permeability for monodisperse dilute solutions for a series of molecular weights can be compared well with the diffusive permeability curve of one polydisperse dilute polystyrene solution. In case of very dilute solutions the polymer coils have no interaction with each other, and the whole range of molecular weight dependent permeabilities can be determined from only one measurement.
The diffusion behaviour of polydisperse solutions through various polyimide membranes has been investigated as well. It was found that the diffusive permeability curve is strongly dependent on the type of membrane, i.e., on the pore size distribution.
It was not possible to calculate a pore size distribution from diffusion experiments, due to mathematical limitations. Nevertheless, it was shown that hindered diffusion measurements are useful to estimate a maximum pore size for each membrane.

## 6.1 Introduction

Characterization of ultrafiltration membranes is still prone to several experimental and theoretical problems, like membrane-solute or solute-solvent interactions, flow-induced deformation of flexible solutes, the occurrence of concentration polarization, and the necessity for some methods to dry the membranes (e.g., gas permeation and permporometry). A comparison of characterization techniques for non-aqueous systems with those for aqueous systems reveals many additional problems. In non-aqueous systems many disturbing interactions can be prevented by choosing the right model system.
In chapter 5 retention measurements were performed on dilute solutions of polystyrene in ethyl acetate, in which the permeate flows were determined by convection; it was shown that flow-induced deformation is a commonly occurring phenomenon for very dilute solutions of flexible polymers.

In this chapter transport measurements will be described for the same systems, in the absence of convection: now, the transport mechanism through the membrane is exclusively diffusive, and flow-induced deformation does not occur. The measurements are performed at very low feed concentrations, which means that the chains have no interaction with each other. Diffusion of polystyrene molecules through a porous membrane is strongly hindered; the theory of hindered diffusion of flexible polymers through porous systems will be reviewed shortly in the theoretical part of this chapter.
Polystyrene (PS) has been chosen as a model polymer for three reasons. Firstly, there are many publications in literature on the diffusive behaviour of this system, and PS may be considered as a polymer coil without long-range interactions with most membrane materials. Secondly, PS is commercially available in both monodisperse fractions and with a broad molecular weight distribution. Thirdly, there are many data available on radii of gyration, bulk diffusion coefficients and solvent quality of polystyrene solutions.
Diffusion of mono- and polydisperse polystyrene solutions in various membranes will be compared. The possibility to use diffusion measurements for the determination of pore size distributions in ultrafiltration membranes will also be discussed.

## 6.2 Theoretical background

### 6.2.1 Hindered diffusion of rigid particles in porous systems

The resistance to Brownian motion of a spherical solute molecule, which is much larger than the surrounding solvent molecules, can be obtained from the

Stokes-Einstein equation [1]:

$$D_o = \frac{k\,T}{f_o} \qquad (6.1)$$

where $D_o$ is the bulk diffusion coefficient [$m^2/s$], k is the Boltzmann constant [J/K] and T the temperature [K]. The molecular friction or wall drag coefficient, $f_o$, is given by equation (6.2):

$$f_o = 6\,\pi\,\eta\,r_s \qquad (6.2)$$

where $\eta$ is the solvent viscosity [$Ns/m^2$] and $r_s$ is the Stokes-Einstein radius of the particle [m]. For non-spherical particles, this radius is defined as the radius of a sphere with the same diffusivity.

Diffusion of particles inside the pores of a porous medium, like a membrane, is highly hindered because of the increased friction by the presence of a confining pore wall. Furthermore, the partition coefficient between "bulk" and "pore" is of importance for the overall diffusive transport, too. When particles are large enough, steric exclusion might take place which turns the diffusivity to zero. With smaller particles, the distribution inside and outside the pores can be influenced by steric effects and long-range intermolecular forces.
The hindrance factor, H (with $0<H<1$), is defined as $D_m/D_o$, where $D_m$ is the effective diffusion coefficient through the porous membrane. H is often related to $\lambda_s$, i.e., the ratio of the solute Stokes-Einstein radius to the pore radius: $\lambda_s = r_s/r_p$. As an example, the Renkin equation is given here [2,3]:

$$\frac{D_m}{D_o} = H = K_R\,f_R = (1-\lambda_s)^2(1- 2.1044\,\lambda_s + 2.0888\,\lambda_s^3 - 0.948\,\lambda_s^5) \qquad (6.3)$$

Here, the index "R" stands for "rigid". The static part $K_R$, is the steric partition coefficient of a spherical rigid particle in a cylindrical pore, and is a function of $\lambda_s$. This is analogous to the relation of Ferry [4]. The dynamic part $f_R$ or molecular friction or wall drag coefficient, represents the hindrance caused by the reduction in mobility of a rigid solute entering a pore, and is also a function of $\lambda_s$. For a solute that is only 0.1 times the pore size, i.e., $\lambda_s = 0.1$, the calculated diffusion hindrance factor is already 0.64, which has been confirmed experimentally by Deen [5].

In practice, the Renkin equation describes quite accurately the transport of spherical rigid particles (e.g., asphaltenes [6]), cross-linked macromolecules [7,8] or small macromolecules with $\lambda_s < 0.4$ through cylindrical pores [7-9].
However, problems arise when charges are involved or other pore shapes are

applied. Malone and Anderson [10] described the hindered diffusion of latices through rhombic (diamond-shaped) pores. Their results indicate that the charged latices, influenced by surfactants and solution ionic strength, show a much higher hindrance factor than similar neutral particles. A correction factor was found necessary for the rhombic pore shape. Weinbaum [11] and Pawar and Anderson [12] calculated hindered diffusion in slit-shaped pores.
Robertson and Zydney [13] measured hindered BSA-diffusion in asymmetric polymeric membranes; they also found a higher hindrance than was predicted by hard-sphere theories, due to charge effects.
In literature many modifications based on the Renkin equation can be found. Deen [5] wrote an excellent and extensive review on the theory of hindered diffusion and convection of large molecules in porous systems.

### 6.2.2 Hindered diffusion of flexible macromolecules in porous systems

Flexible polymers in solution are regarded as random coils instead of rigid spheres. The size of such a coil is usually indicated as the radius of gyration, $r_g$, which is a statistical average of all kinds of configurations the coil can adopt. Flexible polymers are allowed to diffuse through pores with pore sizes smaller than the radius of gyration. The hydrodynamic radius of a polymer coil, $r_h$, is defined as the Stokes-Einstein radius ($r_s$) of a rigid spherical particle that has the same bulk diffusion coefficient. It is assumed that the diffusion of a polymer through pores that are *smaller* than its hydrodynamic radius is negligible, i.e., the diffusion is effectively zero when $\lambda_s>1$.

Based on the ideas of Debye and Bueche [14] and Brinkman [15], Davidson and Deen [16] considered a polymer random coil as a porous body, that is permeable for solvent molecules (for this reason generally the radius of gyration is somewhat larger than the Stokes-Einstein radius which is defined for an impermeable rigid sphere). They proposed a model for the hindrance factor for flexible polymers, based on the variable $\lambda_g=r_g/r_p$, which is the ratio of the radius of gyration of the solute to the pore radius. For flexible polymers equation (6.3) becomes:

$$\frac{D_m}{D_o} = H = K_F f_F \qquad (6.4)$$

Here, the index "F" stands for "flexible". Both the partition coefficient of a flexible polymer coil, $K_F$, and the wall drag coefficient of a flexible polymer coil, $f_F$, are functions of $\lambda_g$. The partition coefficient $K_F$ was described analytically by Casassa for cylindrical pores, using random-flight statistics [17]:

$$K_F(\lambda_g) = 4 \sum_{m=1}^{\infty} -\frac{1}{\beta_m^2} \exp\left(-\beta_m^2 \frac{\langle r_g^2 \rangle}{r_p^2}\right) \qquad (6.5)$$

Here, $\beta_m$ is the $m^{th}$ root of the $zero^{th}$-order Bessel function $J_0(\beta) = 0$; $\langle r_g^2 \rangle$ is the mean square of the radius of gyration of the polymer. Results from a Monte Carlo approach were in good agreement with the results of Casassa [18]. The calculated results for the partition coefficient show that when the equivalent $\lambda_s < 0.4$, the value for a porous polymer coil is close to that of a rigid sphere, which explains the rigid sphere-like behaviour of macromolecules at low $\lambda_s$.

A wall drag coefficient for flexible polymers inside a confining pore has been deduced by Davidson and Deen, based on a porous-body friction coefficient in bulk solution that was derived by Wiegel and Mijnlieff [19]. This modified friction coefficient, $f_F$, gives a concentration distribution of the polymer *inside* the pore. The distribution combined with a set of equations that describe the flow past a stationary solute determines the wall friction [16]. $f_F$ is only dependent on $\alpha$ and $\lambda_g$. $\alpha$ is a dimensionless measure of the resistance to solvent flow through the porous-body polymer, and is dependent on the polymer-solvent combination and the molecular weight of the polymer. For most polymer-solvent systems $10 \leq \alpha \leq 60$ [16], where in general $\alpha$ is low for a polymer in a good solvent, and $\alpha$ is high for a polymer in poor solvent. In addition, this approach led to a relation between $r_s$ and $r_g$ (and consequently between $\lambda_s$ and $\lambda_g$):

$$\frac{r_s}{r_g} = \frac{2}{3}\sqrt{\frac{2}{3a}}\,\alpha\,\xi\{\alpha\} \qquad (6.6)$$

Here, a [-] is a measure of the solvent quality [20].
By using some experimental values for $r_s/r_g$ from literature combined with numerical solutions for the $\xi\{\alpha\}$-functions and $f_{F,o}$ for porous spheres in bulk solution, diffusive hindrance factor curves were calculated as a function of $\lambda_s$ (and $\lambda_g$) for three discrete values of $\alpha$, $\alpha$=10, $\alpha$=34 and $\alpha$=60. These calculations made clear that H as a function of $\lambda_s$ of a flexible polymer is smaller than H as a function of $\lambda_s$ of a rigid solid sphere.
Davidson and Deen also reasoned that for a given polymer the choice of solvent has only little effect on the diffusive hindrance, based on entropic and hydrodynamic considerations; as a result the H-curves for $\alpha$=34 and $\alpha$=60 are almost similar.
In figure 1, the H-$\lambda_s$-curves are given for $\alpha$=10 and $\alpha$=60, together with the curve for rigid spheres (Renkin equation (6.3)).

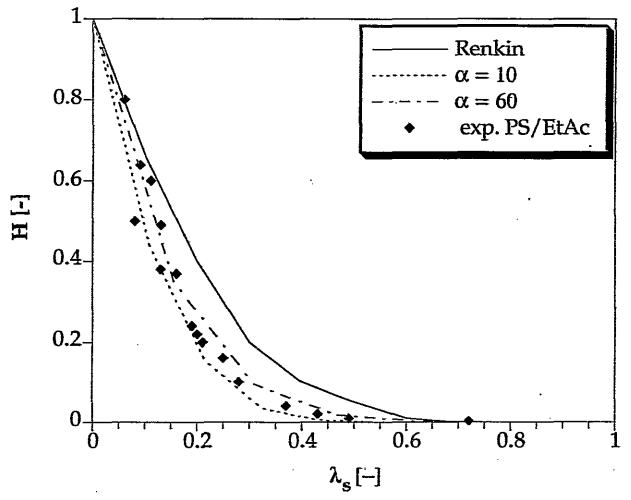


*Figure 1. Comparison of hindered diffusion for rigid spheres (Renkin) and flexible polymers (porous-body approach) as a function of $\lambda_s$. $\alpha$=10: polymer in good solvent, $\alpha$=60: polymer in poor solvent. The points represent experimental data obtained by Cannell and Rondelez for PS in ethyl acetate [23] (see section 6.2.3)*

Diffusion of flexible polymers through pores can also be described by a scaling analysis [21]. For long-chain flexible polymers in good solvents with $r_f \geq r_p$ (with $r_f$ the Flory radius, i.e., the root mean square end-to-end distance of the chain), the following scaling law was obtained:

$$\frac{D_m}{D_o} = H \cong \alpha' \left(k' \frac{r_f}{r_p}\right)^{\frac{2}{3}} e^{\left(-k' \frac{r_f}{r_p}\right)^{\frac{5}{3}}} \qquad (6.7)$$

Here $\alpha'$ and $k'$ are proportionality factors. Equation (6.7) is a scaling law, which means that it is not possible to predict exact numerical coefficients [22]. Nevertheless, Cannell and Rondelez [23] and Guillot et al. [24] were able to fit their experimental data of diffusion of polystyrene (PS) with $\lambda_s$<1 in ethyl acetate through Nuclepore membranes using equation (6.7).
This scaling approach is especially useful for higher polymer concentrations, when the bulk concentration ($c_o$) approaches the overlap concentration $c^*$ [22] or even exceeds it. Below $c^*$ the polymer coils have no interaction with each other and can be treated as independent molecules. The overlap concentration is dependent on the polymer molecular weight (see also chapter 5).
Scaling arguments predict for semi-dilute solutions the possibility of large chains to enter pores even if $r_h > r_p$, because the typical hydrodynamic size of a polymer above the overlap concentration is no longer the Stokes-Einstein radius, but a

smaller radius that decreases with increasing concentration [25,26,27]. In this study, attention will be focused only on dilute concentrations, so with $c_o \ll c^*$.

A comparison between the porous-body approach and the scaling analysis is difficult, because they apply to a different regime. The porous-body approach is limited for $\lambda_s \leq 1$, while the scaling analysis was derived especially for cases where $\lambda_s > 1$. For the specific case presented in figure 1, the differences are not large; nevertheless, more research is needed in order to compare both theories.

### 6.2.3 Experimental diffusion studies from literature

In figure 1 experimental diffusion data obtained as reported by Cannell and Rondelez for dilute solutions of PS in ethyl acetate, through track-etched polycarbonate membranes were represented [23]. These results are comparable with later results obtained by Guillot et al. [24] and Guillot [27]. The PS samples were commercially available monodisperse fractions, with molecular weights ranging from $1.07*10^5$ g/mol to $20.6*10^6$ g/mol. The $\lambda_s$-values, defined as $r_h/r_p$ with $r_h$ the hydrodynamic radius determined by quasi elastic light scattering, varied from 0.1 to 0.993.
The scaling approach was used to fit the experimental data.
Kathawalla and Anderson [28] measured diffusion of dilute monodisperse PS solutions in THF through track-etched mica membranes with rhombic pores ($\lambda_s<1$). Their results agree qualitatively well with the results of Cannell and Rondelez and Guillot et al.
In a later article, Kathawalla et al. [29] described the hindered diffusion of disk-like porphyrin molecules in chloroform and of low molecular weight polystyrenes ($M_w$ < 7000 g/mol) in THF ($\lambda_s<1$). The short-chain polystyrenes were hindered less than the long-chain polystyrenes ($M_w$: $10^5$ - $10^6$ g/mol) that were described in the previous article; these short-chain polymers can better be described as rigid rods than as random coils.
Bishop et al. [30] and Teraoka et al. [31] used dynamic light scattering to measure directly the diffusion of polystyrene in 2-fluorotoluene through porous glasses. Their results are also consistent with the previously mentioned studies.
In addition, Teraoka et al. were able to determine diffusion coefficients of PS *inside* the pores. They found that when the feed concentration is lower than 20% of the overlap concentration ($c_o < 0.2\ c^*$), the diffusive behaviour is almost constant, indicating a dilute concentration regime *inside* the pores. In practice, this means that feed concentrations should never exceed 0.2 c*, to avoid disturbing semidilute diffusive effects.

Deen et al. [8] and Bohrer et al. [7] measured the hindered diffusion of dextran and ficoll, a cross-linked polysaccharide, in water through polycarbonate track-

etched membranes. For dextran the H-$\lambda_s$-curve was significantly higher than the curve for rigid spheres. Deen [5] suggested that interactions between the dextran molecules and the pore wall material cause the increase in the value of H. Davidson et al. [18] theoretically showed by Monte Carlo simulations, that even weak interactions drastically increase the partition coefficient. The presence of interactions causes an increase in friction with the pore wall, which should result in a decrease in the value of H. That experimental results show an increase in H, means that the influence of interactions on the partition coefficient is larger than that on the wall drag coefficient.
The diffusive hindrance curve for linear polyisoprenes ($\lambda_s$<1) in amyl acetate, as measured by Bohrer et al. [32], was situated slightly above the curve for rigid spheres. They also determined hindrance curves for branched, star-shaped polyisoprenes, which were in agreement with the results described previously for polystyrene. In this case the discrepancy cannot be explained by interactions, because linear and star-branched polyisoprenes are supposed to be chemically identical. It is not yet clear where this discrepancy originates from.

### 6.2.4 Diffusion experiments using asymmetric membranes

Diffusion experiments are usually carried out in a simple diffusion cell, consisting of two compartments separated by a membrane. One compartment is filled with a dilute polymer solution, while the other contains pure solvent only. These solutions are well stirred to enable a uniform concentration. In the case of polystyrene as diffusing polymer, the stirring rate cannot exceed a certain value, because of a possible cleavage of the polymer chain [33-35].
Because of a concentration gradient the polymer diffuses through the membrane. From a mass balance, equation (6.8) can be derived (see appendix in section 6.7):

$$\ln \frac{(c_f - c_d)_o}{(c_f - c_d)_t} = \frac{A}{R_{tot}} t \left( \frac{1}{V_f} + \frac{1}{V_d} \right) \qquad (6.8)$$

where $c_f$ and $c_d$ are the polymer concentrations [g/l] on the solution (feed) side and the solvent (diluate) side, respectively. A is the membrane surface area [$m^2$], $V_f$ and $V_d$ are the volumes of the two compartments [$m^3$]. The subscripts o and t indicate the concentration differences at time zero and time t, respectively.
$R_{tot}$ [s/m] is the total resistance to diffusive transport. The total diffusive permeability, $P_{tot}$ [m/s], is the inverse of the total diffusive resistance. When diffusion results are plotted as the logarithm of the ratio of the concentration differences in the feed and diluate versus the diffusion time t, a straight line is the result with a slope of $(A/R_{tot})*(1/V_f + 1/V_d)$. A schematic representation is given in figure 2.

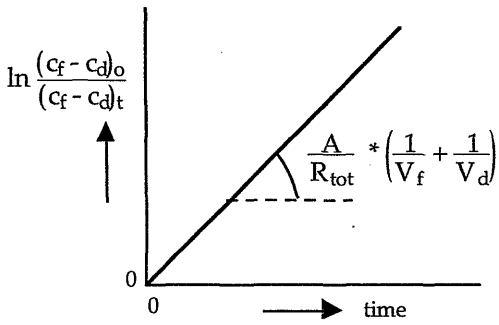


*Figure 2. Graphic representation of equation (6.8): determination of the diffusive resistance $R_{tot}$.*

$R_{tot}$ is the summation of the resistances of the membrane and boundary layers, the feed and diluate phase (resistance in series), and can be represented by:

$$R_{tot} = \frac{1}{k_{tot}} = \frac{1}{k_{feed}} + \frac{2}{k_{bl}} + \frac{1}{k_{membr}} + \frac{1}{k_{diluate}} \qquad (6.9)$$

Since the feed and diluate phase are well mixed:

$$R_{tot} \approx \frac{2}{k_{bl}} + \frac{1}{k_{membr}} = \frac{2}{k_{bl}} + R_{matrix} + R_{skin} \qquad (6.10)$$

where $k_{bl}$ [m/s] is the mass transfer coefficient of the liquid boundary layers on both sides of the membrane.

The asymmetric membrane consists of a thin symmetric toplayer with a diffusive resistance $R_{skin}$ and a thicker symmetric support layer with a diffusive resistance $R_{matrix}$. The resistances are assumed to be in series, and a schematic drawing of the process is given in figure 3.

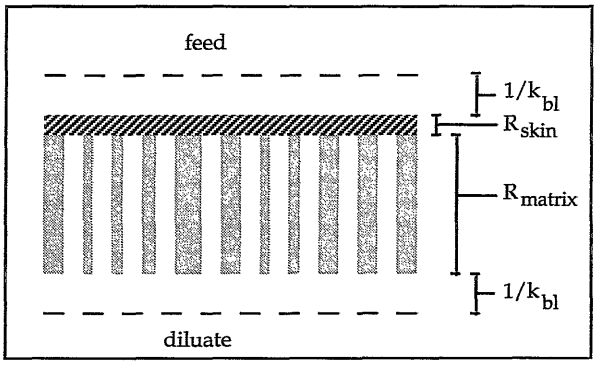


*Figure 3. Schematic overview of resistances to diffusive transport through a membrane plus two boundary layers (at the well mixed feed and diluate side).*

The boundary layer mass transfer coefficient in a stirred cell (see figure 7) can be described by [36]:

$$k_{bl}\, b_{cell} = 0.285\, D_o * \left(\frac{\nu}{D_o}\right)^{0.33} * \left(\frac{\omega\, b_{cell}^2}{\nu}\right)^{0.57} \qquad (6.11)$$

where $b_{cell}$ is the radius of the compartment of the diffusion cell [m], $\nu$ is the kinematic viscosity [$m^2/s$] and $\omega$ is the stirring speed [/s]. Equation (6.11) is only valid for a ratio of cell radius to stirrer bar radius of 1.11 [36], which is equal to the ratio used in the present study.

The resistance of the polymer matrix can be represented by equation (6.12), assuming that the matrix consists of symmetric straight cylindrical pores of radius $r_{matrix}$ [m]:

$$R_{matrix} = \frac{l_{matrix}}{n_{matrix}\, \pi\, r_{matrix}^2 * D_{matrix\ pore}} \qquad (6.12)$$

where $l_{matrix}$ is the length [m] of the matrix pores (≈ membrane thickness), $n_{matrix}$ is the number of matrix pores per membrane surface area [$/m^2$], $n_{matrix}\pi r_{matrix}^2$ is equal to the matrix porosity $\varepsilon_{matrix}$ [-] and $D_{matrix\ pore}$ is the effective diffusion coefficient of the solute in the matrix pore [$m^2/s$].

The resistance of the skin is determined by two factors: the diffusion resistance by the toplayer combined with entrance and exit effects to diffusion into and out of the pores. Entrance and exit effects each add an equivalent length of $0.25*\pi*r_p$ to the diffusion path [37]. Assuming that the toplayer is a symmetric layer with

straight cylindrical pores of radius $r_p$ [m] and pore length or skin thickness $l_{skin}$ [m], the resistance of the skin becomes [37]:

$$R_{skin} = \frac{l_{skin}}{n_{skin}\,\pi\,r_p^2\,D_p} + \frac{0.5\,\pi\,r_p}{n_{skin}\,\pi\,r_p^2\,D_o} \qquad (6.13)$$

where $D_p$ is the diffusion coefficient inside the skin pores [$m^2/s$], $n_{skin}$ is the number of pores in the skin per membrane surface area [$/m^2$] and $\Sigma n\{r_p\}\pi r_p^2$ is a measure of the pore size distribution in the toplayer.

It will be shown below that the resistances of the boundary layers and of the matrix are negligible compared to the resistance of the skin (see experimental section). The total diffusive permeability for a solute is then given by the inverse of the toplayer resistance; the permeability is determined experimentally by monitoring the concentration difference in time, according to equation (6.8). The effective diffusion coefficient through the membrane is in that case equal to the diffusion coefficient inside the skin pores: $D_m = D_p$.
Measurements are carried out in the dilute regime, which implicitly excludes the possibility of concentration-induced deformation.
The Stokes-Einstein radius, which is the radius of a rigid sphere that is impermeable to solvent molecules, is taken as the hydrodynamic radius of the polymer. This is the smallest size a polymer coil can adopt in a dilute solution. This implies that a polymer chain in a dilute solution cannot diffuse through a membrane pore with a radius smaller than the hydrodynamic radius. The pore size distribution of the accessible pores for a certain polymer is between $r_h$ as minimum and $r_{p,max}$ as maximum. $r_h$ depends on the polymer molecular weight via the hydrodynamic radius, while $r_{p,max}$ is the largest pore radius that is present in the membrane, which is a fixed value that is determined only by the membrane morphology.

In principle, $r_{p,max}$ can be determined by diffusion measurements: it is equal to $r_h$ of the largest polymer molecule that can pass through the membrane, which is the highest molecular weight that can be detected at the diluate side. Based on equation (6.13), the permeability of the polymer, a, with the maximum molecular weight that is still permeable can be represented by equation (6.14):

$$P_a = \frac{n_{p,a}\,\pi\,r_{p,a}^2\;D_p\left\{\frac{r_{h,a}}{r_{p,a}}\right\}\;D_{o,a}}{l_{skin}\,D_{o,a} + 0.5\,\pi\,r_{p,a}\;D_p\left\{\frac{r_{h,a}}{r_{p,a}}\right\}} \qquad (6.14)$$

Here, the braces indicate that $D_p$ is a function of $r_{h,a}/r_{p,a}$. When values are

obtained for the skin thickness $l_{skin}$ (estimated from SEM) and the bulk diffusion coefficient $D_{o,a}$ (from literature), an estimation of $D_p$ as a function of solute size to pore size ratio, $r_{h,a}/r_{p,a}$ (from theory), provides us the number of pores with radius $r_{p,a}$ (=$r_{p,max}$): $n_{p,a}$.
A slightly smaller polymer chain, b, can then pass through somewhat smaller pores ($r_{p,b} < r_{p,a}$), but also through the pores that were already accessible for polymer a. The effective diffusion coefficient of b through these largest pores is *larger* than the diffusion coefficient of a: the solute size to pore size ratio (pore size $r_{p,a}$) is smaller for polymer b than for polymer a.
Now for polymer b the permeability is given by:

$$P_b = \frac{n_{p,a}\,\pi\, r_{p,a}^2\, D_p\left\{\frac{r_{h,b}}{r_{p,a}}\right\}\, D_{o,b}}{l_{skin}\, D_{o,b} + 0.5\,\pi\, r_{p,a}\, D_p\left\{\frac{r_{h,b}}{r_{p,a}}\right\}} + \frac{n_{p,b}\,\pi\, r_{p,b}^2\, D_p\left\{\frac{r_{h,b}}{r_{p,b}}\right\}\, D_{o,b}}{l_{skin}\, D_{o,b} + 0.5\,\pi\, r_{p,b}\, D_p\left\{\frac{r_{h,b}}{r_{p,b}}\right\}} \qquad (6.15)$$

and $D_p\left\{\frac{r_{h,b}}{r_{p,a}}\right\} > D_p\left\{\frac{r_{h,b}}{r_{p,b}}\right\}$

For the "smallest polymer n" the permeability is given by:

$$P_n = \sum_{i=1}^{n} \left( \frac{n_{p,i}^{*}\,\pi\, r_{p,i}^2\, D_p\left\{\frac{r_{h,n}}{r_{p,i}}\right\}\, D_{o,n}}{l_{skin}\, D_{o,n} + 0.5\,\pi\, r_{p,i}\, D_p\left\{\frac{r_{h,n}}{r_{p,i}}\right\}} \right) \qquad (6.16)$$

The values of the number of pores, $n_{p,i}^{*}$, are indicated with an asterisk and they have to be calculated for each step in pore size.
The summation of $n_{p,i}^{*}\pi r_{p,i}^{2}$ over all pore sizes gives the pore size distribution of the membrane; equation (6.16) shows the dependence of the diffusive permeability on the membrane pore size distribution. In fact, it should be possible to estimate a pore size distribution from a diffusive permeability measurement of a polymer with a broad molecular weight distribution. However, the intricate dependence of the effective diffusion coefficient on the solute size to pore size ratio will be a complicated factor, and is not well defined.
A certain period of time will be required to allow the higher molecular weight polymer chains to diffuse.
Furthermore, the effect of a polydisperse feed solution has to be investigated (most literature data were obtained with monodisperse polymer fractions). Guillot [38], until now, was the only one who reported both on monodisperse solutions and solutions of mixtures of two molecular weights. He found that in the dilute regime, a solute molecule with a certain $M_w$ did not influence the diffusion kinetics of a molecule with a different molecular weight. An increase of the concentration of one of the components close to the overlap concentration

c* resulted in a blockage of small solutes by large solutes or a diffusion enhancement of large solutes by small solutes.

## 6.3 Experimental

### 6.3.1 Membranes and materials

Several polyimide membranes were used for diffusion experiments, all coagulated in ethanol. Special care was taken to ensure that the membranes were not dried during preparation, storage and installation. The membranes were pre-conditioned at least 48 hours in an ethyl acetate bath prior to installation in a diffusion cell. Ethyl acetate (synthesis quality) was purchased from Merck and used as received.
Some of the polyimide membranes were dried according to an ethanol-hexane-air exchange procedure: the ethanol-wet membranes were placed for three days in hexane to replace the ethanol, and after that, the membranes were dried (see also chapter 4). These membranes were rewetted again following the opposite procedure.

### 6.3.2 Polystyrene solutions: characteristics and concentration analysis

Six monodisperse polystyrene (PS) samples with molecular weights from 4070 to 1447000 g/mol were obtained from Aldrich.
The bulk diffusion coefficients [$m^2/s$] for these samples were obtained by quasi elastic light scattering [23,39] and fitted using a power law dependence, according to the method that Kathawalla and Anderson [28] used for PS in tetrahydrofuran (THF). An additional temperature and viscosity correction was necessary, because the measurements were performed at 25.0°C in our case. Since low molecular weight polystyrenes ($M_w < 10000$) can be better considered as rigid rods than as random coils [29], two power law relations were used,
for $M_w > 10000$:

$$D_o \sim 3.296*10^{-8} * M_w^{-0.533} \qquad (6.17)$$

and for $M_w < 10000$:

$$D_o \sim 1.75*10^{-8} * M_w^{-0.511} \qquad (6.18)$$

Hydrodynamic radii (i.e., Stokes-Einstein radii) were calculated from these bulk diffusion coefficients according to the Stokes-Einstein equation (equations (6.1) and (6.2)). Overlap concentrations are calculated according to two methods:

equation (6.19) represents the c* as given by Doi and Edwards [40] ($c^{*a}$), while equation (6.20) is the estimation Des Cloizeaux and Jannink used [41] ($c^{*b}$) (see also chapter 5):

$$c^{*a} = \frac{M_w}{\frac{4}{3}\pi r_g^3 N_A} \qquad (6.19)$$

$$c^{*b} = \frac{M_w}{(\sqrt{2}\, r_g)^3 N_A} \qquad (6.20)$$

Here $N_A$ is Avogadro's number and $r_g$ is the radius of gyration; $r_g$ was estimated from relation (6.21) which is applicable for good solvents [42-44]:

$$\frac{r_g}{r_h} = 1.48 \pm 0.03 \qquad (6.21)$$

The characteristics of the various monodisperse polystyrenes and the feed concentrations are summarized in table 1. The values of $M_w/M_n$ are a measure of the polydispersity, i.e., the ratio of the weight-average molecular weight to the number-average molecular weight.

***Table 1.*** *Characteristics of the various monodisperse polystyrenes used.*

| $M_w$ [g/mol] | $M_w/M_n$ [-] | $D_o$ [$m^2/s$] | $r_h$ [nm] | $c^{*a}$ [g/l] | $c^{*b}$ [g/l] | $c_o$ [g/l] |
|---|---|---|---|---|---|---|
| 4075 | 1.04 | $2.5 * 10^{-10}$ | 2.1 | 57 | 84 | 1.76 |
| 45730 | 1.05 | $1.1 * 10^{-10}$ | 4.8 | 52 | 77 | 3.17 |
| 95800 | 1.04 | $7.3 * 10^{-11}$ | 7.1 | 33 | 50 | 3.31 |
| 401340 | 1.02 | $3.4 * 10^{-11}$ | 15.1 | 14 | 21 | 1.72 |
| 850000 | 1.06 | $2.3 * 10^{-11}$ | 22.5 | 9.1 | 14 | 1.01 |
| 1447000 | 1.14 | $1.7 * 10^{-11}$ | 29.9 | 6.6 | 9.8 | 1.00 |

Below the overlap concentration c*, polymer chains have no interaction with each other. The concentrations of the feed solutions were in all cases far below the overlap concentration ($c_o < 0.2\ c^*$, see figure 5). The concentrations of solutions at the diluate side were determined by UV-spectrophotometry (Philips PU UV/Vis 8720 Scanning Photospectrometer) at a wavelength of 260 nm. Samples were returned to the diluate solution after analysis.
A commercially available polystyrene was purchased from BDH-Chemicals with a broad molecular weight distribution for diffusion measurements of polydisperse PS-solutions (see figure 4). The feed concentrations during these

measurements was about 2 g/l. In figure 5, $c^{*a}$ is given as a function of the molecular weight. It is clear from these figures that the concentrations of the separate fractions are well below the overlap concentration.

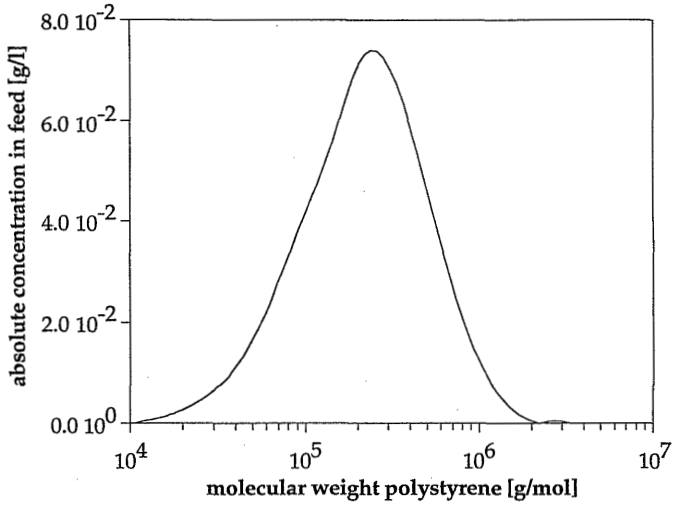


*Figure 4.* *Molecular weight distribution of polydisperse PS as a function of the molecular weight determined by GPC.*

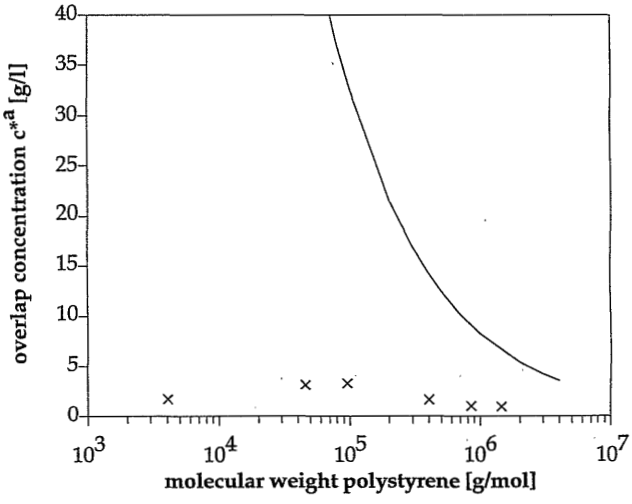


*Figure 5.* *Overlap concentration (line) of PS in ethyl acetate as a function of the molecular weight calculated from equation (6.19). Crosses are experimental feed concentrations for monodisperse PS (see table 1).*

Samples at the diluate side were analysed with Gel Permeation Chromatography, consisting of an HPLC-pump (Waters 510) with an autosampler (Hewlett Packard HP 1050 TI), a variable UV-detector (Waters 486), a differential refractometer (Waters 411) and two μStyragel-HT columns (Waters $10^4$ Å and $10^5$ Å). The total volume of the samples taken from the diluate side was about 3% of the total compartment volume. The diluate compartment was refilled with clean ethyl acetate.

The concentrations of the various fractions in the polydisperse sample are much lower than with monodisperse samples, because the "overall" concentrations are of the same order of magnitude. As a consequence, a small increase in concentration at the diluate side affects the diffusive permeability of other fractions perceptively when polydisperse samples are used. For this reason, only measurements of separate fractions are discussed where the concentration at the diluate side ($c_{dt}$) does not exceed 10% of the original feed concentration ($c_{fo}$).
Samples are taken at different times, varying from 4 to 14 days. The permeability is constant in time, according to equation (6.8). To verify this, an example is given in figure 6: this graph shows the diffusive permeability of a certain PI membrane for polystyrene, determined after 7 days and 14 days, respectively. The small differences in permeability may be ascribed to detection errors.

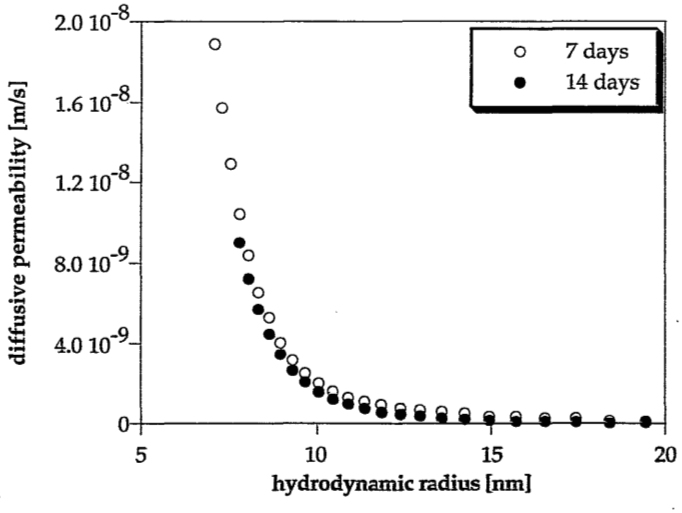


***Figure 6.*** *Diffusive permeability of polystyrene in a membrane (made from a casting solution of 20% polyimide in DMF and coagulated in ethanol) after 7 days (open circles) and 14 days (closed circles).*

### 6.3.3 Diffusion measurements

The diffusion test cell set-up is schematically drawn in figure 7. It consists of two glass compartments, which were kept at 25.0°C. The volume of each compartment was $56*10^{-6}$ $m^3$, and the membrane surface area $13.2*10^{-4}$ $m^2$. The membrane was clamped tightly into the cell using Kalrez® O-rings, to ensure chemical resistance to ethyl acetate and to prevent evaporation. One compartment was filled with the PS-solution, while the other was filled with ethyl acetate. The toplayer of the membrane was faced towards the solution side. Refilling and sampling in both compartments was done through teflon taps. Each compartment contained a magnetic stirrer, which was driven externally. The stirrer speed was set at 180 rpm, and the ratio of the cell radius to the stirrer radius was 1.11.
Sometimes a leak in the membrane was observed, caused by the tight clamping of the membrane. In these cases the diffusive permeability graphs expressed clearly an independence of P on the molecular weight.

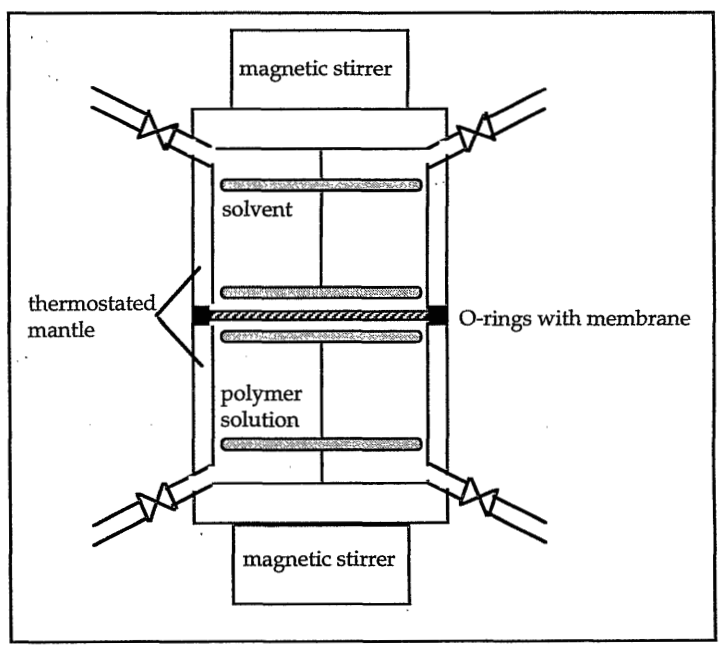


*Figure 7. Diffusion measurement set-up.*

The boundary layer mass transfer coefficient of the high molecular weight monodisperse polystyrene was estimated by equation (6.11), resulting in: $k_{bl} = 2.96*10^{-6}$ m/s. The combined resistances of the boundary layers are then $2/k_{bl} = 6.7*10^{5}$ s/m, which is less than 0.1% of the total resistance over the membrane (see below).

To determine the resistance of the membrane matrix (equation (6.12)), estimations of the thickness and porosity should be made. From a typical Scanning Electron Micrograph, the following values were obtained: $l_{matrix}$ = 75 μm, $\varepsilon_{matrix}$ = 0.80, $r_{matrix}$ = 200 nm. Consequently, for a PS chain with $r_h$ = 15 nm ($M_W$=401,340), $\lambda_s$ = 15/200 = 0.08. Then, from figure 1, H is determined to be 0.8, so the effective diffusion coefficient of this polymer in the matrix is $0.8*D_o$, with $D_o = 3.4*10^{-11}$ $m^2/s$.
The resistance of the matrix, $R_{matrix}$, can now be calculated from equation (6.12): $R_{matrix} = 3*10^6$ s/m. A typical value of the total resistance of the membrane for this polymer is in all experimental cases more than $1*10^9$ s/m, which is more than 300 times higher. For smaller PS molecules the resistance by the matrix is even less.

From these considerations it may be concluded that the total resistance of the membrane to diffusive transport is almost completely determined by the toplayer. Therefore, equation (6.13) is valid for this system. One has to keep in mind that a model description is used, where the pores are regarded as straight cylindrical channels. This assumption also applies for other characterization methods like retention measurements or permporometry. In practice, the configurations of the pores are quite different. In addition, there will be a gradient in pore size across the toplayer. Introduction of this gradient into equation (6.13) means that $l_{skin}$ will be dependent on the pore size as well.

## 6.4 Results and discussion

### 6.4.1 Diffusive permeability of monodisperse and polydisperse solutions

A batch of similar membranes was used to compare the diffusion of polystyrenes in monodisperse solutions and in polydisperse solutions. For this purpose, films cast from a 20 wt% polyimide solution in DMF containing 3 wt% tartaric acid were coagulated in ethanol. After preconditioning in ethyl acetate, the membranes were installed in the diffusion test cell set-up. For each measurement, a fresh membrane was applied.

If the natural logarithm of the ratio of the concentration differences is plotted versus time for the monodisperse polystyrenes, according to equation (6.8), the diffusive permeabilities can be calculated from the slope of each line. The results are summarized in table 2, as a function of the molecular weight, $M_w$, and the hydrodynamic radius, $r_h$.

*Table 2.* *Diffusive permeability of monodisperse polystyrenes.*

| $M_w$ [g/mol] | $r_h$ [nm] | P [m/s] |
|---|---|---|
| 4075 | 2.1 | $4.7 * 10^{-8}$ |
| 45730 | 4.8 | $1.4 * 10^{-8}$ |
| 95800 | 7.1 | $6.2 * 10^{-9}$ |
| 401340 | 15.1 | $1.9 * 10^{-9}$ |
| 850000 | 22.5 | $8.9 * 10^{-10}$ |
| 1447000 | 29.9 | $5.3 * 10^{-10}$ |

Diffusion measurements with a polydisperse PS-solution were done using membranes from the same batch. Samples were taken from the diluate side and analysed by GPC. The diffusive permeabilities for the different fractions of the polydisperse sample can be calculated in a similar way, using a graphical evaluation of the total resistance to diffusive transport (see figure 2). Figure 8 shows the diffusive permeability as a function of the polymer hydrodynamic radius. In this graph also some "monodisperse permeabilities" are given as comparison, i.e., the molecular weights of 45730, 95800 and 401340 g/mol.

The concentrations of the highest molecular weight fractions are very low (see figure 4) and the determination of the permeability may become inaccurate. It is preferred to employ a more uniform molecular weight distribution as a feed rather than a Gaussian distribution. The concentration of the lowest molecular weights is also very low, but these fractions are already divided over the two compartments after a short period of time, so that the concentration at the diluate side is larger than 10% of the original feed concentration. For this reason, these fractions are not recorded in the diffusive permeability graphs.

From figure 8 it can be seen that the monodisperse PS permeabilities fit nicely into the polydisperse PS permeabilities. This means that the different fractions in the polydisperse sample do not influence the diffusive permeability of other fractions by blockage or enhanced diffusion, i.e., each molecule diffuses independently from the other for solutions in the dilute concentration regime.

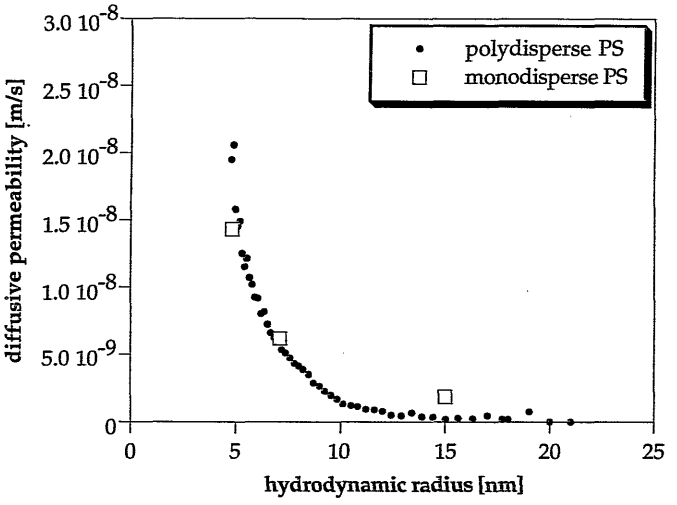


*Figure 8. Diffusive permeability of polydisperse polystyrene as a function of the hydrodynamic radius; the monodisperse values are given as reference.*

The results presented here are in agreement with Guillot's work [38]. Diffusion measurements of a series of monodisperse polymer samples can be approximated by employing a polydisperse polymer, as long as all the separate fractions are below the overlap concentration.

### 6.4.2 Diffusive permeability: suitability as characterization technique for membranes with a pore size distribution

Equations (6.13) already described the dependence of the diffusive permeability on the membrane pore size distribution for each molecular weight of the polymer. The main conclusion of the last section indicates that the diffusive permeabilities of a polymer with a distribution of molecular weights can be determined by only one experiment. This makes diffusive permeability measurements suitable as characterization technique for ultrafiltration membranes.

In case of a molecular weight distribution, equation (6.16) is a summation of n different equations, with n the number of polymer molecular weight fractions. The objective of this characterization technique is to obtain a permeability for polystyrene as a function of the membrane pore radius, $r_p$, which then can be related to the polystyrene hydrodynamic radius, $r_h$. Therefore, the total diffusive permeability integral, equation (6.16), has to be differentiated to $r_h$. The mathematical procedure to solve this integral is described in the appendix to this chapter.

It was already discussed in section 6.2.2 of this chapter that there are two different theories that describe hindered diffusion. $D_p$ may be determined from the porous-body approach, or from the scaling analysis. These theories have in common that $D_p$ is a function of the ratio of the polymer hydrodynamic radius to the membrane pore radius, which means that the diffusive permeability integral function becomes even more complicated.
The diffusive permeability integral cannot be solved analytically, and also a numerical solution was not found. However, if one succeeds in finding a solution for this "ill-posed" mathematical problem (e.g., by making an assumption about the shape of the pore size distribution [45,46]), the diffusive permeability measurements may form a promising ultrafiltration membrane characterization technique, especially for non-aqueous systems where long-range interactions are absent and polymers behave like random coils, so many disturbing effects do not occur. Until then, these measurements are useful to determine a maximum pore radius for a certain membrane and to compare different membranes qualitatively.

A remark has to be made about the effective diffusion times, calculated by Guillot et al. [24]. These values were determined for diffusion through track-etched membrane pores with a length of 10 μm. For asymmetric membranes, the skin thickness is generally only 0.2 μm, so the effective diffusion distance is much smaller here. An effective diffusion time for $\lambda_s = 0.993$ and a pore length of 0.2 μm was calculated at 8 days, while for the system of Guillot et al. the comparable effective diffusion time was about 1 year. One has to realize that the maximum pore radius that can be determined by diffusion experiments, in fact will be slightly too low because the polystyrene chains with a $\lambda_s$ approaching 1 might not have had enough time to diffuse through the membrane skin. Despite this small possible discrepancy, the qualitative comparison of the maximum pore radius for different membranes is still valid.
It has been assumed here that the polymer coil in dilute solution cannot pass pores smaller than the hydrodynamic radius at a reasonable time scale, analogous to the scaling analysis and the porous-body approach. This allows to determine the maximum pore radius, which is shown in the next section for different membranes.

### 6.4.3 Results of measurement of diffusive permeability for different membranes

To verify the dependence of the diffusive permeability on the pore size distribution, various membranes were employed for diffusion experiments of polydisperse PS-solutions. In figure 9 the diffusive permeability curve of a membrane prepared from a 20 wt% polyimide casting solution in DMF and

coagulated in ethanol, is compared with the curve of a membrane from a 25 wt% polyimide casting solution in DMF, that was prepared under equal conditions.

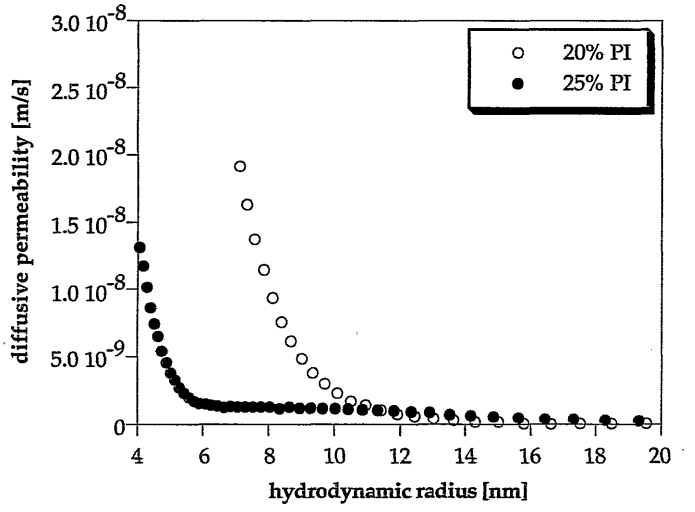


***Figure 9.*** *Diffusive permeability for polyimide membranes, prepared from an initial polyimide concentration in the DMF casting solution of 20% wt and 25 wt%, respectively.*

From this figure it can be seen that the membrane prepared from a casting solution containing 20 wt% PI has a higher diffusive permeability over almost the whole range. The membrane that was prepared from a 25 wt% PI casting solution shows permeability through pores with a radius of about 16 nm. This is probably caused by the presence of pinholes, because it is not expected that there are pores present of 16 nm radius. Therefore, the maximum pore radius for this membrane is estimated to be 6 nm. For the membrane cast from a 20 wt% PI-solution a maximum pore radius of about 14 nm was determined.
Previously, the pure ethanol hydraulic permeabilities of these membranes were determined at 291 kg/m$^2$hr bar for the membranes cast from a 20 wt% PI-solution and 49 kg/m$^2$hr bar for membranes cast from a 25 wt% PI-solution, respectively (see chapters 2 and 4). These results can be explained well by the diffusive permeability results presented in figure 9: the higher permeability of the membrane from a 20 wt% casting solution is caused by the presence of larger pores than in the case of the membrane from a 25 wt% casting solution.
In chapter 5 it was concluded from polystyrene retention measurements that the major part of the pores of these wet membranes are smaller than 7 nm, and this is quite reasonable when considering that the largest pores are 6 and 14 nm, respectively. Permporometry results for these membranes (after a drying procedure!) showed that the maximum pore sizes are about 7 nm and 14 nm for

the membranes prepared from a 25 wt% PI casting solution and prepared from a 20 wt% solution, respectively (see chapter 4). This is in agreement with the diffusive permeability results described in this chapter, which implies that during drying of these membranes the radii of the largest pores will hardly change, and that swelling of the membrane by the wetting liquid has only a minor influence.

Some membranes that were prepared from a casting solution in DMF containing 20 wt% PI and coagulated in ethanol, were dried according to an ethanol-hexane-air displacement sequence. After this drying procedure, they were rewetted and preconditioned in ethyl acetate. The diffusive permeability curves of two of these dried membranes are compared with the diffusive permeability of an untreated wet-state membrane, and the results are given in figure 10.

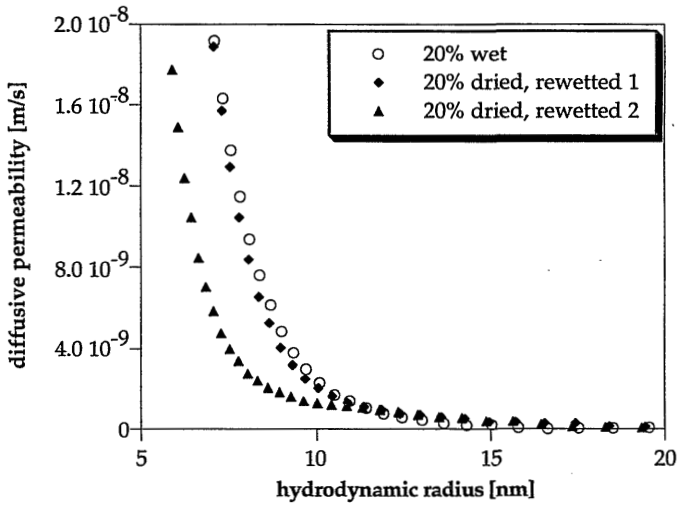


***Figure 10.*** *Diffusive permeability for membranes prepared from a 20 wt% polyimide casting solution and coagulated in ethanol, dependent on the application of a drying-rewetting procedure.*

In contradiction to the results of the wet untreated membranes, the reproducibility of the diffusion measurements for dried-rewetted membranes was rather bad, as can be seen from the different curves in figure 10. One of the membranes shows only a small decrease induced by the drying-rewetting procedure in the number of pores < 10 nm radius, whereas the other one shows a larger decrease in this area.

It was already discussed that the pure ethanol or water permeability of rewetted membranes shows a large variation, as shown in the appendix to chapter 4 and

results by McDonogh et al. [47]. The bad reproducibility in diffusive permeability for dried-rewetted membranes follows this trend.

The diffusive behaviour of membranes prepared from 20 wt% polyimide casting solutions is compared with similar membranes that were prepared from 20 wt% polyimide casting solutions containing 3 wt% oxalic acid (OA) or tartaric acid (TA), and the results are given in figure 11. All membranes were coagulated in ethanol.

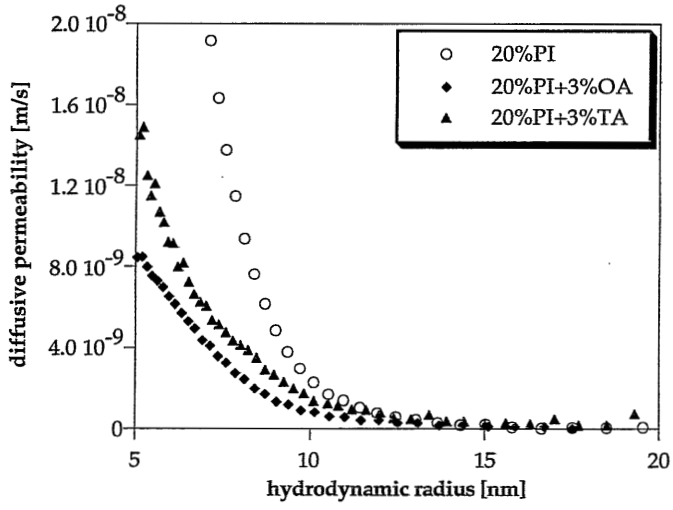


*Figure 11. Diffusive permeability of membranes prepared from casting solutions containing 20 wt% polyimide, with and without addition of 3 wt% oxalic or tartaric acid to the casting solution.*

From figure 11 it can be seen that the additives do not influence the maximum pore radius. The lower permeability at lower PS hydrodynamic radius for the "additive-membranes" indicates that the number of pores in this region is drastically decreased by the addition of OA or TA to the casting solution. The effect of OA is stronger than the effect of TA. These findings are in agreement with the results described in chapter 3. The addition of OA or TA to a 20% polyimide casting solution results in a decline in pure ethanol permeability when compared to membranes casted from solutions without additives. The ethanol permeability decline is stronger for OA than for TA. Furthermore, permporometry results showed that the presence of the additives in the casting solution has only a minor effect on the pore peak maximum, whereas it decreases the number of pores.

## 6.5 Conclusions

The diffusive permeabilities of dilute solutions of monodisperse polystyrene fractions in ethyl acetate, measured for polyimide ultrafiltration membranes, correspond well with the diffusion results for a polydisperse polymer for the same membrane.
The experiments were employed to compare qualitatively the hindered diffusion of polystyrene molecules through polyimide membranes, which were prepared in a different way to obtain various morphologies. The effect of drying and rewetting of the membranes was studied as well. It was shown that the maximum pore radius that was determined by the diffusive permeability measurements, could be related to membrane formation and pretreatment processes. In addition, the results are in qualitative agreement with results obtained by retention and pure ethanol permeability measurements and permporometry.
An attempt was made to calculate membrane pore size distributions from the experimental diffusive permeability curves. Because this is an ill-posed mathematical problem and the description of the diffusion coefficient inside the membrane is not uniform, this was not yet possible. Until these problems are solved, the experimental results can be used to compare maximum pore radii and permeability curves for different membranes.

## 6.6 References

[1] A. Einstein; Investigations on the theory of Brownian movement; R.Furth (Ed), Dover, New York, 1956

[2] E.M. Renkin; Filtration, diffusion and molecular sieving through porous cellulose membranes; J. Gen. Physiol., 38(1954)225

[3] J.R. Pappenheimer, E.M. Renkin, L.M. Borrero; Filtration, diffusion, and molecular sieving through peripheral capillary membranes; Am. J. Physiol., 167(1951)13

[4] J.D. Ferry; Ultrafilter membranes and ultrafiltration; Chem. Rev., 18(3)(1936)373

[5] W.M. Deen; Hindered transport of large molecules in liquid-filled pores; AIChE J., 33(1987)1409

[6] R.E. Baltus, J.L. Anderson; Hindered diffusion of asphaltenes through microporous membranes; Chem. Eng. Sci., 38(1983)1959

[7] M.P. Bohrer, G.D. Patterson, P.J. Carroll; Hindered diffusion of dextran and ficoll in microporous membranes; Macromolecules, 17(1984)1170

[8] W.M. Deen, M.P. Bohrer, N.B. Epstein; Effects of molecular size and configuration on diffusion in microporous membranes; AIChE J., 27(1981)952

[9] R.E. Beck, J.S. Schultz; Hindrance of solute diffusion within membranes as measured with microporous membranes of known pore geometry; Biochim. Biophys. Acta, 255(1972)273

[10] D.M. Malone, J.L. Anderson; Hindered diffusion of particles through small pores; Chem. Eng.

Sci., 33(1978)1429

[11] S. Weinbaum; Strong interaction theory for particle motion through pores and near boundaries in biological flows at low Reynolds number; Lect. Math. Life Sci., 14(1981)119

[12] Y. Pawar, J.L. Anderson; Hindered diffusion in slit pores: an analytical result; Ind. Eng. Chem. Res., 32(1993)743

[13] B.C. Robertson, A.L. Zydney; Hindered protein diffusion in asymmetric ultrafiltration membranes with highly constricted pores; J. Membrane Sci., 49(1990)287

[14] P. Debye and A.M. Bueche; Intrinsic viscosity, diffusion and sedimentation rate of polymers in solution; J. Chem. Phys., 16(1948)573

[15] H.C. Brinkman; A calculation of the viscous force exerted by a flowing fluid on a dense swarm of particles; Appl. Sci. Res., A1(1947)27

[16] M.G. Davidson, W.M. Deen; Hydrodynamic theory for the hindered transport of flexible macromolecules in porous membranes; J. Membrane Sci., 35(1988)167

[17] E.F. Casassa; Equilibrium distribution of flexible polymer chains between a macroscopic solution phase and small voids; J. Polym. Sci., B 5(1967)773

[18] M.G. Davidson, U.W. Suter, W.M. Deen; Equilibrium partitioning of flexible macromolecules between bulk solution and cylindrical pores; Macromolecules, 20(1987)1141

[19] F.W. Wiegel, P.F. Mijnlieff; Intrinsic viscosity and friction coefficient of permeable macromolecules in solution; Physica, 89A(1977)385

[20] P.F. Mijnlieff, F.W. Wiegel; Intrinsic viscosity and friction coefficient of polymer molecules in solution: porous sphere model; J. Polym. Sci., Polym. Phys. Ed., 16(1978)245

[21] M. Daoud, P.G. de Gennes; Statistics of macromolecular solutions trapped in small pores; J. Phys. (Paris), 38(1977)85

[22] P.G. de Gennes; Scaling concepts in polymer physics; Cornell University Press, Ithaca, New York, 1979

[23] D.S. Cannell, F. Rondelez; Diffusion of polystyrenes through microporous membranes; Macromolecules, 13(1980)1599

[24] G. Guillot, L. Leger, F. Rondelez; Diffusion of large flexible polymer chains through model porous membranes; Macromolecules, 18(1985)2531

[25] P.G. de Gennes; Dynamics of entangled polymer solutions. 1. The Rouse model/ 2. Inclusion of hydrodynamic interactions; Macromolecules, 9(1976)587/594

[26] M. Daoud, J.P. Cotton, B. Farnoux, G. Jannink, G. Sarma, H. Benoit, R. Duplessix, C. Picot, P.G. de Gennes; Solutions of flexible polymers. Experiments and interpretation; Macromolecules, 8(1975)804

[27] G. Guillot; Diffusion of polystyrene through model membranes. 1. Diffusion kinetics of monodisperse solutions; Macromolecules, 20(1987)2600

[28] I.A. Kathawalla, J.L. Anderson; Pore size effects on diffusion of polystyrene in dilute solution; Ind. Eng. Chem. Res., 27(1988)866

[29] I.A. Kathawalla, J.L. Anderson, J.S. Lindsey; Hindered diffusion of porphyrins and short-chain polystyrene in small pores; Macromolecules, 22(1989)1215

[30] M.T. Bishop, K.H. Langley, F.E. Karasz; Dynamic light-scattering studies of polymer diffusion in porous materials: linear polystyrene in porous glass; Macromolecules, 22(1989)1220

[31] I. Teraoka, K.H. Langley, F.E. Karasz; Diffusion of polystyrene in controlled pore glasses: transition from the dilute to the semi-dilute regime; Macromolecules, 26(1993)287

[32] M.P. Bohrer, L.J. Fetters, N. Grizzuti, D.S. Pearson, M.V. Tirrell; Restricted diffusion of

linear and star-branched polyisoprenes in porous membranes; Macromolecules, 20(1987)1827
[33] A.J. Müller, J.A. Odell, S. Carrington; Degradation of semidilute polymer solutions in elongational flows; Polymer, 33(1992)2598
[34] T.Q. Nguyen, H.H. Kausch; Chain extension and degradation in convergent flow; Polymer, 33(1992)2611
[35] A. Keller, J.A. Odell; The extensibility of macromolecules in solution; a new focus for macromolecular science; Colloid Polym. Sci., 263(1985)181
[36] K.A. Smith, C.K. Colton, E.W. Merril, L.B. Evans; Convective transport in a batch dialyzer: determination of true membrane permeability from a single measurement; Chem. Eng. Progr. Symp. Ser., no. 84, 64(1968)45
[37] D.M. Malone, J.L. Anderson; Diffusional boundary-layer resistance for membranes with low porosity; AIChEJ, 23(1977)177
[38] G. Guillot; Diffusion of polystyrene through model membranes. 2. Experiments with mixture solutions; Macromolecules, 20(1987)2606
[39] J. Brandrup, E.H. Immergut; Polymer Handbook; 3d edition, Wiley, New York, 1989
[40] M. Doi, S.F. Edwards; The theory of polymer dynamics; Clarendon Press, Oxford, UK, 1986
[41] J. des Cloizeaux, G. Jannink; Polymers in solution: their modelling and structure; Clarendon Press, Oxford, UK, 1990
[42] M. Fukuda, M. Fukutomi, Y. Kato, T. Hashimoto; Solution properties of high molecular weight polystyrene; J. Polym. Sci., Polym. Phys. Ed., 12(1974)871
[43] N. Nemoto, V. Makita, Y. Tsunashima, M. Kurata; Dynamic light scattering studies of polymer solutions. 3. Translational diffusion and internal motion of high molecular weight polystyrenes in benzene at infinite dilution; Macromolecules, 17(1984)425
[44] B.K. Varma, Y. Fujita, M. Takahashi, T. Nose; Hydrodynamic radius and intrinsic viscosity of polystyrene in the crossover region from θ to good-solvent conditions; J. Polym. Sci., Polym. Phys. Ed., 22(1984)1781
[45] E.A. Mason, R.P. Wendt, E.H. Bressler; Similarity relations (dimensional analysis) for membrane transport; J. Membrane Sci., 6(1980)283
[46] J.K. Leypoldt; Determining pore size distributions of ultrafiltration membranes by solute sieving - mathematical limitations; J. Membrane Sci., 31(1987)289
[47] R.M. McDonogh; unpublished results

## 6.7 Appendix: derivation of permeability - concentration relation

For the diffusion cell, a mass balance can be given by:

$$\left(V\frac{dc}{dt}\right)_f = -\left(V\frac{dc}{dt}\right)_d = V_f\left(\frac{dc}{dt}\right)_f = -V_d\left(\frac{dc}{dt}\right)_d = \frac{A}{R_{tot}} * (c_f(t) - c_d(t)) \qquad (A1)$$

since the volumina of the two compartments are constant. The concentrations at the feed and diluate sides are a function of time, t.
Rearrangement of equation (A1) results in:

$$\left(1 + \frac{V_f}{V_d}\right) * \left(\frac{dc}{dt}\right)_f = \frac{d\,(c_f - c_d)}{dt} \qquad \text{(A2)}$$

Combination of equations (A1) and (A2) gives:

$$\frac{d\,(c_f - c_d)}{(c_f - c_d)} = -\left(1 + \frac{V_f}{V_d}\right) * \frac{A}{R_{tot}\,V_f}\,dt \qquad \text{(A3)}$$

The boundary conditions are:

t=0: $c_f\{t\} = c_{fo}$

$c_d\{t\} = c_{do}$

t=t: $c_f\{t\} = c_{ft}$

$c_d\{t\} = c_{dt}$

With these boundary conditions, integration of equation (A3) from time zero to time t results in equation (A4) (which is equal to equation (6.8)):

$$\ln \frac{(c_f - c_d)_o}{(c_f - c_d)_t} = \left(1 + \frac{V_f}{V_d}\right) * \frac{A}{R_{tot}\,V_f}\,t = \frac{A}{R_{tot}}\,t * \left(\frac{1}{V_f} + \frac{1}{V_d}\right) \qquad \text{(A4)}$$

# Appendix to chapter 6

## Derivation of diffusive permeability integral

M.A.M. Beerlage, R.H.B. Bouma, M.H.V. Mulder, C.A. Smolders, H. Strathmann

### 6.A.1 Introduction

In chapter 6 polystyrene diffusion experiments through different polyimide membranes were described. The diffusive permeability was shown to be dependent on the membrane pore size distribution. Therefore, these diffusion experiments might in principle serve as a technique to characterize ultrafiltration membranes. For this purpose, a relation has to be found between the polymer hydrodynamic radius distribution and the membrane pore size distribution, including the theory of hindered diffusion of flexible polymer chains.
The derivation of this relation, which is presented in this appendix, is based on the equations (6.14)-(6.16) from chapter 6; equation (6.16) is the basis of a set of n relations describing the diffusive permeabilities of n different polymer hydrodynamic radii through the accessible pores of the membrane. The derivation presented here processes these n relations into one single integral.

### 6.A.2 Derivation

For one type of polystyrene molecules, i, the diffusive permeability through the pores that are accessible for these molecules, i.e., in the interval $r_h$ to infinity, can be written in the form of an integral:

$$P_{tot,i}(r_h) = \int_{r_h}^{\infty} \frac{\frac{dn}{dr}(r_p)\,\pi r_p^2 * D_p\left(\frac{r_h}{r_p}\right) * D_o(r_h)}{l_{skin}\,D_o(r_h) + 0.5\,\pi\,r_p * D_p\left(\frac{r_h}{r_p}\right)}\,dr_p \qquad (6.A.1)$$

This is a more generalized form of equation (6.16), valid for any molecule i. The bulk diffusion coefficient, $D_o$, is written here as a function of the polymer hydrodynamic radius. Note that the number of pores is written here in the differential form, representing the pore size distribution.
To obtain the dependence of the diffusive permeability on the molecular weight, or better the hydrodynamic radius $r_h$, the integral in equation (6.A.1) is differentiated with respect to $r_h$. For this purpose, Leibniz's theorem for differentiation of an integral is used [1]:

$$\frac{dP_{tot}\{r_h\}}{dr_h} = \int_{r_h}^{\infty} \frac{d}{dr_h}\left[\frac{\frac{dn}{dr}\{r_p\}\,\pi r_p^2 * D_p\left\{\frac{r_h}{r_p}\right\} * D_o\{r_h\}}{l_{skin}\,D_o\{r_h\} + 0.5\,\pi\,r_p * D_p\left\{\frac{r_h}{r_p}\right\}}\right] dr_p$$

$$-\left[\frac{\frac{dn}{dr}\{r_h\}\,\pi\,r_h^2 * D_p\{1\} * D_o\{r_h\}}{l_{skin}\,D_o\{r_h\} + 0.5\,\pi\,r_h * D_p\{1\}}\right] \qquad (6.A.2)$$

Further development of the integral results in:

$$\frac{dP_{tot}\{r_h\}}{dr_h} = \int_{r_h}^{\infty} \frac{\frac{dn}{dr}\{r_p\}\,\pi r_p * \frac{dD_p}{d\left\{\frac{r_h}{r_p}\right\}}\left\{\frac{r_h}{r_p}\right\} * D_o\{r_h\}}{l_{skin}\,D_o\{r_h\} + 0.5\,\pi\,r_p * D_p\left\{\frac{r_h}{r_p}\right\}} dr_p$$

$$+\int_{r_h}^{\infty} \frac{\frac{dn}{dr}\{r_p\}\,\pi r_p^2 * D_p\left\{\frac{r_h}{r_p}\right\} * \frac{dD_o\{r_h\}}{dr_h}}{l_{skin}\,D_o\{r_h\} + 0.5\,\pi\,r_p * D_p\left\{\frac{r_h}{r_p}\right\}} dr_p$$

$$-\int_{r_h}^{\infty} \left[\frac{\frac{dn}{dr}\{r_p\}\,\pi r_p^2 * D_p\left\{\frac{r_h}{r_p}\right\} * D_o\{r_h\}}{\left[l_{skin}\,D_o\{r_h\} + 0.5\,\pi\,r_p * D_p\left\{\frac{r_h}{r_p}\right\}\right]^2} * l_{skin} * \frac{dD_o\{r_h\}}{dr_h}\right] dr_p$$

$$-\int_{r_h}^{\infty}\left[\frac{\frac{dn}{dr}\{r_p\}\,\pi r_p^2 * D_p\left\{\frac{r_h}{r_p}\right\} * D_o\{r_h\}}{\left[l_{skin}\,D_o\{r_h\} + 0.5\,\pi\,r_p * D_p\left\{\frac{r_h}{r_p}\right\}\right]^2} * 0.5\,\pi * \frac{dD_p\left\{\frac{r_h}{r_p}\right\}}{d\left\{\frac{r_h}{r_p}\right\}}\right] dr_p$$

$$-\left[\frac{\frac{dn}{dr}\{r_h\}\,\pi\,r_h^2 * D_p\{1\} * D_o\{r_h\}}{l_{skin}\,D_o\{r_h\} + 0.5\,\pi\,r_h\,D_p\{1\}}\right] \qquad (6.A.3)$$

The combination of these five parts finally gives equation (6.A.4):

$$\frac{dP_{tot}\{r_h\}}{dr_h} = \int_{r_h}^{\infty} \frac{\frac{dn}{dr}\{r_p\}\,\pi r_p * \left[\frac{dD_p\left\{\frac{r_h}{r_p}\right\}}{d\left\{\frac{r_h}{r_p}\right\}} * D_o\{r_h\} + r_p * D_p\left\{\frac{r_h}{r_p}\right\} * \frac{dD_o\{r_h\}}{dr_h}\right]}{l_{skin}\,D_o\{r_h\} + 0.5\,\pi\,r_p * D_p\left\{\frac{r_h}{r_p}\right\}} dr_p$$

$$-\int_{r_h}^{\infty} \frac{\frac{dn}{dr}\{r_p\}\,\pi r_p^2 * D_p\left\{\frac{r_h}{r_p}\right\} * D_o\{r_h\}\left[l_{skin} * \frac{dD_o\{r_h\}}{dr_h} + 0.5\,\pi\,\frac{dD_p\left\{\frac{r_h}{r_p}\right\}}{d\left\{\frac{r_h}{r_p}\right\}}\right]}{\left[l_{skin}\,D_o\{r_h\} + 0.5\,\pi\,r_p * D_p\left\{\frac{r_h}{r_p}\right\}\right]^2} dr_p$$

$$-\left[\frac{\frac{dn}{dr}\{r_h\}\,\pi\,r_h^2 * D_p\{1\} * D_o\{r_h\}}{l_{skin}\,D_o\{r_h\} + 0.5\,\pi\,r_h\,D_p\{1\}}\right] \qquad (6.A.4)$$

In all these equations the effective diffusion coefficient, $D_p$, is not defined further. It is a function of the ratio of the polymer hydrodynamic size to the pore radius. In section 6.2.2 of chapter 6 of this thesis two theories for the description of the effective diffusion coefficient are summarized, the quantitative porous body approach and the qualitative scaling analysis. Both theories describe $D_p$ as an intricate function of the ratio of polymer hydrodynamic radius to the pore radius. The introduction of these $D_p$-functions into the already complicated

integral (6.A.4) results in a relation that cannot be solved analytically; it is doubtful whether it can be solved numerically: we did not yet find a solution for this ill-posed mathematical problem.

## 6.A.3 Reference

[1] M. Abramowitz, I.A. Stegun; Handbook of mathematical functions with formulas, graphs, and mathematical tables; 10th printing, Wiley, New York, 1972; p 11, nr. (3.3.7)

# Chapter 7

## Ultrafiltration of organic paint waste

M.A.M. Beerlage, H.H.M. Rolevink, P. Adamczak*, M.H.V. Mulder, C.A. Smolders, H. Strathmann

**Summary**

Ultrafiltration of an organic paint waste stream has been investigated as an application in non-aqueous solution. For this purpose dilute organic paint was used as a feed solution. The ultrafiltration experiments were performed under cross flow conditions using polyimide membranes. These membranes proved to be very effective, since all pigments and solid particles were retained. To decrease the fouling of the membranes, a high cross flow velocity is required. In addition, less porous membranes are less sensitive to fouling. At higher feed concentrations fouling is less severe, probably because a stable "dynamic membrane" has been formed.
It can be concluded that the concentration polarization layer and fouling deposit layer determine the separation performance, while the membrane has hardly any influence and only serves as a kind of chemically resistant support.

*: Nicolaus Copernicus University, Torun, Poland

## 7.1 Introduction

Today, the pollution of the environment has been recognized as a major problem, and the need to develop new non-polluting technologies is growing very fast. Membrane technology is gaining importance as environmental technology. In many cases membrane processes are good alternatives to conventional separation processes, such as distillation, extraction or adsorption techniques.
Environmental technologies can be classified as cleaning technology or clean technology. Cleaning technology implies that processes are used for cleaning of waste streams or contaminated sites, whereas clean technology involves process integrated technologies to recover valuable products and/or energy, to reduce waste streams, and to avoid emission of polluting compounds to the environment.
An introduction on the use of membrane processes to solve environmental problems is given by Mulder [1]. Examples are the treatment of landfill leachates by reverse osmosis, and the removal of volatile organic compounds from air by vapour permeation. An example of a commercially very successful clean technological process is the recovery of electrocoat paint by ultrafiltration. After electrophoretic deposition of the paint, the surface is rinsed with water generating an aqueous waste stream; this stream is fed to an ultrafiltration module, where a separation is obtained into clean water (permeate) which can be reused, and reusable electrophoretic paint (retentate).

The treatment of the rinsing waste streams resulting from rinsing of tanks and filling lines during manufacture and transport of aqueous latex paints, is also a very promising membrane process. The treatment of similar organic paint waste streams that occur during manufacture and transport of conventional paint based on organic solvents, is more problematic because the membranes and modules have to be chemically stable in the environment of their application.
In this chapter the employment of newly developed polyimide ultrafiltration membranes will be described. They are used to separate an organic paint waste stream into two new product streams, the permeate containing pure solvent and a retentate stream with concentrated paint.

## 7.2 Paint technology

In literature there are a number of textbooks that give information about paint technology [2-4]. Commercially available organic paints are often complex mixtures of many components with different functions. These components can be divided in several classes, as illustrated in figure 1.

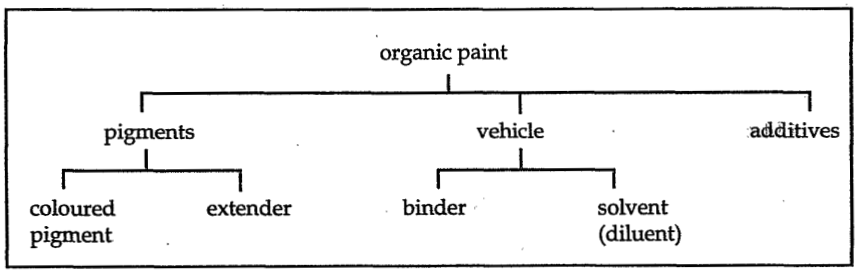


***Figure 1.*** *Classes of components of organic paint.*

*Pigments* are very fine particles that are insoluble in the paint solvent. The main pigments in paints provide the colour and opacity. In addition to this, secondary mostly colourless pigments (*extenders*) may be present to improve adhesion of the film to the substrate or to enlarge the hardness of the film.
The paint *vehicle* is the combination of the binder with the paint solvent; the term "vehicle" is used because the pigments can be dispersed in this mixture. A *binder* is a polymer or mixture of prepolymers which polymerize during the drying process, and is able to form a film that adheres well to the substrate to be painted. The binder also provides the framework that "binds" the different components in the film together and it determines the mechanical and chemical properties of the dried film. There are several different binders, dependent on the type of organic paint. For the traditional oil paints, various unsaturated oils are used, of which linseed oil is the most important one. Cross-linking occurs during film drying by oxidative polymerization at the unsaturated bonds. Examples of synthetic polymers are phenolic resins, polyesters and alkyd resins (oil modified polyester resins), amino resins, fatty acid modified polyamides, epoxy resins, urethane polymers, cellulose esters and ethers, vinyl chloride and vinyl acetate polymers, and acrylic and methacrylic ester polymers.
The *solvent* in the vehicle transforms the binder into a tractable accessible liquid with a low viscosity; in some cases the "solvent" does not dissolve the binder, hence the term "diluent" is more correct [2]. The solvents are generally very volatile aliphatic and aromatic hydrocarbons, such as hexane, xylene, toluene, ethyl acetate, methyl ethyl ketone, etc. When the paint is spread out on a surface, the solvent evaporates. This is a major environmental problem, because the emitted solvents are often toxic.
*Additives* are substances of various kinds, such as catalysts, surfactants, stabilizers, flow agents, plasticizers, drying or wetting agents, emulsifiers, gloss enhancers and many more, which are added in small quantities to modify the properties of the paint.
Commercial paints do not simply consist of one pigment, one binder, one solvent and some additives. The composition is often a combination of several

pigments, extenders, binders, solvents and additives. Because of this complexity it is difficult to determine the influence of one specific component on the filtration process, i.e., on membrane fouling. Another factor is that the combination and concentration of the ingredients determine the specific properties.

Paint technologists were about the first to develop some quantitative theory about polymer solubility. This resulted in the practical use of the Hildebrand solubility parameter [5] by Burrell, who presented lists of solubility parameters for 250 solvents and 30 polymers. He also divided solvents into three classes: poorly, moderately and strongly hydrogen bonded [6]. With this theory some very specific solvent combinations were developed. White spirit is a well known example of such a solvent combination. Later, Hansen improved the solubility parameter concept by the introduction of three-dimensional parameters that represent dispersion, polar, and hydrogen bonding interactions, respectively [7]. Several Hildebrand-parameters and Hansen-3D-parameters have been summarized for a range of components by Barton [8,9].
The best solvents usually contain a large amount of aromatic hydrocarbons, such as xylene; since these aromatics also differ in solubility behaviour, two standard tests were developed: the Kauri-Butanol [10] test and the Aniline Point [11] both give a rough measure of the content of aromatics in the paint solvent.
The solubility parameter approach and the aromatic content tests illustrate the need for a more reliable quantitative theory of polymer solubility; they only give rough estimates, and it shows that paint technology is still an empirical science.

## 7.3 Environmental problems of paints based on organic solvents

Paint solvents evaporate from the drying paint film, resulting in serious air pollution problems and health risks for the painter. For these reasons, paint manufacturers attempt to decrease the aromatic content of the solvent mixture. In addition, environmental regulations for volatile organic compounds (VOC's) will become more severe (e.g., the Dutch program to reduce emission of VOC's: VOC 2000 [12]). There is also a trend towards "new" products: high solid coatings, paints partially based on water as solvent and powder coatings. Despite these new developments, the need for traditional organic paints will remain.
An overview of emitted amounts of VOC's in the Netherlands is given in table 1.

*Table 1.* *Emission of VOC's in the Netherlands.*

| VOC emission | ktons/year | reference (period) |
|---|---|---|
| total [a] | 908 | [13] (1985-1987) |
| from: | 225 | [12] (1985) |
| - industry | | |
| - small companies | | |
| - households [b] | | |
| by professional painters | 32 | [12] (1985) |

a: including emission by incineration

b: excluding emission by traffic and agriculture

Paint production generates a tremendous waste stream as well. The mixing vessels and can filling lines in a paint factory have to be cleaned when different colours and different types of paint are produced or transported. For this cleaning procedure pure paint solvent is used, resulting in a huge waste stream of solvent with all kinds of paint components. This waste stream is usually incinerated.
Techniques to recover the solvent from these waste streams, like solvent extraction and distillation, are economically not feasible and require much energy [14]. Moreover, the remaining non-volatiles and solids (i.e., thermo-setting resins) may cause problems. Membrane technology seems to be a good alternative, provided that the membrane material is chemically resistant to the waste stream components.

In literature there are not many references about ultrafiltration of organic paint waste. Nitto has developed a polyimide membrane (NTU 4200 series) for non-aqueous ultrafiltration applications. These membranes are available in a tubular configuration, and according to the supplier they have a molecular weight cut-off (MWCO) of 8,000 or 20,000 g/mol and a pure toluene permeability of 45 or 100 l/m$^2$hr bar, respectively [15]. There is no information available about the pore size distributions of these membranes, but the pure toluene permeabilities are rather low when compared to the membranes developed in this project (see chapter 2).
Isooka et al. [16] used a Nitto MWCO 8,000 membrane for the treatment of a paint solvent waste stream at 3.5 bar and 25°C with 18% non-volatile parts. They found that the flux through the membrane, and hence fouling of the membranes, is strongly dependent on the feed flow rate. It was concluded from a cost analysis that ultrafiltration is economically a very promising technique for paint solvent recovery. However, no specific information was given about the feed system: the solvents, pigments, binders, and concentration factor. This makes a comparison with our results very difficult.

Ultrafiltration membranes are expected to retain the pigments and binders, as well as the larger additives (polymers in solution and solid particles), while the solvent and the smaller additives pass through the membrane. The ultrafiltration process turns the waste stream into two product streams. The permeate, i.e., the purified solvent, can be reused to rinse the tanks, mixing vessels and filling lines or even serve as new paint solvent, while the concentrate might be used as rough basis for a primer, eventually after addition of some extra components. The process is schematically represented by figure 2.

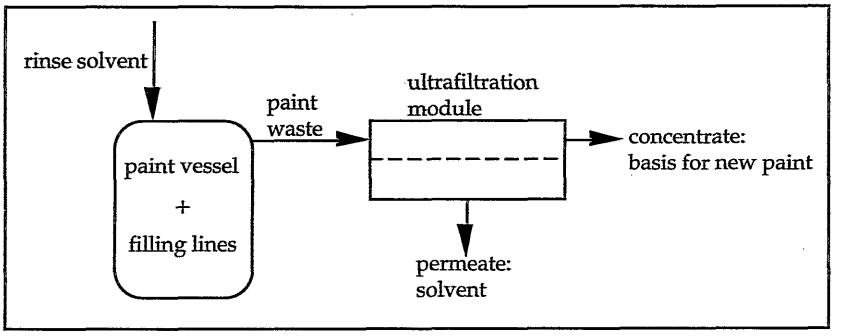


*Figure 2. Schematic drawing depicting the use of ultrafiltration for the treatment of paint waste.*

At Tollens Coatings BV at Breda, the Netherlands, a research program has been started to investigate the application of ultrafiltration to treat latex paint waste based on water [17,18]. For this purpose, a commercial ultrafiltration system with capillary modules has been used. The permeate was recovered and reused as paint solvent. The retentate caused some conservation problems, because it contained a high amount of bacteria and fungi. For paint based on organic solvents no such problem is expected.

## 7.4 Concentration polarization and membrane fouling

During an ultrafiltration application, the actual permeate flux is generally much lower than the pure solvent flux; moreover, the flux is often decreasing with time. This flux decline can be very severe, and is caused by concentration polarization and fouling.
Concentration polarization occurs when solutes are retained totally or partially by the membrane, and accumulate at the membrane surface. The accumulation leads to backdiffusion of the solutes to the bulk, because of the concentration gradient. Based on the film model under steady-state conditions and at low concentrations, the solute convective flow towards the membrane and the solute

backdiffusion equals the solute permeate flow [19]:

$$J\,c + D\frac{dc}{dx} = J\,c_p \qquad (7.1)$$

Here, J is the permeate flux [m/s], D is the solute diffusion coefficient [$m^2/s$], $c_p$ is the solute concentration in the permeate and c is the concentration [$kg/m^3$] of the solute in the concentration polarization boundary layer, while dc/dx is the concentration gradient in this layer [$kg/m^4$]. The boundary condition for c at the membrane surface (x=0) is: $c=c_m$, while at the bulk side (x=δ): $c=c_b$. Integration of equation (7.1) results in:

$$\frac{c_m - c_p}{c_b - c_p} = \exp\left(\frac{J\,\delta}{D}\right) = \exp\left(\frac{J}{k}\right) \qquad (7.2)$$

where δ is the laminary boundary layer thickness [m], and $c_m$ and $c_b$ are the solute concentrations at the membrane surface and in the bulk, respectively [$kg/m^3$]. The term D/δ represents k, the mass transfer coefficient [m/s], which is determined by the hydrodynamics of the system and which is an important parameter to reduce concentration polarization, as can be seen from figure 3. Here, the flux is schematically given as a function of the transmembrane pressure. During ultrafiltration of a solution, the flux becomes independent of pressure, and reaches a limiting flux, $J_\infty$, which decreases with increasing feed (bulk) concentration and/or decreasing mass transfer coefficient.

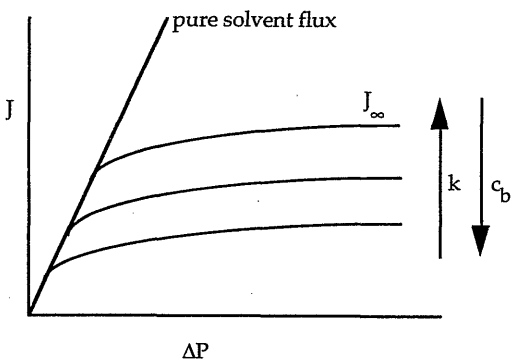


*Figure 3. Schematic illustration of the typical flux vs. pressure behaviour during ultrafiltration: limiting flux of a solution as a function of feed concentration and mass transfer coefficient.*

In general, the feed concentration is not a variable for a practical application, therefore, to reduce concentration polarization, k should be as high as possible. This can be achieved in several ways [19]. Very often the feed flow velocity, v, is

increased for this purpose.
There are several quantitative models that describe the concentration polarization, such as the gel layer model [20], the osmotic pressure model [21], and the boundary layer resistance model [22].
The flux reaches a constant value in time when steady-state conditions are reached. Concentration polarization is always reversible.

However, during most ultrafiltration applications the flux decreases continuously to very low values and a stable flux is not reached. This drastic flux decline is caused by membrane fouling. Fouling can be reversible or irreversible. During fouling, solutes can adsorb at the membrane surface or inside the pores, and eventually plug the pores. Moreover, often a cake layer has been formed, and the summation of all the hydrodynamic resistances explains the very strong flux decline:

$$J = \frac{\Delta P}{\eta R_{tot}} \qquad (7.3)$$

Here, J is the permeate flux [m/s], $\Delta P$ is the transmembrane pressure [Pa], $\eta$ is the liquid viscosity [Pa s] and $R_{tot}$ is the sum of the hydrodynamic resistances [/m].
It is very difficult to theoretically describe fouling processes, because fouling is very system-specific and also dependent on the process conditions. In practice, some fouling tests have been used, mostly based on cake filtration, and this approach can be applied generally.
The cake filtration theory is based on the assumption that a fouling layer is formed. The thickness of this layer, with a constant concentration, increases with increasing permeate volume and is independent of the applied pressure. The presence of the cake layer implies an extra hydrodynamic resistance to the flux superimposed on the membrane resistance:

$$J = \frac{\Delta P}{\eta (R_m + R_c)} \qquad (7.4)$$

Here, $R_m$ and $R_c$ are the hydrodynamic resistances caused by the membrane and the cake layer, respectively [/m].
It is assumed that the specific resistance is constant over the thickness of the cake. The cake resistance is then given as:

$$R_c = r_c l_c \qquad (7.5)$$

Here, $l_c$ is the thickness of the cake layer [m] and $r_c$ is the specific resistance [/m$^2$].
When the retention R=1, the reciprocal flux can be written as [23]:

$$\frac{1}{J} = \frac{1}{J_o} + \frac{\eta\, c_b\, r_c}{c_c\, \Delta P} * \frac{V_p}{A} \qquad (7.6)$$

where $J_o$ is the pure liquid flux [m/s], $\eta$ is the liquid viscosity [Pa s], $c_c$ is the concentration of the cake layer [kg/m$^3$], $c_b$ is the feed bulk concentration [kg/m$^3$], $\Delta P$ is the transmembrane pressure [Pa], $V_p$ is the permeate volume [m$^3$] and A is the membrane area [m$^2$].
If $\eta$, $\Delta P$, $c_b$, $r_c$, and $c_c$ are constants, a plot of $1/J$ as a function of $V_p/A$ gives a straight line, which is an indication of cake filtration. With $J = 1/A*dV/dt$, a relationship of $V_p \sim t^{0.5}$ and $J \sim t^{-0.5}$ can be derived [24,25].

Cake filtration is a very simple fouling model. Several other models have been proposed, based on (semi)empirical or fundamental basis. Reviews on fouling models can be found in literature [26-29].

## 7.5 Experimental

### 7.5.1 Membranes

Ultrafiltration tests were performed on flat sheet polyimide (PI) membranes, made from casting solutions containing 16, 18, 20 or 25 wt% polyimide P84 in DMF and subsequently immersed in an ethanol coagulation bath; details on the preparation conditions can be found in chapters 2 and 5.
The membranes were stored in ethanol after preparation. Prior to the ultrafiltration experiments, the membranes were preconditioned in "white spirit 15%" (i.e., a commercial solvent) for at least two days. White spirit is a mixture of aliphatic and aromatic hydrocarbons (17% aromatics), with a boiling point range of 160-192 °C. Some membrane samples were stored in white spirit in small sealed containers; after one year no visual changes could be observed.
The pure ethanol fluxes have been determined for these membranes (see chapters 2 and 4). The flux of white spirit has been estimated, based on a white spirit viscosity of $1.5*10^{-3}$ Pa s (assumption), according to:

$$J_{\text{white spirit}} = \frac{\eta_{\text{ethanol}}}{\eta_{\text{white spirit}}} * J_{\text{ethanol}} = \frac{1.08}{1.5} * J_{\text{ethanol}}$$

The pressure normalized flux of ethanol and white spirit are summarized in table 2.

*Table 2.* *Pressure normalized flux of ethanol (measured) and white spirit (estimated).*

| membrane | $J_{ethanol}$ [kg/m$^2$ hr bar] | $J_{white\ spirit}$ [kg/m$^2$ hr bar] |
|---|---|---|
| PI-16 (16 wt% PI) | 924 | 665 |
| PI-18 (18 wt% PI) | 526 | 379 |
| PI-20 (20 wt% PI) | 285 | 205 |
| PI-25 (25 wt% PI) | 49 | 35 |

### 7.5.2 Model feed solutions for organic paint waste

The red toluidine pigment ($M_w$ = 307 g/mol) was expected to be one of the most difficult components to retain from paint waste by ultrafiltration [30]. On the other hand, white titanium dioxides are about 0.2 µm in size, and they will be retained completely by ultrafiltration membranes in all cases.
A paint waste stream was simulated by dilution of a commercially available red paint, Rotoll Red RN, to 5 or 1 weight % in the paint solvent white spirit 15%. The paints were kindly supplied by Tollens Coatings BV, Breda, the Netherlands. The compositions of the original paints are summarized in table 3.

*Table 3.* *Composition of undiluted paints.*

| properties | red paint | white paint |
|---|---|---|
| binding resins | 56.1 wt% | 42.2 wt% |
| pigments | 14.0 wt% | 33.1 wt% |
| solvents | 29.9 wt% | 24.5 wt% |

The binders in these paints are alkyd resins. The molecular weights of these resins are unknown, but according to Turner [4], typical molecular weights of the order of 1000-5000 g/mol may be expected. The radius of the binder molecules in solution is about 0.5-1 nm. The solutes that are present in the diluted paint probably consist of small clusters of pigments surrounded by one or more binder molecules. The solute radius will then be somewhat larger than the radius of one binder molecule.

### 7.5.3 Ultrafiltration experiments

The ultrafiltration experiments were performed on a cross flow filtration set-up

from SEMPAS Membrantechnik GmbH, Horb am Neckar, Germany. All parts in this set-up are made of stainless steel or Teflon which allows to employ organic solvents. A schematic representation is shown in figure 4.

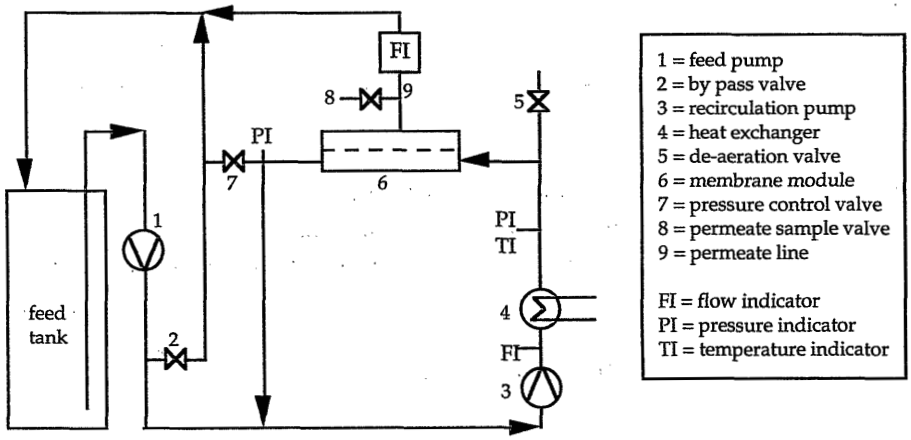


*Figure 4. Cross flow ultrafiltration set-up*

The effective membrane area is 84 $cm^2$. The cross flow velocity and the feed pressure can be adjusted independently. The feed temperature is controlled by water cooling and kept between 18-25°C. The transmembrane pressure was kept constant at 4 bar, by regulation of the feed pump, the bypass and the pressure regulating valves. The permeate stream was fed back to the feed tank. The cumulative volume of the permeate samples was always much lower than 0.1 % of the feed solution volume, so changes in feed concentration were negligible. A part of the measurements was performed using the flow meter (see figure 4 between the circulation pump 3 and the heat exchanger 4); this flow meter did not function anymore after some experiments, and the measurements were continued using the value of the gear speed of the circulation pump 3 as a measure of the cross flow velocity.
The permeate samples were analysed with a Philips PU UV/Vis scanning spectrophotometer.

Some assumptions have to be made for the mass transfer calculations. The solvent viscosity is estimated at $1.5*10^{-3}$ Pa s (the value for turpentines), and the solvent density at $0.78*10^3$ $kg/m^3$. The diffusion coefficient of a particle with a Stokes-Einstein radius of 0.5-1 nm is $D = 4.4*10^{-10}$ $m^2/s$. The Schmidt number is then: $Sc=\eta/\rho D=4370$.
The hydraulic diameter of the module calculated for a rectangular pipe: $d_h=(2*width*height)/(width+height)=17.2*10^{-3}$ m.
Reynolds numbers (Re) are calculated for the different cross flow velocities v

according to:

$$Re = \frac{\rho \, v \, d_h}{\eta} \qquad (7.7)$$

where v [m/s] is calculated by multiplying $\Phi_v$ (i.e., the volumetric cross flow [l/min]) by $1/(6*10^4 \, A_{cf})$, where $A_{cf}$ is the module cross sectional area, with $A_{cf} = 0.62*10^{-3}$ m$^2$.

The entrance length of a module is defined as $L' = 0.029*Re*d_h$ [31]; the module length L (0.201 m) is in all experimental cases smaller than L'.
According to Wiley et al. [31], the Sherwood number Sh can be calculated, depending on the flow regime:

for laminar flow (Grober equation, L<L'):

$$Sh_L = 0.664 \, Re^{0.5} \, Sc^{0.33} \left(\frac{d_h}{L}\right)^{0.5} \qquad (7.8)$$

for turbulent flow (Harriot-Hamilton equation, Sc>1000):

$$Sh_T = 0.0096 \, Re^{0.91} \, Sc^{0.35} \qquad (7.9)$$

The mass transfer coefficient k can be calculated from the Sherwood numbers according to:

$$Sh = \frac{k \, d_h}{D} \qquad (7.10)$$

The results for different cross flow velocities are summarized in table 4.

***Table 4.*** *Mass transfer conditions as a function of cross flow velocity.*

| $\Phi_v$ [l/min] | v [m/s] | Re [-] | $Sh_L$ [-] | $Sh_T$ [-] | $k_L$ [m/s] | $k_T$ [m/s] |
|---|---|---|---|---|---|---|
| 2.0 | 0.05 | 481 | 67 | | $1.7*10^{-6}$ | |
| 4.0 | 0.11 | 962 | 95 | | $2.4*10^{-6}$ | |
| 6.0 | 0.16 | 1449 | 116 | | $3.0*10^{-6}$ | |
| 8.0 | 0.22 | 1931 | 135 | 176 | $3.5*10^{-6}$ | $4.5*10^{-6}$ |
| 10.0 | 0.27 | 2415 | | 216 | | $5.5*10^{-6}$ |
| 12.0 | 0.32 | 2898 | | 255 | | $6.5*10^{-6}$ |

For the cross flow velocity of 0.22 m/s, the flow regime is in between the laminar and the turbulent regime; therefore, in this case two mass transfer coefficients have been calculated.

## 7.6 Results and discussion

The influence of the cross flow velocity on the permeate flux for the PI-20 and PI-25 membranes is shown in figures 5 and 6. The feed was 5% red paint, and the temperature was 20°C. In both figures two curves are given: one for a stepwise increase of the velocity and one for a stepwise decrease of the velocity. The cross flow velocity can be varied to a desired value by adjustment of the gear speed of the circulation pump and can be determined by the flow meter.

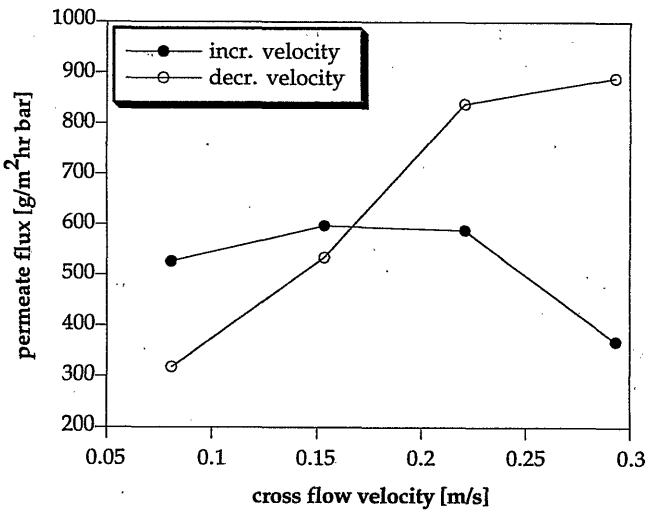


*Figure 5. Influence of a stepwise increasing and decreasing cross flow velocity on the permeate flux of PI-20 membranes.*

From both figures it is obvious that with an increase in velocity the permeate flux remains low and almost independent of the velocity. On the other hand, when the cross flow velocity has been decreased stepwise, the permeate flux is strongly dependent on the cross flow velocity. At higher velocities, the "starting flux" of the decreasing velocity curve is much higher than the "end flux" of the increasing velocity curve.

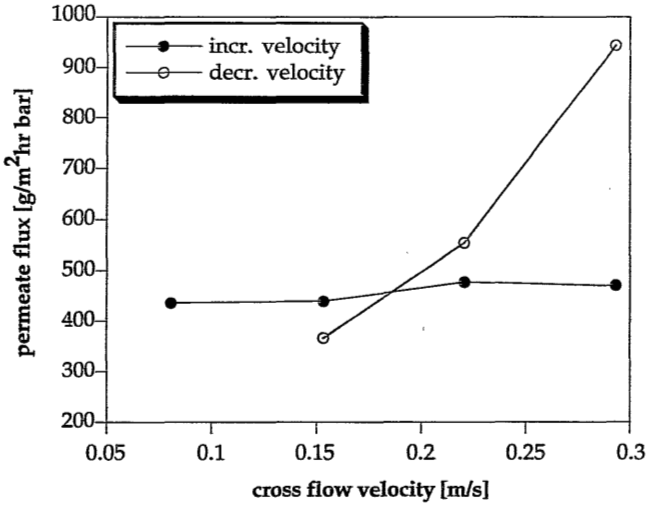


***Figure 6.*** *Influence of a stepwise increasing and decreasing cross flow velocity on the permeate flux of PI-25 membranes.*

These results can be explained by considering the effects of concentration polarization and fouling. Starting at a high velocity, concentration polarization and fouling are less severe. When the velocity is decreased, these effects become more severe. Starting at low velocity, the permeate flux is very low. When the velocity during this measurement is increased, the permeate flux stays constant at this low level, while polarization should be less. Probably, at low cross flow velocities irreversible fouling is very important: the paint binder polymers might form a gel layer, or might partially enter the porous substructure and thereby plug the pores. The additional hydrodynamic resistance in this case cannot be removed by increasing the cross flow velocity: an increase in k of a factor 4 (see table 4) does not increase the limiting flux (see figure 3). This indicates the existence of a kind of cake layer which has been formed at the membrane surface. In addition, the observed fluxes are less than 1% of the pure solvent flux, in the case of a PI-20 membrane (compare figure 5 and table 2).

The permeate fluxes at high cross flow velocity are about the same for PI-20 and PI-25 membranes, despite their large difference in clean solvent fluxes. This result shows as well that fouling determines almost the entire flux, while the original membrane characteristics become relatively unimportant. The system can be considered as a dynamic membrane, where the fouling layer is the actual separating layer and the membrane itself serves only as a support for this secondary layer.
From the experiments, it seems that the PI-20 membranes are more sensitive to fouling than the PI-25 membranes. The pore size distributions of these

membranes are different; from permporometry measurements (see chapter 4) and hindered diffusion measurements (see chapter 6), it appeared that the PI-20 membranes have more large pores than PI-25 membranes. This indicates that the membrane resistance is negligible when compared to the resistance of the cake layer.

In some experiments the pressure was raised to 6 bar, but this did not result in a flux increase. This gives additional support to the importance of the fouling process.
Between two measurements at different velocities a stabilization time was used of at least one hour. The permeate fluxes were constant after 15 to 20 minutes and additional tests showed that fluxes were still constant after two to three hours, for these particular membranes.

For PI-18 and PI-16 membranes only the cross flow velocity was varied. Since the flow meter did not give reliable values anymore, the velocities were compared through the gear speed of the circulation pump. These values are given on a scale from 0 - 100%; for the measurements values of 60, 45 and 30% were used. No exact values are obtained and the numerical results cannot be compared with the results described in figures 5 and 6.

The permeate flux of a 5% red paint solution is plotted as a function of time for various gear speeds of the circulation pump, using PI-18 and PI-16 membranes, respectively (see figures 7 and 8). Note that the cross flow velocity has been changed stepwise.
The flux curve for the PI-18 membrane also shows a stepwise behaviour: a lowering of the cross flow velocity results in a flux decline. After 6 hours the gear speed was increased to the initial level, but the flux declined further, which indicates that a stable cake has been formed. Moreover, it shows an irreversible fouling as well.
The flux curve for the PI-16 membrane did never reach a stable value. Probably fouling is already very severe at a high gear speed. The flux value of the PI-16 membrane is even lower than of the PI-18 membrane at the end of the experiments.
It seems that at the same feed concentration and cross flow velocity the more open membranes are more sensitive to fouling. Although the pure solvent permeability differs about 20 times, the end flux for the various membranes is almost the same. It is expected that PI-16 membranes contain even more large pores than PI-18 membranes, but these will be plugged completely.
The results described by van Kooij for the same feed systems, showed similar values for the end flux [17]. A more detailed comparison is difficult to make, since the membrane module configuration is different (spiral wound), and the

preparation conditions of the polyimide membranes were not given.

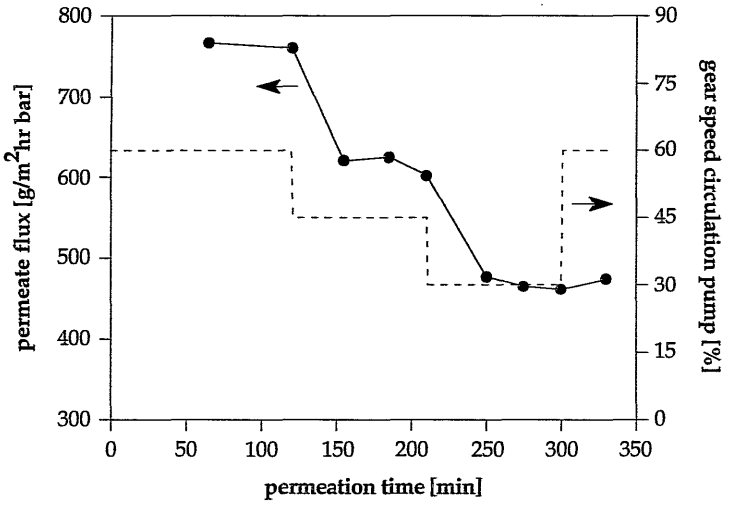


*Figure 7. Permeate flux of a 5% red paint solution as a function of time for various gear speeds measured with a PI-18 membrane.*

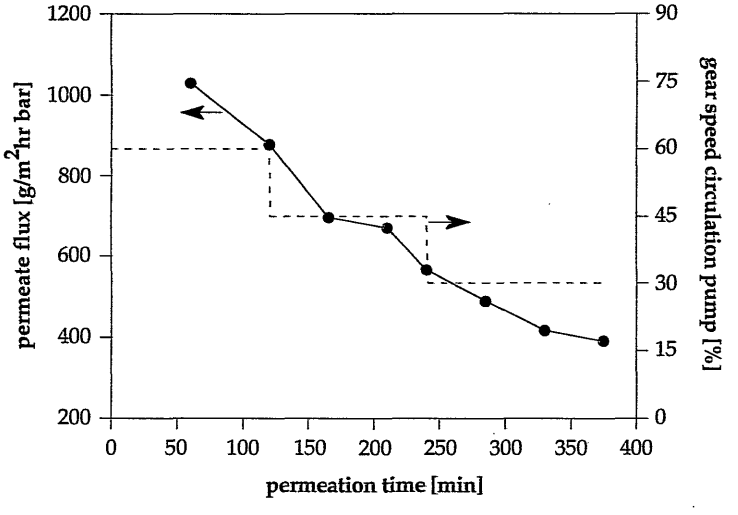


*Figure 8. Permeate flux of a 5% red paint solution as a function of time for various gear speeds measured with a PI-16 membrane.*

Experiments were also performed at paint feed concentrations of 1% for PI-18 and PI-20 membranes. The results are given in figures 9 and 10.

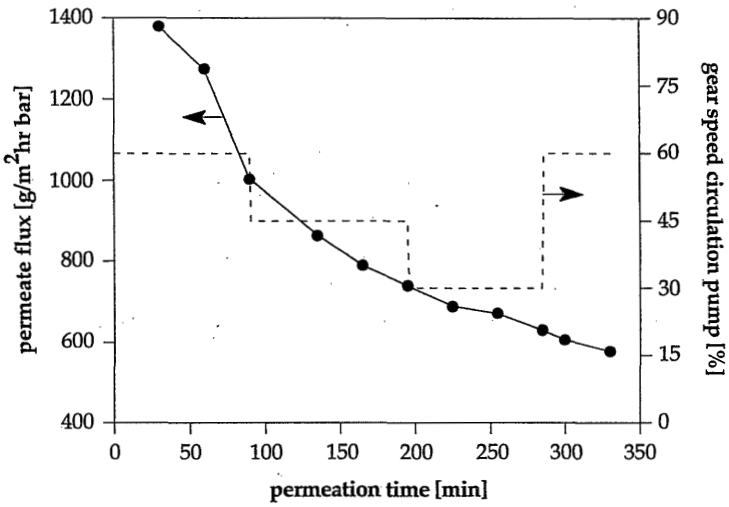


*Figure 9.* *Permeate flux of a 1% red paint solution as a function of time for various gear speeds measured with a PI-18 membrane.*

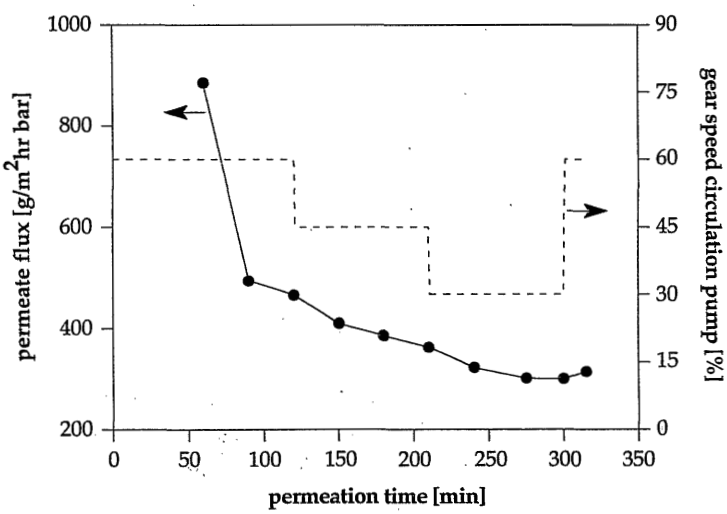


*Figure 10.* *Permeate flux of a 1% red paint solution as a function of time for various gear speeds measured with a PI-20 membrane.*

Comparison of figures 7 and 9 shows a clear difference. At a low feed concentration (1%) no stable permeate fluxes could be obtained during the measurement. The form of the flux curve in figure 9 is determined by a further increase in fouling of the membranes and is comparable to figure 7 (5% feed and PI-16 membrane).

For the filtration of a 1%-solution with a PI-20 membrane, the same behaviour was found: the flux never became constant, while in the case of 5%-solutions the flux was constant after 15 or 20 minutes.

When cake filtration occurs, the permeate flux must be dependent on time according to $J \sim t^{-0.5}$ (see theory). The results presented in figures 8, 9, and 10 are an indication of this dependency; these results have been replotted according to equation (7.6), and the reciprocal flux is given as a function of the permeate volume divided by the membrane area, $V_p/A$ (see figure 11). In this way it is possible to determine whether the fouling behaviour can be described as cake filtration.

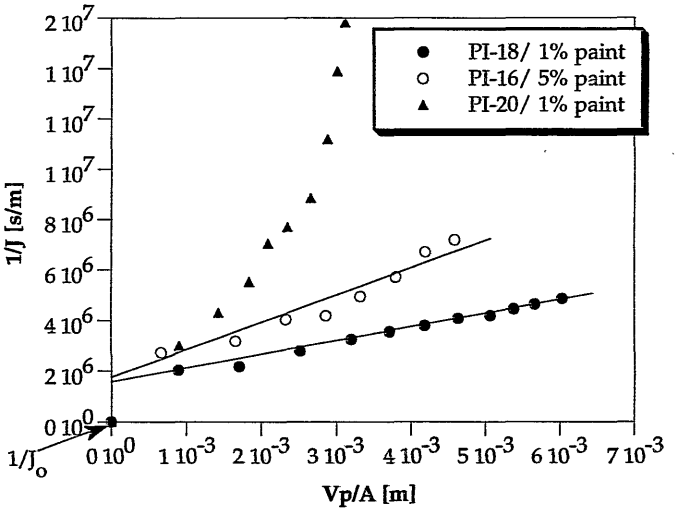


*Figure 11. Reciprocal flux as a function of the permeate volume.*

The results indicate that the fouling behaviour of both the PI-18 membrane/1%-feed and the PI-16 membrane/5%-feed can be described reasonably well by cake filtration. An increase in cross flow velocity has no effect on the fouling layer.
It is obvious from figure 11 that an extrapolation of the results for PI-16 and PI-18 to $V_p/A=0$ results in a significantly higher value than the reciprocal of the pure solvent flux ($1/J_o$). This means that the resistance to permeation is not only the result of the cake layer, but that additional fouling takes place due to solute adsorption (pore narrowing) and pore plugging. Probably, this process of adsorption/plugging occurs immediately at the start of the experiments, before the cake layer is formed. In addition, the cake layer in the case of PI-16 has a higher resistance than in the case of PI-18, due to the higher feed concentration.
The PI-20 membrane/1%-feed shows some irreversible effects, for which we have no explanation yet. The results for the PI-18 membrane/5%-feed deviate

strongly from cake filtration behaviour (results are not given in figure 11). For the latter two cases additional experiments are necessary to investigate the fouling behaviour.

The 1% and 5% feed solutions remain red and opaque, whereas during the experiments the permeate was light-orange, very clear and looked very much the same in all cases, independent of type of membrane and feed concentration.
An attempt was made to estimate a "retention" for the components in the feed. For this purpose the feed solution was diluted to determine a calibration curve for UV/Vis spectrophotometry. However, at a 1/1000 dilution the feed was still red and opaque and very different from the actual permeate samples. Also the UV/Vis scans showed another spectrum and it was concluded that a retention value is meaningless, because of the different compositions between permeate and diluted samples of the feed.
Anyway, the very small red pigments, responsible for the red colour, clearly are retained to a large extent by all membranes. This can also only be explained by the formation of a fouling layer at the membrane surface or within the pores: the binder polymers bind the pigments very effectively and are retained by the membrane. No affine deformation takes place (see chapter 5), because the permeate flow is hindered by the fouling layer, and the feed or better the surface concentration is far too high. The pigments are tightly bound to the binders and are not able to diffuse through this network.
An additional experiment has been carried out for a 5 wt% white paint solution in white spirit through a PI-20 membrane, using a stirred dead-end filtration set-up. As expected, the permeate was completely clear and colourless: all the pigments are completely retained by the membrane.

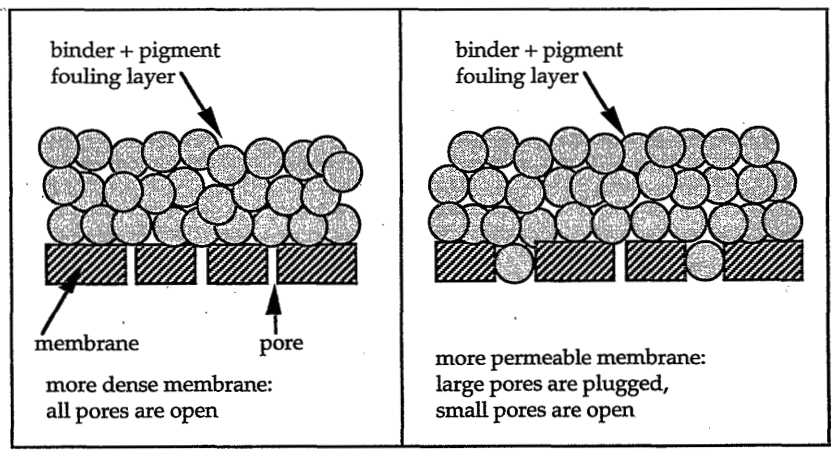


*Figure 12. Schematic representation of fouling during ultrafiltration of diluted paint, for different membranes.*

If a layer is formed at the membrane surface, the transmembrane flux will exclusively be determined by the transport of solutes from the layer into the bulk solution, independent of the pore size and pore size distribution of the membrane. With more open membranes, the permeate samples look similar to the permeate of the more dense membranes. In the former probably all larger pores are plugged by the solutes. A schematic representation of this situation is shown in figure 12.

The effect of the feed concentration is not clear. For the filtration of 5%-feed solutions through PI-18 and PI-20 membranes, the flux stabilized within a very short time (half an hour), whereas for the combinations of PI-16 membrane/5% feed, PI-18 membrane/1% feed, and PI-20 membrane/1% feed, the flux continuously decreased. It may be possible that the combination of a dense membrane with a high feed concentration reduces the number of pores plugged or delays this process, because the layer at the membrane surface is formed almost instantaneously so that the solute drag into the pores is hardly possible. Further research is necessary to test this hypothesis.

The paint waste ultrafiltration experiments that were performed by Isooka et al. [16] were done by using a feed stream containing 18% solids. Our 5 wt% diluted paint effectively contains only 3.5 wt% solids (see table 3), which is much lower in concentration. Isooka et al. used tight membranes, which give better flux results, as can be concluded from our work. In their case, membrane fouling is also severe. It is obvious that for these systems fouling cannot be avoided, since the function of the binder polymers in paint is to initiate and enhance the film formation properties, which promotes the formation of a stable fouling (cake) layer.

## 7.7 Final remarks and conclusions

The results described in this chapter illustrate well the suitability of polyimide membranes for ultrafiltration of non-aqueous organic paint waste. Even the diluted red paint, which was expected to be the most difficult component, could be retained quite effectively by ultrafiltration. For comparison, a 5% white paint (Rotoll White by Tollens) was filtrated as well through a PI-20 membrane. In this case the permeate was completely clear and colourless.
If the feed concentration is too low, then the membranes are severely fouled and the permeate flow is very low and declines relatively fast. At higher concentrations, the binder polymers can form a stable cake or gel layer at the membrane surface, which can be considered as a dynamic membrane. A high cross flow velocity from the start is beneficial, because at lower velocities the

membranes are fouled more severely and irreversibly.
It is also shown that at constant feed concentration the more dense membranes give better results; since they are less sensitive to fouling inside the membrane pores and give more stable permeate fluxes, which are higher than those of the more open membranes. Nevertheless, it is obvious that in all cases the membrane performance is completely determined by fouling.
More future research is necessary to study the long-term behaviour of these ultrafiltration systems under the desired conditions.

## 7.8 References


[1] M.H.V. Mulder; The use of membrane processes in environmental problems - an introduction; J. Crespi, K. Böddeker (Eds.); Membrane processes and separation and purification; Kluwer, Dordrecht, in press

[2] Z.W. Wicks, F.N. Jones, S.P. Pappas; Organic coatings science and technology, vol. 1; Wiley, New York, 1992

[3] P. Nylén, E. Sunderland; Modern surface coatings; Wiley, London, 1965

[4] G.P.A. Turner; Introduction to paint chemistry; Chapman and Hall, London, 1990

[5] J. Hildebrand, R. Scott; The solubility of non-electrolytes; Reinhold Publ. Corp., New York, 1949

[6] H. Burrell; Solubility parameters; Interchem. Rev., 14(1955)3,31

[7] C.M. Hansen; The three-dimensional solubility parameter - key to paint-component affinities: 1. solvents, plasticizers, polymers, and resins; J. Paint Technol., 39(1967)104

[8] A.F.M. Barton; Handbook of solubility parameters and other cohesion parameters; 2nd edition, CRC Press, Boca Raton, 1991

[9] A.F.M. Barton; Handbook of polymer-liquid interaction parameters and solubility parameters; CRC Press, Boca Raton, 1990

[10] American Society for Testing and Materials; test D 1131-61

[11] American Society for Testing and Materials; test D 1012-60T

[12] Projektgroep Koolwaterstoffen 2000; Bestrijdingsstrategie voor de emissies van vluchtige organische stoffen; Dutch Ministry of Environment (VROM), february 1989; p A22, p B9

[13] C.W.A. Evers, C.A. van Mameren; Industriële emissies in Nederland. Derde inventarisatieronde 1985 t/m 1987; Proces Technologie, march 1992, 40

[14] I. Smallwood; Solvent recovery handbook; Edward Arnold, London, 1993; p. 133

[15] Nitto Electric Industrials Co.; Nitto membrane modules and systems, general catalogue; technical brochure, 1985

[16] Y. Isooka, Y. Imamura, Y. Sakamoto; Recovery and reuse of organic solvent solutions; Metal Finishing, 82(1984)113

[17] E. van Kooij; Hergebruik van spoelvloeistof door middel van membraantechnologie met nullozing als doel; Novem-report, projectnr. 51310/0910, 1993

[18] E. van Kooij; Recovery of rinse solvent in the paint industry; lecture presented at NPT/NMG symposium on membranes; Utrecht, the Netherlands, december 1992

[19] M.H.V. Mulder; Basic principles of membrane technology; Kluwer, Dordrecht, 1991

[20] W.F. Blatt, A. Dravid, A.S. Michales, L. Nelsen; Solute polarization and cake formation in

membrane ultrafiltration: causes, consequences, and control techniques; J.E. Flinn (Ed.); Membrane Science and Technology; Plenum Press, New York, 1970, 47

[21] G. Jonsson; Boundary layer phenomena during ultrafiltration of dextran and whey protein solutions; Desalination, 51(1984)61

[22] J.G. Wijmans, S. Nakao, J.W.A. van den Berg, F.R. Troelstra, C.A. Smolders; Hydrodynamic resistance of concentration polarization boundary layers in ultrafiltration; J. Membrane Sci., 22(1985)117

[23] G.B. van den Berg, C.A. Smolders; Flux decline in membrane processes; Filtration and Separation, march/april (1988)115

[24] V.L. Vilker, C.K. Colton, K.A. Smith; Concentration poraization in protein ultrafiltration. Part 2. Theoretical and experimental study of albumin ultrafiltered in an unstirred cell; AIChE J., 27(4)(1981)637

[25] D.R. Trettin, M.R. Doshi; Ultrafiltration in an unstirred batch cell; Ind. Eng. Chem. Fundam., 19(1980)189

[26] E. Matthiasson, B. Sivik; Concentration polarization and fouling; Desalination, 35(1980)59

[27] A.G. Fane, C.J.D. Fell; A review of fouling and fouling control in ultrafiltration; Desalination, 62(1987)117

[28] A.G. Fane; Ultrafiltration: factors influencing flux and rejection; R.J. Wakeman (Ed.); Progress in filtration and separation,4; Elsevier, Amsterdam, 1986, chapter 4, p 101

[29] R.H. Davis; Chapter 33; W.S.W. Ho, K.K. Sirkar (Eds.); Membrane Handbook; Van Nostrand Reinhold, New York, 1992, p. 480

[30] Private communication, E. van Kooij, Tollens Coatings BV.

[31] D.E. Wiley, C.J.D. Fell, A.G. Fane; Optimisation of membrane module design for brackish water desalination; Desalination, 52(1985)249

# Summary

Polymeric ultrafiltration membranes have already been employed in numerous aqueous separation processes. On the other hand, the number of non-aqueous applications is still rather limited. This is mainly due to the often poor chemical resistance of the polymers used for membrane preparation; most membranes have been developed for aqueous applications only. In this thesis the preparation, characterization, and application of polyimide ultrafiltration membranes has been described, which may be applicable in non-aqueous separation processes.

Chapter 1 gives a general introduction to the ultrafiltration process. Special attention is paid to the chemical resistance of polymers and to literature references on non-aqueous applications.

In chapter 2, the resistances of various commercially available polymers to a range of solvent classes have been compared. Based on this comparison, a polyimide has been chosen as membrane material. This polymer is well soluble in amide solvents and insoluble and poorly swelling in almost all other organic solvents. The solubility in amides implies that asymmetric polyimide membranes can be prepared by means of phase inversion by immersion precipitation. The influence of several immersion precipitation membrane formation parameters on the membrane morphology and permeability for ternary membrane forming systems is discussed in chapter 2. Dimethylformamide (DMF) was found to be the most suitable casting solvent, and ethanol the most suitable non-solvent, i.e., precipitation medium. The polymer concentration in the casting solution is the main parameter studied here to obtain differences in membrane morphology and permeability.

Polyimide membranes are very brittle and sensitive to defects in the toplayer, especially when macrovoids are present. In chapter 3, it is shown that the addition of some selected low molecular weight aliphatic dicarboxylic acids to the casting solution of polyimide in DMF, suppresses the formation of macrovoids for membranes that are precipitated in water or ethanol (i.e., quaternary membrane forming systems). A mechanism is proposed to explain the effect for these specific systems, based on steric conformations of the additives and the polyimide and interaction between these components. In addition, the solubility of the additives in the coagulation bath has been taken into account as well.

In chapter 4, some of the characterization methods are discussed in more detail, particularly liquid and gas permeation measurements and permporometry. Permporometry is a technique to determine pore size distributions for membranes in a dry state. Theoretical gas fluxes (calculated from pore size distributions obtained by permporometry) were of the same order as the experimental gas fluxes, whereas theoretical ethanol permeabilities (calculated from permporometry results) were about 100 times lower than the experimental values. This discrepancy is probably caused by a change in membrane morphology, which occurs upon drying of the membranes. Therefore, permporometry is a good method to characterize polymeric membranes which will be employed in the dry state. However, for application in the wet state, wet-state membrane characterization techniques are preferred.

Drying of an ultrafiltration membrane results usually in a shrinkage. In the appendix to chapter 4, it is shown that various drying procedures cause an identical overall shrinkage, applied to one type of membrane. One of the few effective variables seems to be the membrane casting solvent, which implies that the membrane preparation conditions determine the final shrinkage of the membrane. It is suggested that during membrane formation by immersion precipitation many small voids are created *inside* the polymeric nodules of the toplayer. These voids collapse during drying, which causes a structural reorganization of the toplayer and surface shrinkage. The ethanol permeabilities were very irreproducible when the membranes were rewetted after drying.

Retention measurements of a flexible monodisperse polystyrene in a very dilute ethyl acetate solution through polyimide ultrafiltration membranes are presented in chapter 5. The retention of the model polymer itself is strongly influenced by convective flow-induced deformation, which means that the employed non-aqueous model system (i.e., flexible polymer molecules) is not suitable to characterize membranes by means of retention measurements. However, flow-induced deformation experiments with non-aqueous dilute solutions can be used to compare qualitatively the critical flux (i.e., the flux necessary for deformation) through different membranes, which is dependent on the pore size distribution.
A new mechanism is proposed which describes the typical flux behaviour of the solution, and is based on energy loss caused by deformational and wall-drag resistances of the deforming polymer chain.
Retention measurements have also been performed with non-deformable silver sols in mixtures of ethanol and water. The interpretation of the results is difficult, since the hydrodynamic radii of the sol particles are expected to be larger than the radii determined by TEM, due to the presence of an electric double layer.

The same polymeric model system, polystyrene in dilute ethyl acetate solutions, has been used to investigate hindered diffusion of flexible polymers through polyimide ultrafiltration membranes. In chapter 6, it is shown that the diffusive permeabilities of monodisperse polymer fractions correspond well with the fractional permeabilities obtained for a polydisperse dilute solution, where all the different molecular weights are present in the feed mixture.
The experimental results also indicate that the diffusive permeability curve as a function of the polystyrene hydrodynamic radius (molecular weight) is strongly dependent on the membrane pore size distribution. However, the determination of a pore size distribution from these hindered diffusion measurements is very difficult, as is also shown in the appendix to chapter 6. Nevertheless, estimations on the maximum pore radius present in each membrane can be made.

The developed polyimide ultrafiltration membranes can in principle be applied for separation in a wide range of chemical media (except the amide solvents). The ultrafiltration of an organic rinsing paint waste stream generated during the manufacture of conventional paints (with white spirit as paint solvent), is a special non-aqueous application of environmental and economical interest and is described in chapter 7. Experiments with diluted red paint in white spirit as feed solution under cross flow conditions have shown that the membranes are able to separate the paint waste stream into one "solvent" stream without pigments and solid particles, and one "concentrated paint" stream that may be used as a basis for a primer paint.
During this separation, a fouling layer has been formed which acts as a dynamic membrane that determines the separation performance.

# Samenvatting

Polymere ultrafiltratiemembranen worden tegenwoordig toegepast in een groot aantal waterige scheidingsprocessen. Het aantal niet-waterige toepassingen is daarentegen tot nu toe erg beperkt. De voor de membraanbereiding gebruikte polymeren hebben vaak een geringe chemische resistentie en zijn bijna zonder uitzondering speciaal ontwikkeld voor waterige toepassingen. In dit proefschrift is de bereiding, karakterisering en toepassing van polyimide ultrafiltratiemembranen beschreven; deze membranen zijn met name geschikt voor toepassing in niet-waterige scheidingsprocessen.

Een algemene inleiding op het gebied van ultrafiltratieprocessen is gegeven in hoofdstuk 1. In dit hoofdstuk worden tevens de chemische resistentie van polymeren en de in de literatuur beschreven niet-waterige toepassingen van ultrafiltratie besproken.

In hoofdstuk 2 worden de chemische resistenties van enkele commercieel verkrijgbare polymeren ten opzichte van een aantal klassen van oplosmiddelen vergeleken. Op basis hiervan is gekozen voor een polyimide als membraanmateriaal; dit polymeer is goed oplosbaar in amides en onoplosbaar (met geringe zwelling) in bijna alle andere organische oplosmiddelen. De oplosbaarheid impliceert dat asymmetrische polyimide membranen bereid kunnen worden door middel van fasenscheiding via immersie precipitatie. In hoofdstuk 2 wordt tevens de invloed van verschillende membraanvormingsparameters op de membraanmorfologie en permeabiliteit besproken, voor ternaire membraanvormende systemen. Dimethylformamide (DMF) bleek het meest geschikte oplosmiddel voor membraanbereiding te zijn, en ethanol het meest geschikte niet-oplosmiddel of precipitatiemedium. De polymeerconcentratie in de oplossing is de belangrijkste onderzochte parameter om verschillende membraanmorfologieën en permeabiliteiten te verkrijgen.

Polyimide membranen zijn erg bros en bevatten veel toplaagdefecten wanneer er macrovoids aanwezig zijn in het membraan. In hoofdstuk 3 is aangetoond dat de toevoeging van bepaalde alifatische dicarbonzuren met een laag molecuulgewicht aan oplossingen van polyimide in DMF effectief de vorming van macrovoids tegengaat, wanneer de membranen gecoaguleerd worden in water of ethanol (quaternair membraanvormend systeem). Een mechanisme is beschreven dat dit effect kan verklaren voor deze systemen, gebaseerd op de

sterische conformaties van de additieven en het polyimide en de interactie tussen deze componenten. Ook de oplosbaarheid van de additieven in het coagulatiebad is een belangrijke factor.

In hoofdstuk 4 worden de verschillende karakteriseringsmethoden nader beschreven: vloeistof- en gaspermeatiemetingen en permporometrie. Met behulp van permporometrie kunnen poriegrootteverdelingen worden bepaald voor membranen in de droge toestand. De theoretische gasfluxen (berekend uit permporometrieresultaten) waren van dezelfde ordegrootte als experimentele gasfluxen, terwijl de theoretische vloeistofpermeabiliteiten (berekend uit permporometrieresultaten) ongeveer 100 keer lager waren dan de experimenteel bepaalde waarden. Dit verschil wordt waarschijnlijk veroorzaakt door veranderingen in membraanmorfologie, die geïnduceerd worden door het noodzakelijke droogproces. Permporometrie is daarom een geschikte methode om polymere membranen te karakteriseren die gebruikt zullen worden in de droge toestand, terwijl voor membraantoepassingen in de natte toestand bij voorkeur "natte" karakteriseringstechnieken gebruikt dienen te worden.

De meeste ultrafiltratiemembranen krimpen wanneer ze worden onderworpen aan droogprocessen. De resultaten die beschreven zijn in de appendix bij hoofdstuk 4 laten zien dat voor één type membraan verschillende droogprocedures resulteren in dezelfde oppervlaktekrimp. Eén van de weinige factoren die invloed lijken te hebben op deze krimp is het gebruikte oplosmiddel tijdens de membraanbereiding, wat betekent dat de oppervlaktekrimp gecorreleerd is aan de membraanbereiding. Er is een hypothese opgesteld, gebaseerd op de veronderstelling dat tijdens het immersie precipitatieproces een groot aantal erg kleine holtes ontstaan binnen in de nodules in de toplaag. Tijdens het droogproces verdwijnen deze holtes, wat gepaard gaat met een verandering in morfologie in de toplaag en met oppervlaktekrimp. De ethanolpermeabiliteiten van membranen die zijn herbevochtigd met vloeistof na het drogen bleken zeer irreproduceerbaar te zijn.

Retentiemetingen met sterk verdunde oplossingen van een flexibel monodispers polystyreen in ethylacetaat door polyimide ultrafiltratiemembranen zijn beschreven in hoofdstuk 5. Het retentiegedrag van het polymeer zelf wordt sterk bepaald door convectieve stromingsvervorming, wat inhoudt dat het gebruikte niet-waterige modelsysteem (flexibele polymeermoleculen) niet geschikt is om membranen te karakteriseren door middel van retentiemetingen.
Stromingsvervormingsexperimenten met niet-waterige verdunde polymeeroplossingen kunnen echter wel worden gebruikt om de "kritische flux" (de flux die noodzakelijk is voor het optreden van vervorming) door verschillende membranen kwalitatief te vergelijken, omdat deze waarde afhankelijk is van de

poriegrootteverdeling van het membraan.
Een nieuwe verklaring is gevonden voor het typerende fluxgedrag van de oplossing, gebaseerd op energieverlies dat optreedt als gevolg van vervormings- en wand-wrijvingsweerstanden van het vervormende polymeermolecuul.
Retentiemetingen zijn tevens uitgevoerd met niet-vervormbare zilversolen in mengsels van ethanol en water. De interpretatie van de verkregen resultaten brengt problemen met zich mee, omdat verwacht wordt dat de hydrodynamische stralen van de soldeeltjes groter zijn dan de stralen die bepaald zijn met behulp van TEM, vanwege de aanwezigheid van een electrische dubbellaag.

Hetzelfde polymeer-modelsysteem, polystyreen in verdunde ethylacetaat-oplossing, werd gebruikt om de gehinderde diffusie van flexibele polymeren door polyimide ultrafiltratiemembranen te onderzoeken. In hoofdstuk 6 zijn resultaten gepresenteerd die aantonen dat de diffusieve permeabiliteiten van monodisperse polymeerfracties goed overeen komen met de corresponderende permeabiliteiten die bepaald zijn voor een polydisperse verdunde oplossing, waar al deze fracties tegelijkertijd in de voeding aanwezig zijn.
De experimentele resultaten laten eveneens zien dat de diffusieve permeabiliteitscurve als functie van de hydrodynamische straal van polystyreen (mol. gewicht) sterk afhankelijk is van de poriegrootteverdeling van het membraan. De bepaling van een poriegrootteverdeling uit deze gehinderde diffusie-experimenten is problematisch, wat tevens aangetoond wordt in de appendix bij hoofdstuk 6. Desalniettemin, schattingen van de grootst aanwezige poriestraal in het membraan kunnen goed worden gemaakt.

De ontwikkelde polyimide ultrafiltratiemembranen kunnen in principe toegepast worden in een reeks verschillende organische media (met uitzondering van de amide oplosmiddelen). Hoofdstuk 7 beschrijft een niet-waterige toepassing die milieutechnisch en economisch aktueel is: ultrafiltratie van een organische spoelafvalstroom die ontstaat bij de productie van conventionele verven (met white spirit als verfoplosmiddel). Crossflow-experimenten met verdunde rode verf in white spirit als voeding hebben aangetoond dat met behulp van de ontwikkelde membranen de afvalstroom gescheiden kan worden in een oplosmiddelstroom zònder pigmenten en vaste bestanddelen, en een geconcentreerde verfstroom die hergebruikt zou kunnen worden als basis voor bijvoorbeeld grondverf.
Tijdens de scheiding wordt een vervuilingslaag gevormd. Deze laag dient als een dynamisch membraan dat de scheiding volledig bepaalt.

# Levensloop

Monique Beerlage werd op 26 augustus 1965 geboren te Oldenzaal. In 1983 behaalde zij het VWO-diploma aan het Pius-X-College te Almelo. In datzelfde jaar begon zij haar studie Chemische Technologie aan de Technische Hogeschool Twente (later Universiteit Twente). In het kader van deze studie werd een stage verricht bij het Koninklijke/Shell-Laboratorium te Amsterdam, alwaar werd gewerkt aan modificatie van katalysatoren voor polymeerproduktie. De afstudeeropdracht, getiteld "Eiwitadsorptie aan microporeuze membranen" werd uitgevoerd in de onderzoeksgroep Membraantechnologie, waarna zij in juni 1989 het ingenieursdiploma behaalde.
Vanaf 1 augustus 1989 was zij als assistent in opleiding werkzaam in de onderzoeksgroep Membraantechnologie (vakgroep Grensvlak- en Scheidings-Technologie) van de Universiteit Twente, waar het in dit proefschrift beschreven onderzoek werd verricht onder supervisie van prof. dr. ing. H. Strathmann en prof. dr. C.A. Smolders.

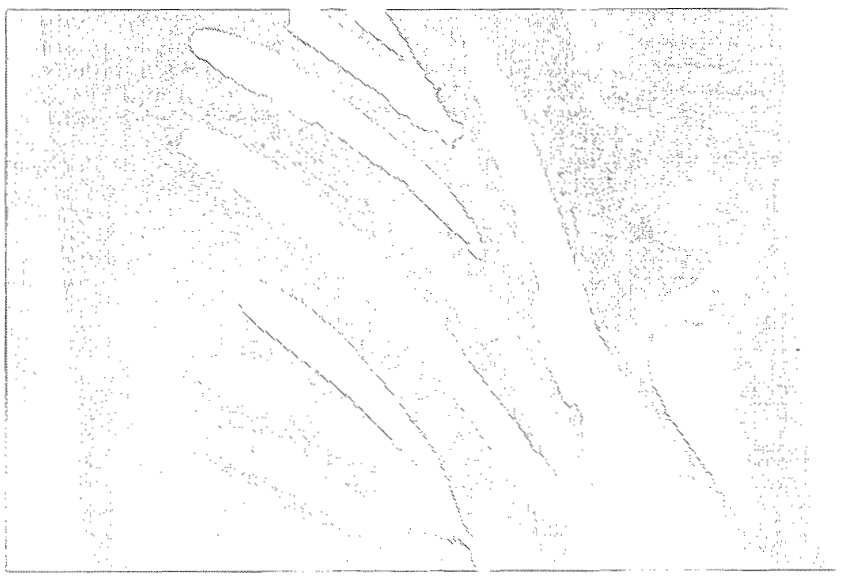

ISBN 90-9007140-7